CONTROL AND ENERGY MANAGEMENT OF STANDALONE INTERCONNECTED AC MICROGRIDS

Submitted by

Ezenwa Ethelbert Udoha

to the
University of Exeter
as a thesis for the degree of

Doctor of Philosophy in Renewable Energy

January 2024.

I certify that all materials in this thesis, which is not my own work, has been identified and that no material has previously been submitted and approved for the award of a degree by this or any other University.

Signature: …… …….

Dedication

This thesis is dedicated to God of all creations, the fountain from whom all wisdom, knowledge, love and kindness come. And to my late Dad, Sir Godwin C. Udoha (KSJI), and ever-prayerful and supportive Mom, Lady Scholastica Udoha (Laux), for being the source of inspiration.

Acknowledgement

My sincere appreciation goes to my supervisor, Prof. Mohammad Abusara, for your selfless effort, starting from supporting me with the documentation that helped to acquire some funding that made this research a reality and to your top-notch professorial mentorship, which is the first of its kind, and diligently seeing me through this PhD journey. Your mentorship has made me acquire more skills and widen my intellectual scope. I want to say thank you. I sincerely appreciate Dr Saptarshi Das for your immense support and guidance throughout my PhD studies. Our insightful engagements would always point me to the fine details of the research work. You have inspired and widened the horizon of my learning and skill acquisition.

I sincerely thank the management of the Tertiary Education Trust Fund (TETFUND) under the leadership of the former Board Chairman and Minister of Education (State), Honourable Barr. Chukwuemeka Nwajiuba for the financial grant approval and encouragement under the Federal University of Petroleum Resources, Effurun (FUPRE) Academic Staff Training and Development (AST&D) intervention grant.

Many thanks to the management and staff of the Federal University of Petroleum Resources, Effurun (FUPRE), for the immeasurable support.

I remain indebted to my ever-lovely wife, Oluchi, and sons, Chukwukere and Uchenna, for their patience, understanding, love and support throughout this journey. I thank you immensely. And to my siblings, Engr and Dr (Mrs) Catherine Oparaji, Engr & Dr (Mrs) Uche Udoha and Engr (Mrs) Chioma, for your prayers, unconditional love, kindness, and encouragement.

My research experience would be incomplete without your support and encouragement, Dr Ajit, Dr Ian Ashton, Dr Essam Hussain, the staff of the Faculty of Environment, Science and Economy, and the following friends, turn brothers: Dr Marvin, Dr Yusuf and Ibrahim and my colleagues, Dr Miguel, Dr Ali and Raul. Thank you very much for the unquantifiable support and warmth; you all made my PhD studies at the University of Exeter, Penryn Campus, worthwhile.

Abstract

This thesis considered microgrids as local area distribution mini-power grids formed by distributed generation sources, energy storage systems and loads. They are reliable and can operate at different voltages and frequencies to meet the requirements of the load. Microgrids have limited renewable energy source (RES) capacity, which can only supply a limited load and increasing the load beyond a specifically designed limit can lead to stability issues. Irrespective of its limited capacity, there has been an increased widespread deployment of renewable energy-based microgrids worldwide orchestrated by the 2015 Paris Agreement and the war in Ukraine and as a solution to meet the global demand for energy in electricity deficit zones aimed to achieve universal access to affordable, reliable, and sustainable energy. Fast forward to the future, flooded singly operated microgrids face the problem of more curtailing of RES and load shedding. Multiple microgrids can be interconnected to mitigate the limitations of single microgrids and improve supply reliability, enhance power supply availability, stability, reserve capacity, reduce investment in new generating capacity and control flexibility.

As a result, this thesis proposes a new structure and control technique for interconnecting multiple standalone AC microgrids to a common alternating current (AC) bus using a back-to-back power electronic converter and a traditional transformer. Each microgrid considered in this thesis comprises a renewable energy source (RES), battery, auxiliary unit, and load. The battery maintains the AC bus voltage and frequency and balances the difference in power generated by the RES and that consumed by the load. Each microgrid battery's charge/discharge is maintained within the safest operating limit to maximise the RES power utilisation. The back-to-back converters are used to decouple the connecting standalone microgrid frequencies and facilitate power exchange between microgrids. The transformer is used to transmit electric power over long distances efficiently. The control technique for all the connecting bidirectional back-to-back converters is developed to manage the bidirectional power flow between each microgrid and other microgrids in the network and to balance the energy in the global bus of the interconnected microgrid with no communication. The control strategy uses a frequency signalling mechanism to limit the power demand of individual global converters and adjusts its droop coefficients accordingly and in proportion to deviation in frequency. The global droop controllers of the global connecting converters receive information about the status of the frequencies of individual microgrids using a low bandwidth communication link to enhance network power flow. MATLAB/Simulink results validate the performance of the proposed structure and control strategy.

A decentralised control scheme is further proposed for the standalone interconnected AC microgrid structure. This thesis presented a high-level global droop controller that exchanges power between the interconnected microgrids. Renewable power curtailment and auxiliary power supplement mechanisms are designed based on the bus frequency signalling technique to achieve balance and continuity of supply. In case of power shortage in one microgrid, priority will first be given to power import from other microgrids. A power supplement is used if the power imported is insufficient to control the battery state of charge (SOC). Similarly, in case of a power surplus, priority will be given to power export, and if this is not enough, power from RES will be curtailed. Performance evaluation shows that the proposed controller maximises renewable power utilisation and minimises auxiliary power usage while providing better load support. The performance validation of the proposed structure and control strategy has been tested using MATLAB/Simulink.

Furthermore, this thesis investigated a centralised control and energy management of multiple interconnected standalone AC microgrids using the Nelder-Mead simplex algorithm (Fminsearch optimisation toolbox in MATLAB) based on the new proposed model. The main objective is to minimise the total cost of energy from the auxiliary unit produced from gas. The results obtained are compared with those obtained from an unoptimised system. The performance evaluation investigation results are compared with the unoptimised results to determine the percentage optimal performance of the system. The comparison outcome shows that the proposed optimisation method minimises the total auxiliary energy cost by about 9% compared with the results of the unoptimised benchmark.

Table of Contents

List of Figures

List of Tables

Nomenclature

Acronyms	Description
AC	Alternating current
ADMM	Alternating direction method of multipliers
ASEAN	Association of South East Asia Nations
ATC	Analytical target cascading
ATS	Automatic transfer switch
BESS	Battery energy storage system
Cdc	DC link capacitor
CHP	Combined Heat and Power
CO_2	Carbon dioxide
COP27	27th Conference of the Parties
DC	Direct current
DG	Distributed Generation
DN	Distribution network
DSO	Distribution system operator
ED	Economic dispatch
EM	Energy management
EMS	Energy management system
GA	Genetic algorithm
GC	Global converter
GHG	Greenhouse gas
GNCC	Global network central controller
GW	Gigawatt
HVDC	High voltage DC
IEA	International Energy Agency
IGBT	Insulated-gate bipolar transistor
IM	Interconnecting medium
kWh	Kilo-Watt-hour
LC	Local controller
LC	Local converter
LCL	Inductor-capacitor-inductor
LPF	Low pass filter
LV	Low voltage
MCS	Monte Carlo Simulation
MENA	Middle East and North Africa
MG	Microgrid
MG1 GC	Microgrid one Global Converter
MG1 LC	Microgrid one Local Converter
MG2 GC	Microgrid two Global Converter
MG2 LC	Microgrid two Local Converter
MG3 GC	Microgrid three Global Converter
MG3 LC	Microgrid three Local Converter
MGCC	Microgrid central controller
MMG	Multi-Microgrid
MPC	Model predictive control
MPPT	Maximum power point tracking
MV	Medium voltage

MVAC	Medium voltage alternating current
OF	Objective function
PCC	Point of common coupling
PSO	Particle swarm optimisation
PV	Photovoltaic
PWM	Pulse Width Modulation
RES	Renewable Energy Sources
SDG 7	Sustainable Development Goal 7
SOC	State of charge
THD	Total Harmonic Distortion
UT	Unscented transform
VSC	Voltage Source Converter
VSC-HVDC	Voltage source converter—high voltage direct current
VSI	Voltage Source Inverter
P_L	Global load
T_g	Utility grid transformer
S_g	Grid breaker
ω	Output frequency
ω_0	Nominal bus frequency
m	Frequency drooping coefficient
P	Active power
P^*	Active power demand
V	Voltage amplitude
V_0	Nominal voltage
n	Voltage drooping coefficient
Q	Reactive power
Q^*	Reactive power demand
$\Delta\omega$	Frequency deviation
ω_{max}	Frequency maximum
ω_{high}	Frequency high
ω_{low}	Frequency low
ω_{min}	Frequency minimum
$\Delta\omega_{max}$	Maximum frequency deviation
$\Delta\omega_{high}$	High-frequency deviation
SOC_{max}	Maximum state of charge
SOC_{high}	High state of charge
SOC_{low}	Low state of charge
SOC_{min}	Minimum state of charge
P_{pv}	PV power
P_{pv}^*	PV power demand
m_p^{pv}	Proportional droop control coefficient of PV

m_i^{pv}	Integral droop control coefficient of the PV
P_{MPPT}	Maximum power point tracking of PV power
P_{aux}	Auxiliary power
m_p^{aux}	Proportional droop control coefficient of the auxiliary unit
m_i^{aux}	Integral droop control coefficient of the auxiliary unit
m_p^{local}	Proportional droop control coefficient of local converter
P_{local}	Output power of the local converter
P_{local}^*	Local converter power demand
k_p^{vdc}	Proportional droop control coefficient of the DC link
k_i^{vdc}	Integral droop control coefficient of the DC link
V_{dc}	DC link voltage
V_{dc}^*	DC link voltage demand
ω_{global}	Output frequency of the global converter
m_p^{global}	Proportional droop control coefficient of global converter
P_{global}	Output power of the global converter
P_{global}^*	The power demand of the global converter
k	The slope of the power demand of the global converter
$\Delta\omega_{local}$	Frequency deviation of the local converter
C_{gas}	Summation of the cost of gas function
$\lambda_{(t)}$	Cost of energy from gas per kWh (£/kWh)
$P_{gas,i}$	The total amount of gas the auxiliary utilises
P_L	Load at the global bus
$P_{\exp,i}$	Power export of the ith microgrid
$P_{\exp,i}^*$	Power export demand of the ith microgrid
N	Total number of connecting global converters
i	Number of microgrids
$P_{\exp,avg}^*$	Average power export demand

Publications

- **Udoha Ezenwa, Saptarshi Das, Mohammad Abusara.** A Power Management System for Interconnected AC Islanded Microgrids Using Back-to-Back Converter: In Grid Connection, IET Powering Net Zero Week, Renewable Power Generation and Future Power Systems Conference 2023, Crowne Plaza Glasgow, UK, 15th – 16th Nov. 2023.

- **Udoha, E., Das, S., & Abusara, M.,** Power Flow Management of Interconnected AC Microgrids Using Back-to-Back Converters. *Electronics 2023*, 12, 3765. https://doi.org/10.3390/electronics12183765.

- **Udoha, E., Das, S., & Abusara, M.,** Centralised Control and Energy Management of Multiple Interconnected Standalone AC Microgrids. Batteries (undergoing review)

CHAPTER 1: INTRODUCTION

1.1 Background

The global call for climate and ecological emergencies and the devastating consequences has been at the forefront of all conversations in the committee of nations. According to a United Nations report [1], billion tons of carbon dioxide (CO_2) emissions from coal, oil, and gas production are released into the atmosphere annually. The last four years have been described as the hottest in history, and understanding the lives that are most affected by climate change stimulates the action for help. Temperature is expected to rise above three degrees Celsius by 2100 if action is not taken to slow global emissions. Hence, the 2015 Paris Agreement on climate change has been reiterated to target progress at the 27th Conference of the Parties (COP27) on the global call to limit the increase of eventual warming to a further 1.5 degrees. The consequential need to reduce CO_2 emissions by 45% by 2030 from the 2010 levels and reach net-zero emissions by 2050, as posited in [2][3], has deepened the scope of developments of research in renewable energy with cutting-edge technologies to generate clean and affordable energy for all. According to a World Bank report, 759 million people globally with no electricity access in 2019 significantly increased in sub-Saharan Africa. Hence, there is a need to ramp up efforts in countries with the most significant electricity deficits to achieve Sustainable Development Goal 7 (SDG 7), which aims to achieve universal access to affordable, reliable, sustainable, and modern energy by 2030 [4]. This research proposes solving the electricity problem in sub-Saharan Africa, a Nigerian case with abundant renewable energy resources from sunlight.

The growing demand for clean, affordable, sustainable and efficient power calls for decentralised Renewable Energy Source (RES)-based electrification solutions expansion in the form of solar photovoltaics (PV), energy storage devices: Battery Energy Storage Systems (BESSs), and flywheel, wind, tidal, bioenergy, fuel cells, geothermal, hydropower, and micro gas turbine etc. RES are clean, inexhaustible energy sources and make a good Distributed Generation (DG) source. They produce near zero CO_2 emission in the atmosphere when compared to fossil fuel-based sources, which is in the

opposite direction. The most common are solar PV and wind energy sources. However, global renewable capacity is expected to increase by almost 75%, about 2400 GW, between 2022 and 2027[5]. This growth in renewable technologies is propelled by more ambitious expansion policies in critical markets and partly in response to high fossil fuel and electricity prices from the current energy crisis. Additionally, the Russian invasion of Ukraine has caused fossil fuel importers, especially in Europe, to value the energy security benefits of renewable energy. It is forecasted that solar PV and wind are expected to account for almost 95% of all new renewable energy installations. Annual capacity additions are expected to increase, reaching a record high of 460 GW in 2027[5]. Table 1.1 illustrates the projected growth of renewable energy regions outside China.

Table 1.1: Renewable capacity growth outside of China, main and accelerated cases

Region	2010 – 2015 (GW)	2016 – 2021 (GW)	2022 – 2027 Main Case (GW)	2022 – 2027 Accelerated Case (GW)
European Union	142.6	144.3	343.9	450.1
United States	68.8	153	280.6	359.5
India	29.7	71.7	145.6	217.1
Brazil	27.7	47.9	72.1	83.3
MENA	6.3	15.5	45.9	77.2
Sub-Saharan Africa	7.5	16.2	42.3	54.7
ASEAN	21.9	39.1	51.3	78.3
Other Countries	141.9	231.2	329.5	440

MENA: Middle East and North Africa
ASEAN: Association of South East Asian Nations

Table 1.1 illustrates that renewable energy expansion accelerates in all regions, and the three least accelerated regions are the Association of South East Asia Nations (ASEAN) with about 78.3 GW, Middle East and North Africa (MENA) with 77.2 GW, and the least is 54.7 GW in Sub-Saharan Africa. Considering the forecasted future power generations from solar PV and wind, which are expected to form the majority of future RES installations and the intermittent nature of the resource, solar and wind

cause variations in voltage and frequency [6]. Therefore, as the demand for accelerated clean energy grows, RES-powered DGs can be aggregated into a microgrid to enhance the reliability and efficiency of its operations. According to [7], increased penetration of DG sources at the distribution network can result in problems such as voltage rise, unstable voltage and frequency and protection miss-coordination. These problems can be mitigated by aggregating several sources and loads into a controlled microgrid unit. Microgrids have the resources and capability to generate electricity, distribute, regulate and manage power flow to consumers with good power quality and increased reliability, controllability, and power quality.

Microgrids are mini-smart power grids consisting of DGs (or micro-sources: conventional or renewable) units, energy storage devices (BESS, fuel cell, flywheel), and loads with associated control systems. They can connect renewable sources like solar PVs and wind turbines and non-renewable clusters of DGs like diesel generators, micro-turbines, fuel cells and combined heat and power (CHP) plants to supply loads within defined electrical boundaries [8][9]. Microgrids can be connected to operate in standalone (autonomous) and utility grid-connected modes based on their prevailing conditions. They are usually connected at the distribution or load side of the power system network. Depending on the proximity of available power sources and the nature of the connected local load bus, a microgrid can be classified into alternating current (AC) or direct current (DC). However, it can be regarded as a hybrid where a combination of AC and DC are used in a microgrid. Microgrid networks are constructed to produce advanced power quality and reliability to satisfy the load demand, which cannot be achieved by the utility grid alone. They reduce power transmission losses and eliminate the need for cost on investment infrastructure that would have been used on transmission and distribution networks [10], [11]. During the islanding operation of a microgrid from the grid-connected mode, the independent operation of a standalone microgrid may not be reliable enough to meet its load demand due to its limited generation capability [6], [12]. Therefore, due to limited generation options,

microgrids more often shed the loads to achieve supply and demand balance, which causes unhealthy disruptions to business operations on the load side. Hence, microgrids are interconnected to overcome these limited challenges and provide improved reliability and supply availability. By integrating interconnected microgrids, larger bulk and more forecasted accelerated renewable power capacity growth could be achieved in the least accelerated Sub-Saharan Africa region, and these microgrids can exchange power to meet their load demands.

1.2 Interconnected Microgrids: The Trending Concept

The concept of interconnected microgrids presents a unique opportunity for the widespread use of neighbourhood-accessible microgrids to meet the growing load demand. An interconnected microgrid is a power system consisting of coordinated microgrids to improve reliability, resilience and robustness by sharing reserve capacity, supplying external microgrid loads during emergencies, and maximising its normal operations collaboratively. Individual microgrid operations in the network are coordinated to provide a resilient, sustainable, cost-effective electricity supply to the load users [13,14]. However, by interconnecting microgrids, various faults are mitigated to achieve continuity of electricity supply to the local load due to the local generation operation, network control topologies and optimisation [10]. For example, in multiple interconnected microgrids operating in a standalone mode, in the event of a power shortage from one microgrid, other microgrids can work together to keep critical loads powered and also share the capacity of their resources with their respective advantages, complementing each other to maintain load-frequency balance in the network for a longer time [15]. Like the microgrid's operation, interconnected microgrids can be connected to the utility grid (grid-connected mode) or operate autonomously in standalone (islanded) mode. Interconnection of microgrids can be done either with a common AC bus or a common DC bus. However, the interconnection of multiple microgrids with a combination of the common AC and DC can be classified as hybrid. In a hybrid, several AC and DC microgrids are interconnected in a smart grid to exchange

power most economically and efficiently. However, this thesis is focused on standalone interconnected AC microgrids with a common AC bus. Interconnected microgrids are a great alternative to microgrids, allowing for better RES utilisation and load support. The proposed structure of multiple standalone interconnected AC microgrids with a common AC bus is shown in Figure 1.1. This figure consists of three microgrids that can operate independently as standalone and interconnected microgrids, operating at the same and different frequencies based on their local load demand. Each microgrid is connected to the common AC bus (global bus or medium voltage AC (MVAC) bus, through a power electronic AC/DC/AC converter and the traditional power transformer.

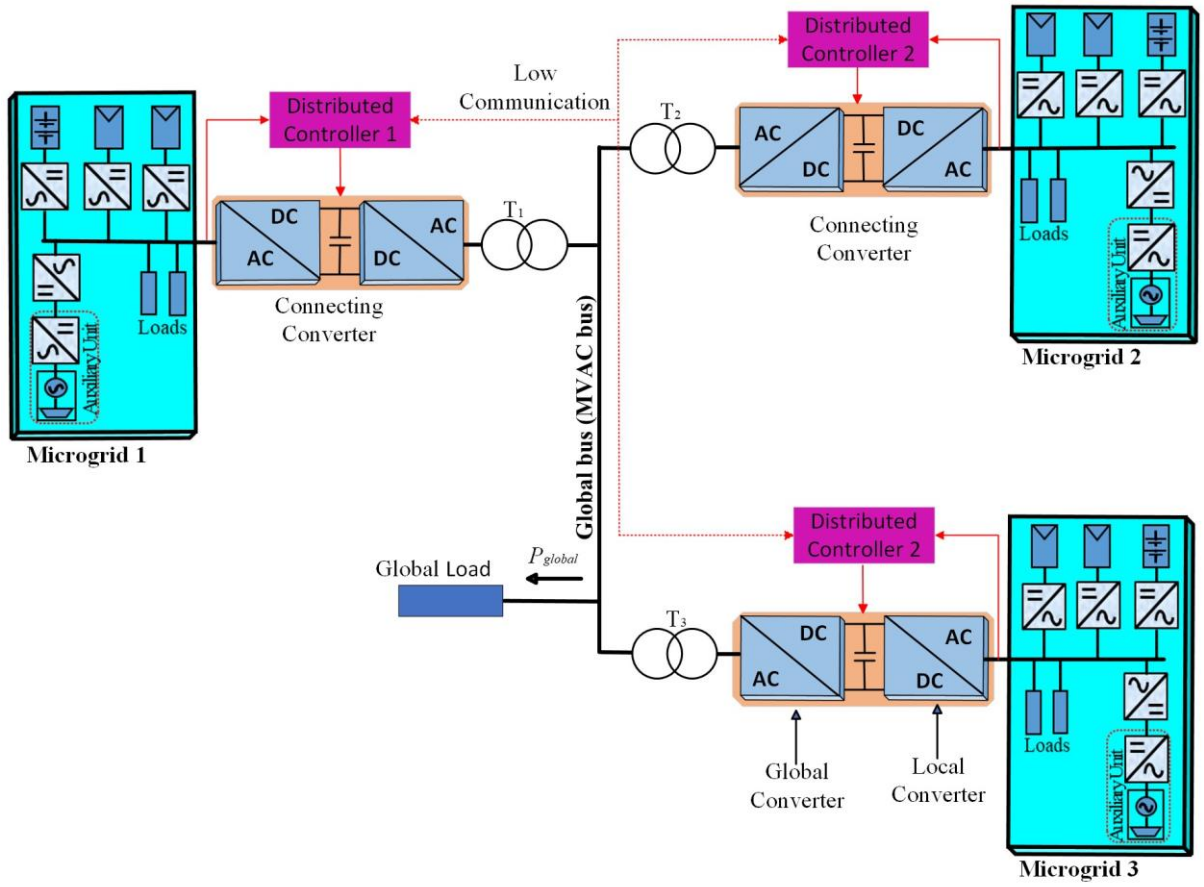

Figure 1.1: Proposed Structure of Multiple Standalone Interconnected AC Microgrids

Figure 1.1: Proposed Structure of Multiple Standalone Interconnected AC Microgrids

At the individual microgrid level, each microgrid described in Figure 1.1 consists of PV-based RES, BESS, auxiliary unit and loads connected to the microgrid's common AC bus. The auxiliary unit is in

the form of a micro-gas turbine or diesel generator. However, the micro-gas turbine and diesel generator provide the same electrical behaviour when a controllable power electronic converter interfaces them. The BESS unit acts as a grid-forming unit that controls the local microgrid AC bus voltage and frequency [16]. The BESS charging or discharging power depends on the difference between PV and load. Each PV-based RES is connected to the local microgrid AC bus via a unidirectional DC/AC inverter [9]. The inverter controls the output power depending on available irradiance. The BESS units are interfaced to the local microgrid common AC bus using bidirectional DC/AC power electronic converters. The auxiliary unit in the form of a micro-gas turbine consists of a unidirectional AC/DC converter that regulates the DC link voltage and the DC/AC inverter that controls power output based on the variation in AC bus frequency [16]. The auxiliary unit AC/DC/AC interfacing converter controls power to ensure that power is delivered at certain times when required. The auxiliary units are not connected directly because if they do, they have to run all the time, and they can respond to very low loads that are not needed. This auxiliary unit supports the BESS unit when the state of charge (SOC) is low and supplements power when the PV-based power cannot meet the load demand. The output AC voltage and current of the PV-based RES and that of the BESS and auxiliary unit are independently controlled to produce power when needed. The combined effect of all sources in the local microgrid common AC bus is used to supply the local loads, and any surplus power can be exported to a deficient microgrid. Hence, the PV-based RES, BESS, auxiliary supply, control system auxiliaries and loads are coupled in microgrid form to operate in standalone (autonomous or islanded) and grid-connected modes.

In standalone mode, the BESS is the grid-forming unit as it controls and maintains the AC bus voltage and frequency and balances the difference in power generated by the RES and the power consumed by the load. Hence, the PV-based RES is the grid-feeding unit that injects power into the local microgrid AC bus. In grid-connected mode, the stiff grid dictates the microgrid AC bus voltage and frequency, and individual RES units control the power flow. Thus, the grid balances any imbalance between the

power provided by the RES and that consumed by the load. However, due to the BESS's limited charging and discharging capacity, overcharging and undercharging boundaries are specified to protect the reserve capacity. In standalone mode, overcharging can be prevented by curtailing the surplus power produced by the RES. Undercharging is prevented by using an auxiliary unit to supplement the power deficit or load shedding. The battery SOC should be controlled to maximise the usable capacity of the BESS most economically to meet the varying load demand.

Microgrids have limited RES and load capacity, and they can only utilise limited available RES to supply a limited amount of load, and increasing the penetration of RES beyond a specific limit can lead to instability. Instability can result if there is a very high load and the generation amount is low, and vice versa. To overcome this limitation, multiple microgrids are interconnected to provide other/more options to stabilise the system, maximise RES power utilisation and offer more load support.

Hence, each microgrid is interfaced with the common AC bus at the interconnected microgrid level using a back-to-back AC/DC/AC converter and traditional power transformer. The AC/DC/AC converter consists of the microgrid side AC/DC local converter, DC link, and the global bus or medium voltage AC (MVAC) side DC/AC converter. The local converter regulates the DC-link voltage. The global converter regulates the power exchanged between the local microgrid and the rest of the system. The global voltage and frequency are controlled by the global controller of the DC/AC global converter. The load at the global bus is supplied by the three global DC/AC inverters, which share the global load equitably. However, all global DC/AC converters use conventional droop control to stay synchronised and collectively control the global AC bus. This implies that each interconnected microgrid in the network shares the power according to its rating. Power management at the global connecting converter employs a frequency signalling mechanism.

Multiple microgrids can be interconnected either with a common-coupling direct current (DC) bus as in [17] or a common-coupling alternating current (AC) bus [18]–[20]. The common AC bus is a simple, easy-to-implement, proven and cost-effective technology that allows for easy integration with existing AC buses, transformers, power system auxiliaries and loads without further investment in power systems infrastructure as would have been the case for a common DC bus. Also, using power transformers helps form a more robust medium AC bus, allowing power transmission over long distances to enhance power quality [21]. Due to excessive conversion equipment, interconnection with a common DC bus is less reliable and available. Using a common DC bus will require high voltage (HVDC) technology, a more complicated and sophisticated technology that still does not exist in the developing world. Using a common AC bus can avoid such complexities. Power electronic AC/DC/AC converters decouple two AC frequencies, and when properly controlled, the system can cope with undesirable disturbances that threaten system stability and robustness. It is simple to interconnect microgrids operating at the same voltage and frequency with static switches or breakers and a good synchronisation algorithm [5].

1.3 System under Study

The multiple standalone interconnected AC microgrids system under study consists of three microgrids, each connected with a connecting power converter to enable the microgrids to operate independently and in interconnected mode, and a traditional power transformer for easy power transmission over long distances. If each microgrid is connected directly to the transformer, it can react even with minor changes in load. The proposed interconnecting control topology of the multiple standalone interconnected microgrids is shown in Figure 1.2, and its operation is as follows:

i) The microgrid side local converter has a bidirectional AC/DC converter that regulates the DC-link voltage.

ii) The global bus side converter is a bidirectional DC/AC converter. The bidirectional DC/AC converter regulates the power exchanged between the local microgrid and the rest of the system. However, all global DC/AC converters use global droop control to stay synchronised and collectively control the global AC bus.

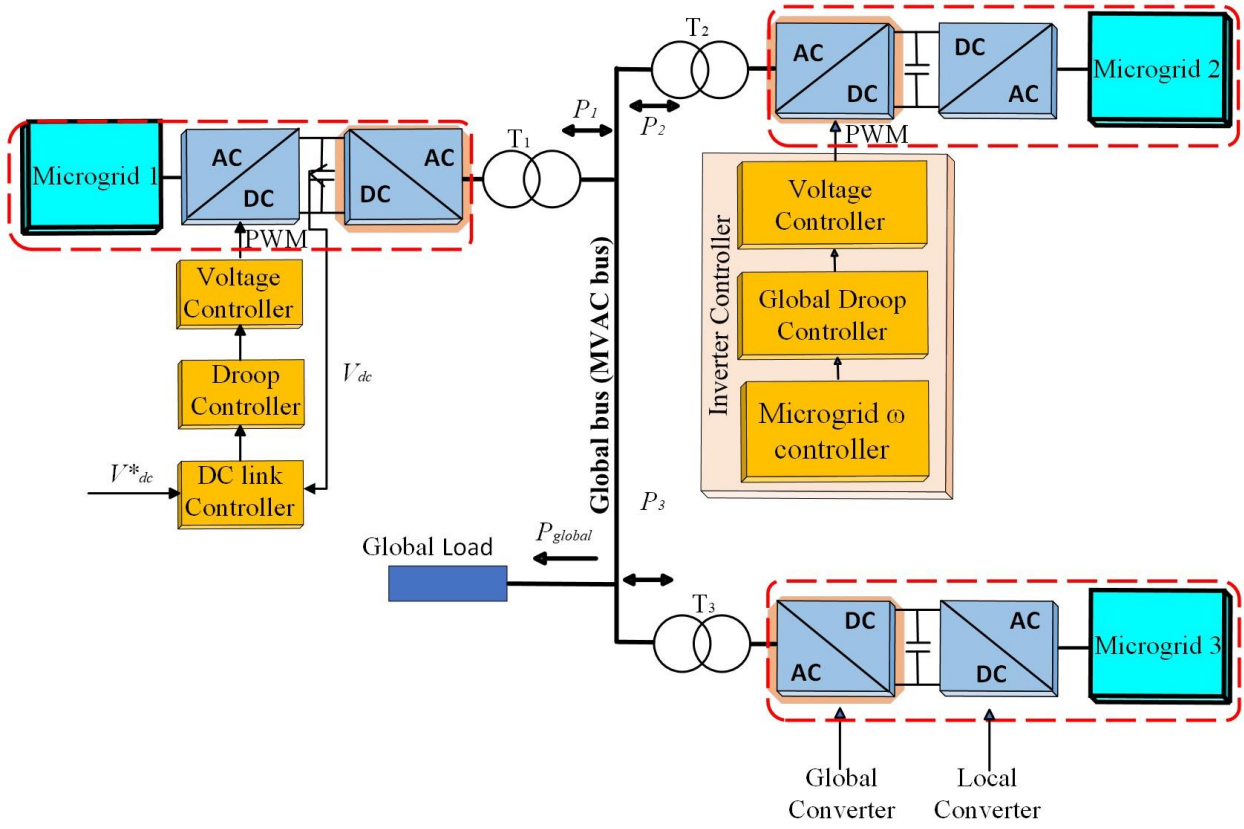

Figure 1.2: Proposed Control Structure of Local and Global Converter Connecting Converters

1.4 Research Motivation and Problem Statement

There has been an increased use of RES from solar, wind, hydropower, biomass, tidal, and wave in combating energy poverty and climate change. Microgrids significantly integrate the bulk of these RES to operate in grid-connected and standalone modes. However, single microgrids have limited energy generation capacity. They can accommodate a limited capacity of RES, which can only supply a limited load and increasing the load beyond a specifically designed limit can lead to stability issues. Hence, the microgrid's stability, reliability, and efficiency decline as the load capacity increases and

the need for expansion arises [7], [22–25]. Thus, if microgrids are interconnected uniquely, it will enable an improved/enhanced way of sharing their respective reserve capacity, improve resilience, improve RES power utilisation and provide better load support [26]. The interconnected microgrid control structure and operation remain challenging due to the complexity and large-scale involvement of power converters with different roles. However, the main motivation of this thesis is to provide some solution to this challenging task by developing functional control strategies that facilitate a more efficient power exchange among interconnected microgrids in the proposed structure.

Therefore, this thesis proposed a structure by which standalone AC microgrids can be interconnected to a common AC bus using the back-to-back converter and traditional power transformer. A back-to-back AC/DC/AC converter provides an electrical mechanism to decouple the two connecting frequencies and ensure independence. At the same time, traditional power transformers help transmit power over long distances and boost the system's robustness.

Hence, this thesis tackled the following problems: How the proposed connecting back-to-back (bidirectional) converters are controlled to exchange power and balance energy between interconnected microgrids with no communication (with decentralised controllers), how the multiple interconnected standalone microgrids are managed to reduce RES power curtailment and auxiliary power usage. Then, a centralised control mechanism is developed to optimise the control and energy management in the interconnected network.

1.5 Aims and Objectives

This thesis proposes a new structure and energy management for interconnecting multiple standalone microgrids to a common AC bus using back-to-back converters. The thesis presents a wireless high-level global droop controller that exchanges power between interconnected microgrids. Each microgrid considered in this paper comprises PV-based RES, BESS, auxiliary units in the form of micro gas turbines, and loads. Renewable power curtailment and auxiliary power supplement

mechanisms are designed based on the bus frequency signalling technique to achieve balance and continuity of supply. The objectives of the thesis are summarised as follows:

i) To review different structures and control architectures for interconnected standalone AC microgrids.

ii) To design a decentralised power management system and wireless global droop controller for power flow management for interconnected standalone AC microgrids using the back-to-back converter.

iii) To design a RES power curtailment unit that curtails surplus RES power according to the local microgrid bus frequency and auxiliary power supplement unit to ensure the system operates within the specified limit.

iv) To evaluate the proposed controllers' effective performance using load and RES power profiles.

v) To investigate the centralised optimal controller performance for energy management in multiple interconnected standalone AC microgrids.

1.6 The Novel Contributions

The following are the main contributions of the thesis:

- This thesis provides a novel structure and control topology of interconnected microgrid design for better RES utilisation and load support. The structure uses back-to-back converters and traditional power transformers to achieve a more robust network.
- Design of distributed controllers that limit the power demand of global converters by measuring each microgrid bus frequency deviation and adjusting its droop coefficient accordingly and in proportion to the bus frequency deviation.

- Design of a global droop control mechanism for power management of multiple standalone interconnected AC microgrids. This controller ensures the right amount of power is exchanged between the interconnected microgrids.
- Performance evaluation of how well the suggested global droop controller satisfies the control priorities and design requirements following the limitations of the controllers. The evaluated results are compared based on three operating scenarios: i) independent operation of multiple microgrids, ii) multiple microgrids interconnected with the global droop control, and iii) interconnected multiple microgrids operating with global droop control and global load.
- An investigation into the centralised optimal controller performance for energy management of multiple interconnected independent AC microgrids using the Fminsearch optimisation toolbox in MATLAB.

1.7 Outline of the Thesis

The outline of the thesis is organised as follows:

Chapter 2 reviews the literature on different structures and power flow management topologies of interconnected microgrids. This chapter provides an extensive literature review of the main research work reported about the control and energy management of interconnected AC microgrids using back-to-back converters, including optimal power-flow management strategies for interconnected microgrids. In addition, reviews of grid-connected and standalone interconnected microgrid studies are also presented.

Chapter 3 describes the proposed novel structure for standalone interconnected AC microgrids. The microgrids are interconnected to a common AC bus using back-to-back converters and traditional power transformers for power management. Each microgrid comprises a hybrid system consisting of PV-based RES, BESS, auxiliary units and loads. Global droop control is proposed for each global connecting converter to manage power exchange among the connecting converters, while the local

droop controller is proposed for each local connecting converter. The chapter overviews a typical detailed inverter-based interconnected AC microgrid and its operation in standalone and grid-connected modes. The chapter also details droop control strategies for BESS and PV-based units and different control strategies for DC link voltages in two-stage converters (local and global) and other relevant DC/AC converters. Simulation results from MATLAB/Simulink validate the performance of the connecting converters and power management using the novel structure.

Chapter 4 illustrates a decentralised high-level control and energy management of interconnected standalone AC microgrids using back-to-back converters. Each microgrid interconnected to the common AC bus manages its energy in a decentralised way. The proposed global droop control enables power to be exchanged from one microgrid to another following some frequency deviation. The detailed performance of the system is assessed with PV-based RES and load profiles, and this chapter provides simulation results for both long- and short-term effects. The long and short real-time simulation provides the performance evaluation conducted for the proposed global droop controller to satisfy the control priorities and design requirements over three operating scenarios: i) independent operation of multiple microgrids, ii) multiple microgrids interconnected with the global droop control, and iii) interconnected multiple microgrids operating with global droop control and global load.

Chapter 5 investigates the centralised optimal controller performance for energy management in multiple interconnected standalone AC microgrids using the Fminsearch optimisation toolbox in MATLAB.

Chapter 6 summarises the research outcomes and conclusion and further provides recommendations for future work.

CHAPTER 2: LITERATURE REVIEW

2.1 Introduction

This chapter reviews the literature to provide detailed insight into microgrids and their structures, followed by the different structures for interconnected microgrids and their possible power flow management topologies. It examines the leading research works in the literature concerning the control and energy management of interconnected microgrids using back-to-back converters, including optimal power-flow management strategies for interconnected microgrids. It reviews the control strategies and droop concept applied to grid-connected and standalone interconnected microgrids for inverter-based and hybrid systems. However, this chapter further highlights in detail the main limitations to the development of both inverter-based and hybrid microgrid systems and aids in improvements in active power sharing of interconnected microgrids with recent related outcomes. This literature concentrates on the interconnecting structure and power flow management strategies, especially in standalone mode.

The need to have improved participation of RES-based DG sources, adequate coordination and controllability at the distribution side of the network to improve supply availability led to the development of interconnected microgrids. Primarily weather dependent RESs, like the PVs and wind turbines, are characterised by strong fluctuations, differentiating them from conventional power plants. Integrating a large amount of RES into the power system is challenging, considering the resource's intermittent nature and distributed location [27], [28], adding to the fact that they are small-scale units widely distributed over a particular geographical area and the shift from the conventional radial (unidirectional) power system to the distributed or dispersed (bidirectional) power system. Hybrid RES and storage devices like the BESS form the building blocks of microgrids that maximise renewable power utilisation and minimise CO_2 emission. A new complex structure of traditional and distributed power systems emerges when two or more microgrids are interconnected. Therefore, energy

management is essential to effectively control the power flow from source to load in new integrated power systems.

2.2 Microgrids

Microgrids provide an interface by which distributed sources from RES can be aggregated into controllable electrical boundaries. The concept of microgrids is to integrate a limited number of DG sources that optimally operate in a simplified network within a geographical boundary/region. According to [29]–[31], microgrids are considered localised clusters of heterogeneous DGs and loads placed in low voltage (LV) or /and medium voltage (MV) distribution networks, which can be either coupled to the main utility grid or operated autonomously in standalone mode The major components of the microgrids are the hierarchical control approach, a point of common coupling (PCC), and distributed (decentralised) controls, which involve the use of local information and a specific region that allows reliable operation of the system [32]. Microgrids are classified into three categories depending on the voltage or type of power on the common bus [33] of the distribution system that connects from the source to the load. Microgrids are classified into AC and DC microgrids. A combination of both is called hybrid (combined AC-DC) microgrids, usually linked by power electronic interfaces, static switches, circuit breakers, etc. The hybrid microgrids are built to minimise conversion stages, reduce interfacing devices, boost reliability in the network, lower energy costs, and improve the network's overall efficiency [34], [35]. Power electronic converters are used to decouple the AC and DC parts of the hybrid microgrids. They provide improved flexibility that allows the distribution bus to supply both the AC and DC, thereby making customers connect and use electricity according to individual needs [36]–[38].

2.2.1 DC Microgrids

DC microgrids are formed by connecting the DGs and DC loads to the common DC bus. DC microgrids enable direct connection of DC output power types from RES like the PV systems, fuel

cells, and BESS to modern electronic loads. Due to the intermittent nature of DC-based sources from RES, the BESS must be connected to DC microgrids during standalone operation. Batteries and capacitors can be directly connected to the DC bus, but flywheels are connected through a machine and converter to enable complete system controllability. In [33], DC microgrids exhibit higher efficiency. They have a lower conversion process for DC loads than AC loads. They are proposed for electrical power supply applications for isolated systems like electric vehicles, space crafts, data centres, naval ships, submarines, telecom systems or rural areas with sensitive DC loads. Wiring hardware can become a significant constraint as the number of units or the distribution of those units over space or geographical location increases [39]–[41]. Additionally, physical variations between converters and lines can result in the circulating current issue. The control objectives in DC microgrids are as follows [29]:

- There is a critical need for DC voltage regulation to be at the specified level.
- The control needs to share the current (power) according to the ratings of the converters.
- There is also a control need to regulate the flow of current (power) to/from an external stiff DC source, which might be a medium voltage DC system, another DC microgrid, or a DC-AC power converter connected to the AC system.

2.2.2 AC Microgrids

AC microgrids are formed by connecting the DGs and loads based on the common AC bus. Energy generated from the DGs is controlled per the load requirement to maintain good power quality and reliability. Power electronics interfaces are essential in realising AC microgrids because most DGs from RES directly produce DC or variable frequency/voltage AC output power that is incompatible with the AC systems. DGs that produce direct AC output power include wind, hydro, biogas, and wave turbines. These DGs typically need AC-DC-AC power converters to ensure stable coupling with the AC distribution networks. Also, DC-AC inverters can be used to connect the DGs with DC output to the system's AC bus [42], [43]. AC microgrids are paramount to this research due to their simple

structure and cost-effectiveness. AC microgrids can be connected easily to the existing utility grid without special conversion requirements and their control approaches, and AC loads are connected directly to the common AC bus. In contrast, DC loads can only be connected to AC microgrids using AC-DC power electronic converters. The control objectives of the power converters in inverter-based AC microgrids are as follows:

- The voltages and frequencies of the power converters need to be controlled and maintained within a specified value.
- The active and reactive powers must be shared in proportion to the rating of their loads.
- Ancillary services are provided to the main utility grid.

Since the advent of microgrids, AC microgrids have been the most researched topic, with the most literature on control and operation because their distribution system consists of a single phase or three phases with or without neutral and has the most compatible modes of electrical and electronic devices [44]–[47]. Table 2.1 briefly summarises the main advantages and disadvantages of each type of microgrid, viz: DC and AC microgrids [48].

Table 2.1: Summarised Advantages and Disadvantages of AC and DC Microgrids

Type of Microgrid	**Advantages**	**Disadvantages**
AC Microgrid	• Versatility as they can integrate easily with the utility grid or in standalone mode. • Easily compatible with existing power system appliances, equipment, and AC loads.	• It has a lower efficiency of conversion. • Require cost-prohibitive converters like the DC-AC converters.

	• There is no need to use inverters for AC loads. • Cost efficiency in power protection systems due to mature technology. • There's increased load availability for AC loads.	• Control complications with frequency, voltage regulation and unbalanced compensation. • Equipment that demands a sufficient power supply for high-performance needs can suffer from lower power supply dependability.
DC Microgrid	• They are the best option for powering high-performance electrical machinery due to their higher conversion efficiency. • Ease of control without complexities from frequency control, harmonics and reactive power control.	• Immature power protection systems can be dangerous, especially in locations with sensitive loads. • The greater initial cost of investment can hamper implementation. • DC microgrids are less known in the electrical market.

	• It has higher supply reliability, even in far-off places. • Systems with lower costs for energy conversion can add additional cost benefits. • There is no reactive current, so there is high transmission efficiency. • The cabling is relatively tiny due to high voltage at low amperages.	• There's reduced compatibility with AC loads proportional to the quantity of AC-based loads. • Voltage drop problems are more likely to occur mainly in bigger systems with no reactive power sources because reactive power is needed to maintain the voltage. • There are more complexities and cost implications in attempting to convert an existing AC system to DC.

2.3 Operation Modes of Microgrids

Microgrids generally operate in two modes, namely, grid-connected and standalone modes. The grid-connected mode operates in close coordination with the utility grid, while the standalone mode operates autonomously with self-regulation of voltage and frequency [49], [50].

2.3.1 Grid-Connected Microgrids

A typical grid-connected microgrid consisting of PV panels, a battery, an auxiliary power supply in the form of a gas turbine, point of common coupling (PCC) and the utility grid is shown in Figure 2.1(a). Each connecting DG source is interfaced to the common AC bus using a voltage source converter (VSC). The microgrid operates to exchange power with the utility grid via the PCC. All DC/AC inverters connected to the DG and BESS operate in the current controlled mode to share the load demand. The real and reactive powers of the inverters are regulated at the desired reference values [49]–[51]. The overall combination can help to reduce costs and improve the reliability of the renewable energy supply. Any surplus power from the RES is injected into the utility grid. During a shortage of power from RES, power is imported from the grid to meet the load demand. The utility grid also dictates the voltage and frequency of the microgrid. The microgrid purchases electricity from or supplies power to the grid during transients with little volatility in frequency thanks to the grid's rigid and reliable frequency regulation [51], [52]. However, the microgrid's main responsibility in grid-connected mode is to ensure accurate power sharing among the microgrid's utility grid and DG units. Intermittent power production due to changes in solar radiation and wind speed over time is a serious issue since it can lead to voltage fluctuations in solar and wind energy sources. The type and magnitude of the load, the strength and size of the connected electrical grid, and the effect of the disturbance are all essential factors [11], [53]–[55].

2.3.2 Standalone Microgrids

A typical standalone microgrid consisting of PV panels, a battery, and an auxiliary power supply in the form of a gas turbine is shown in Figure 2.1(b). A VSC interfaces each connecting DG source to the common AC bus. However, power electronic interfaces can achieve a common DC bus depending on the objectives and control structure. The DG and BESS maintain the bus voltage and frequency. The BESS is used as the grid-former in standalone mode to regulate the bus voltage and frequency, as it is a more stable and reliable power source than the intermittent DG sources connected to the same bus [50], [51]. When there is a power deficit, especially from the RES, a standalone system must rely on its internal backup system from the battery to supply the necessary power to the connected loads. If the DG and BESS units cannot meet the load demand in the standalone microgrid, power can be supplemented by the auxiliary unit to avoid frequency deterioration. If the islanded microgrid is an AC microgrid, voltage and frequency management, supply and demand balance, and power quality requirements should all be met by a standalone microgrid. Standalone microgrids are an excellent option for remote locations without access to the utility grid. A storage system is essential to ensure continuous power supply to loads. This thesis proposes a new structure of interconnected standalone AC microgrids to maximise RES power utilisation and minimise auxiliary power usage. The proposed system structure is subjected to various operating system performance tests to determine its efficiency.

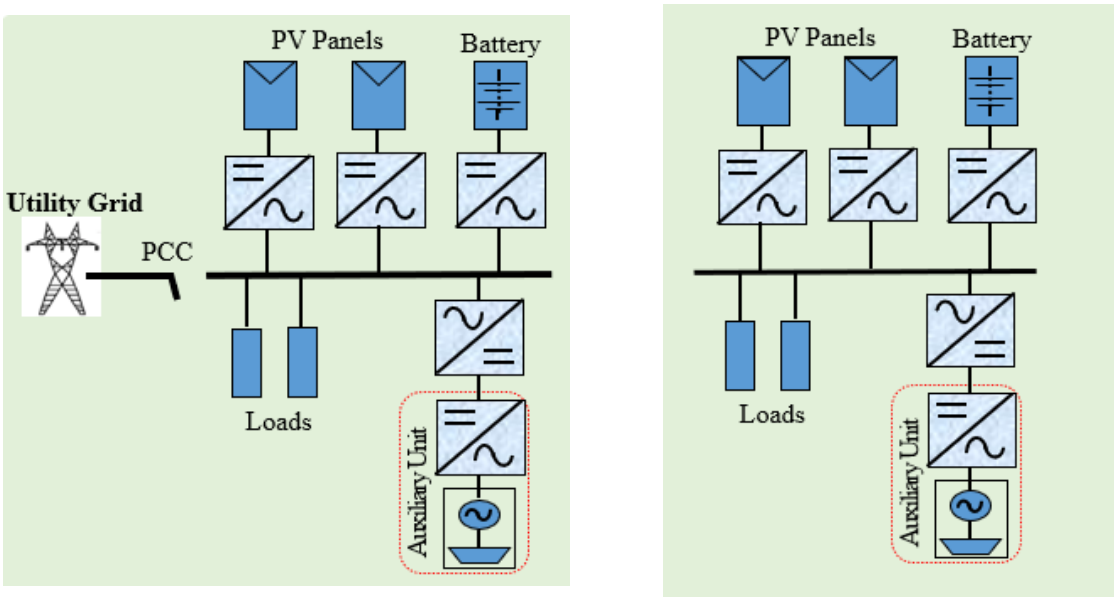

(a) **(b)**

Figure 2.1: (a) Grid-connected Microgrids, (b) Standalone Microgrid

2.4 Control Operation of Converter-based DGs

Power electronic interfaces in VSC are fundamental building blocks of microgrids and interconnected microgrids, and they integrate newly developed DGs and microgrids. Depending on the goals and the control structure, a VSC can be classified as either a voltage-controlled VSC or a current-controlled VSC. The voltage-controlled VSC is structured to have an input DC-link voltage from an independent source like a battery, producing a controlled AC output power at the load side. They can be connected in single-phase, three-phase and multiphase output voltage phases. Single-phase VSCs provide single-phase voltages and are used in low-power applications; three-phase VSCs provide controllable three-phase voltage source amplitudes, phase and frequency, which are used in medium to high-power applications [55], [56]. Current-controlled VSCs regulate active and reactive power delivery. In contrast, voltage-controlled VSCs can regulate the voltage and frequency of the AC bus. Using RESs in MPPT mode and batteries in charging mode as a current-controlled VSC is preferable. However, RES and BESS can participate in frequency and voltage regulation. However, BESS is superior to a

voltage-controlled VSC due to its bidirectional capability. The current-controlled VSC inputs a constant DC, and the voltage changes with the load [55]–[57].

2.4.1 Switching Operation of a DC/AC Inverter

In a PV-based power converter consisting of a DC/DC converter and DC/AC inverter, the DC/DC converter is designed to step up the voltage of the PV system to a higher constant value, and it has the capability of increasing the overall efficiency of the inverter system. In addition, it regulates and boosts the system's DC output voltage. The DC/AC inverter's switching operation per phase is shown in Figure 2.2, as detailed in [58]–[60].

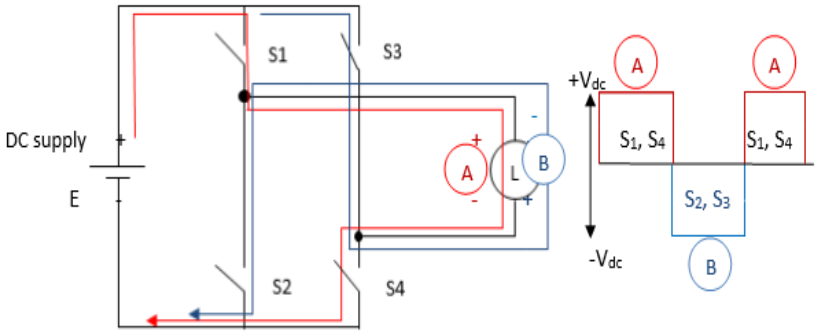

Figure 2.2: Switching Operation per phase of a DC/AC Inverter

The DC/AC inverter in Figure 2.2 consists of four switches: S_1, S_2, S_3 and S_4. When switches S_1, S_4 and S_2, S_3 are alternately turned ON and OFF respectively, current flows through the circuit and the voltage across the load "L" changes direction between A ($+V_{dc}$) and B ($-V_{dc}$), thereby causing the inverter output voltage to change direction periodically producing an AC output waveform with three voltage levels viz; $+V_{dc}$. 0, and $-V_{dc}$. The output waveform usually has two major types: sine wave and modified sine wave. Nevertheless, specific domestic electrical loads cannot operate using modified sine waves because of their significant harmonic frequencies. To function appropriately, such domestic loads must require pure sine wave inverters with sinusoidal AC output identical to AC grid voltage [59]–[61]. The time taken for the output signal to complete one cycle is known as the period of output voltage, while the inverse of the period is called the frequency. Figure 2.3 shows the voltage regulation

method [61], [62] If the switches S_1, S_4, S2, and S_3 are not constantly turned ON in the corresponding half cycle, the average amplitude of the AC inverter output voltage would be lower than the amplitude of the DC power voltage. Therefore, the shorter the turn ON time, the lower the average amplitude.

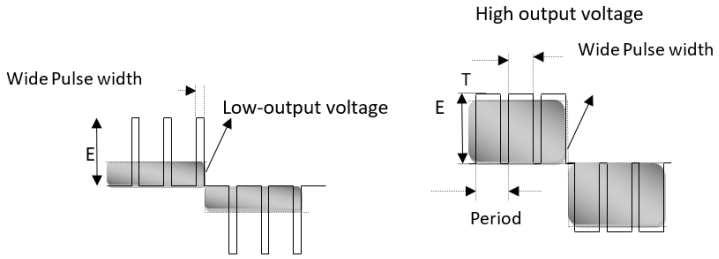

Figure 2.3: Method of Voltage Regulation

The higher output voltage is achieved with broader pulse widths, while the lower output voltage is achieved with narrower pulse widths. However, the voltage could be controlled by controlling the pulse width, frequency and amplitude of the inverter. The method by which this process can be completed is called Pulse Width Modulation (PWM). The PWM technique is widely used to control switching devices to achieve the desired output. As long as the switching frequency is high enough, the pulses are amplified to control the state of the switches to generate the inverter output voltage. The modulation index (ratio between the modulation amplitude and carrier amplitude) can control the inverter output voltage. Thus, the inverter output voltage can be controlled by the modulating signal passed through a low pass filter to reduce the Total Harmonic Distortion (THD), producing the final pure sine wave output.

2.4.2 Control of Three-Phase Inverter

Figure 2.4 shows the three-phase full bridge inverter with six insulated-gate bipolar transistors (IGBTs), an inductor-capacitor-inductor LCL filter connected to a constant DC input and a DC link capacitor, which can be controlled in standalone and grid-connected modes. During standalone mode, the inverter is controlled to operate in voltage control mode. In this case, the controller is required to actively regulate the output voltage of the VSI, and the outer voltage control loop generates the current

reference. In grid-connected mode, the inverter is controlled to operate in power control mode. The grid determines the voltage and frequency. Here, the output power flow is controlled by current regulation (controlling the real and reactive current). The controller calculates the current reference of the inverter produced by the outer power control loops using the measured voltage and desired power levels [62], [63].

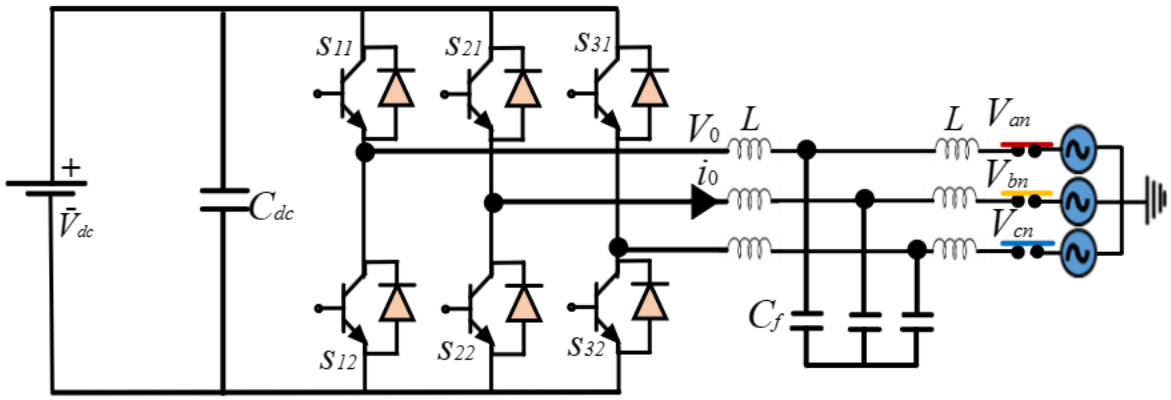

Figure 2.4: Three-Phase Full Bridge Inverter

2.5 Control Methods and Operation of Microgrid

The main control objective of a microgrid control scheme is to adequately maintain good regulation of voltage, frequency and energy management among microgrids. It should provide a solution well before all possible control operations that may arise during operation and accommodate different RES into a desired structure that can operate in plug-and-play mode [63], [64]. However, microgrid sources are controlled to achieve the following purposes:

- Enable new DG sources to synchronise without modification of the existing system.
- The system under control can operate independently.
- To help microgrids to connect and disconnect from the grid seamlessly.
- Active and reactive power can be controlled independently.
- Voltage sag and system imbalances can be corrected

- To enable microgrids to meet the grid load dynamic requirements.

The two main control strategies used to achieve the above control objectives in microgrids are master-slave mode (Communication link) control, peer-to-peer mode (without Communication link) control and the combined mode [46], [47], [64], [65].

2.5.1 Master-Slave Control Mode

This is also known as the communication link control or the wired control strategy. It uses some form of direct interconnection among the other units contributing to the microgrid [64], [65]. Here, one of the DG unit controllers in the microgrid serves as the master unit, controlling the load bus voltage. In contrast, the other DG controllers serve as slave units by following voltage reference fixed by the master unit. The later controllers obey the regulation/instruction of the master controller based on communication connection. It uses high-speed communication links between inverters to achieve accurate power sharing. Different DG units with variable outputs, such as PV or stable, controllable DG units, such as fuel cells, batteries and microturbines, can be used as master units. The master-slave control mode is widely used in the literature [58], [66] and has several advantages. Only a simple control algorithm is required at each component level. Unlike other peer-to-peer control modes, master-slave control does not depend on the impedances of the lines interconnecting the microgrid systems in the multi-microgrid (MMG) system. The main disadvantage is that it depends on high-speed communication links, which is costly. Still, a reliable and high-speed communication and cabling system will improve efficiency and reliability. Also, if the master DG control unit fails, there is a chance of collapse of the whole microgrid. Thus, it does not provide seamless mode transfer from grid-connected mode to island [66], [67]. An integrated microgrid laboratory system is presented in [66] as a cluster of multiple microgrids consisting of various DGs and energy storage systems, with backup diesel generators that work in synergy with flywheel energy storage to provide an uninterrupted power supply. The master-slave control strategy is adopted for the microgrids to operate using switches

as the interconnecting medium between islanded, grid and interconnected modes of operation. Disconnection can occur from the utility grid should any fault arise.

2.5.2 Peer-to-Peer Control Mode

This control mode is commonly referred to as no-communication link control or the wireless control method that solely relies on the droop control strategy. The peer-to-peer control mode is based on plug-and-play and decentralised control that uses feedback from locally measured variables for control. The main advantage is that it is very simple and easy to implement using local voltage and current measurements of the DG sources. It does not require a high-speed communication link between the different sources. Its operation increases redundancy and simplicity of expansion. It is highly reliable and flexible and enables plug-and-play operation [63], [64], [67], [68]. The droop control strategy uses a peer-to-peer control scheme for its operation in that if the load changes, then that load change will be distributed among the DG units according to their droop gains [68]–[70]. Hence, this allows for the autonomous control of the DG units, especially During standalone mode; the droop control will enable the DG units to share the real power proportionally to regulate the microgrid system frequency f to its nominal value f_0. Also, droop control will facilitate proportional sharing of reactive power demand by the DG units in the islanded microgrid to regulate the load voltage V to its nominal value V_0 [50].

2.5.3 Droop Control Concept

The concept of droop control originated from synchronous generators in power systems, where the synchronous generator presents a rotor inertia which limits the frequency variation. The inverter mimics the function of a synchronous generator, whereby grid–connected synchronous generators drop in frequency and voltage magnitude due to an increase in active and reactive power [64], [65], [70], [71]. Droop control is employed in the parallel operation of inverters to achieve accurate active and reactive power sharing and maintain good microgrid regulation of output voltage and frequency. However, this control strategy requires a low communication link between each unit and a supervisory

Controller for electric power monitoring and management concerns. It enables good sharing of linear and non-linear loads [72]–[74].

Conventional Droop Control

Whenever an inverter is connected to the grid network, the inverter control system must establish the following inherent conditions to reach a stable operation. DG unit can be modelled as an equivalent voltage source connected to a common bus through a coupling impedance, as shown in Figure 2.5 [64], [65], [74], [75].

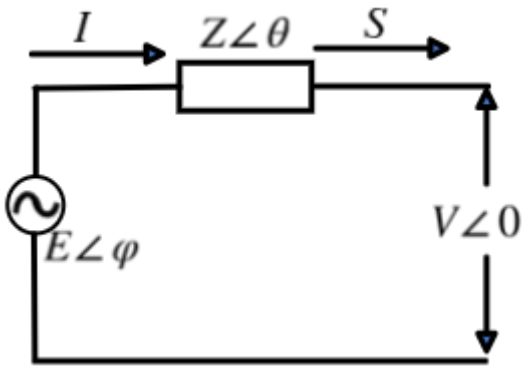

Figure 2.5: Equivalent Circuit per-phase model of a VSI Connected to a common AC bus

Complex power S injected by the inverter to the common bus is given as[53], [54]:

$$S = P + jQ = V \times I^{*} \tag{2.1}$$

where I^{*} is the complex conjugate of the inverter current and is given by:

$$I^{*} = \left[\frac{E\cos\varphi + jE\sin\varphi - V}{X} \right] \tag{2.2}$$

Substituting (2.2) in (2.1) gives

$$S = V \times I^{*} = V\left[\frac{E\cos\varphi + jE\sin\varphi - V}{X} \right] \tag{2.3}$$

where the active and reactive power is defined as

$$P = \frac{EV}{Z}\cos(\theta - \varphi) - \frac{V^2}{Z}\cos\theta$$
$$Q = \frac{EV}{Z}\sin(\theta - \varphi) - \frac{V^2}{Z}\sin\theta \qquad (2.4)$$

where E is the output voltage amplitude of the inverter measured at the filtered bus, V is the common AC bus voltage at the point of common coupling, φ is the power angle. Z and θ are the magnitude and phase angle of the overall system impedance, which consist of the resistance and inductive reactance, R and jwL.

Therefore, for a purely inductive output impedance of the systems, which is often associated with high and medium power lines or low voltage lines with large output inductance, it can be assumed that the resistance is negligible $Z = X$ and $\theta = 90^0$.

Hence, the active and reactive powers drawn to the bus, as shown in equations (2.4), can be simplified as shown in equation (2.5) [60], [75], [76].

$$P = \frac{EV\sin\varphi}{X}$$
$$Q = \frac{EV\cos\varphi - V^2}{X} \qquad (2.5)$$

Based on equation (2.5), assuming that If the power angle is very small, such as $\sin\varphi \approx \varphi$ and $\cos\varphi \approx 1$, then active power P injected to the common AC bus predominantly depends on the power angle φ, and also the reactive power Q mainly depends on the output voltage amplitude difference $(E - V)$. Also, changing frequency causes a dynamic change of the phase error φ. Therefore, active power P is controlled by the power angle, while the voltage amplitude controls reactive power Q. Thus, wireless control by the conventional droop control method of paralleled inverters is developed from the decoupled control of active and reactive power through the output voltage amplitude E and frequency ω droops. Equations (2.6) and (2.7) illustrate the frequency and voltage droop control equations for parallel connected inverters.

$$\omega = \omega^* - mP_m \tag{2.6}$$

$$E = E^* - nQ_m \tag{2.7}$$

where ω^* is the inverter output angular frequency at no load, E^* is the voltage amplitude at no load, m is the frequency droop coefficient, n is the droop coefficient of the voltage amplitude, P_m is the measured active output power, and Q_m is the measured reactive output power. Figure 2.6 represents the active power (P)-frequency (ω) and reactive power (Q)-voltage (E) characteristics of the droop control equation.

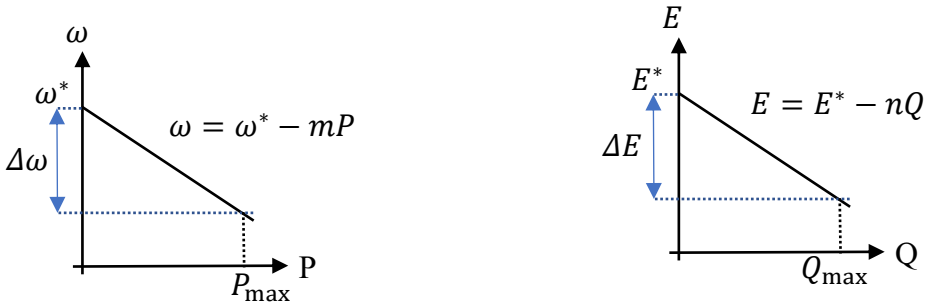

a) $P-\omega$ Droop Control b) $Q-E$ Droop Control

Figure 2.6: ($P-\omega$) and ($Q-E$) Droop Control Characteristics

From the droop control equation, only the droop coefficients m and n can be adjusted to effect change in the power-sharing formula and dynamic response of the system. These droop coefficients can be designed based on the available nominal real power P_{nom} and reactive power Q_{nom} and with the maximum allowable voltage and frequency deviation, $\Delta\omega_{max}$ and ΔE_{max} respectively [69], [77], [78]. The droop coefficients can be obtained as follows:

$$m = \frac{\Delta\omega_{max}}{P_{nom}} \tag{2.8}$$

$$n = \frac{\Delta E_{max}}{Q_{nom}} \tag{2.9}$$

However, the equation (2.6) and (2.7) can be rewritten as follows for the grid-connected mode:

$$\omega = \omega^* - m\left(P_m - P^*\right) \tag{2.10}$$

$$E = E^* - n\left(Q_m - Q*\right) \tag{2.11}$$

where P_m and Q_m are measured active and reactive power, P^* and Q^* are the reference (setpoints) of the active and reactive power in $P \sim \omega$ and $Q \sim E$ droop control, respectively. When two parallel inverters are actively involved in active power sharing using a droop controller, the power-sharing accuracy also depends on the impedance ratio of the line.

Doop control strategies are used in different forms based on the type of output impedance. The active power–frequency and reactive power–voltage droops are used when the output impedance is inductive [77], [79]; the reactive power-frequency, $Q \sim \omega$, and active power-voltage, $P \sim V$, droops are employed when the output impedance is resistive [69], [78].

2.5.4 Combined Control Mode

The combined control mode of operation, which is relatively new, allows for the implementation of peer-to-peer and master-slave controls for various DG units with different characteristics. In grid-connected and islanded microgrids, various control modalities, such as master-slave and peer-to-peer controls, can be simultaneously used due to various DG units, including PV, fuel cells, microturbines, etc [50]. Because DG units come in various forms and functionalities, the combined mode allows for utilising the benefits of both master-slave and peer-to-peer systems.

2.5.5 Hierarchical Control

This control approach is proposed to standardise the performance and functions of smart grids, categorising the control structure into three different control layers, namely the primary, secondary and tertiary controls, as shown in Figure 2.7. The primary control is the first level of control hierarchy that consists of the inner control loop and droop control. This inner control action is performed at every DG inside the microgrid based on local measurements to ensure that the system voltage and frequency

follow their setpoints, avoid the flow of circulating currents and islanding detection, which offers the ability to detect the operational mode of the microgrid viz a viz grid-connected and standalone mode [79]–[81]. Secondary control is the second-level control decoupled from primary control with a slower timeframe in the hierarchy that slows control loops and low-bandwidth communication systems. The main control objective of the secondary control loop is to restore the microgrid voltage and frequency levels to the nominal values by determining the setpoint of the primary control and shifting or adjusting the droop characteristics of connected DGs for power quality enhancement and allowing synchronisation between the microgrid system and the main electrical network [29], [79], [80]. Hence, the primary control loop reaches its steady state before the secondary controller updates the setpoints. The tertiary control is the third level in the control hierarchy that ensures optimal operation in both modes by regulating the power flow exchange with the external grid and other microgrids. It also includes advanced control functions at higher management levels that involve economic improvement and efficiency. The tertiary control hierarchy uses the information obtained regarding the DGs' state, market signals, and other system requirements to set the long-term setpoints of the lower levels. However, the bandwidth of the control level decreases gradually as control action ascends the hierarchy, as illustrated in Figure 2.7. The hierarchical control layers can be implemented side-by-side in both distributed and control structures. Thus, a centralised control structure can be used for primary control. In contrast, the decentralised control structure is employed locally at each microgrid without using upper control levels like digital communication technologies. Hence, the centralised control strategy is employed for the tertiary level, while secondary control is employed at both centralised and distributed control structures.

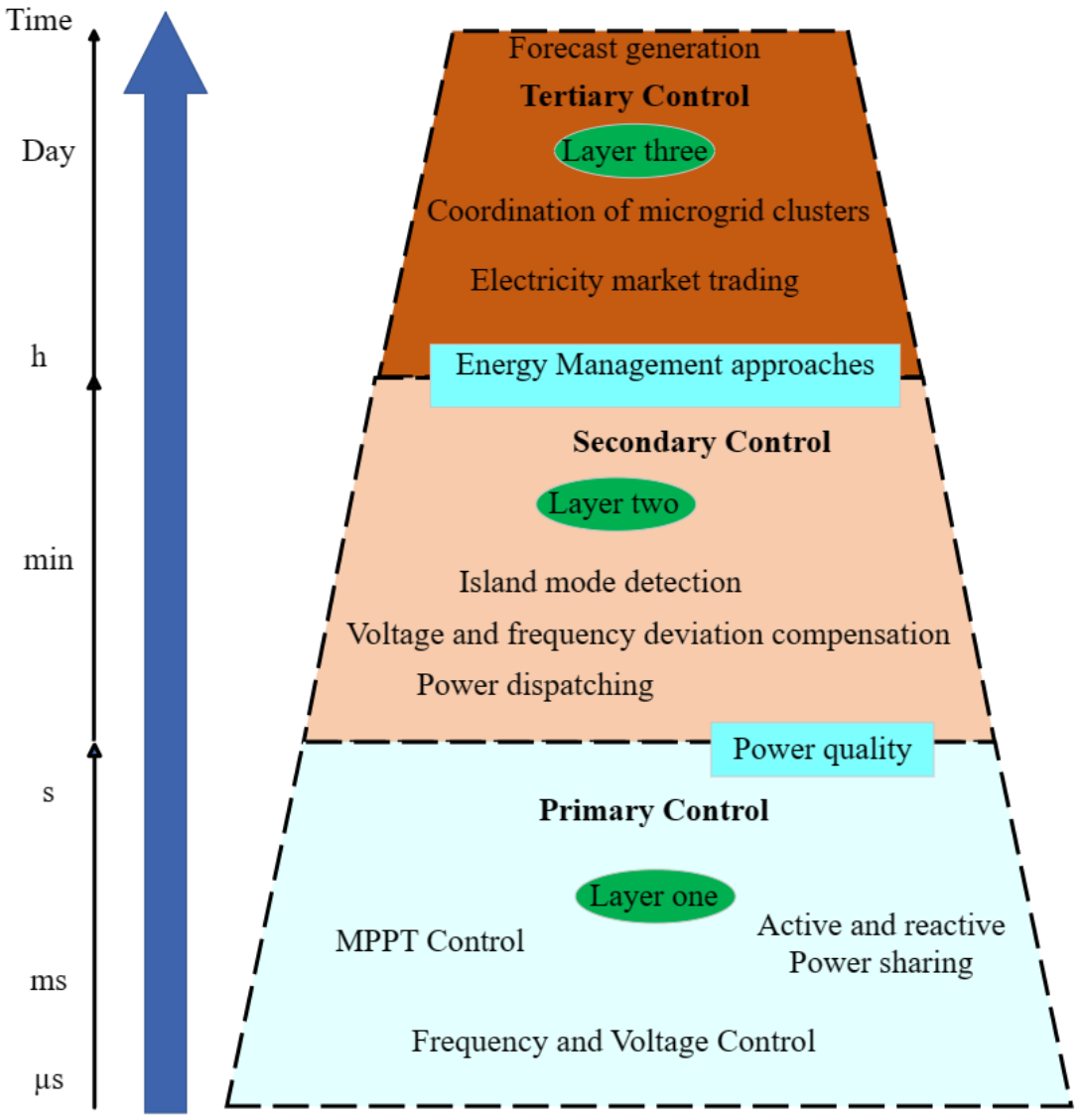

Figure 2.7 Hierarchical Control Structure

2.6 Interconnected Microgrids

Multiple interconnected microgrids consist of two or more individual microgrid networks, which are sometimes geographically located nearby and may or may not be connected to a distribution bus. The control objective is to improve RES power utilisation and effectively share their neighbouring reserve capacities. This allows the interconnected microgrids to accommodate more loads and meet the demand of those loads most economically [82], [83]. Power management and controls for interconnected microgrids ensure maximum power extracted from the distributed generation (DG) source is transferred to the load. Effective energy coordination and transfer of microgrids can help

improve the network's reliability and stability. However, there are numerous benefits to highly efficient RES power utilisation and sharing renewable power among interconnected microgrids. Interconnected microgrids allow energy sharing among microgrids to satisfy their individual power demands using their locally sourced cheaper RES. By so doing, the cost of energy from alternative means like fossil fuel-based sources can be reduced [84]. Compared with the traditional single-operated microgrids, limited power is extracted from microgrid generation sources comprising limited RES participation, even though intermittency in hybrid RES systems is boosted by using an auxiliary unit like the micro-gas turbine and sufficient storage systems like batteries. There are limitations to the amount of RES that can be added to a microgrid to supply load. The role of the auxiliary unit in the microgrid systems is minimised to reduce its greenhouse gas (GHG) effect on the environment. Hence, the study of interconnected microgrids cannot be overemphasised to overcome the above limitations. Substantial literature, e.g.[20], [85]–[89], has been focused on interconnected microgrid system operation, control and management with little or no details on the structure and medium of interconnection between defined interconnected microgrids. Figure 2.8 shows the configuration of a typical grid-connected interconnected Microgrid. The figure comprises multiple standalone AC microgrids interconnected with static switches as the interconnecting medium (IM) and the main grid. Each AC microgrid is connected to another via a common AC tie-line and static switch, and the grid is connected with a static switch and traditional power transformer. Each microgrid operates independently during nominal operation and meets its respective load demands. All the microgrids are expected to exchange energy among each other and also with the main utility grid. In grid-connected mode, the voltage and frequency at the grid switch are dominantly determined by the utility grid; hence, the main role of the microgrid is to accommodate the local load demand and the active/reactive power generated by the respective DGs [29].

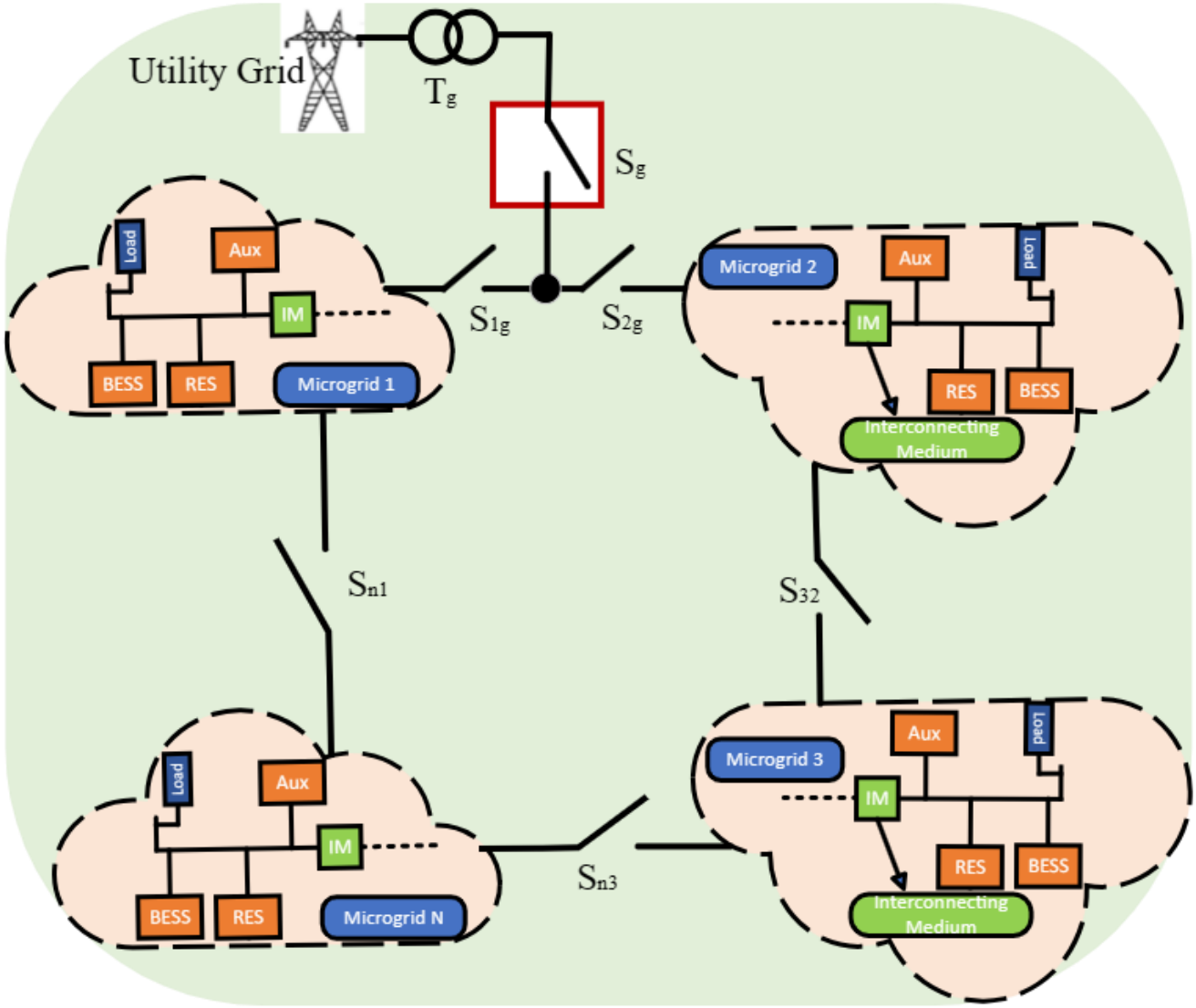

Figure 2.8: Configuration of a typical Grid-Connected Interconnected Microgrid

2.6.1 Structures for Interconnected Microgrids

The integration of RES at the distribution system has transformed the existing power system from a passive network to an active distribution network characterised by assorted control systems and bidirectional power flows. Therefore, this trending concept of interconnected microgrids accommodates more RES and improves power quality, load support, reliability and efficiency by expanding the active distribution networks with microgrids as the building block. Interconnected microgrids provide some flexibility and can allow the benefits of AC and DC microgrids, improve reliability and efficiency, and provide mutual support during contingencies [28], [89]–[92]. Modern

literature [17], [92], [93] has enumerated different ways and interconnecting mediums by which microgrids can be interconnected. Some use tie-lines, conventional circuit breaker/ static switches, power electronics-based switches/converters, back-to-back power converters or power transformers, depending on the prevailing condition. These interconnecting mediums serve unique purposes and can be deployed based on functionality. It is easier to interconnect standalone AC microgrids at the same voltage and frequency than to interconnect at different voltages and frequencies. According to [17], [89], [93], standalone microgrids that operate at the same voltage and frequency can be easily interconnected with static switches or breakers and a good synchronisation algorithm. Operating microgrids at different voltages and frequencies provides more flexibility to connected loads across the network. It also presents some potential demerits that cause them to require power electronic AC/DC/AC converters to be used as the interconnecting mediums to decouple the two frequencies. Using power converters as a medium of interconnection of different AC microgrids with varying voltage amplitudes and frequencies presents more complexities to the system than using breakers or static switches [93][94] in the sense that interconnecting power converters can introduce harmonics and imbalance without an adequate control mechanism. Several studies [13], [15], [28], [85], [95] have suggested different architectures of interconnected microgrids; this thesis reviews all possible structures for interconnected microgrids and classify the different structures of interconnected microgrids in two ways:

1) Design layout: The layout of the design defines the structure or placement of multiple standalone interconnected microgrids from one point of common coupling (PCC) to another. The design layout depends on the number of microgrids to be interconnected and the geographical location.

2) Interconnection medium defines the interface or medium by which two or more microgrids are interconnected. This interface depends on whether the microgrid PCC is an AC, DC or hybrid and the type of flexibility required. Interconnecting mediums can be based on tie-line, breakers or static switches, power electronic converters or traditional power transformers, or a combination of those, as illustrated in Figure 2.9.

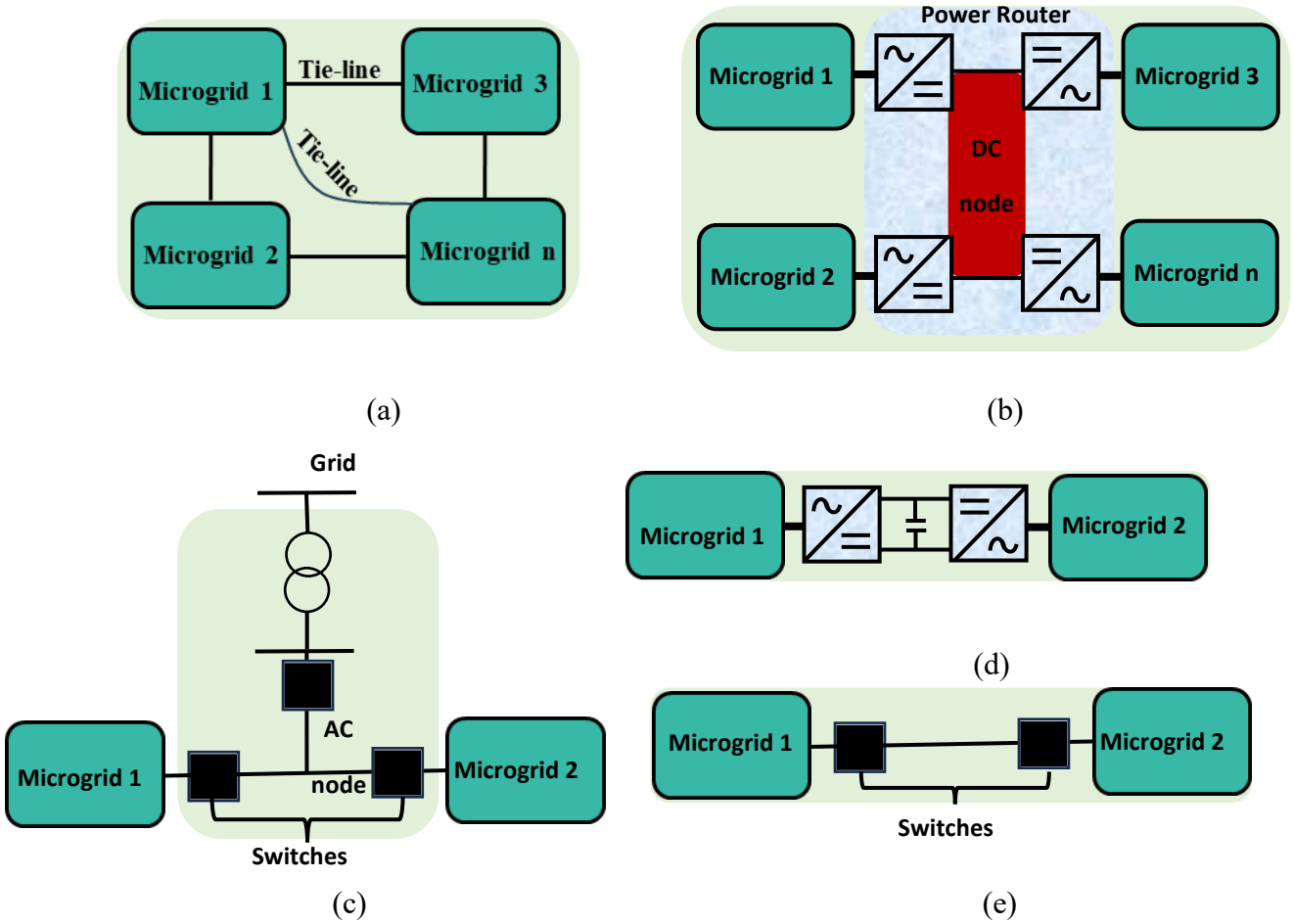

Figure 2.9: Interconnected Microgrids with Different Interconneting Medium (a). Tie-line lines, (b). Double Power Electronic Converters, (c). Static Switches and Power Transformer, (d). Single back-to-back converter, (e). Static switches/Breakers.

The figure shows interconnected microgrids with different interconnecting mediums. Sometimes, it is interesting to have a combination of the structure. So far, this illustration describes all possible interconnecting mediums identified in this thesis. Figure 2.9(a) shows the structure of interconnected microgrids with tie-lines as the interconnection medium representing a common AC link [20], [85].

The layout represented in Figure 2.9(b) shows multiple back-to-converters used to form a power router representing a common DC link [28], [96]. The structure in Figure 2.9(c) shows a combination of breakers/ static switches and power transformers, and the utility grid represents a common AC bus. The combination in Figure 2.9(d) shows two microgrids interconnected with a back-to-back power converter representing a common DC link, as in [92], [93], [97], [98] while in Figure 2.9(e), two microgrids interconnected with two circuit breaker representing a common AC bus [85], [99]. However, the above illustrations are simplified examples of the mediums by which multiple microgrids can be interconnected. In summary, apart from Figure 2.9(a) with four microgrids interconnected with tie-lines only, Figures 2.9(b) with only two microgrids and 2.9(d) are similar with a common DC bus and Figures 2.9(c) with only two microgrids and 2.9(e) are also similar with a common AC bus. More complex interconnected structures can be formed from various simplified system combinations.

2.6.2 Energy Management Techniques of Interconnected Microgrids

An energy management system (EMS) of interconnected microgrids maintains the power quality and generally optimises the operation of the network. This is essential for the seamless operation of a network of microgrids in both grid-connected and standalone modes [94], [100]. Therefore, effective energy management ensures that energy is moved efficiently and securely across all interconnected networks. This ensures that the global performance of the interconnected networks is improved to maximise RES power utilisation and continuous availability of electric power to the connected load [17], [80]. In this way, three main categories of energy management techniques considered in this literature include centralised, decentralised and distributed approaches.

2.6.2.1 Centralised Control

The centralised control approach relies on operating a single central controller to manage the microgrids interconnected to the global network. Hence, all the interconnected microgrid dispatchable units and controllable loads are managed by a central controller, which is also responsible for the

interaction among microgrid operating modes, stability control and energy market bidding functions [101], [102]. The centralised controller uses high-performance computation and communication infrastructure to obtain global information about all the network microgrids and makes decisions by executing an optimisation algorithm [17], [85]. In the centralised control architecture of interconnected microgrids shown in Figure 2.10, the centralised controller executes the management operation algorithm and the control command is communicated to each microgrid supervisory controller. This method employs higher communication and computation requirements as the penetration of renewable generation increases, and coordination can be satisfied. The centralised control approach requires point-to-point communication. Additionally, the reliability of the system is compromised in the event of a failure because the entire system depends on the centralised controller functioning well [102], [103]. Numerous works of literature have employed centralised control to optimise operations, including [95], which proposed a centralised controller to optimise the operation of interconnected microgrids. A centralised optimal EMS operation of interconnected microgrids is proposed in [104], [105], and the optimal power exchange is determined by an imperialist competitive algorithm considering the reliability indices of each microgrid. The optimal results are compared when the microgrids are interconnected and standalone. In [105], the authors presented an energy management (EM) that minimises the operating cost of all microgrids in multi-microgrid with sequentially coordinated operations. The authors carried out the economic perspective of optimal power scheduling using a central controller, and results showed individual microgrids avoided cost by adjusting their local generations. However, the proposed model does not represent detailed microgrid component operation. A model predictive control (MPC) based on global centralised control of an interconnected network of renewable energy-based microgrids is presented in[105], aimed to maximise the overall benefits from a cluster/network of interconnected microgrids. Simulation results demonstrate significant advantages of the cooperation among clusters of microgrids when compared to each single microgrid operation. The reliability evaluation framework for multi-microgrid distribution systems

based on a sequential Monte Carlo Simulation (MCS) approach is proposed in [106]. Suitable centralised and hierarchical control schemes are investigated for multi-microgrid operations during outages, and the proposed MPC approach minimises total load curtailment in the system. However, in these works, multiple microgrids are randomly interconnected, focusing on overall energy management in individual and interconnected operations. The structures of interconnecting medium are not of interest. The common characteristics of the interconnecting medium in the investigated centralised EMS of interconnected microgrids in the literature are tie-lines and circuit breakers that interconnect the microgrid network.

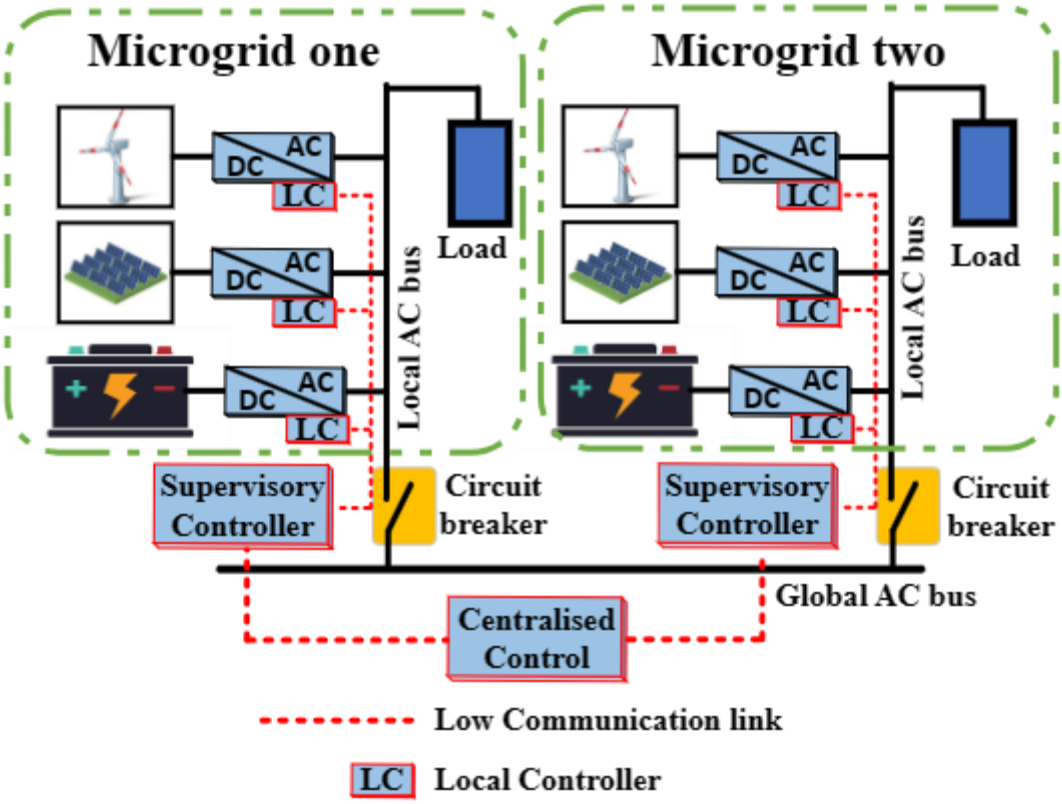

Figure 2.10: Centralised Control Architecture of Interconnected Microgrid

2.6.2.2 Decentralised Control

A decentralised control of interconnected microgrids ensures that each microgrid in the network operates as a fully autonomous entity with local controllers based on local information. In the case of Figure 2.11, which illustrates a decentralised control architecture of interconnected microgrids, there

is no communication between the different microgrid supervisory controllers. Each microgrid seeks to utilise its resources to optimise its operation independently [84]. The interconnected microgrid network can still operate when a local controller fails. The local controllers of MGs work independently without any information exchange with other entities, which enhances the MGs' autonomy and improves immunity against external disturbances and attacks. Individual microgrids cannot exchange information directly with one another, so achieving global optimum control becomes difficult [103]. They possess high computation efficiency and strong plug-and-play functionality. A decentralised EMS for autonomous poly-generation microgrid topology, which allows controlling each microgrid unit independently, is presented in [107]. The system design was based on a multi-agent system, and Fuzzy Cognitive Maps was employed for its implementation. The results obtained are compared with a centralised EMS case study, and the technical performance of the decentralised solution is as good as the centralised one. A decentralised power dispatch model for the coordinated operation of multiple microgrids and distribution systems is presented in [108]. The model considered the RES-based DG output uncertainties, distribution network operators, and microgrids as different entities with different objectives and formulated a stochastic bi-level problem. A scenario reduction technique is used to improve the trade-off between the computational load and the correctness of the solution. Case studies illustrating a distribution system with various MGs show the success of the suggested methodology. A decentralised energy management system is proposed in [109]to coordinate the operation of networked microgrids in a distribution system. A decentralised bi-level algorithm is proposed to coordinate the operation, including the first level to conduct negotiations among all entities and the second to update the non-converging penalties. The problem is formulated as a two-stage stochastic program, and the results of the case studies demonstrate the method's effectiveness in grid-connected and standalone modes. A communication-less multi-frequency control in a standalone multi-microgrid system using a back-to-back converter is proposed in [110], operated based on a droop control strategy.

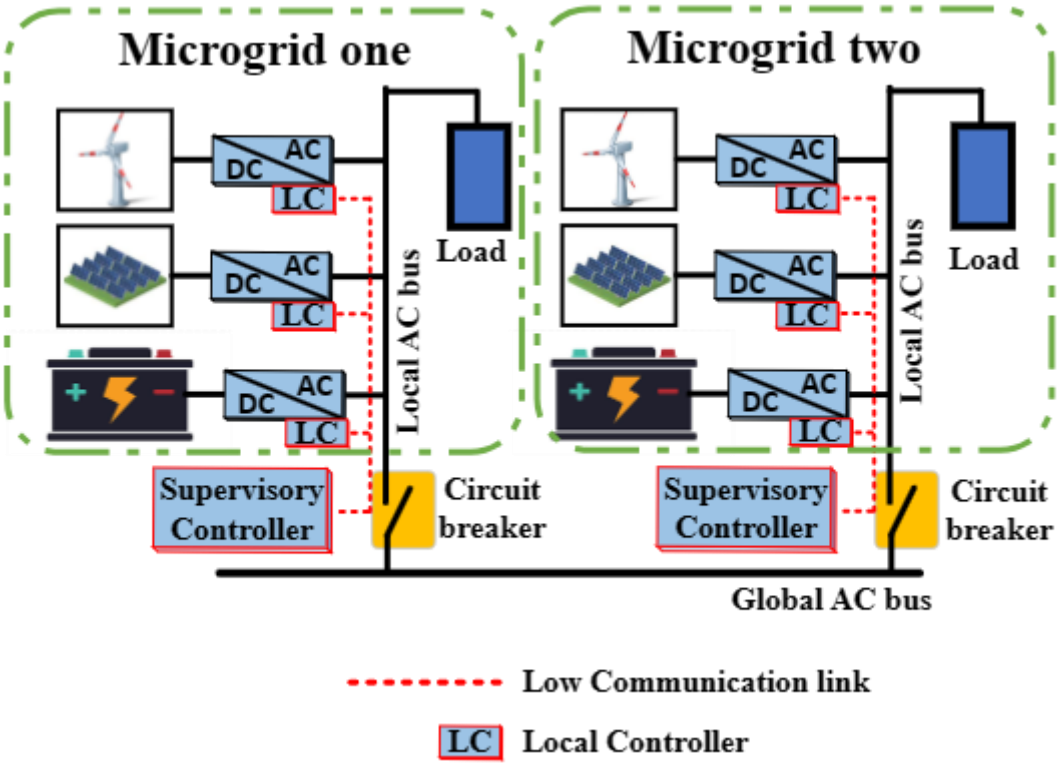

Figure 2.11: Decentralised Control Architecture of Interconnected Microgrid

2.6.2.3 Distributed Control

Distributed control is the intermediary of centralised and decentralised control, which requires less information exchange and lower computational complexity. Distributed control methods are proposed to overcome the disadvantages of centralised and decentralised energy management approaches. Figure 2.12 illustrates a distributed control architecture of an interconnected microgrid, which shows the communication between different microgrid supervisory controllers that cooperate to achieve a common goal [104]. The distributed energy management approach requires minimal information exchange among interconnected microgrids to coordinate power exchanges and achieve optimal energy distribution through coordinated operation [84]. Adding a DG in a local microgrid requires updating the local parameters in the optimisation problem of that microgrid, as opposed to updating a global centralised model, which may be problematic as DG penetration increases. A drawback of the distributed approach is the dependency on a communication network to coordinate the interactions

among the microgrids and the required infrastructure to enable power transactions [111]. The multi-agent distributed management approach is applied for energy scheduling optimisation involving different participating microgrids. The basic principle of distributed control is information exchange through neighbouring communications in a distributed manner. However, distributed control can be exploited to generate a common signal compared with a reference and passed through a local PI controller, producing an appropriate control signal to be sent to the primary level to remove associated steady-state errors [29]. A new distributed economic model predictive control scheme for the coordinated stochastic energy management of multi-microgrids is proposed in [112]. The system optimally coordinates the operation of individual microgrids and economically maintains the supply and demand balance. The results show that the proposed scheme successfully reduces the system's operating cost, and the energy exchange between the distributed network operator and the main grid is within a predefined trajectory. In [113] a distributed control regulates power flow among multiple islanded microgrids and minimises dynamic interactions. A distributed robust control problem based on partially nested information of power flows in a team of cooperating microgrids is presented [114] to maximise the maximum divergence from an agreed power exchange among microgrids. A distributed coordination of multiple networked microgrids aimed at overall operating cost reduction by enabling energy trading among microgrids and the utility grid is presented in [115]. The alternating direction method of multipliers (ADMM) algorithm is proposed for the distributed optimisation problem to minimise the overall operating cost and optimise other network operational objectives. A bilevel model to simulate the market behaviour of networked microgrids in the distribution market is proposed in[116]. In the lower-level model, each microgrid determines its schedule for the day ahead and bids into the distribution market. At the upper level, the distribution system operator (DSO) clears the distribution market through distribution locational marginal price. The optimal day-ahead coordination scheme among networked microgrids is obtained iteratively. Results show the effectiveness of the proposed method. However, distributed energy management techniques in

interconnected microgrids are more popular when compared with the centralised approach. A summary of the benefits and drawbacks of each interconnected microgrid EMS technique in [96], [104] is presented in Table 2.2.

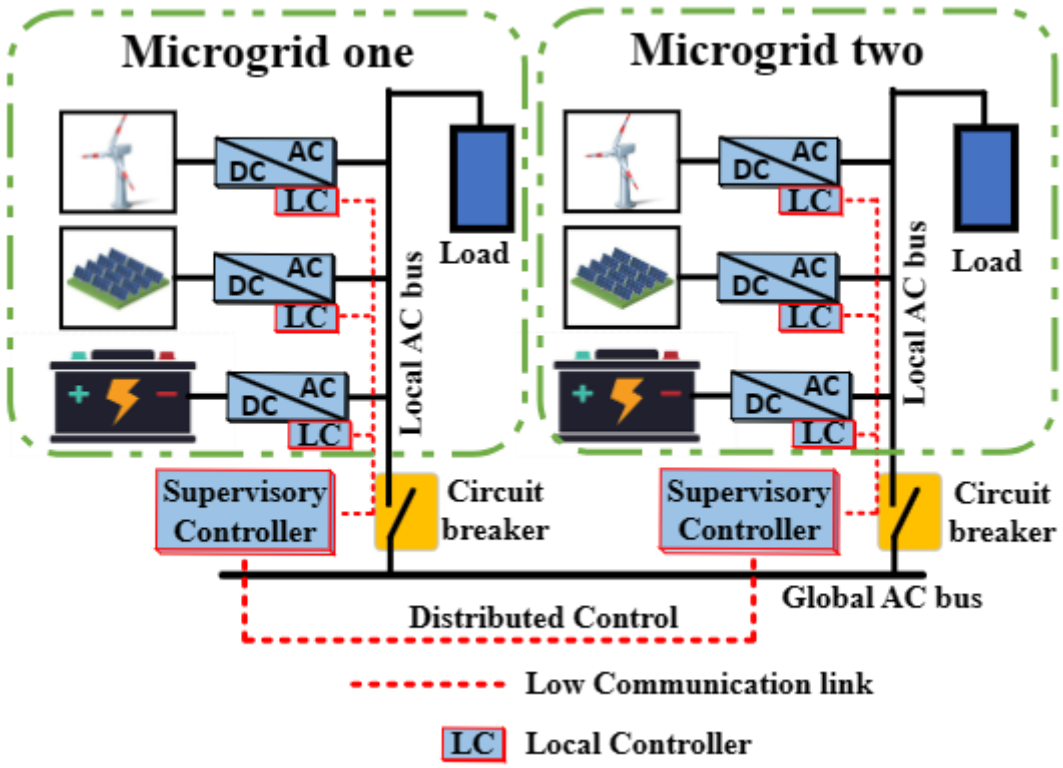

Figure 2.12: Distributed Control Architecture of Interconnected Microgrid

Table 2.2: Advantages, Disadvantages and Suggested Applications of Control Techniques.

Control Approach	**Advantages**	**Disadvantages**
Centralised	• Ease of implementation and coordination. • The single control action is responsible for all the control decisions. • Global optimum operating point is attainable due to access to all the required information.	• High communication and computation burden. • High risk of single-point failure. • Limitation on expandability and scalability. • Full dependence on a central controller.

	• Reduced operation cost. • Effective use of microgrid components.	• Issues with preserving data privacy.
Suggested Applications	• Small-scale systems • Systems with fixed architecture and less probability of expansion. • When sufficient computational resources are available.	
Decentralised	• Controllers operate independently, and there is no communication infrastructure to exchange information among controllers. • Local controllers communicate using locally measured information like the system voltage and frequency changes. • Enhances microgrid autonomy and their immunity to external disturbances. • High plug-and-play functionality. • Reduced computational burden for local controllers. • High privacy protection.	• Difficult to reach the global optimum operating point of the interconnected microgrid. • Lack of cooperation among microgrids. • Risk of instability due to lack of information. • High cost of operation. • High energy exchange between interconnected microgrid network and main grid. • More complex implementation and coordination.
Suggested Applications	• When attaining the global optimum point, it is not necessary. • Preserving the privacy and autonomy of microgrids is sought.	
Distributed	• Benefits of the advantages of centralised and decentralised techniques.	• Complex implementation. • Communication delays might introduce new challenges.

	• Communication among multiple controllers is required to achieve a common goal. • Reduces the need for powerful computational resources by including several local controllers. • It allows easy system expansion and facilitates the plug-and-play operation and integration of new microgrids. • Low operation cost. • Reduced communication and computation burden of the central controller.	• Preserving the privacy of individual microgrids might be challenging. • Coordinated operation still relies on a central controller. • High dependence on communication networks. • Disclosing of partial information is required.
Suggested Applications	When there is a possibility for system expansion and the plug-and-play operation is required. Sharing private data of microgrids is not critical.	

2.7 Related Studies

Several contemporary literature surveys that focus on different control structures and energy management of interconnected standalone AC microgrids are discussed in this section. Amongst these, considerable literature, e.g. [11], [16], [117]–[119], has focused on microgrid controls and power management. Nevertheless, these microgrid operations are widely known to reduce power transmission loss and enhance power system resilience and their capability to integrate DGs from RES [120]. It has been established in [26] that microgrids have limited capacity when operated in standalone mode, and a single-use microgrid system's stability, reliability, and efficiency decline as the load

capacity of the microgrid increases. Microgrids are interconnected to overcome the limitations of a single microgrid. Therefore, the functional structure of interconnected microgrids and effective power flow coordination strategy can boost the system's stability and reliability [6], [14], [106]. However, interconnected microgrid operational goals include power generation, energy storage, and consumption at the microgrid level, power exchange and the medium of interconnection with other connected microgrids or the utility grid at the network level following the operating objectives. Typical objective functions used in literature for interconnected microgrid operation and management include voltage-frequency profile improvement, operation cost minimisation, RES power utilisation maximisation, transmission loss minimisation, reliability improvements, etc. [104].

Much literature has addressed microgrid interconnection in different control structures, considering the classification of connecting common AC buses with static transfer switches, tie-lines and breakers, or common DC buses using back-to-back converter classifications and energy management approaches. Some have focused on microgrid interconnection with the common DC bus [121], and most microgrids are randomly interconnected with tie-lines representing the common AC bus [122]. However, using back-to-back converters can improve power quality and limit the fault current in the network [123].

Multiple interconnected microgrids can support one another to enhance the support of their respective load and minimise RES power curtailment by using the global droop controller proposed in [26]. A robust distributed control for interconnected microgrids was designed in [6] to regulate the power flow among multiple microgrids in island mode. The microgrids are connected directly via a common bidirectional VSC-HVDC link, which uses modal analysis and time-domain simulations to deal with critical issues that degrade stability. In [15], [86], [95], [124], microgrids are interconnected via a common DC link. A multi-microgrid power management system was proposed in [92], based on energy routers to handle network congestion and issues in a multi-microgrid system. The system consists of a fixed grid connected to a voltage source converter (VSC), a circuit breaker, and an energy

router with back-to-back converter technology connected in parallel with four microgrids. A distributed optimal tie-line power flow control for multiple interconnected AC microgrids in[88] consists of microgrids connected to the grid through a grid-tied switch. Autonomous power electronic interfaces between microgrids presented in [125] use the back-to-back converter representing a common DC link to interface microgrids and the utility grid. It demonstrated the design of a two-microgrid interface control method using a dynamic phasor model to preserve the microgrid operation and power transfer across the interfaces. Two microgrids in [126], [127] are interconnected with a back-to-back converter to improve the power quality and stability of the interconnected microgrids. The two microgrids of different frequencies presented in [128] are interconnected with a back-to-back converter (common DC bus), and each microgrid is connected to the utility grid with a breaker. Hence, simulation results show that the back-to-back converter and proposed control strategy improved the frequency control. The microgrids can operate in grid and standalone modes and supply power to each other without needing a communication link between the two microgrids.

An energy management system for controlling interconnected microgrids is presented in [129] to manage the power exchange between microgrids and each microgrid with the utility grid. The microgrids are interconnected with static switches and tie-lines, and multi-layer neural networks are used to predict the uncertainty parameters. A multi-microgrid alliance protocol interconnected to a common AC bus with tie-lines based on cooperative game theory is presented in [130] to maximise the benefits of the microgrids. In [131], each of the two microgrids is connected with a circuit breaker to a common AC bus and is utility grid-connected. Each microgrid consists of renewable DG sources like wind turbines, photovoltaics, battery storage systems, controllable units and loads. A community market structure based on energy trading among interconnected microgrids with adjustable power is presented in [132] to manage energy trading among microgrids and also with the utility grid. Three microgrids with 15 kW, 30 kW, and 60 kW are interconnected to a common AC bus via an automatic transfer switch (ATS) and a traditional transformer [133], which operates in standalone and utility grid

mode and a power dispatching control strategy is proposed to enhance the resilience of system operation in the islanded mode. In [134], an energy-sharing provider to minimise the cost of power loss, together with a distributed optimal model and two-level iterative algorithm for the microgrids and energy-sharing providers, are proposed to minimise the total cost.

In [135], an optimal scheduling strategy for interconnected microgrids considering the uncertainty of wind power is proposed to minimise the operation cost of individual microgrids. The ADMM is used to protect the privacy of individual microgrids and achieve a decentralised solution to the proposed model. An optimal energy management strategy for minimising the operation cost of an MMG network proposed in [136] considered operation constraints and carbon emissions. An optimised framework for energy management of multi-microgrid systems is presented in [137], suggesting a hierarchical energy management system for the optimal operation of multi-microgrids, which is considered two-level optimisation. The paper in [138] compares three models of predictive control (MPC) coordination strategies based on decentralised, centralised and hierarchical-distributed MPC operations for interconnected home microgrids. A power management strategy for interconnected microgrids proposed in [19] uses a power-sharing framework and local objectives of multiple microgrids to maintain the power balance between generation and load. A power dispatch strategy for interconnected microgrids-based hybrid RES proposed in [139] ensures load demand in each microgrid is met through interaction with the utility grid. An optimal energy control hosting the BESS and electric vehicles through multiport converters in interconnected microgrids is presented in [140] to connect to different sources and loads and eliminate uncertainty from RESs. A new efficient stochastic energy management technique for interconnected AC microgrids in [141] investigates the optimal operation and scheduling of interconnected microgrids with high penetration of RES—a framework based on the unscented transform (UT) method to model uncertainties. An energy management system for multiple grid-connected interconnected microgrids uses the ADMM strategy presented in [142] to minimise operational costs and maximise benefits from RES. A hierarchical decentralised system of systems

architecture for energy management of a multi-microgrid system was proposed in [143] as a bilevel optimisation considering individual microgrids and multi-microgrid operation. An autonomous optimisation model of an active distribution system with multi-microgrids is presented in [144]. The model consists of three microgrids and the distribution network (DN), which can autonomously utilise their distinct resources to optimise the operation and benefits of the interconnected microgrids. The proposed analytical target cascading (ATC) theory decouples the active DN and microgrids dispatching by modelling the tie-line flow as a pseudo-generator/load.

2.8 Summary and Research Gap

This chapter reviewed the leading background topics relevant to the development of this thesis. A review of microgrids, different operation modes and the types based on AC, DC and hybrid microgrids was presented. This literature review addressed converters as the fundamental component of microgrids. It explained how three-phase inverter management and DC/AC inverter switching work and discussed the hierarchical control levels, methods and operation. The concept of interconnected microgrids was introduced, describing their different features, types, and structures, followed by a detailed description of the centralised, decentralised and distributed control approaches was presented. Finally, a thorough survey of related literature was introduced, which provided an in-depth review of research papers that have proposed different structures, control and energy management of interconnected microgrids.

Based on the broadly published literature related to the control and energy management of interconnected AC microgrids, it is found that existing research work has focused on the random interconnection of neighbouring microgrids using back-to-back converters, which represents a common DC bus between the connecting microgrids and the following research gaps have been identified and addressed:

There is no clear report of literature on interconnected microgrids using back-to-back converters to form the structure of a common AC bus. Therefore, to fill this research gap, this thesis presents a novel structure contribution to interconnecting multiple standalone microgrids to a common AC bus using back-to-back converters and traditional transformers.

Also, as far as the author knows, the decentralised control and power flow management of interconnected AC microgrids, including the centralised control and energy management of interconnected microgrids, are not yet fully resolved. Thus, research into decentralised and centralised optimal control continued to gain more attention. Therefore, optimal control in this specific area of research on interconnected microgrids remains untouched, and no study has addressed this problem clearly and in detail. More research is required on interconnected AC microgrids optimal control and energy management.

Hence, the aim of the emergence of the research embedded in this thesis is to fill the gap and provide detailed structure, robust controllers and energy management of interconnected standalone AC microgrids using back-to-back converters to form a common AC bus and traditional power transformers to transmit electric power over long distances. The control scheme for the bidirectional power flow of the back-to-back converters has been developed to balance the power flow in the interconnected microgrid network. The controllers are implemented using a low-link communication network. A global droop controller is proposed to enable power exchange among the interconnected microgrids.

CHAPTER 3: PROPOSED STRUCTURE FOR INTERCONNECTED AC MICROGRIDS USING BACK-TO-BACK CONVERTERS

3.1 Introduction

This chapter proposes a novel structure and control technique for interconnecting standalone AC microgrids to a common AC (global AC or MVAC) bus. The technique uses back-to-back converters to decouple the connecting frequencies and facilitate power exchange between microgrids. The control technique for all the connecting bidirectional back-to-back converters is developed to manage the bidirectional power flow between each microgrid and the rest of the microgrids in the network and to balance the power in the global bus of the interconnected microgrid.

The chapter gives a generalised overview of a typical structure of grid-connected interconnected microgrids AC microgrids and the mode of operation in independent microgrid operational mode and interconnected standalone mode. The proposed novel structure is presented with its operation in independent microgrids and interconnected modes. The chapter shows the control strategy and the details of different droop control strategies of the PV-based RES and BESS units. It reveals different control strategies for the converters and other relevant DC/AC converters. The bidirectional back-to-back converters, classified as the local and global converters, are presented together with the associated modified local and global droop control strategies. The detailed model of the global droop controller for power flow management of interconnected standalone AC microgrids is investigated in detail. Simulation results from MATLAB/Simulink validate the performance of the proposed global droop controllers.

3.2 System Overview

A typical existing structure of a grid-connected interconnected AC microgrid is shown in Figure 3.1 [8]. The Figure consists of four microgrids operating individually in standalone and grid-connected modes. Each microgrid local AC bus comprises RES-based DG, BESS, auxiliary unit and local load. In this case, the auxiliary unit is a micro-gas turbine and can also be a fuel cell, a diesel generator, or

BESS. A circuit breaker is an interconnecting medium that interfaces each microgrid to the global AC bus. The global AC bus is interfaced with the utility grid by a grid transformer (T_g), utility grid breaker (S_g), and a global synchronisation algorithm. At the individual microgrid level, the RES-based DG in the form of PV units producing DC is interfaced by a DC/AC inverter, and a bidirectional DC/AC inverter interfaces the BESS. The auxiliary unit is interfaced by two-stage AC/DC and DC/AC power electronic converters.

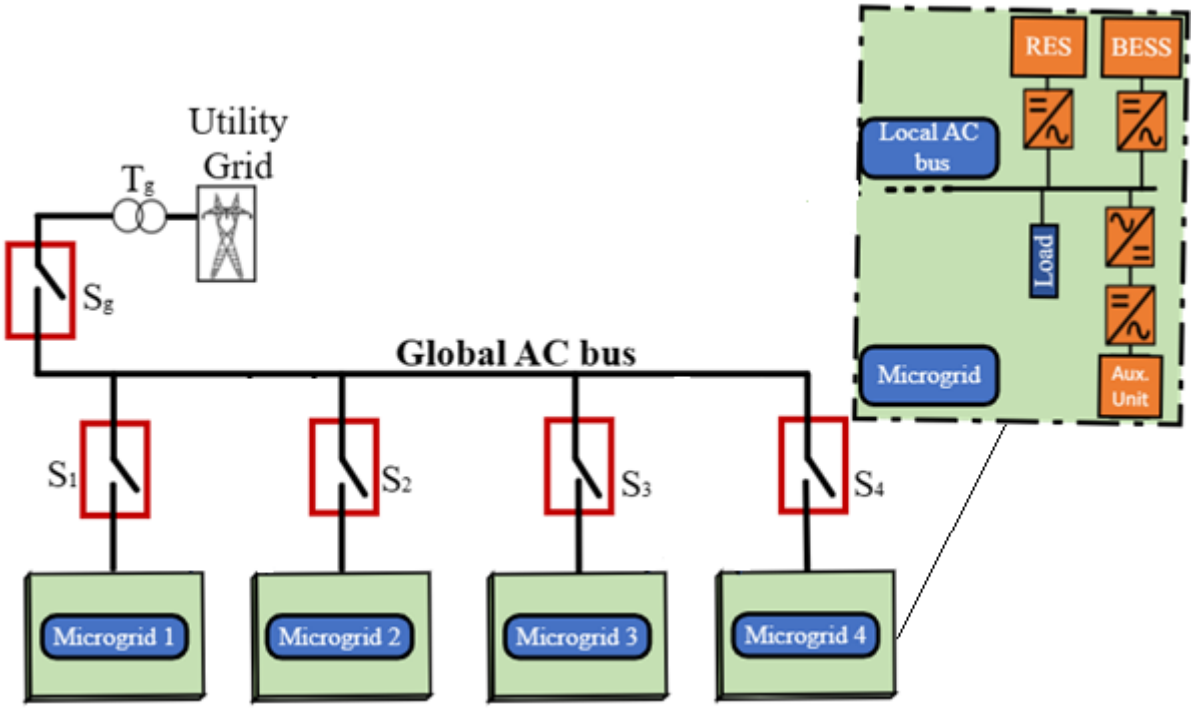

Figure 3.1: Typical Structure of Grid-Connected Interconnected AC Microgrids

The AC output voltages from individual DG units are connected to the local AC bus to power the local loads and global AC bus via an interface system comprised of a circuit breaker. The output voltage from each DG unit is independently controlled. The BESS is the grid-forming unit that controls and maintains the AC bus voltage and frequency. However, overcharging and undercharging boundaries can be set to preserve the reserve capacity of BESS. The surplus power from RES can be curtailed to prevent overcharging the BESS. Furthermore, the auxiliary unit in the form of a micro-gas turbine can supplement the power. But, in the case of no auxiliary unit, an eventual load shed must happen to keep

the frequency within the limit. The rates of charging/discharging of BESS affect their rated capacity. Suppose the BESS is rapidly discharged; this lowers the battery capacity and reduces the amount of energy that can be extracted from the battery. However, more energy is extracted when the BESS are discharged at a prolonged rate, and the capacity is higher, thus dissipating greater energy. It is desired that the SOC be operated and maintained within the safest operable limit. Exceeding the SOC maximum charging/discharging operable limits can put the BESS at risk by reducing its lifespan. Effective coordination and control of each microgrid SOC are vital in determining different operational modes to utilise more RES to provide better load support. The different PVs (RES-based DG) act as the current sources and inject power directly into the AC bus according to their Maximum Power Point Tracking (MPPT).

Though a low-speed communication link between the breaker and the DG units is required to detect the status of the breaker and to isolate or re-connect the microgrid to or from the global AC bus seamlessly, the switch operates the Point of Common Coupling (PCC), which can be monitored and controlled by the microgrid central controller (MGCC). The local loads are connected to the microgrid side of the local bus to achieve uninterruptable power supply from generation to loads. At the interconnected microgrid level, the local microgrid breaker connects or isolates each microgrid from the interconnected global AC bus. At power balance, each microgrid operates at a nominal frequency to meet the demand of its local load. During power imbalance, the microgrids with surplus power export power to microgrids with a power deficiency and vice versa. Similarly, a utility grid breaker and a synchronisation algorithm operate the grid PCC to connect or isolate the global AC bus of microgrids seamlessly to or from the utility grid, which can be performed by the global network central controller (GNCC).

The utility grid dictates the global networked bus and the microgrid bus voltage and frequency in grid-connected mode. Also, the grid balances any difference between the power generated by the RES and that consumed by the load. All microgrid DG units act as current sources, controlling the power

injected directly from the microgrid to the grid. The role of the BESS is to control the amount of power exchanged between the microgrids in the network and the grid.

Power can be imported from the utility grid to the global AC bus during lower electricity import tariffs. Similarly, power can be exported from the networked microgrids to the utility grid when there is a surplus of power from the PV, the microgrid feeding unit. Each BESS is the grid-forming unit that is interfaced with a bidirectional converter to regulate the voltage amplitude and frequency of the individual microgrid bus. In standalone operational mode, the global AC bus is detected and maintained by the various microgrids in the network. Hence, this thesis is concerned with standalone interconnected AC microgrids.

3.3 Proposed Novel Structure of Interconnected Standalone AC Microgrids

The proposed new structure and control model of standalone interconnected AC microgrids is shown in Figure 3.2. Figure 3.3 shows the equivalent structure of the standalone interconnected microgrids representing the BESS as voltage sources, PV-based RES, auxiliary units and load as sources. The interconnected microgrid model consists of three standalone AC microgrids interconnected to the global bus, also known as the medium voltage AC (MVAC) bus, capable of transmitting voltages greater than 1kV and less than 100kV, using back-to-back converters and traditional power transformers. However, there is no limit to the number of microgrids that can be interconnected because the interconnection medium is a controllable interface that may require some adjustment to the controller for optimal performance. At the same time, each microgrid consists of a PV-based RES unit, BESS, and auxiliary unit (micro gas turbine) connected to the local AC bus, which supplies the local loads.

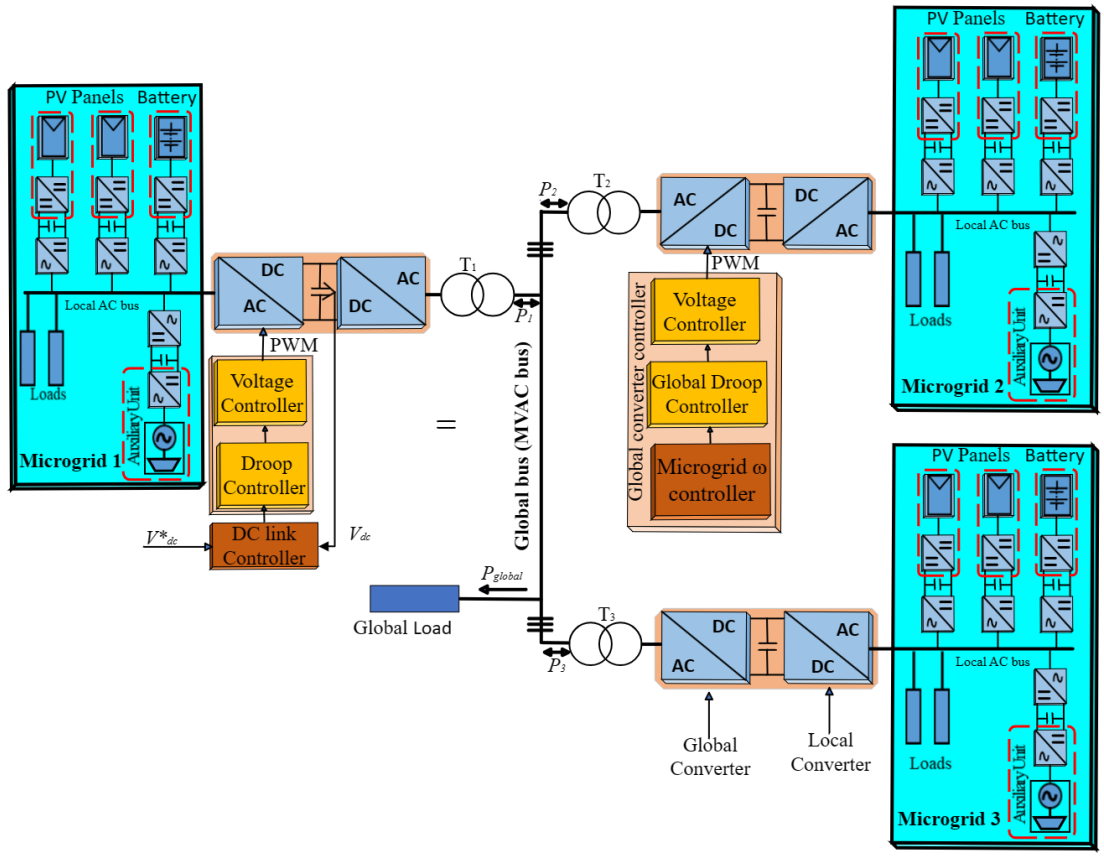

Figure 3.2: New Structure and Control of Standalone Interconnected Microgrids

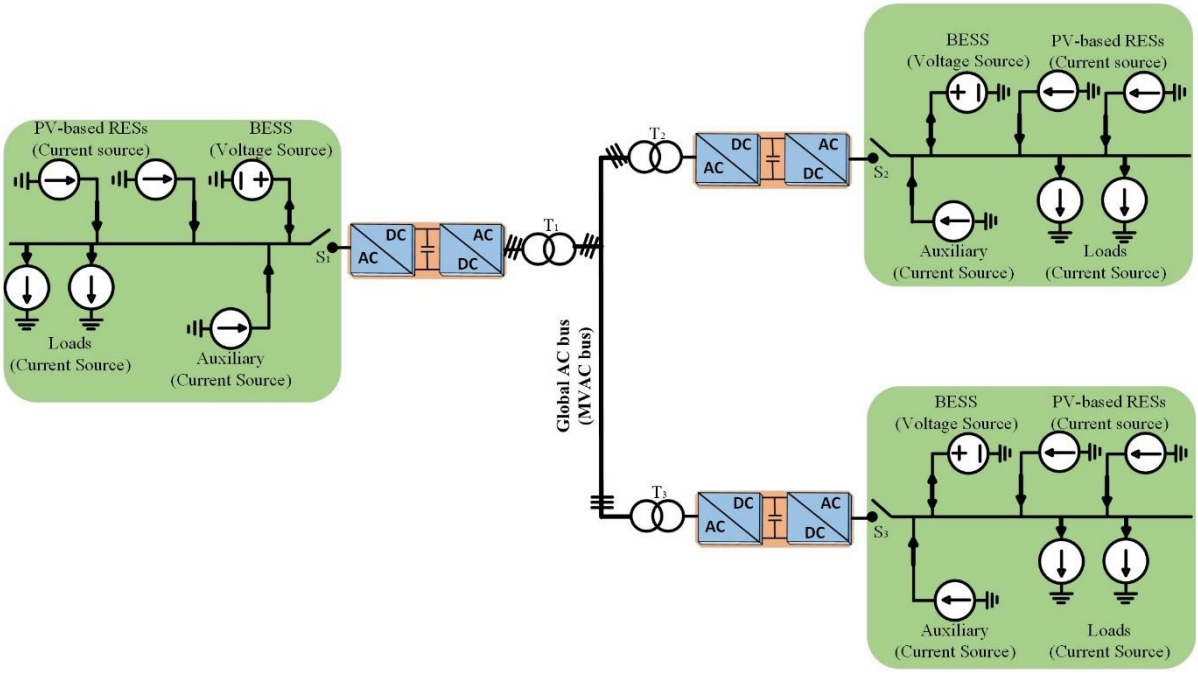

Figure 3.3: Interconnected Microgrids with BESS as Voltage Source PV-Based RES Auxiliary and Load as Current Sources

3.3.1 Independent Mode of Operation

The BESS unit acts as the grid-forming unit that controls the microgrid bus's local AC voltage and frequency. The BESS is interfaced with a bidirectional DC/DC converter that regulates the DC-link voltage and the bidirectional DC/AC inverter that controls and maintains the voltage and frequency of the local AC bus. The PV-based RES is the grid-following unit that injects maximum power available irradiance. The PV is interfaced with a DC/DC converter that controls the voltage output to achieve maximum power point tracking (MPPT) and the unidirectional DC/AC inverter that regulates the DC-link voltage. The grid-forming and grid-following (grid-feeding) units are controlled to supply power to the AC bus. The auxiliary unit is a micro gas turbine that operates at a very high frequency, interfaced by a unidirectional AC/DC and DC/AC converter. The role of the auxiliary unit is to supplement power based on the load requirements at low SOC and low PV power supply [16].

If the PV-based RES unit generates more power than the load can use, the BESS absorbs it and supplies power when the PV power is less than the amount of power needed by the load. When there is a power surplus, and the SOC of the BESS reaches its maximum, the PV's power curtailment is required to protect the BESS. Also, when there is a power shortage and the SOC is approaching its low limit, the auxiliary unit generates power to supplement the deficiency. The BESS can provide the system balance, but the smaller the BESS unit, the quicker the SOC will reach its limit. Ideally, the usage of the auxiliary unit and the PV curtailment should be minimised

3.3.2 Interconnected Mode of Operation

The microgrids are interconnected to facilitate the exchange of a bidirectional power flow, such as a power surplus in one microgrid compensates for power deficiency in another microgrid. Each microgrid is interfaced with the global bus via a bidirectional power electronic back-to-back AC/DC converter, a DC/AC inverter, and a traditional power transformer. The AC/DC converter (microgrid side or local converter) and the DC/AC inverter (global bus side converter) are known as the local and

global bus converters. The global converter regulates the power flow from the local microgrid to the rest of the network. The global bus converter, however, controls the power import and export to/from the global bus according to the global droop controller. The global converters use a frequency signalling technique and modified droop control strategy to regulate power flow in and out of the microgrid. The main advantage of the global controller is that it uniformly and harmoniously regulates the voltage and the frequency of the global/MVAC bus equitably, collectively and wirelessly.

It is important to state categorically that this research focuses on interconnected standalone AC microgrids and not grid-connected. Therefore, the novelty of this research can be highlighted in the structure and control strategy of interconnection via back-to-back AC/DC/AC converter and power transformer to form an MVAC bus. A back-to-back AC/DC/AC converter is an electrical mechanism to decouple the two connecting frequencies so that microgrids and the MVAC bus can autonomously utilise their distinct resources and benefits. However, traditional power transformers transmit electrical energy over long distances, making the system more efficient and robust.

At the global bus (MVAC bus) level, the sum of the powers from the three global converters of the three microgrids $\left(P_1 + P_2 + P_3 \right)$ equals the power that goes to the global load $\left(P_{global} \right)$ as shown in Figure 3.2. Each microgrid must meet its load demand within the nominal frequency range. The PV-based RES is the primary power source for the load, while the BESS is the secondary power source. The BESS supplies the power shortage during discharging mode if the PV power is insufficient to supply the load. The auxiliary power supply unit only supplements power when the SOC is low and there is a low power supply from the PV-based RES. In the charging mode and discharging mode of the BESS, it is presumed that the BESS power is negative and positive, respectively.

If the frequency of the microgrid bus is increased above the nominal range, the power from the microgrid PV-based RES can be exported to the microgrid with a deficient power supply. Similarly, the auxiliary unit supplies power if the frequency is decreased below the nominal range. But, if there

is a further decrease in frequency and the BESS unit runs out of charge, the BESS will reduce its frequency. So, the global connecting converter will start to demand power, and the microgrid will start asking for power import. The frequency deviation range is between ±1% the nominal value of 50 Hz, giving a deviation in frequency between 49.5 Hz and 50.5 Hz. The power import and export in the system are proportional to the variation in microgrid frequency, and the system is implemented to work automatically. The BESS's SOC variations reflect changes in the bus frequency. The microgrid can export power if the BESS SOC and frequency are high. Similarly, the microgrid can import power if the BESS SOC and frequency are low. The amount of power exported or imported is proportional to the frequency deviations.

All the units' DC/AC inverters use wireless droop technology to eliminate the need for direct links between the connecting networks. Suppose the microgrid local bus frequency is reduced substantially below its nominal value. In that case, this sends a signal to the power demand of the global converter to start demanding power import from the global AC bus. The global droop control is implemented such that the global converter unit only imports or exports electricity when needed. However, any substantial deviation in frequency in the microgrid brings about imbalance, and the DC/AC global converter control uses a global wireless droop control strategy that responds to keep the system balanced.

3.4 Droop Control Strategy

This thesis adopts the wireless droop control strategy to facilitate parallel connection among the connecting microgrid converters and avoid circulating currents between the connected units [11], [145]. Droop control in AC systems allows for decentralised control of individual converters with either no or very little communication, like a power line connection [16]. The primary inverter controller mimics the behaviour of a synchronous generator in terms of the drop in frequency and voltage due to an increase in active and reactive power [66], [73]. Hence, Droop control will be applied

to the DC/AC converters inside the microgrid and the DC/AC inverters interfacing with the MVAC. The concept of droop control originated from synchronous generators in power systems, where the synchronous generator presents a rotor inertia which limits the frequency variation.

3.4.1 Basic Droop Control

The fundamental active power–frequency $P \sim \omega$ and reactive power-voltage $Q \sim V$ droop control curves are represented in Figures 3.4(a) and (b), respectively. The Figure illustrates that frequency deviates farther from its nominal value as more active power is generated. Also, the voltage drop increases as supplied reactive power increases.

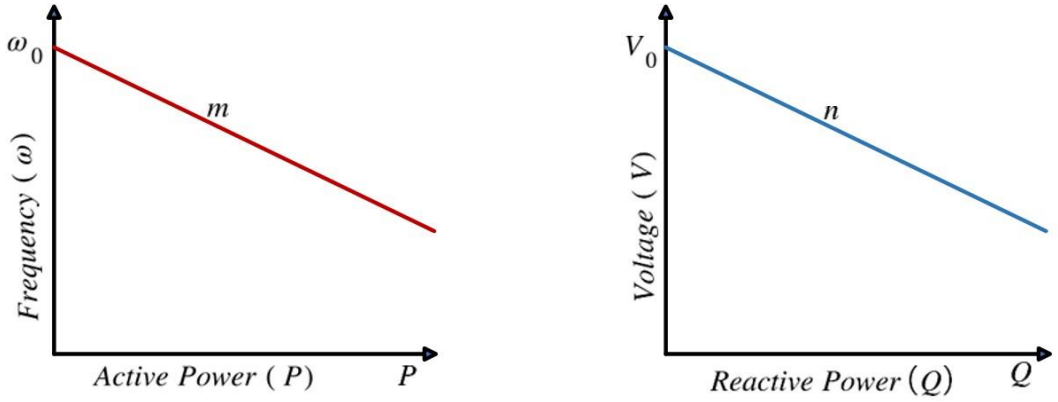

(a) (b)

Figure 3.4: Droop Control Characteristics: (a) $P \sim \omega$ and (b) $Q \sim V$ Droop Control Curves

The primary controller in the active power droop strategy mimics the behaviour of the synchronous generator in terms of decreasing the frequency when the active power is increased and vice versa, as detailed in [16]. Hence, the conventional $P \sim \omega$ and $Q \sim V$ droop controls are defined by equation (3.1) and are employed in all DC/AC converters.

$$\begin{aligned} \omega &= \omega_0 - m(P - P^*) \\ V &= V_0 - n(Q - Q^*), \end{aligned} \tag{3.1}$$

where ω, V, ω_0, V_0, m, and n represent the output frequency, the voltage amplitude, the nominal frequency, the nominal voltage, the frequency droop coefficient, and the voltage droop coefficient,

respectively. Here, P and Q are the measured active and reactive power, while P^* and Q^* are active and reactive power setpoints, respectively.

3.4.1.1 Control of the BESS Unit

The stage 1 DC/DC converter and stage 2 DC/AC inverter interfaces the BESS unit. The BESS stage 1 DC/DC is a bidirectional buck/boost circuit regulating the DC link voltage to a suitable value. The BESS stage 2 bidirectional DC/AC converter operates in voltage mode with a droop control coefficient set to zero. The droop coefficient is set to zero to enable the BESS to detect the frequency of the local microgrid AC bus and not allow the frequency to droop. The DC/AC converter becomes the grid-forming unit by setting the droop coefficient to zero, as illustrated in Figure 3.5. Based on this functionality of the BESS, the power absorbed or delivered by the BESS unit depends on the power from the PV-based RES and the load. Hence, its power output is determined only by the difference between local generation and load. However, the bus frequency is varied by, $\Delta\omega$ as a signalling mechanism to control the other units connected to the local AC bus. The output frequency of the BESS unit is given by the expression in equation (3.2).

$$\omega = \omega_o + \Delta\omega \tag{3.2}$$

The microgrid SOC determines the frequency deviation $\Delta\omega$ according to the control strategy illustrated in Figure 3.6. The proposed SOC–-frequency variation curve represents how each local microgrid bus former responds to frequency variation at the global bus. The deviation in frequency occurs within the maximum (ω_{max}) and minimum (ω_{min}) values, and the change in SOC occurs between the maximum (SOC_{max}) and minimum (SOC_{min}).

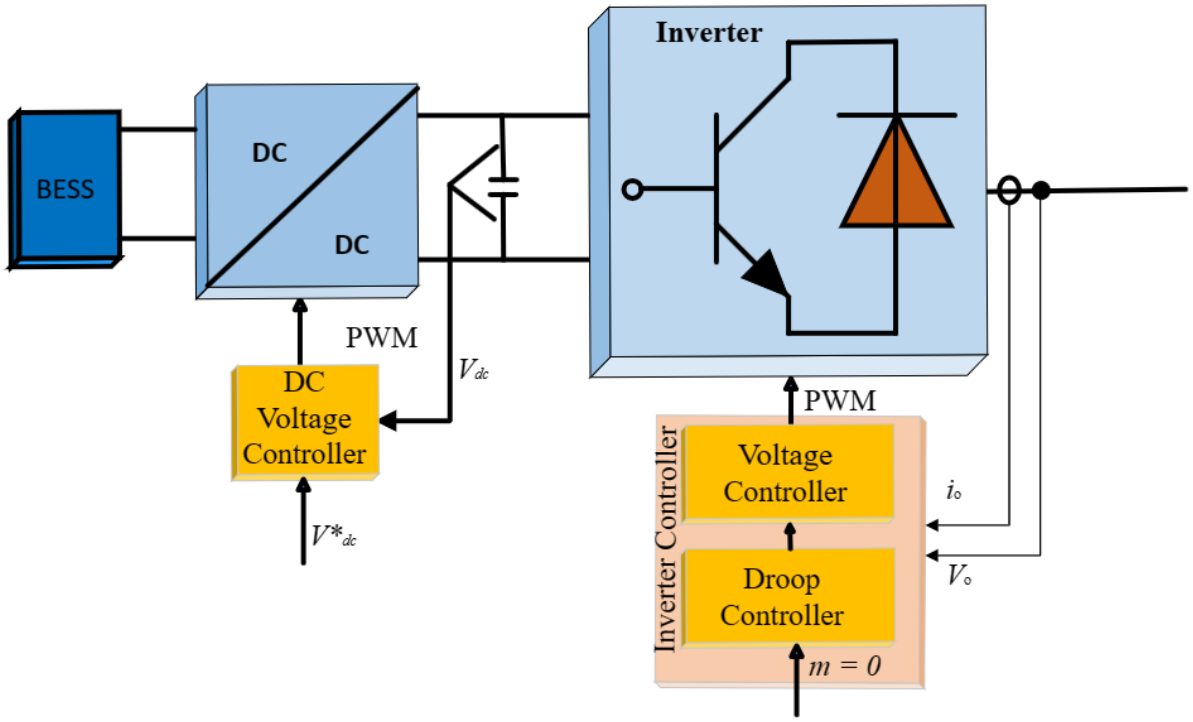

Figure 3.5: Control Scheme of the BESS

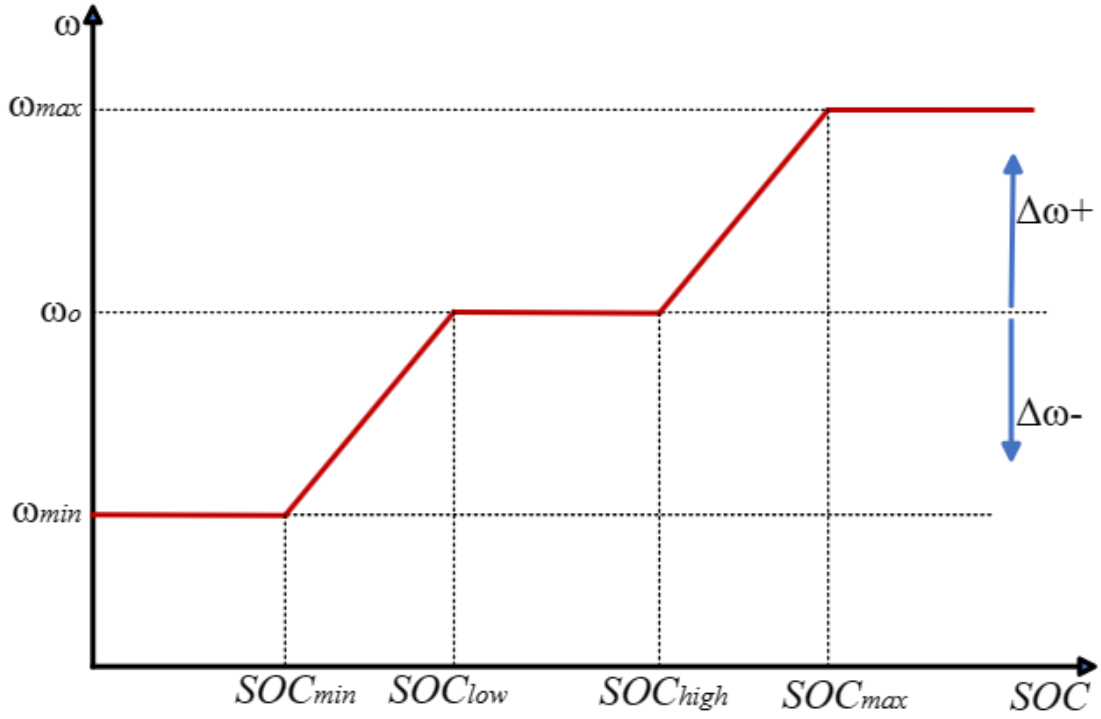

Figure 3.6: Microgrid SOC relationship to frequency variation

At the nominal frequency operation of the interconnected microgrids, the variation in frequency is within its limit, and the system is balanced. Each microgrid operates to meet the demand of its local load and frequency; hence, there is no power exchange. The SOC of each microgrid varies in direct proportion to the variation in frequency $\left(SOC_{batt} \rightarrow \Delta\omega\right)$. The variation in frequency reflects the status of the battery storage system; if the storage goes low, the frequency goes low, depicting a power shortage. If the storage and frequency go up, that implies a power surplus. Hence, the battery SOC operated in three control limits: 1) ranges between SOC_{low} and SOC_{high}, 2) ranges between SOC_{min} and SOC_{low}, and 3) ranges between SOC_{high} and SOC_{max}. The range of curves illustrates that at a very good range of the SOC in control limit 1, indicating a state of power balance, the frequency variation remains limited within the nominal frequency range (ω_0).

In the case of system imbalance due to a power shortage for SOC in control limit 2, and the SOC start to go down, shifting away from SOC_{low} to SOC_{min}, the frequency variation also goes down. If the SOC approaches low-frequency variation (ω_{low}), power can start to be imported into the microgrid with a power shortage. Suppose the power imported into the microgrid is not enough to meet the demand of the load, and SOC goes further down on approaching the minimum frequency variation ($\Delta\omega_{min}$). In that case, the auxiliary unit starts to supplement power to avoid frequency degradation and over-discharging of the BESS. However, priority is given to importing power into the microgrid with a deficient power supply over power supplement by the auxiliary unit.

Similarly, considering the case of surplus power in SOC control limit 3, If the SOC approaches high-frequency variation (ω_{high}), power is exported from the microgrid with the surplus of power to the microgrid with deficient in power (evidenced by negative frequency variation). Suppose the power generated from the PV-based RES into the microgrid continues to be in excess, frequency variation continues to increase in the positive sense until it approaches the maximum variation in frequency

(ω_{max}) corresponding to SOC_{max}, PV-based RES power is curtailed to prevent the battery from overcharging. Priority is given to exporting power from a microgrid with a surplus of power to a microgrid with a power supply shortage over curtailment. However, the SOC controller is implemented in the BESS of each microgrid, and the bus frequency is either positively or negatively varied to reflect the storage status. The increase in the SOC is an indication that there is a surplus of power, and the battery SOC is getting high. The reduction in the frequency is an indication that there is a shortage in power generation, and the SOC is getting low.

3.4.1.2 Control of the Solar PV Unit

The stage 1 unidirectional DC/DC converter and stage 2 DC/AC inverter interface the solar PV unit. The stage 1 DC/DC converter controls the PV voltage to track the maximum power point depending on solar irradiance. The stage 2 DC/AC inverter operates in three control loops; the outer DC-link voltage regulator loop sets the power demand to the droop control loop, which in turn sets the voltage demand to the inner AC voltage control loop, as presented in Figure 3.7. The DC/AC inverter operates in droop control mode, with its power demand set by a DC link voltage regulator. The Solar PV operates as a power/current source, injecting the maximum available power to the microgrid AC bus [11]. The droop control equation of the Solar unit is shown in equation (3.3).

$$\omega = \omega_0 + m_{pv}(P - P_{pv}^*) \tag{3.3}$$

where P_{pv}^* is the power setpoint of the PV-based RES unit, and the output of this setpoint is determined by the DC link voltage controller. The DC-link voltage is controlled by a proportional-integral (PI) controller whose output sets the power demand of the PV-based RES. At a steady state, the setpoint of the PV-based RES is required to equal the power generated by the DC/DC converter according to the maximum power point tracking. Therefore, the power setpoint of the PV-based RES is determined by the equation (3.4).

$$P_{pv}^{*} = m_{p}^{pv} + \frac{m_{i}^{pv}}{s}(V_{dc} - V_{dc}^{*}) \tag{3.4}$$

where m_{p}^{pv} and m_{i}^{pv} are the proportional and integral controller gain values of the PI controller that regulates the DC-link voltage and 's' is the Laplace operator. V_{dc} and V_{dc}^{*} are the measured DC-link voltage and its setpoint. However, the PV-based proportional gain values and power setpoints remain the same in grid-connected mode.

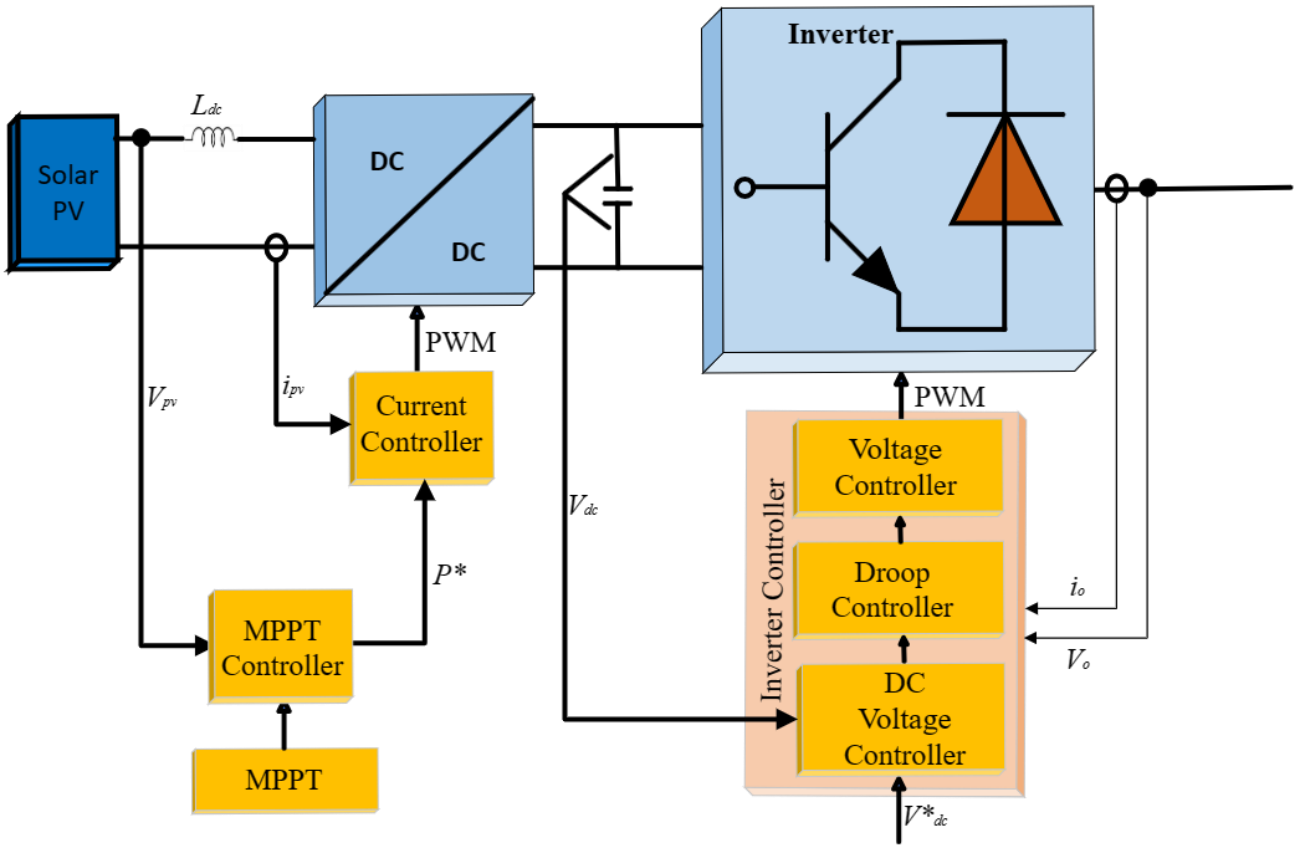

Figure 3.7: Control Scheme of the Solar PV Unit

3.4.1.3 Control of Auxiliary Unit

The stage 1 unidirectional AC/DC converter regulates the DC-link voltage, while the stage 2 DC/AC inverter controls the power output according to the local microgrid AC bus frequency as presented in Figure 3.8. The purpose of the auxiliary unit is to supplement power whenever the SOC is low. There is no need for the unit to run unless the SOC and frequency start to go low. The power can be regulated

by either varying the power setpoint P^* or the nominal frequency ω_0. In each case, the frequency must have deviated below the allowable limit to initiate power supplement from the auxiliary unit. The auxiliary unit supplies power to the microgrid AC bus only when needed according to the amount of deviation by the signalling bus frequency, and the droop control of the DC/AC inverter of the auxiliary unit can be estimated as shown in equation (3.5).

$$\omega = \omega_0 + m_{aux}(P - P^*_{aux}) \tag{3.5}$$

where m_{aux} is the proportional controller gain, P^*_{aux} is the power setpoint, and is set to zero to enable the auxiliary unit to float on the local AC bus and supply auxiliary power automatically only when needed and in response to local microgrid bus frequency deviations. P^*_{aux} is set to the required power level in utility grid-connected mode. However, the auxiliary unit proportional gain m_{aux} and power setpoints remain the same in grid-connected mode.

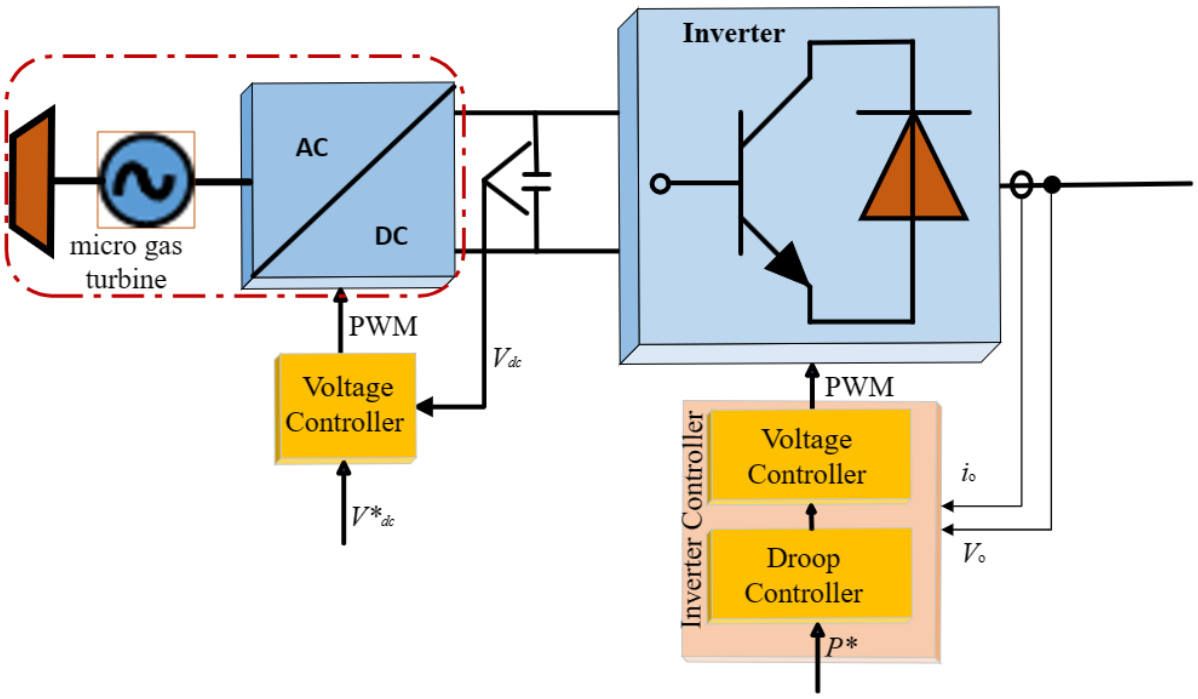

Figure 3.8: Control Scheme of the Auxiliary Unit

3.4.1.4 Control of the Interconnecting Back-to-Back Converter

The control of the two-stage interconnecting back-to-back converter, as presented in Figure 3.2, is described as follows:

1) Local Converter Control

The microgrid-side converter (local converter) operates in three control loops; the outer DC-link voltage regulator control loop of the back-to-back converter sets the power demand to the droop control loop, which in turn sets the voltage demand to the inner AC voltage control loop, as presented in Figure 3.9. The outer DC link voltage control loop uses the proportional-integral controller to regulate the DC link voltage, keep the DC voltage within its limit and set the power setpoint of the droop control (P^*_{local}) as expressed in the equation (3.6).

$$P^*_{local} = \left(k_p^{vdc} + \frac{k_i^{vdc}}{s} \right) \left(V_{dc} - V^*_{dc} \right), \tag{3.6}$$

where k_p^{vdc} is the proportional droop control coefficient, k_i^{vdc} is the integral droop control coefficient, V^*_{dc} are the DC link voltage setpoint, and V_{dc} is the measured voltage of the DC link.

The power setpoint is then used in the droop control of the local side DC/AC inverter,

$$\omega = \omega_o - m_p^{local} \left(P_{local} - P^*_{local} \right), \tag{3.7}$$

where m_p^{local} is the proportional droop control coefficient.

However, there is no need for an integral controller in the droop control because the power setpoint (P^*_{local}) is an output of a PI controller. Hence, it can compensate for any frequency deviation, i.e., the integral term in the equation (3.6) will raise the droop curve up or down depending on the microgrid frequency.

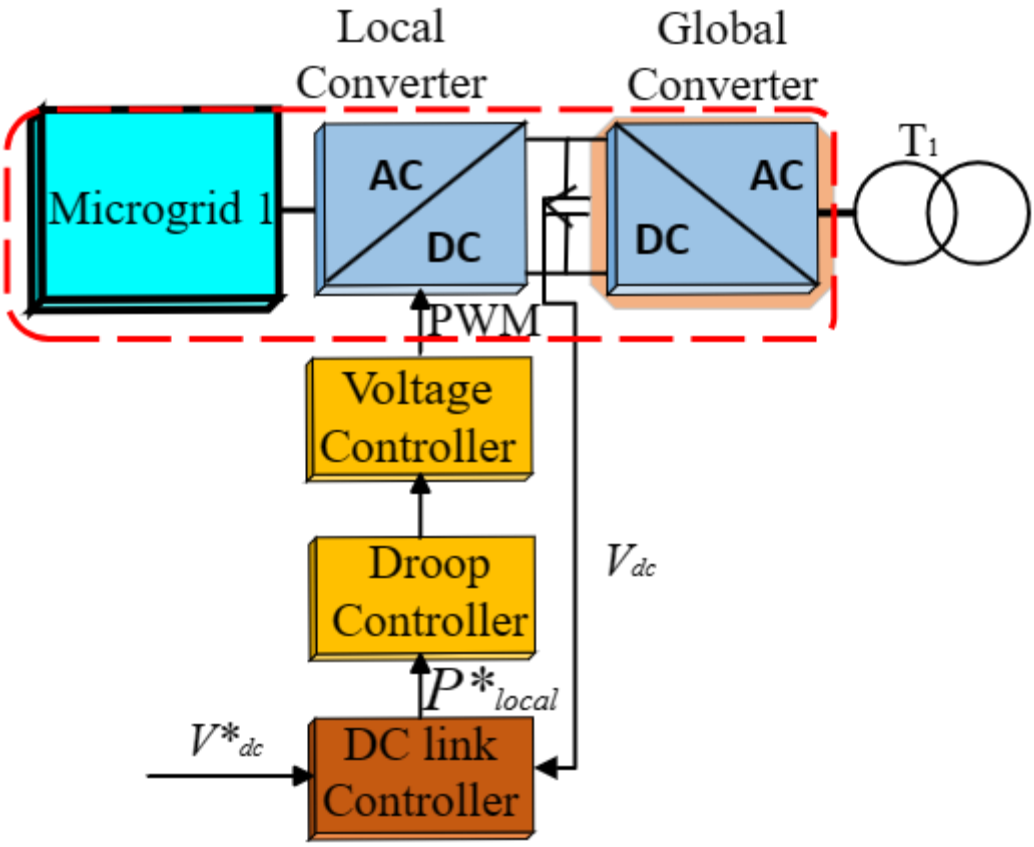

Figure 3.9: Control Scheme of the Local Converter

1) Global Converter Control

The MVAC side converter (global converter) is responsible for the power exchange between the microgrid and the rest of the network. The global converter control operates in three control loops; the local microgrid AC bus frequency control sets the power demand to the global droop control loop, which in turn sets the voltage demand to the inner AC voltage control loop, as presented in Figure 3.10. All the global converters collectively control the MVAC bus via droop control on the global bus sides, as described in equation (3.8). The voltage/reactive power droop equations in [11], [16] as in equation (3.1) specified for the three DC/AC inverters of the global converters in Figure 3.2, are the same. However, the global droop control automatically adjusts its power demand (P^{*}_{global}) based on the controller output from the local microgrid bus frequency.

$$\omega_{global} = \omega_0 - m_p^{global}\left(P_{global} - P^{*}_{global}\right) \qquad (3.8)$$

where m_p^{global} is the global droop proportional controller P_{global} is the measured active power of the global converter. The local microgrid frequency bus controller sets the global power demand (P_{global}^*) for the global droop controller. However, equation (3.9) expresses the global power demand (P_{global}^*) for all three global converters in the interconnected standalone AC microgrid.

$$P_{global}^* = k_{\Delta\omega}\left(\omega_n - \omega_{MG}\right) \tag{3.9}$$

Where ω_n and ω_{MG} are the nominal frequency and individual microgrid frequencies, and $k_{\Delta\omega}$ is the local microgrid frequency deviation proportional controller. This controller uses the AC bus frequency of each microgrid as a low-communication link.

The global converter needs to export or import power depending on the status of the microgrid's local bus frequency and, hence, the SOC of its battery. When the droop coefficient is proportional only, P_{global}, will depend on the setpoints of other global inverters and the global load. This will be explained in more detail in Chapter 4. If the droop coefficient is modified to a PI controller instead, i.e., adding to the integral term, then $P_{global} = P_{global}^*$.

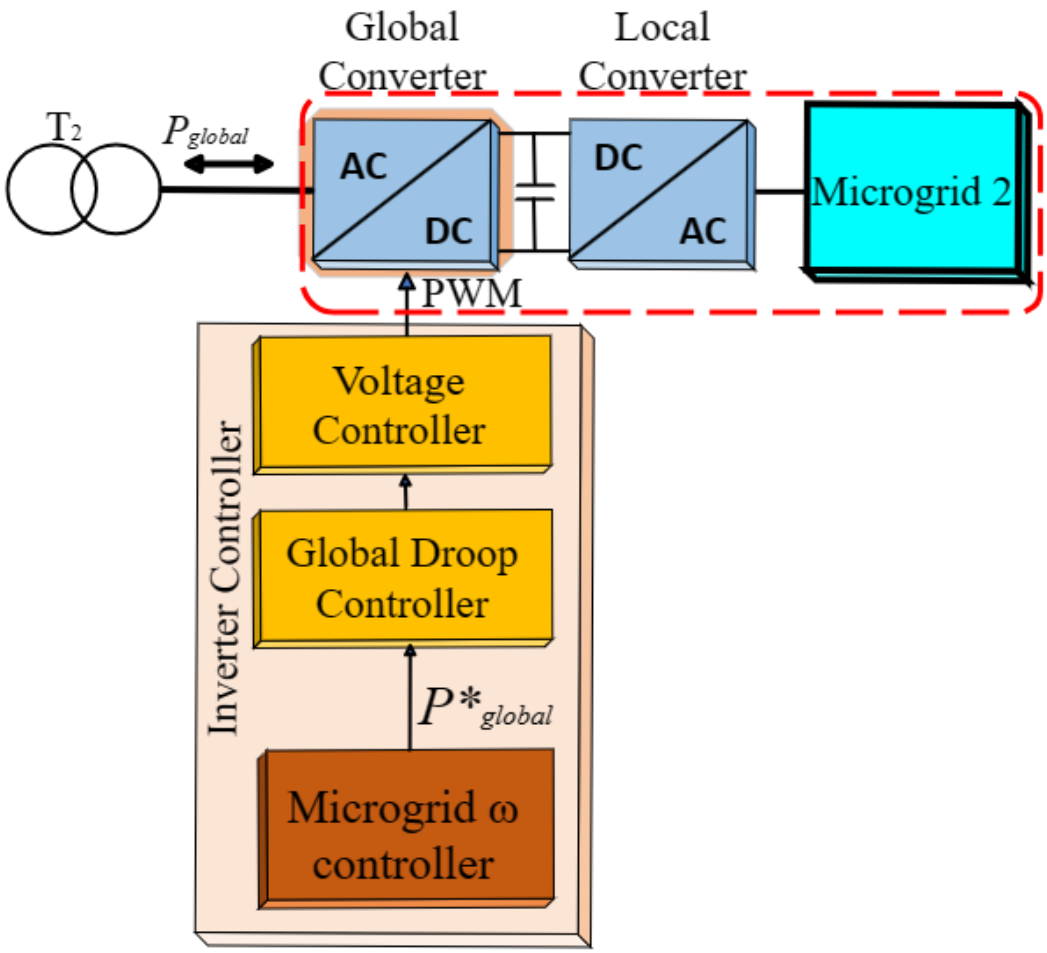

Figure 3.10: Control Scheme of the Global Converter

Figure 3.11 shows the global droop control of the global DC/AC converter unit, given by the equation (3.8). The power demand of the global converter is determined by the local microgrid frequency proportional controller output to import or export power to/from the microgrid in proportion to the variation in the local microgrid bus frequency.

The instantaneous active power used by the droop control equation is measured as a product of 3-phase individual voltages (V_{abc}) and currents (I_{abc}) for all the converters, together with a low pass filter (LPF), which is shown in Figure 3.10. Based on the power calculation approach used in [11], which uses a product of the output voltage and current of the inverters coupled with LPF, the power calculations block is the same for all power units, as illustrated in Figure 3.12.

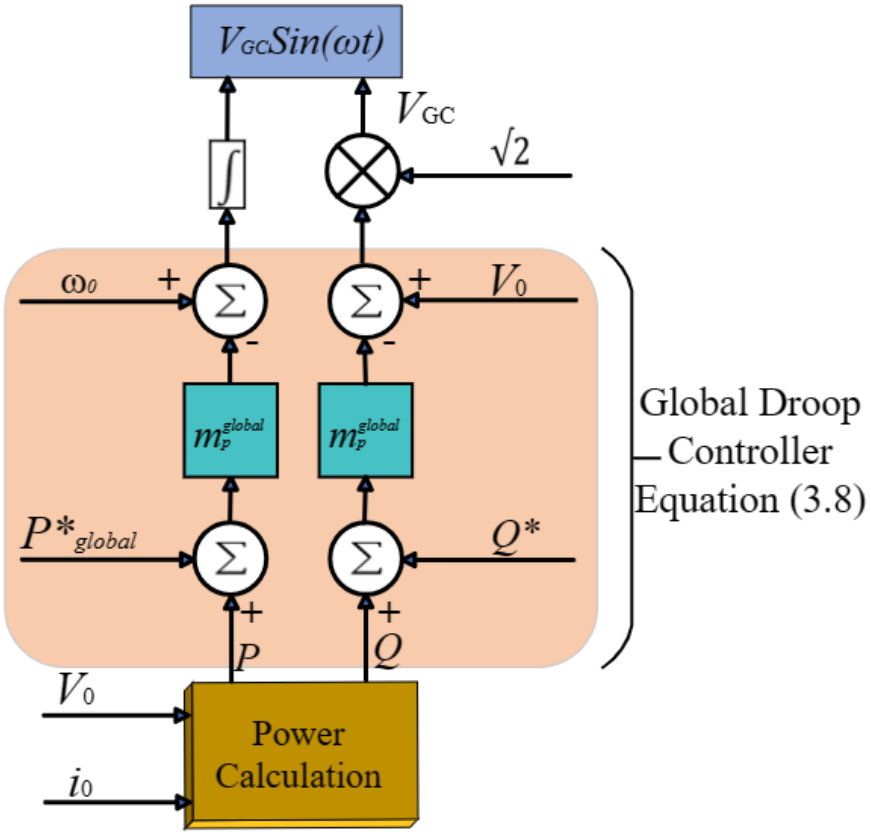

Figure 3.11: Global Droop Control of the Global Converter

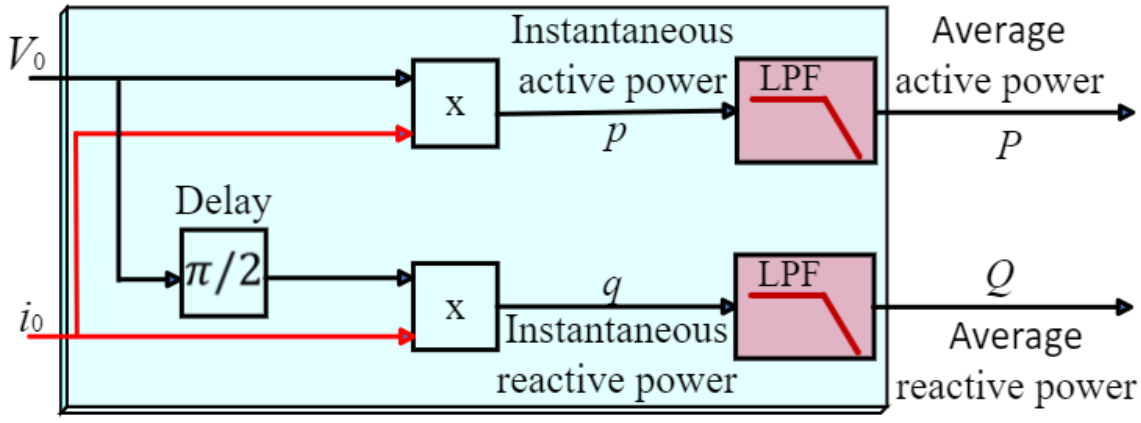

Figure 3.12: Power Calculation Block

3.5 Matlab/Simulink Simulation

3.5.1 Simulation Model

The proposed 3-phase detailed model and control of three standalone AC microgrid units interconnected to the MVAC bus with three back-to-back converters, as presented in Figure 3.2, have been designed and built in MATLAB/Simulink SimPower System. Each microgrid comprises three DG units (PV-based RES, BESS and auxiliary) and the local load. The microgrids are modelled as an ideal voltage source.

The detailed model, which includes all the power converters and all the physical elements, is very slow because all of its power electronics switches are included. Still, the microgrids are modelled and simplified as an ideal voltage source.

1. Each microgrid is modelled as a 3-phase ideal voltage source (a block) in Simulink and connected to a local load with appropriate parameters chosen from the literature as in [145].
2. Each 3-phase local and global converter with the LC filter has been modelled as an averaged model ideal converter. This average model is a block provided in Matlab/Simulink.

Figure 3.13 shows the block diagram representation of the detailed model of the proposed standalone interconnected AC microgrids, with each ideal voltage source connected to a local load used to represent each of the three microgrids and a global load. The global converter unit model is modelled as a controlled voltage source, as shown in Figure 3.14.

Each local connecting AC/DC power electronic converter is modelled as a DC voltage source circuit representing a $750V$ amplitude of rectified voltage, as shown in Figure 3.14.

Each global connecting DC/AC inverter is modelled as an averaged-model-based voltage source converter (VSC) representing the power electronic switches. Figure 3.14 illustrates a three-phase universal bridge block power converter comprising six insulated-gate bipolar transistors (IGBTs) or power switches connected in a bridge configuration. The DC link is represented by a capacitor (Cdc)

that runs parallel to the VSC. The DC link controller regulates the DC link voltage with a proportional-integral controller to keep the DC link voltage always controlled. It measures the reference value of the output voltage signal representing the average voltages generated at the universal bridge ABC terminals to generate the duty cycle for the inverter. The 3-phase series RL branch, which corresponds to the output impedance of the DC/AC inverter, is connected to the ABC terminals of the bridge.

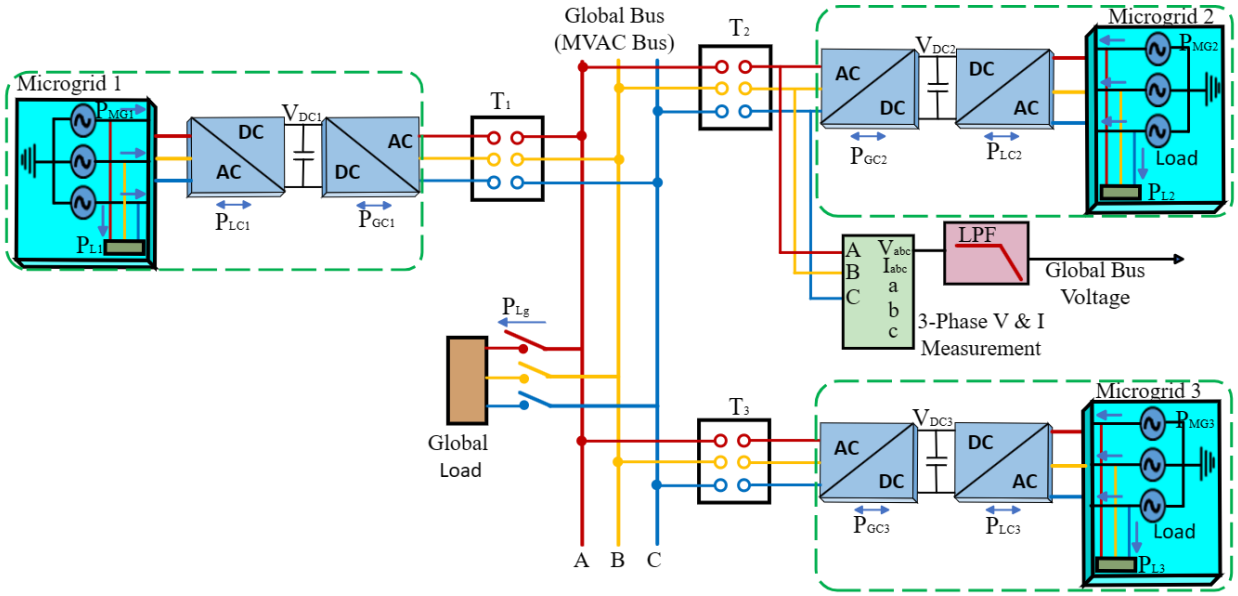

Figure 3.13: Detailed Model of the Proposed Standalone Interconnected Microgrids

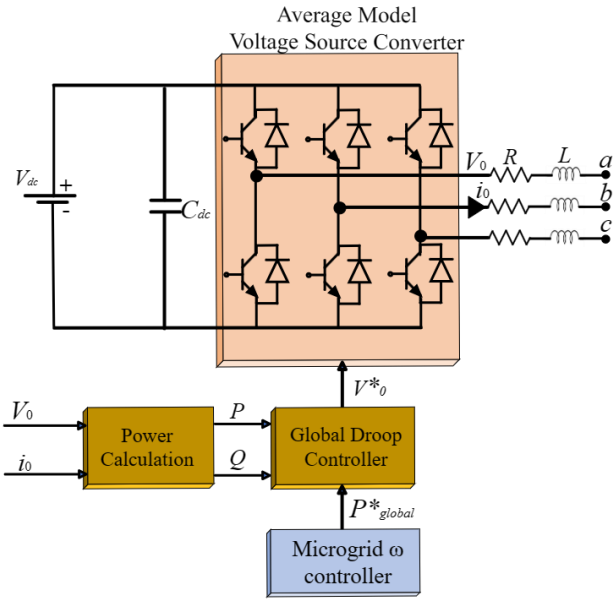

Figure 3.14: Average VSC Model and Global Control Loop

Table 3.1 displays the system parameters that were used in the simulation.

The simulation results are described in two cases, as shown together with the global droop control loop in Figure 3.15.

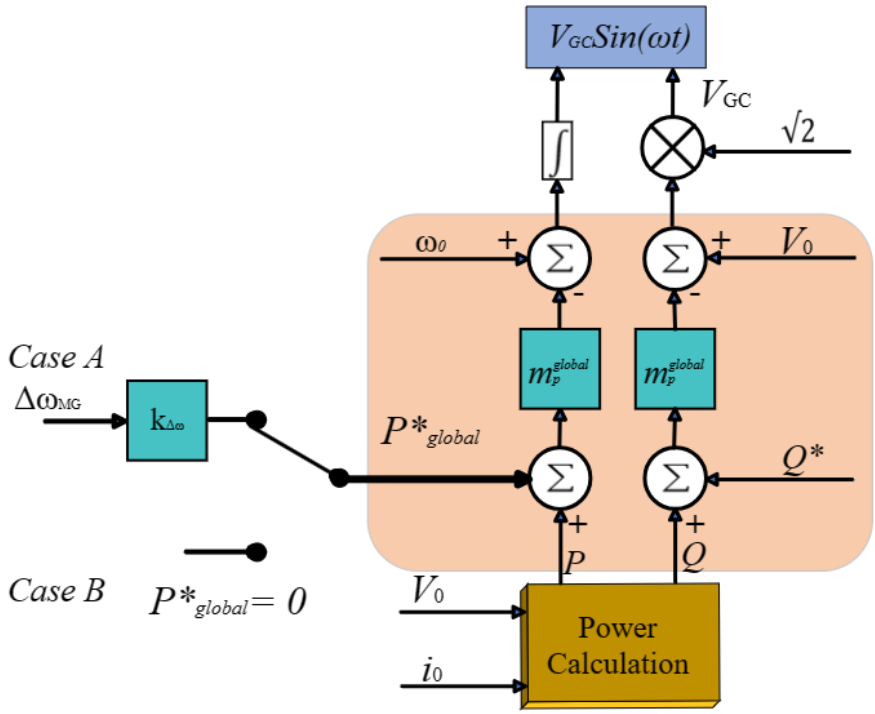

Figure 3.15: Cases A and B with the Global Droop Control Loop

A) The interconnected standalone AC microgrid operates with the power-sharing capability to complement each other in the network, the proportional controller determines the power demand of the global droop controller.

B) The interconnected network operates with no power-sharing capability, when the global power demand is set to zero.

Table 3.1. System Parameters

Parameter	Symbol	Value
Nominal bus frequency	$\omega_0 = 2\pi f_0$	314 rad/s
Nominal bus voltage	V_0	230V
Nominal DC-link voltage	V_{dc}	750V
DC link voltage P-controller gain	k_{p_dc}	20
DC voltage I – controller gain	k_{i_dc}	60

DC link capacitor	C_{dc}	1200μF
Active power droop coefficient	m_p^{global}	0.9e-4 rad/s/W
Reactive power droop coefficient	n	0.9e-4 V/Var
Frequency deviation gain	$k_{\Delta\omega}$	30000

3.5.2 Simulation Results

Case A: Proportional control with power exchange capability

This case describes the simulation results when microgrids one and three operate to meet the respective local load of 30*kW* and within the nominal frequency of 50*Hz,* which indicates a surplus of power in both microgrids. Microgrid two runs at a deficient load of about 22*kW*, reflecting a deviation in frequency of 49.80*Hz*, indicating a power shortage of 8*kW*. Figure 3.16 shows the power output and demand of three microgrids together with the connecting converters, frequencies and DC link voltages. Figure 3.16(a) shows that microgrid one operates to meet its local load demand of 30*kW* and also exports its surplus power of about 4*kW* via its global converters (MG1 GC) through the MG2 GC and MG2 LC to supplement part of the deficient power in microgrid two equitably. However, Figure 3.16(b) shows that microgrid two has a power shortage of 8*kW,* which reflects a deviation in frequency of 49.80*Hz*, as seen in Figure 3.16(d). Also, Figure 3.16(c) shows that microgrid three operates to meet its load demand of 30*kW* and also exports its surplus power of about 4*kW* equitably via its global converters (MG3 GC) through the MG2 GC and MG2 LC to supplement part of the deficient power in microgrid two equitably. It can be shown from Figure 3.16(b) that microgrid two MG2 GC and MG2 LC indicates a power import of 8*kW* from the global bus, which is equivalent to the amount of power shortage. Figure 3.16(d) shows that microgrids one and two operate at a nominal frequency of 50*Hz*, and the global bus frequency automatically adjusts its frequency to 49.94*Hz* to keep the interconnected network balanced. Figure 3.16(e) shows that the DC link voltage of microgrids one and three settled to its steady state at about 1 *Sec* while that of microgrid two reached its steady state value of 750*V* at about 1.5 *Secs*.

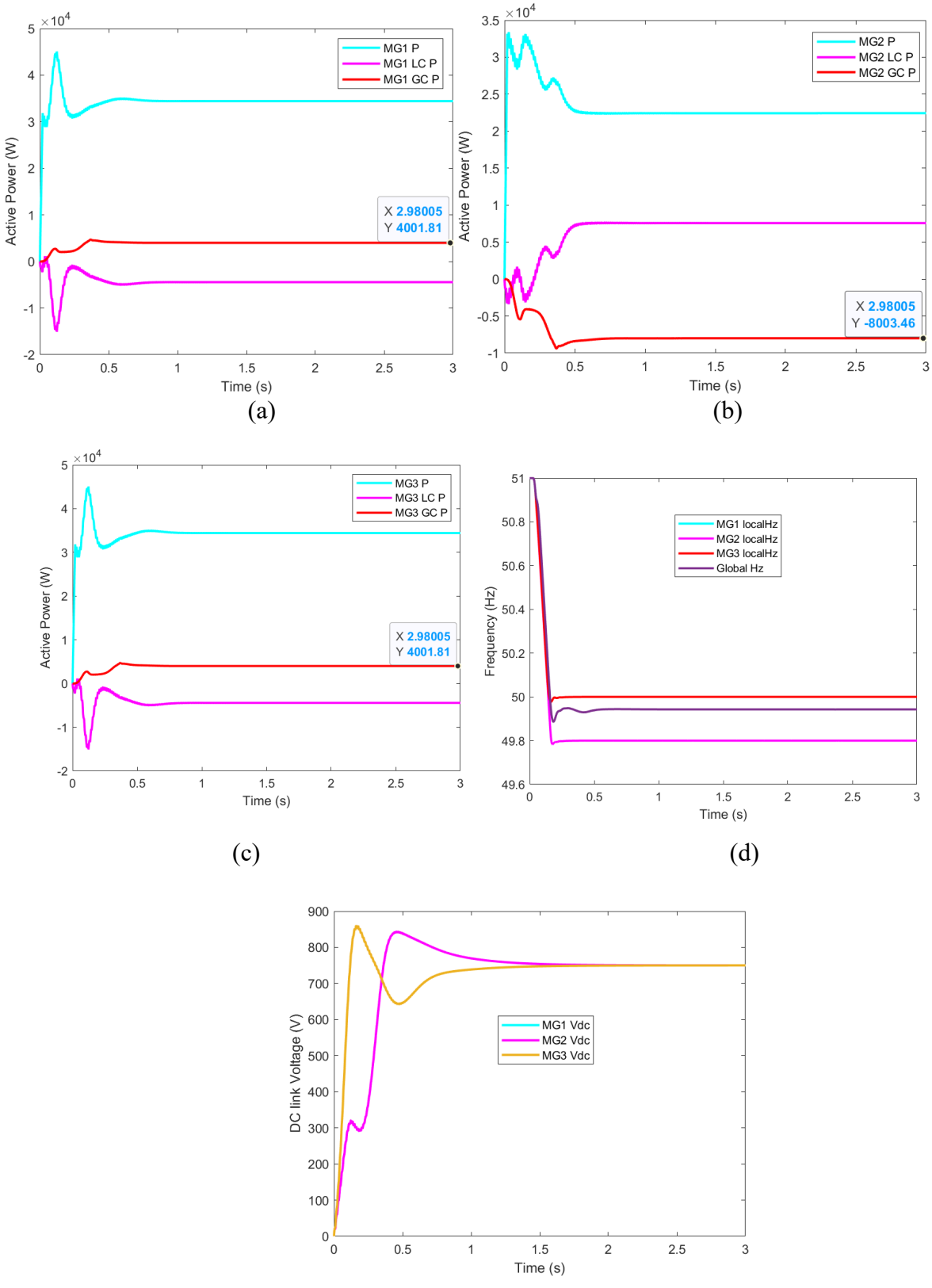

Figure 3.16: Output responses when interconnected islanded microgrids one and three are operated within the nominal frequency of 50*Hz* and microgrid two at 49.80*Hz*: (a) Output power and demand

of microgrid one (b) Output power and demand of microgrid two (c) Output power and demand of microgrid three (d) Frequencies and (e) DC link voltages

Case B: Global power demand is set to zero with no power exchange capability

This case demonstrates the simulation results when the standalone interconnected microgrid operates with no power-exchange capability and the global power demand is zero. Each of the three interconnected microgrids operates at a load of $40kW$ and a nominal frequency of $50Hz$, and microgrid two has a power deficiency that reflects a deviation in frequency to $49.8Hz$. Figure 3.17 shows the power output and demand of the three microgrids together with the connecting converters, frequencies and DC link voltages. The simulation results of Figure 3.17(a) – (c) show that there is no power export or import in the different local and global converters of the interconnected islanded microgrid network even at a deviation of frequency below nominal at $49.80Hz$ of microgrid two as shown in Figure 3.17(d). Each microgrid operates independently to manage its loads; the global frequency remains at $50Hz$. However, each microgrid's local converter (LC) and global converter (GC) output power remain at $0kW$, indicating no power (P) exchange. Figure 3.17(e) shows that the DC link voltage of the connecting converters reaches its steady state value of $750V$ at about 2.5 Secs. The 2.5-second delay is due to the imbalance in the network, and the system takes longer to adjust to its steady state.

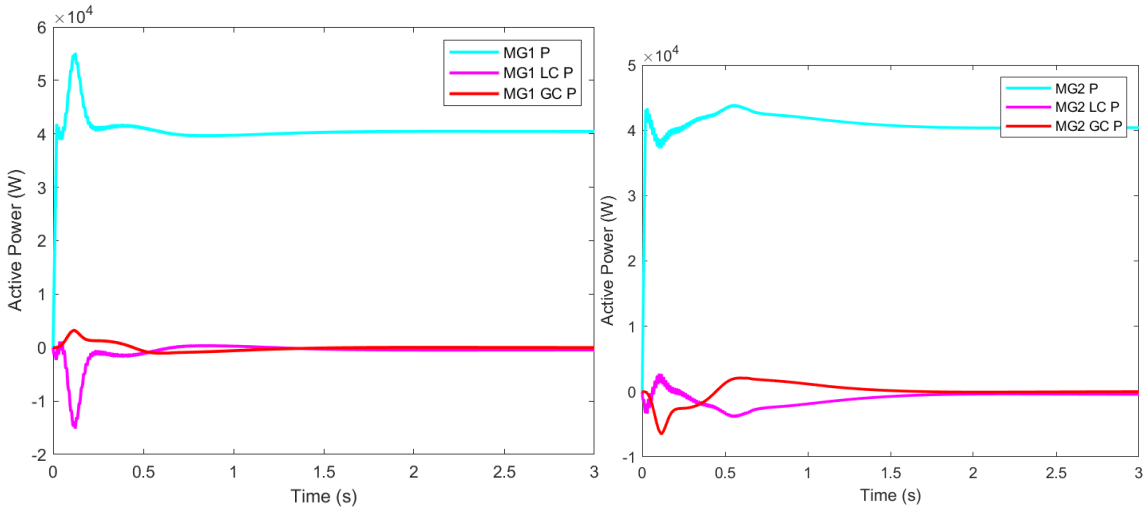

(a) (b)

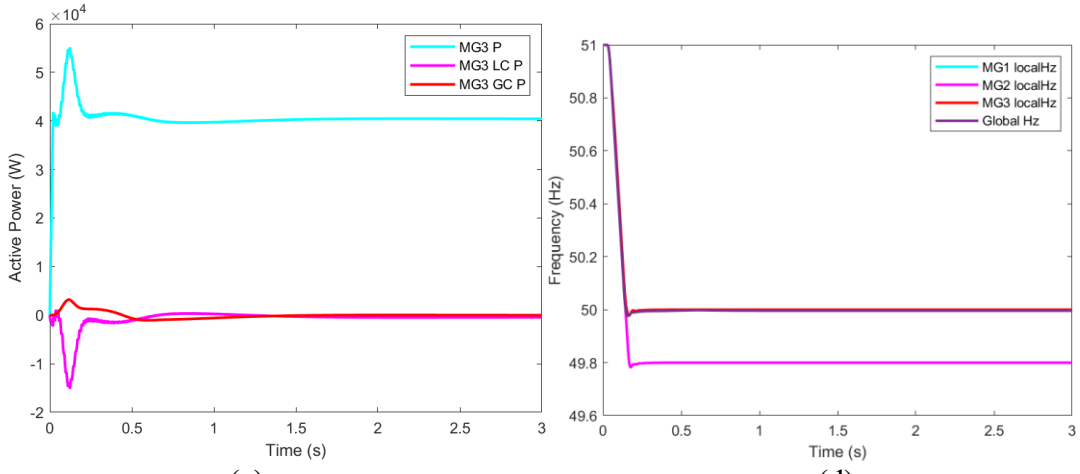

(c) (d)

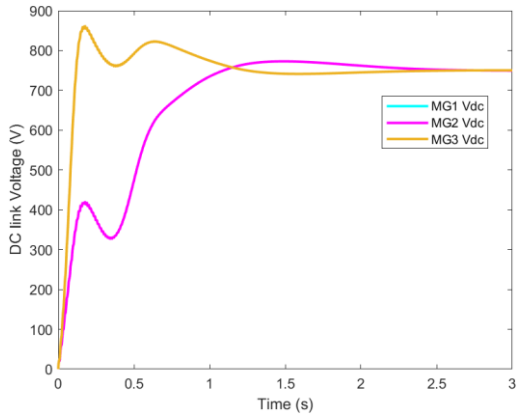

(e)

Figure 3.17: Output responses when power demand is set to zero and microgrids one and three are operated within nominal frequency of 50*Hz* and microgrid two at 49.80*Hz*: (a) Output power and demand of microgrid one (b) Output power and demand of microgrid two (c) Output power and demand of microgrid three (d) Frequencies and (e) DC link voltages

Table 3.2 Summary of the global droop control with the power setpoints.

Table 3.2 Global Droop Control and Power Setpoints

	MG1	**MG2**	**MG3**
P_L (*kW*)	30	22	30
Frequency (*Hz*)	50	49.8	50
P^*_{global} (*kW*) (Proportional Control)	+4	-8	+4
P^*_{global}(*kW*) (PI Control)	0	0	0

MG1 – Microgrid one.
MG2 – Microgrid two.
MG3 – Microgrid three.

3.6. Summary

This chapter proposed and examined a new structure for interconnecting AC microgrids. Each microgrid is interfaced with a back-to-back converter to decouple the microgrid frequency from the MVAC bus. The microgrid side local converter controls the DC link voltage, setting the power demand for the local converter droop control loop. In contrast, the global converter controls the amount of power exchange. Furthermore, the chapter proposed a global droop control strategy based on a frequency signalling technique to control the MVAC bus collectively. This chapter presented an overview of typical grid-connected interconnected AC microgrids and described their operation in standalone and grid-connected modes, as well as their various control strategies. It also examined the two major control techniques, communication-based and non-communication-based control, which gave rise to droop control for control of interconnected microgrids. This chapter discussed the droop control strategy in detail and further presented the global droop control that is applied to the connecting interfaces for the exchange of power in a standalone interconnected microgrid system.

The interconnected microgrid structure uses traditional power transformers to transmit power over long distances and form an efficient and robust network. The global connecting converters and associated global controllers ensure that power leaves the microgrid with a surplus to the microgrid with a deficiency in power and vice versa to keep the interconnected standalone microgrid network balanced. The local converters' DC link voltage is maintained within the limit. However, the controllers use local measurements without direct communication between the individual microgrid buses. This chapter also covered a Matlab/Simulink simulation model, and results are presented to validate the performance of the network structure and proposed controller operation. In conclusion, based on a frequency signalling technique, the proposed interconnected microgrid exchange power among themselves to keep balance in the microgrid networks and proportional control is used to achieve that. When the power demand of the global converter is set to zero, the interconnected microgrid independently operates on its own with no power exchange, even at a deviation in the frequency of

microgrid two. The DC link voltage of all the local converters is controlled and maintained within the limit.

CHAPTER 4: DECENTRALISED CONTROLLER FOR POWER FLOW MANAGEMENT IN INTERCONNECTED MICROGRIDS

4.1 Introduction

This chapter proposes a decentralised control scheme for the interconnected structure presented in Chapter 3. Renewable power curtailment and auxiliary power supplement mechanisms are designed based on the bus frequency signalling technique to achieve balance and continuity of supply. In case of power shortage in one microgrid, priority will first be given to power import from other microgrids. If the power imported is not enough to control the battery SOC, then a power supplement is used. Similarly, in case of a power surplus, priority will be given to power export, and if this is not enough, power from RES will be curtailed. Performance evaluation shows that the proposed controller maximises renewable power utilisation and minimises auxiliary power usage while providing better load support. The performance validation of the proposed structure and control strategy has been tested using MATLAB/Simulink.

4.2 Simplified Model of Interconnected Microgrids

The interconnected standalone AC microgrids presented in Chapter 3, section 3.5.1, are based on a detailed model of the back-to-back converter in addition to ideal sources to represent the microgrid. This chapter develops a simple power flow model considering the droop control level equations, battery capacity and steady-state power balance equations between the interconnected microgrids. Analytical equations are created for three interconnected microgrids to relate the actual active power flow with respect to the power demands at a steady state.

The interconnected standalone AC microgrid system has been modelled, and a series of aggregated PV-based RES and load profiles have been used to obtain detailed simulation results to compare the performance of the controllers when the individual microgrids are operated individually and when they are interconnected and operated with the proposed global droop controller with and without a load connected to the global bus. The profiles used consider PV-based RES fluctuation, and the load

condition changes over the set time. Hence, there is a crucial need to design a time-responsive and effective controller to manage the power flow into and out of the interconnected microgrid global bus. The load at the global bus also varies; therefore, the amount of power required to supply the load at the global bus is not fixed. Similarly, the frequency varies with the SOC, and the amount of power used to charge the battery at each instant varies, and it keeps changing as the system maintains its balance at the global bus. Therefore, a highly responsive proportional change between the microgrid AC bus frequency and active power is required to achieve and maintain balance at the global bus. The real power droop control uses a pure proportional controller and is not proportional-integral for the global inverter because the global power demand is not fixed; hence, there's no reference power. The power set-point/reference is determined according to the deviation of the microgrid frequency. This causes the power exchange to be according to the available power of each microgrid. The simulation case scenarios are evaluated to assess the performance of the proposed global droop controller in ensuring the frequency at the global bus is operated within its limits and also prevents the battery SOC and charging/discharging power from exceeding their limits irrespective of the variations in load and changing conditions of the power from the PV-based RES. The simulation results show that the proposed global droop controller effectively controls the interconnected standalone AC microgrids and exchanges the required amount of power between connected microgrids in compliance with the acceptable frequency limits and designed limits of the battery SOC.

4.2.1. Power Balance Equations

Figure 4.1 illustrates the power flow at the global bus network. The figure shows that individual networked microgrids have back-to-back converters. Each microgrid can have its particular bus frequencies (ω) and their respective SOC of the BESS. The global load (P_L) is connected to the global bus, and each microgrid can produce its power, meet its load demands and exchange power when necessary. The amount of power injected into the global bus is determined by balancing the total power

produced and consumed by the load in the individual units of the interconnected multiple AC microgrids.

Considering the power balance of the standalone interconnected multiple AC microgrids, if none of the microgrids has a power shortage or surplus, this implies that all available power from RES meets the load demand, indicating that there will be no need to exchange power. The varying load at the global bus will be shared among the interconnected microgrids.

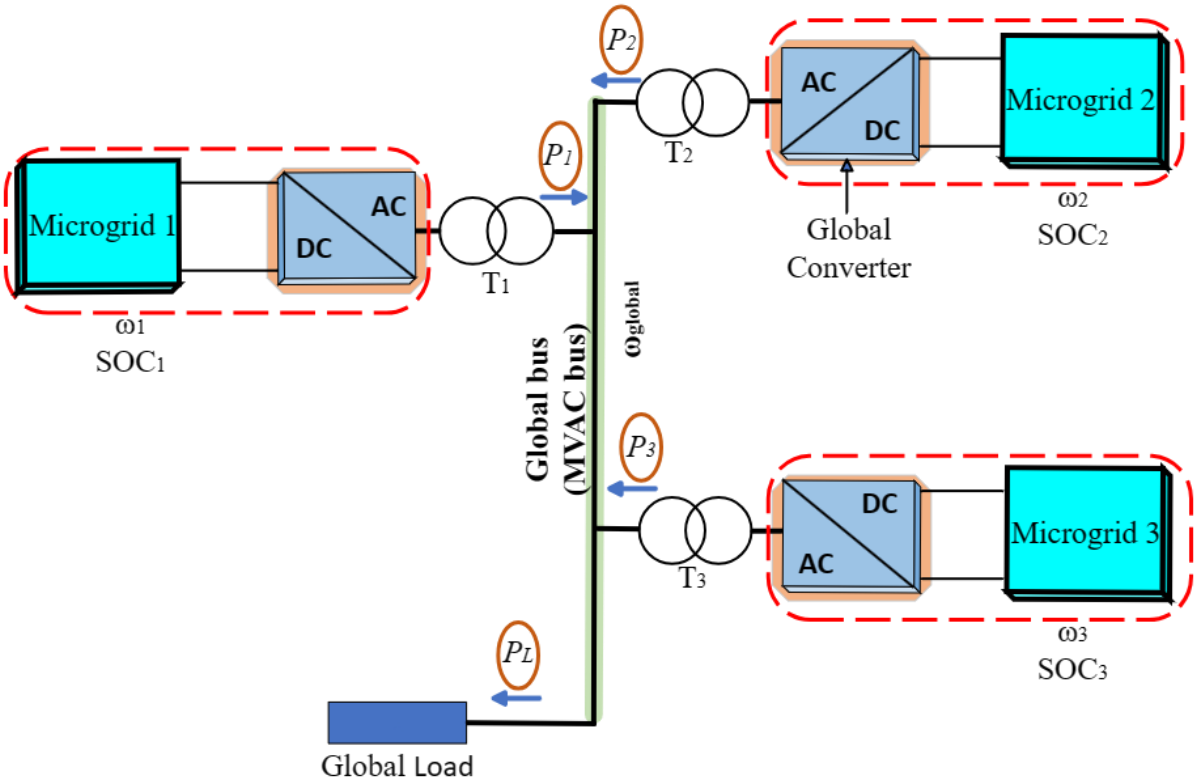

Figure 4.1: Power Flow in the Global Network

Considering the illustrative power flow network diagram in Figure 4.1, the power balance equation at the global bus can be described as shown in the equation (4.1).

$$P_L = P_1 + P_2 + P_3 \qquad (4.1)$$

where P_L is the global load, while $P_1, P_2,$ and P_3 is the power exchange from the individual microgrids.

Therefore, during the standalone mode operation of the individual microgrids where the battery is the grid-forming unit, the battery power (P_{batt}) can be defined as in equation (4.2).

$$P_{batt} = P_{pv} + P_{aux} - P_L \pm P_{exp/imp} \quad (4.2)$$

where P_{pv} is the power from the PV-based RES, P_{aux} the power from the auxiliary unit, P_L the supply to the microgrid load, $-P_{exp}$ the power export, $+P_{imp}$ the power import.

4.2.2. Control Strategies of Different Components

Traditional droop control is used for all DC/AC converters. The conventional active Power-frequency $(P - \omega)$ and reactive power-voltage $(Q - V)$ droop control defined by Equation (4.3) are employed in all DC/AC converters. The primary controller in the active power droop strategy mimics the behaviour of the synchronous generator in terms of decreasing the frequency when the active power is increased and vice versa, as detailed in [11], [16], [26], [146].

$$\begin{aligned} \omega &= \omega_0 - m(P - P^*) \\ V &= V_0 - n(Q - Q^*), \end{aligned} \quad (4.3)$$

Where ω, V, ω_0, m, *and* n represents the output frequency, the voltage amplitude, the nominal frequency, the nominal voltage, the frequency droop coefficient, and the voltage droop coefficient, respectively. Here, P and are the measured active and reactive power, while P^* and Q^* are active and reactive power setpoints, respectively.

4.2.2.1. Control of the BESS

The battery power is given in equation (4.2), and the battery power (P_{batt}) is modelled as a function of the estimated state of charge (SOC), which is calculated based on the coulomb counting principle, as shown in Figure 4.2 [3]–[5].

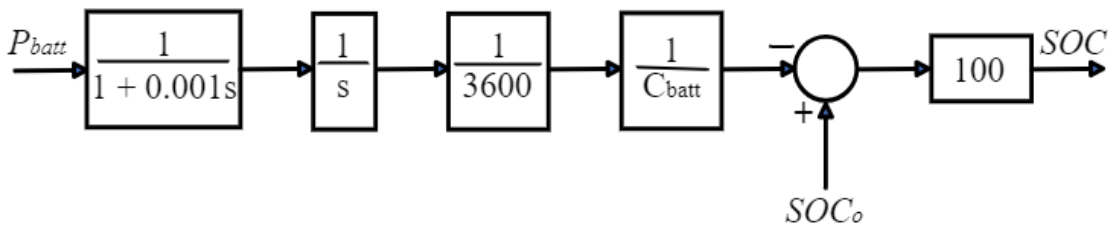

Figure 4.2: Figure 4.2: SOC Calculation Block

where SOC_0 is the initial value of SOC, and the battery's capacity is represented in ampere-hour (Ah). 1Ah represents 3600 coulombs, there are 3600 seconds in 1hour, and V_{batt} is the battery voltage in Volts. The SOC computation block is similar to a low pass filter, where 's' stands for the Laplace operator. It is just necessary to employ (LPF) with a small time constant since the current is moving quickly, and SOC is moving slowly. Therefore, the LPF filters out high frequencies and slows the response of the battery SOC. The SOC of each microgrid is directly proportional to deviation in frequency $\left(SOC \to \Delta\omega\right)$. Hence, the control strategies equations can be described in tandem with Figures 4.3(a-f), which illustrates the SOC—frequency deviation control curves and power–frequency deviation droop control curves at various positions of the bus frequency. However, the frequency varies with the battery SOC as a signalling mechanism to control the other units in the system. The output frequency (ω) of the BESS unit is given in equation (4.4).

$$\omega = \omega_0 \pm \Delta\omega \tag{4.4}$$

The SOC determines the deviation in frequency $(\Delta\omega)$, as illustrated in Figure 4.3a. When the SOC is between SOC_{low} and SOC_{high}, the frequency deviation $\Delta\omega = 0$ and the system is balanced. During this period, there is no need for power export, import, curtailment, or supplement. As the SOC increases, the frequency deviation increases until the SOC reaches $SOC_{\max}$ where $\Delta\omega$ it saturates. A similar trend exists for low SOC when $\omega_0 < \omega < \omega_{high}$ the microgrid should export power to the rest of the system but with no curtailment of the PV power. During further frequency deviation between

the regions, $\omega_{high} < \omega < \omega_{max}$ the microgrid should curtail PV and export power to the rest of the network. Alternatively, as the SOC decreases, the frequency deviation increases in the opposite negative sense until the SOC reaches SOC_{min}, when $\omega_{low} < \omega < \omega_0$ the microgrid should import power from the rest of the network but with no supplement from the auxiliary unit. Furthermore, when $\omega_{min} < \omega < \omega_{low}$ the auxiliary unit should supplement the microgrid power and import power from the global network.

4.2.2.2. Control of the Solar PV

The PV unit will produce the maximum possible power, which is largely dependent on the MPPT and solar irradiance as far as the microgrid bus frequency deviation is less than frequency high $\omega < \omega_{high}$. Suppose that the microgrid frequency, as dictated by the BESS, deviated from its nominal value $\omega \neq \omega_0$ during steady state; the frequency of the PV inverter should also be ω. According to [6], the PV power P_{pv} is given by the expression in the equation (4.5).

$$P_{pv} = P_{pv}^{*} + \frac{\omega_0 - \omega}{m_p^{pv}} \tag{4.5}$$

The PV power (P_{pv}) will differ from the power setpoint (P_{pv}^{*}) depending on how much the frequency deviates from its nominal value. The droop control can be modified to become a proportional-integral (PI) controller, as shown in the equation (4.6). Therefore, to ensure that the power is the same as that of the setpoint, the droop control equation is given as:

$$\omega = \omega_o - \left(m_p^{pv} + \frac{m_i^{pv}}{s} \right) \left(P_{pv} - P_{pv}^{*} \right), \tag{4.6}$$

where m_p^{pv} is the proportional droop control coefficient, and m_i^{pv} is the integral droop control coefficient, and P_{pv}^{*} is the maximum power point $(P_{pv}^{*} = P_{MPPT})$. The integral term will raise or lower

the droop control curve depending on the microgrid frequency. In Figure 4.3b, $\omega = \omega_o$ the PV power equals that of MPPT i.e. $P_{pv} = P_{MPPT}$. In Figure 4.3c, the BESS bus frequency is increased, such as $\omega_o < \omega < \omega_{high}$. This is the region where the microgrid should export power and does not curtail the PV power. Therefore, the PI controller of the PV raises the droop curve (when compared to that of Figure 4.3b), so the PV MPPT is maintained. In Figure 4.3d, the microgrid frequency is pushed higher, such as $\omega_{high} < \omega < \omega_{max}$. In this area, the microgrid should export power and curtail its PV output as described in equation (4.7) at $\omega > \omega_{high}$. The droop control becomes proportional only; the more the frequency increases, the less PV power is generated. When the frequency is $\omega = \omega_{max}$, PV power becomes zero. This can be described as:

$$\begin{aligned} \omega &= \omega_{max} - m_p^{pv} P_{pv}, && \text{for } \omega > \omega_{high}, \\ \omega &= \omega_o - \left(m_p^{pv} + \frac{m_i^{pv}}{s} \right) \left(P_{pv} - P_{MPPT} \right) && \text{for } \omega < \omega_{high}. \end{aligned} \tag{4.7}$$

4.2.2.3. Control of the Auxiliary Unit

The purpose of the auxiliary unit is only to supplement power (produce power) whenever the SOC is low, and the frequency is below ω_{low}, as illustrated in Figure 4.3f, and import power from the rest of the network is insufficient. A fuel cell or micro gas turbine could power the auxiliary unit, and there is no need for the unit to run unless the SOC and frequency start to go low. However, once the system is running, it should produce zero power, but it should only produce power if the frequency is below, ω_{low} as illustrated in Figure 4.3f. Otherwise, it should produce zero power, as in Figure 4.3e. This can be achieved by using a PI controller if the frequency is higher than ω_{low} as shown in the equation (4.8).

$$\begin{aligned} \omega &= \omega_{low} - \left(m_p^{aux} + \frac{m_i^{aux}}{s} \right) P_{aux} && \text{for } \omega > \omega_{low}, \\ \omega &= \omega_{low} - m_p^{aux} P_{aux} && \text{for } \omega < \omega_{low}. \end{aligned} \tag{4.8}$$

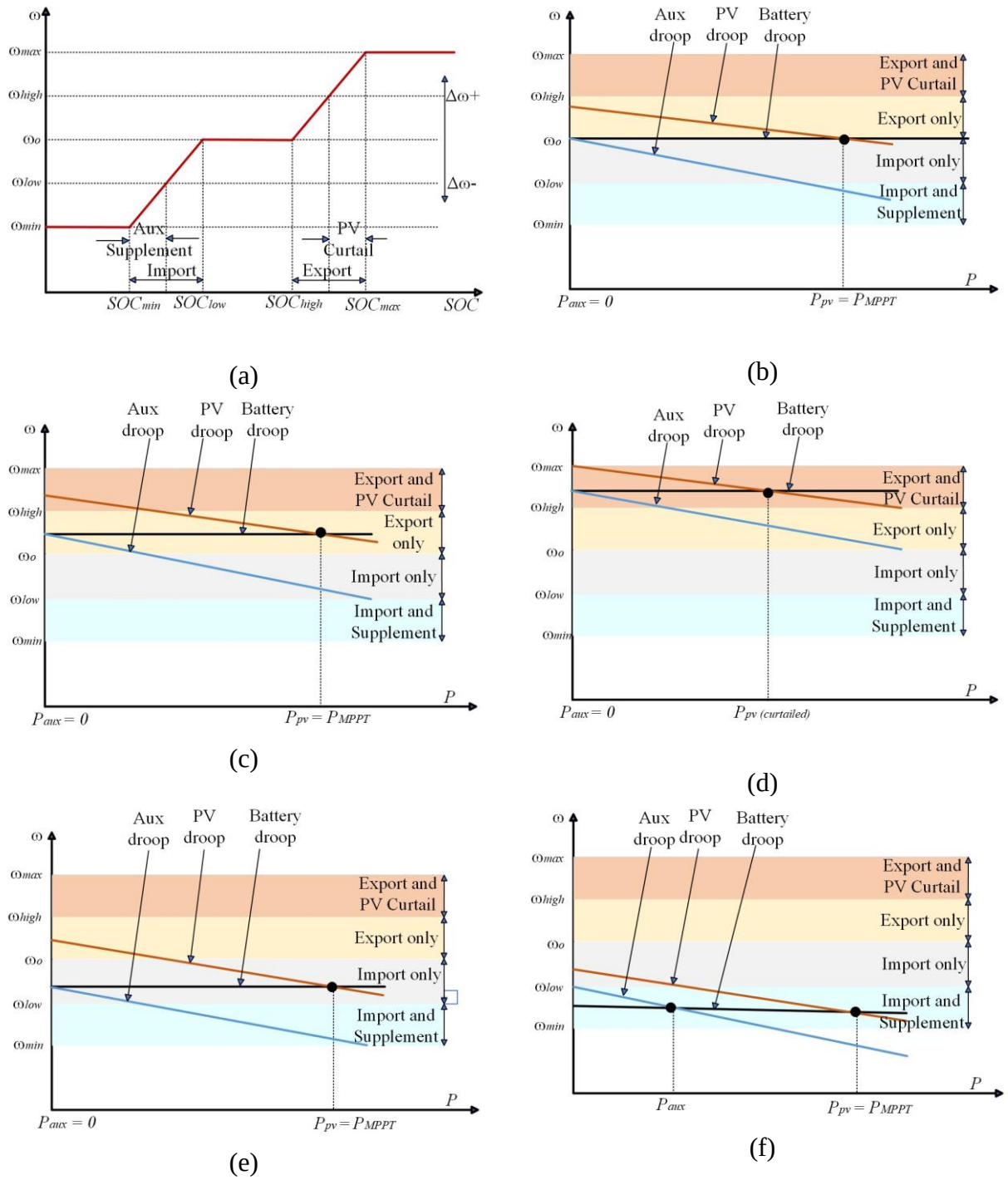

Figure 4.3: SOC, power–frequency deviation control curves. (a). SOC—frequency deviation control curve, power–frequency deviation droop control curves at (b). $\omega = \omega_o$, (c). $\omega_o < \omega < \omega_{high}$, (d). $\omega_{high} < \omega < \omega_{max}$, (e). $\omega > \omega_{low}$, (f). $\omega < \omega_{low}$.

4.2.2.4. Control of the Interconnecting Back-to-Back Converter

The global inverters are set to operate in droop control with their power setpoints set according to their microgrid battery SOC. To have a balanced system with no control signals between the microgrids, no integral term should be used in the droop control. If an integral term is used, the power output from the global inverter (power export/import from the microgrid) must equal the power setpoint. A decentralised controller must collectively determine these setpoints to have a balanced system. However, if a proportional controller is used, then an increase in the power setpoint will increase the power export.

However, the amount of power exchange will depend on the power setpoints of the other global inverters and the load connected to the global bus. The total power the load dissipates should equal the output power exported by the multiple global converters. Therefore, the equation described in (4.1) can be rewritten as shown in equation (4.9):

$$P_L = \sum_{i=1}^{N} P_{\text{exp},i} \tag{4.9}$$

At steady state, all connecting global converters must operate at the same bus frequency. Assuming that all global converters have the same droop coefficient, the global frequency is given in equation (4.10):

$$\omega_{global} = \omega_o - \frac{m_p^{global}}{N} \sum_{i=1}^{N} \left(P_{\text{exp},i} - P_{\text{exp},i}^{*} \right) \tag{4.10}$$

where N is the total number of connecting global converters.

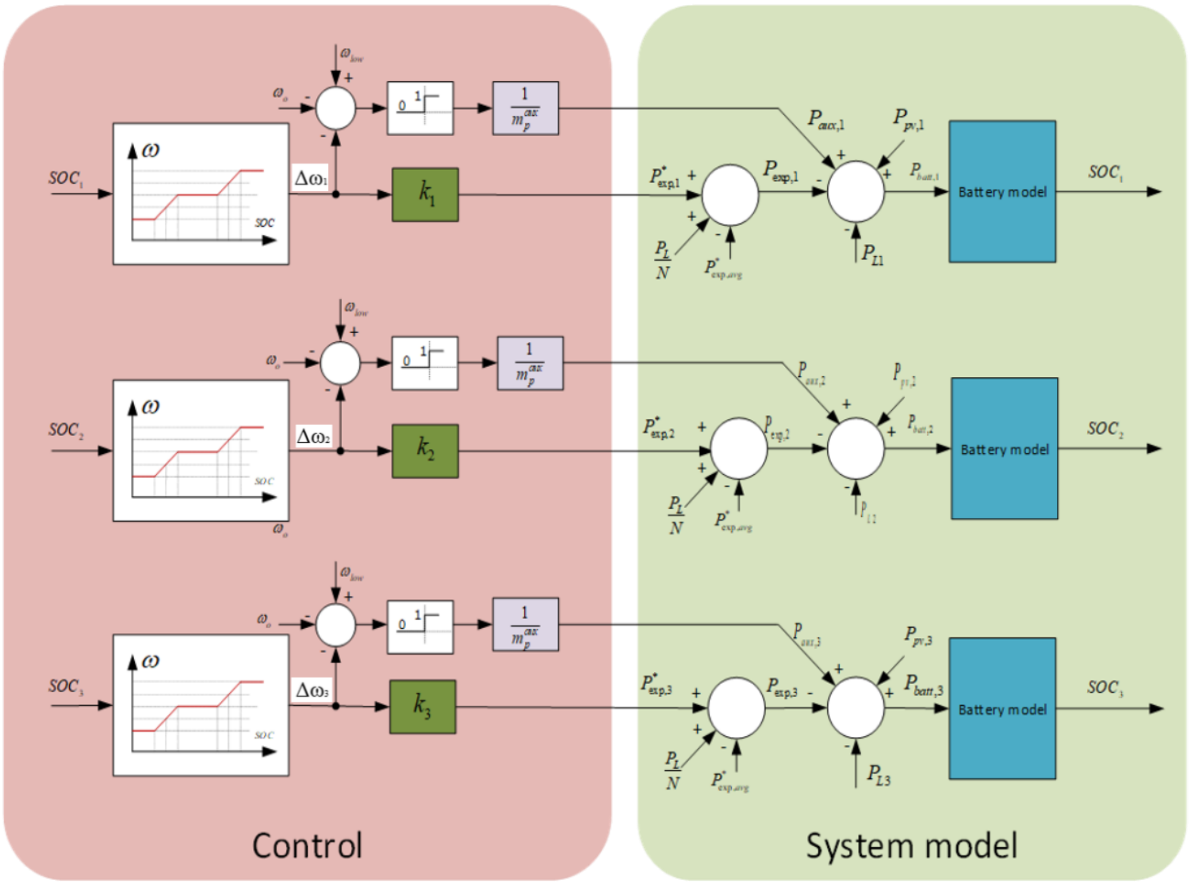

Figure 4.4: High-level control of multiple standalone interconnected microgrids

Substituting equation (4.9) into equation (4.10) gives equation (4.11):

$$\omega_{global} = \omega_o - \frac{m_p^{global}}{N}\left(P_L - \sum_{i=1}^{N} P^*_{\exp,i}\right) \tag{4.11}$$

Substituting equation (4.11) into the active power–frequency droop control equation (4.3) gives equation (4.12)

$$P_{\exp,i} = \frac{P_L}{N} + P^*_{\exp,i} - P^*_{\exp,avg}, \tag{4.12}$$

The expression in equation (4.12) shows that if all units have the same power setpoint, all units will supply the global load equally, and there will be no power exchange between the microgrids.

where,

$$P^{*}_{\exp,avg} = \frac{\sum_{i=1}^{N} P^{*}_{\exp,i}}{N} \tag{4.13}$$

It also shows that each unit will supply its portion of the global load plus a term equal to the difference between that unit's power setpoint $P^{*}_{\exp,i}$ and the average of all setpoints $\sum P^{*}_{\exp,i}$. Additionally, if the average of all setpoints is greater than $P_L/N + P^{*}_{\exp,i}$, the microgrid will import rather than export power. The above equations are represented in Figure 4.4, which shows the system model and its high-level controller. This model will be used for the simulation in the next section.

4.3 Simulations Results and Discussion

4.3.1 Step-Varying Simulation Results

The purpose of this short-varying simulation result is to assess the performance of the proposed global droop controller in managing the power flow between multiple interconnected standalone microgrids while maintaining the BESS SOC within their allowable limits. To adequately test the performance and examine the effect of the global droop controller, the controller is implemented on three interconnected standalone microgrids and its performance is compared with that of individually operated microgrids. Sudden step changes in PV-based RES and loads are applied to simulate various scenarios. The PV-based RES and load data step samples for this simulation case represent the maximum available RES and load demand. The overall aim is to apply the proposed controller to a few step data samples representing the maximum available RES power and load demand at the point through simulation studies to demonstrate that the proposed controller performs well within the given constraint. The performance is also tested with a global load connected to the global bus.

Here, the minimum SOC limit used for this step-varying simulation is 25% instead of 30%, while the low SOC limit also used for this test simulation is 35% instead of 40%. This is because the minimum SOC limit and low SOC limit are controller input parameters that the user can modify. Nevertheless, the dynamics of the results in terms of the proposed controller actions or outcomes are unaffected by this. It is expected that the performance of the proposed controller will demonstrate that the system operation is limited to the new modified values of the SOCs. Hence, the parameters of the system used in the simulation are listed in Table 4.1. At the same time, the simulation results of the interconnected standalone microgrids are compared with the case of individually operated microgrids. After that, interconnected microgrids are connected with the global load.

Table 4.1: System parameters used in the simulation

Parameter	Symbol	Value
Nominal bus frequency	$\omega_0 = 2\pi f_0$	314 rad/s
Battery capacity	$C_{bat1} = C_{bat2} = C_{bat3}$	240 kWh
Maximum SOC	SOC_{max}	100%
Minimum SOC	SOC_{min}	30% long-term simulation (25% Step-varying simulation)
Low SOC	SOC_{low}	40% long-term simulation 35% Step-varying simulation
High SOC	SOC_{high}	90%
Global drooping coefficient	m	1×10^{-4} rad/s/W
Maximum frequency deviation	$\Delta\omega_{max}$	1Hz
High-frequency deviation	$\Delta\omega_{high}$	0.1Hz
Global proportional gains	$k_1 = k_2 = k_3$	1000

From the simplified high-level control model, each microgrid operates within the nominal allowable frequency to meet the demand of its local load and exchange power only when needed. However, the test simulation results of the high-level control simulation model of multiple interconnected microgrids are shown in Figure 4.5 – 4.7.

Case 1: Individually Operated Microgrids with a Minimum SOC of 25% and Low SOC of 35%

Figure 4.5 shows the power output response of the PV-based RES and the curtailed RES, the auxiliary units, the load, and the SOC of three independently operated microgrids having a minimum SOC of 25% and a low SOC of 35%. Figure 4.5(i) shows the simulation results for microgrid one, which illustrates that the maximum available PV-based RES is $3.5kW$ while the maximum load demand is $1.5kW$. Due to the available surplus power from the PV-based RES unit in microgrid one, at all the step changes, the battery SOC goes up to its full limit and stays high, while the RES unit supplies its power to the load and curtails the RES. The auxiliary unit does not supply any power ($P_{aux1} = 0kW$) and remains on standby as the battery SOC reaches its full limit for the day. Figure 4.5(ii) shows the simulation result for microgrid two, which illustrates that the maximum step available power from the PV-based RES exceeds the load demand. The maximum available step PV-based RES is $4.5kW$, while the maximum step load demand is $2.5kW$. The auxiliary unit is on standby at $P_{aux2} = 0kW$ and does not supply any power as the battery SOC climbs to its full limit for the day. However, the load demand is met while the surplus RES power is curtailed in steps as the SOC rises to its full limit. Figure 4.5(iii) shows the simulation results for microgrid 3, indicating the maximum available step load demand exceeds the available PV-based RES power. The PV-based RES unit supplies its maximum available capacity to the load, which is insufficient to meet the load's demand. Due to the insufficient power from the PV-based RES to meet the load demand, the battery SOC goes down to about 32%, and the auxiliary unit supplies the power difference to meet the load demand. Notably, the auxiliary unit does not start until the battery SOC reaches its low limit of 32%. After that, the auxiliary unit starts to supply power to meet the load demand for the rest of the simulation time. The results illustrate that the SOC operated and maintained within its limits amidst the changing RES supply and load demand conditions.

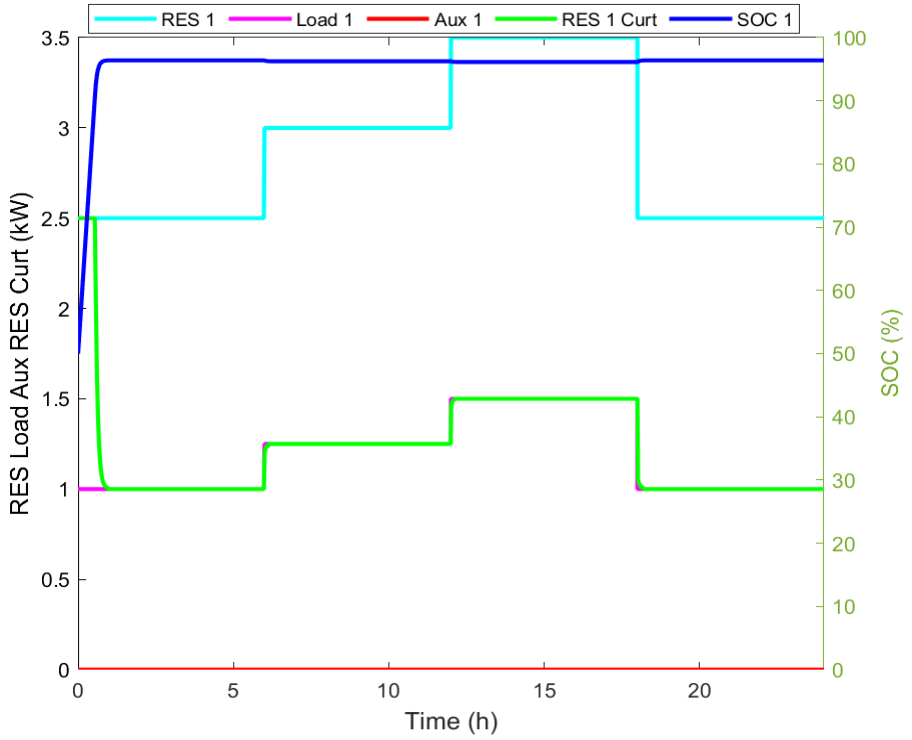
RES 1
Load 1
Aux 1
RES 1 Curt
SOC 1
RES Load Aux RES Curt (kW)
SOC (%)
Time (h)

(i)

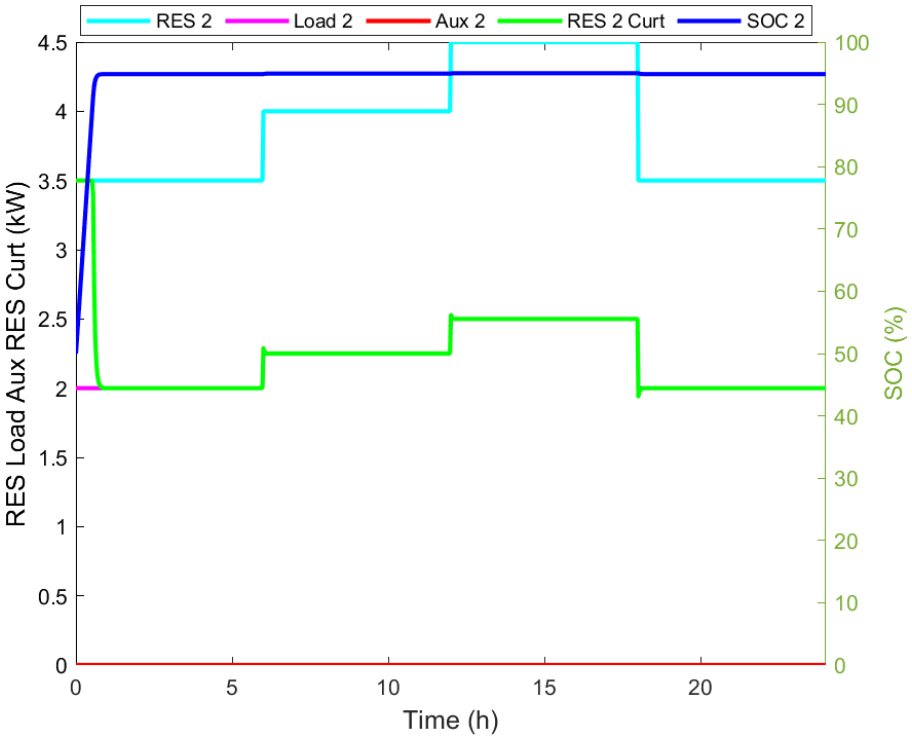
RES 2
Load 2
Aux 2
RES 2 Curt
SOC 2
RES Load Aux RES Curt (kW)
SOC (%)
Time (h)

(ii)

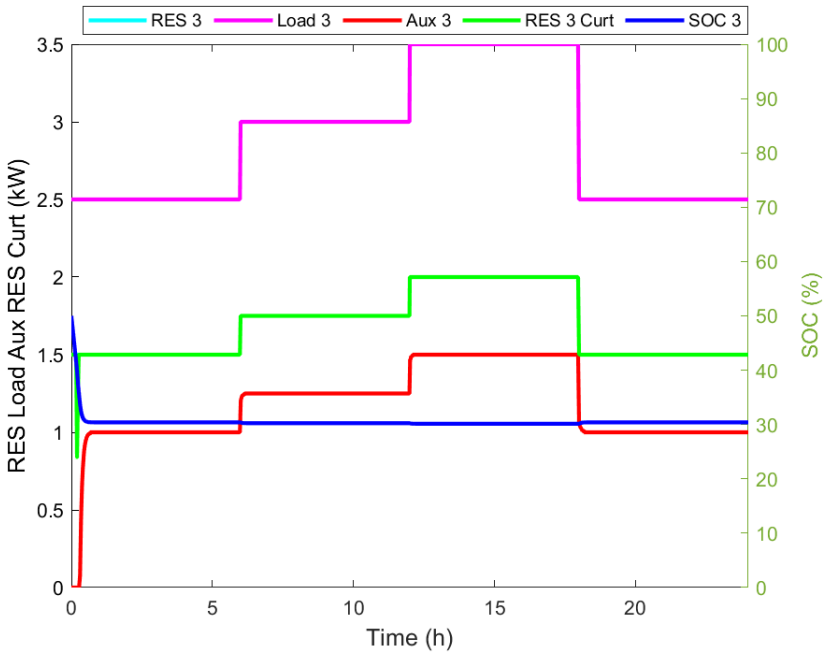

(iii)

Figure 4.5(i)-(iii): Output responses for multiple microgrids independently operated for a minimum SOC of 25% and low SOC of 35%: (i) microgrid one, (ii) microgrid two, (iii) microgrid three

Case 2: Multiple Interconnected Microgrids with the Proposed Controller

Figure 4.6 shows the power output response of the PV-based RES and the curtailed RES, the auxiliary units, the SOC, the load, and the power exported for microgrids one, two and three interconnected with the proposed global droop controller with a minimum SOC of 25% and low SOC of 35%. Figure 4.6(i) shows the simulation results for microgrid one, which illustrates that the maximum available step PV-based RES power is 3.5kW while the maximum step load demand is 1.5kW. Due to the available surplus power from the PV-based RES unit in microgrid one, the battery SOC goes up to its full limit throughout the simulation time at all the step changes. In contrast, the RES unit supplies its power in steps to meet the load demand, some of the available RES power is exported (P_1) and the surplus power from the PV-based RES is curtailed in steps. The auxiliary unit is on standby and does not supply any power ($P_{aux1} = 0kW$). It remains on standby as the battery SOC reaches its full limit for the day. Figure 4.6(ii) shows the simulation result for microgrid two, which illustrates that the maximum step available power from the PV-based RES is greater than the load demand. The maximum available step PV-based

RES is 4.5*kW,* while the maximum step load demand is 2.5*kW*. The auxiliary unit does not supply any power as the battery SOC reaches its full limit. The available RES power supplies to meet the load demand in steps; some of the PV power is exported via P_2, and the surplus power from the PV-based RES is curtailed in steps as the SOC stays at its full limit throughout the simulation time. Figure 4.6(iii) shows the simulation results for microgrid three, which indicates the maximum step load demand is greater than the available maximum step PV power. The PV-based RES unit supplies its maximum available capacity to the load ($P_{RES3} = P_{RES3\ Curtail}$), which is insufficient to meet the load demand. Due to the insufficient power from the PV-based RES to meet the load demand, the battery SOC goes down in steps to about 32%, RES power is imported into microgrid three via P_3, and the auxiliary unit supplies the power difference in steps to meet the load demand. The auxiliary unit starts to supply power to meet the load demand at the low limit of the battery SOC for the rest of the simulation time. Figure 4.6(iv) shows the frequency curves at the global bus, which illustrates that the frequency is operated and maintained within its operating limits irrespective of the surges in RES power and load demands. The results show that the SOC is maintained within its up and low limits irrespective of the step-change RES supply and load demand conditions.

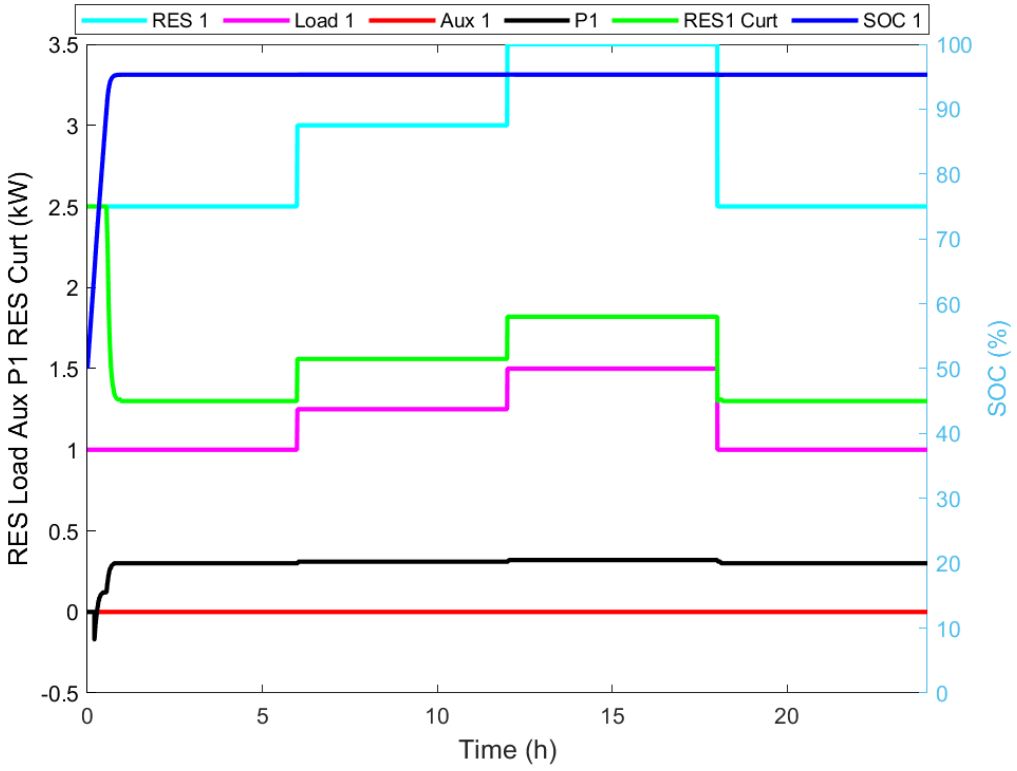
RES 1
Load 1
Aux 1
P1
RES1 Curt
SOC 1
RES Load Aux P1 RES Curt (kW)
SOC (%)
Time (h)

(i)

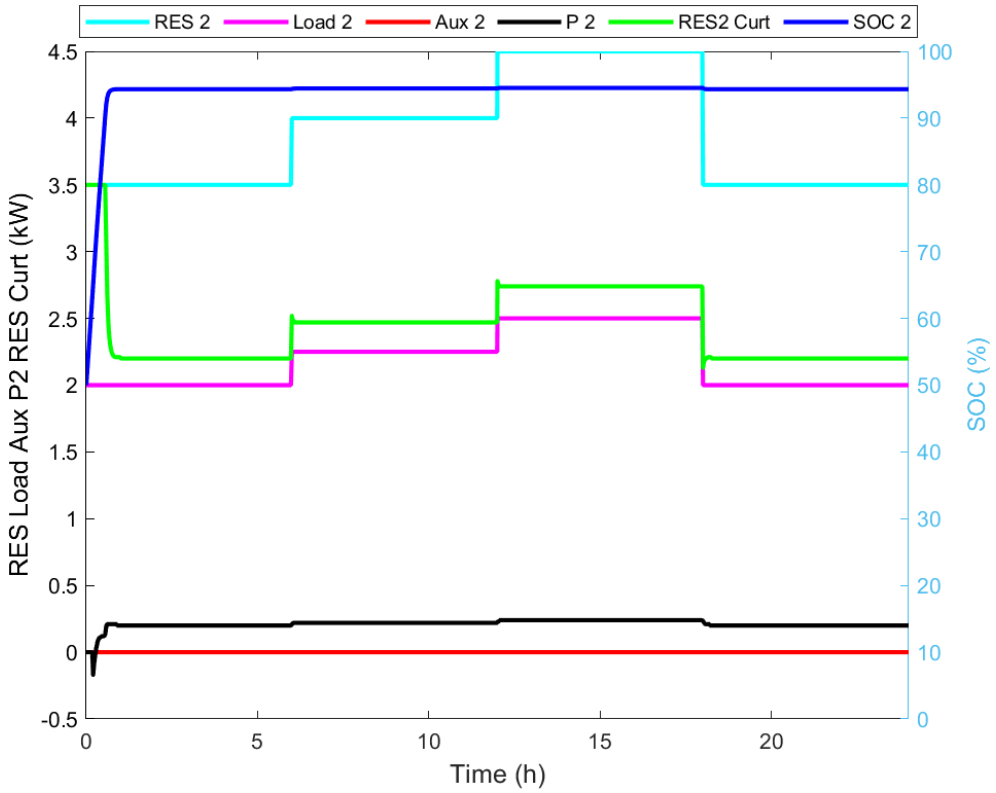
RES 2
Load 2
Aux 2
P 2
RES2 Curt
SOC 2
RES Load Aux P2 RES Curt (kW)
SOC (%)
Time (h)

(ii)

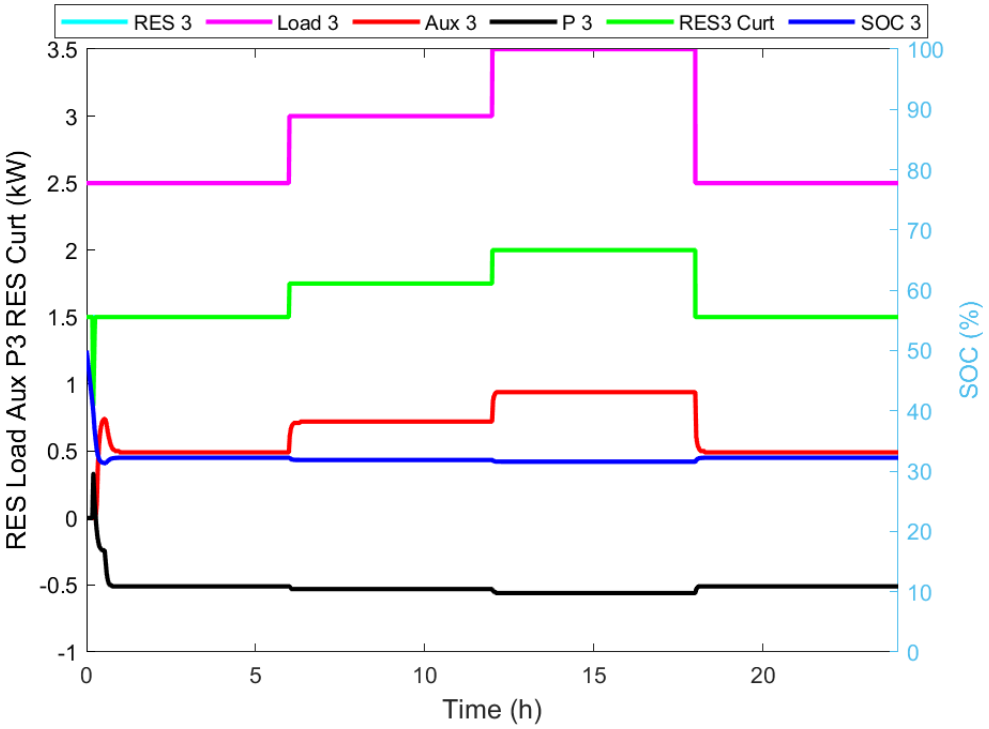

(iii)

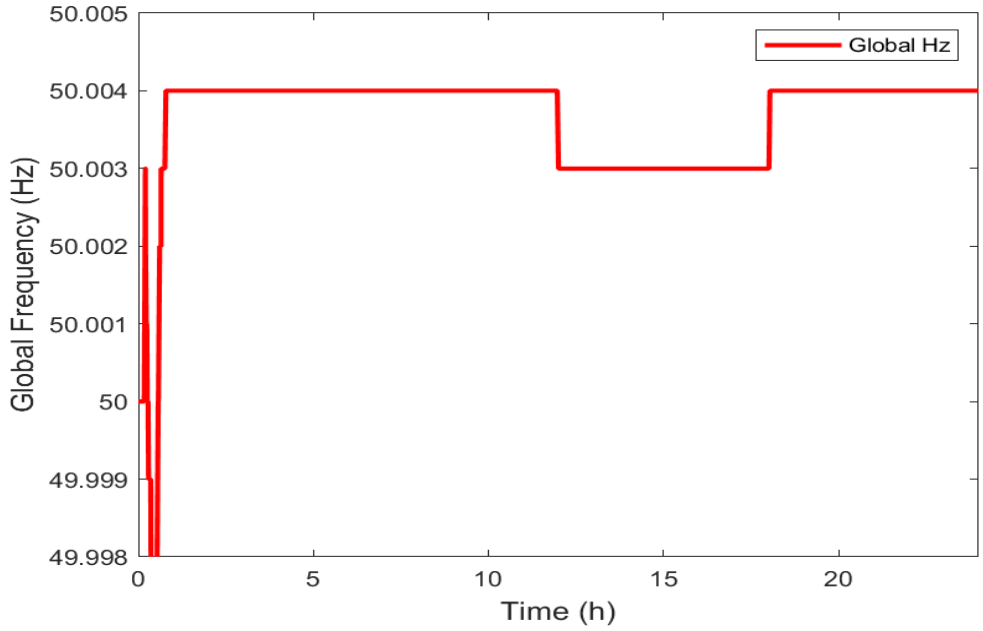

(iv)

Figure 4.6(i)-(iv): Output responses for multiple microgrids interconnected with global droop controller for a minimum SOC of 25% and low SOC of 35%: (i) microgrid one, (ii) microgrid two, (iii) microgrid three, (iv) global frequency.

Case 3: Multiple Interconnected Microgrids with Global Load

Figure 4.7 shows the power output response of three microgrids with the load connected to the global bus. Figure 4.7(i) shows the simulation results for microgrid one, which illustrates that the maximum available step PV-based RES power is $3.5kW$ while the maximum step load demand is $1.5kW$. Due to the surplus power from the RES unit in microgrid one, the battery SOC goes up to its full limit throughout the simulation time and in all the step load changes. The RES unit supplies power to meet the load demand in steps; some of the available RES power is exported via P_1, and the surplus power from the PV is curtailed in steps. The auxiliary unit is on standby and does not supply any power ($P_{aux1} = 0kW$). It remains on standby as the battery SOC reaches its full limit for the day. Figure 4.7(ii) shows the simulation result for microgrid two, which illustrates that the maximum step available power from the PV-based RES is greater than the load demand. The maximum available step PV power is $4.5kW$, while the maximum step load demand is $2.5kW$. The auxiliary unit is on standby at $P_{aux2} = 0kW$ and does not supply any power as the battery SOC rises to its full limit for the day. The available RES power supplies power to meet the load demand in steps; some of the PV power is exported via P_2, and the surplus power from the PV is curtailed in steps as the SOC stays within its full limit throughout the simulation time. Figure 4.7(iii) shows the simulation results for microgrid three, which indicates the maximum step load demand is greater than the available maximum step PV power. The PV-based RES unit supplies its maximum available capacity to the load ($P_{RES3} = P_{RES3\ Curtail}$), which is insufficient to meet the demand of the load. Due to the insufficient power from the PV-based RES to meet the load demand, the battery SOC goes down in steps to about 32%, RES power is imported into microgrid three via P_3, and the auxiliary unit supplies the power difference in steps to meet the load demand. The auxiliary unit starts to supply power to meet the load demand within the low limit of the battery SOC for the rest of the simulation time. Figure 4.7(iv) shows the frequency curves at the global bus. This illustrates that the frequency is operated and maintained within its operating limits irrespective of the RES power and load demand surges. Figure 4.7 (v) shows that the global bus load demand is equitably

met in steps from the supplied PV power surplus. Hence, the results show that the SOC is maintained within its upper and lower limits irrespective of the step-change RES and load and global load demand conditions.

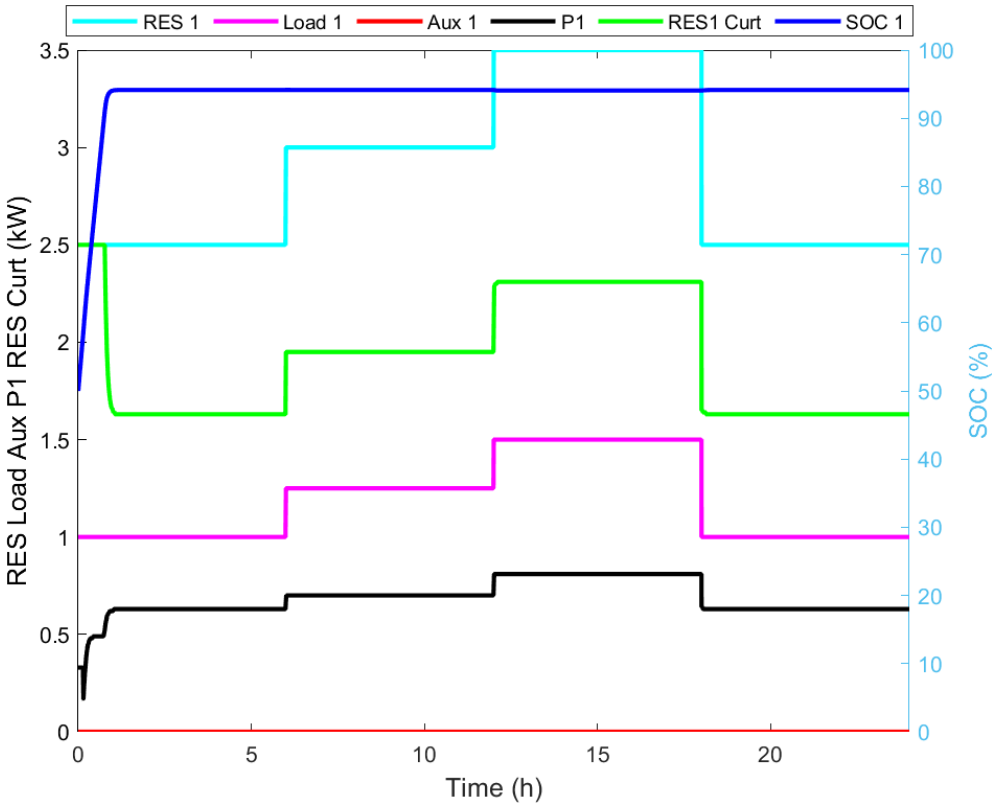

(i)

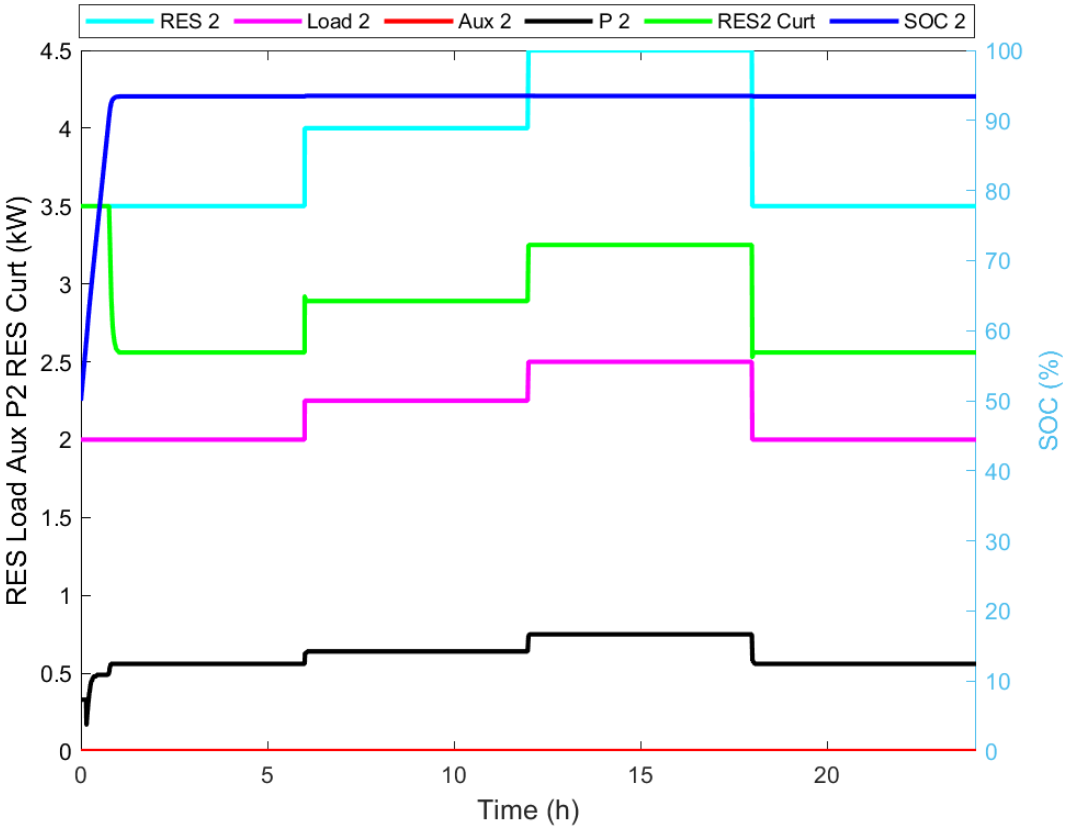
RES 2
Load 2
Aux 2
P 2
RES2 Curt
SOC 2
RES Load Aux P2 RES Curt (kW)
SOC (%)
Time (h)

(ii)

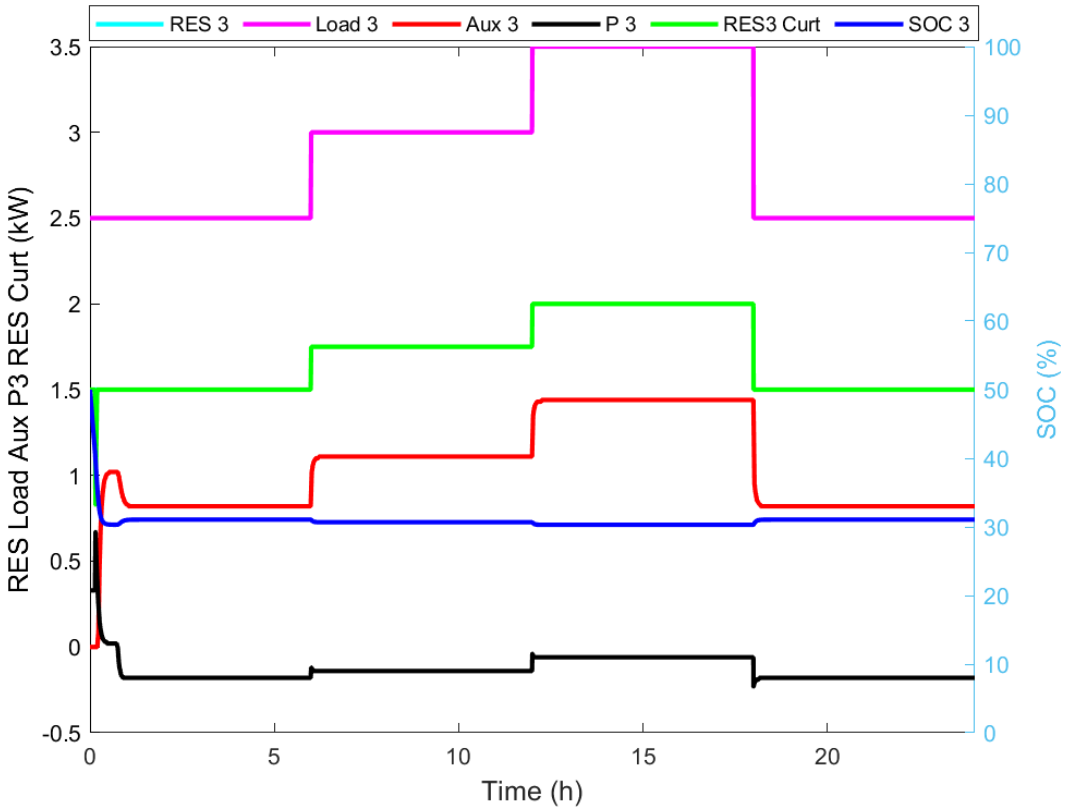
RES 3
Load 3
Aux 3
P 3
RES3 Curt
SOC 3
RES Load Aux P3 RES Curt (kW)
SOC (%)
Time (h)

(iii)

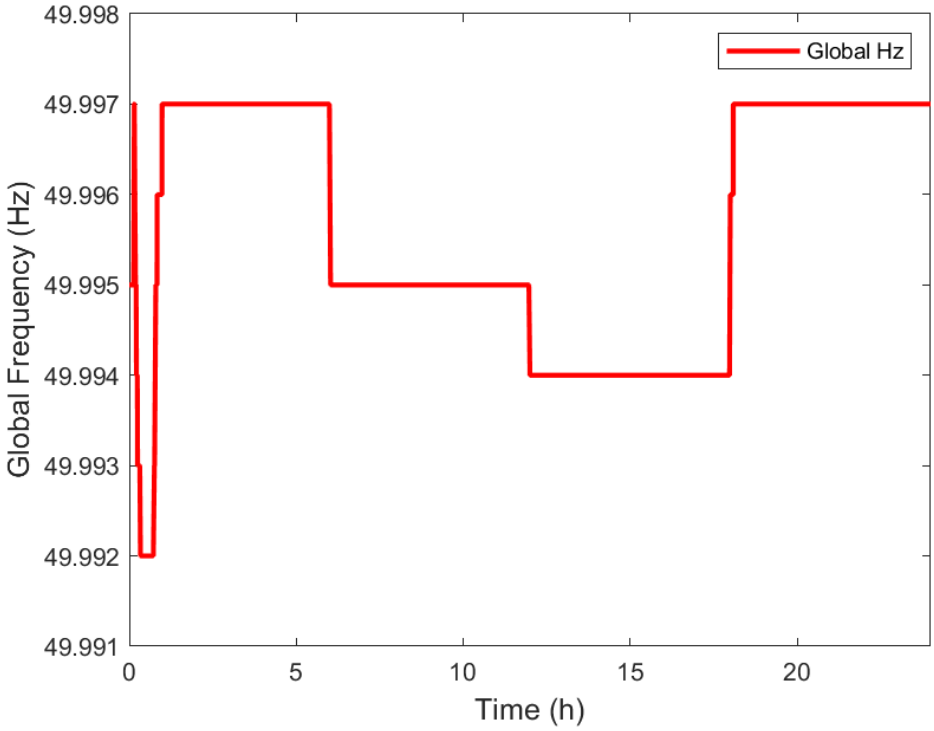

(iv)

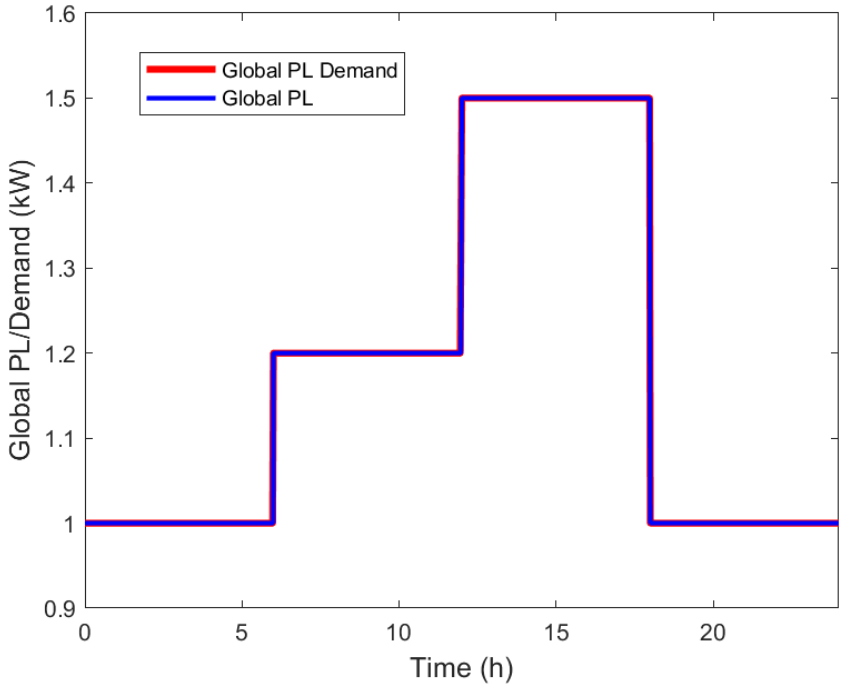

(v)

Figure 4.7(i)-(v): Output responses for multiple microgrids interconnected with global droop controller for a minimum SOC of 25% and low SOC of 35%: (i) microgrid one, (ii) microgrid two, (iii) microgrid three, (iv) global frequency, (v) Global load /Demand

4.3.2 Long-duration Simulation Results

A long-duration simulation result is presented in this section to assess the performance of the proposed structure and controller over an extended time in the utilisation of more RES power while keeping the SOC and global frequency within limits. To test the system structure and controller performance, aggregated profiles of RES power and load data that represent existing power system data are provided and used to run simulations on multiple interconnected microgrids and their performance results are compared with individually operated microgrids with and without global loads. The aim is to validate the proposed structure and controller performance results as they are supposed to be within the given constraint. The simulation case carried out in this section is to test the system with sets of different data profiles under a minimum SOC limit of 30% and a low SOC of 40%.

Case 1: Individually Operated Microgrids

Figure 4.8 shows the output responses for multiple microgrids independently operated at a minimum SOC of 30% and low SOC of 40%. Figure 4.8(i) shows the power output of the PV-based RES and the curtailed RES, the auxiliary unit, the SOC and the load power of microgrid one[1]. Individual microgrids can only curtail their PV-based RES or utilise power from the auxiliary supply and there is no power export and global load. The general expectation from this simulation scenario is that any excess power should be curtailed, and priority should be given to the full utilisation of the PV-based RES to feed the load. In microgrid one, the RES power supply exceeds the load demand. The RES is used to supply power to the load, and the surplus from the RES is curtailed. The auxiliary unit does not supply any power and remains on standby as the battery SOC reaches its limit. At about time (t) = 4 h, the SOC tends to decrease due to a slight increase in the load. At t = 19 h, the SOC reflects the gradual increase in load demand with a gradual slight decline. However, the battery power is always provided to balance the system as priority is given to full utilisation of PV-based RES, the SOC is high, and the auxiliary unit does not supply and only supplies power when needed. Figure 4.8(ii) shows

the simulation result for microgrid two, which illustrates that the power generated from the PV-based RES exceeds the load demand. The auxiliary unit is on standby and does not supply any power as the battery SOC goes up to its full limit for the day. At about t = 4 h, the SOC slightly decreased due to a sharp increase in the load. At t = 19 h, the SOC reflects the gradual increase in load demand with a slight decline, which goes back up at t = 21 h. Figure 4.8(iii) shows the simulation results for microgrid three, indicating that the load demand exceeds the available RES power. The PV-based RES supplies its full capacity to the load, which is insufficient to meet the load demand, and the auxiliary unit provides the difference to meet the load demand. The auxiliary unit starts to supply power at t = 0 h, as the battery SOC reaches its low limit of about 32%. The available power from the PV-based RES is less than the load, and this caused the SOC to stay within its low limit, which triggers supply from the auxiliary unit. At about time t = 12 h, the SOC goes up and down at t = 15 h due to intersecting with the load demand and available RES curves, and at this point, the auxiliary unit supplied zero power. The auxiliary unit supplies power to meet the load demand for the rest of the simulation time. Figure 4.8(iv) shows the 30-day simulation for SOC operated under different load and RES profiles, and the results illustrate that the SOC remains within its limits irrespective of the variations in RES and load demand. Hence, the controller prevents the SOCs from exceeding their maximum and minimum limits.

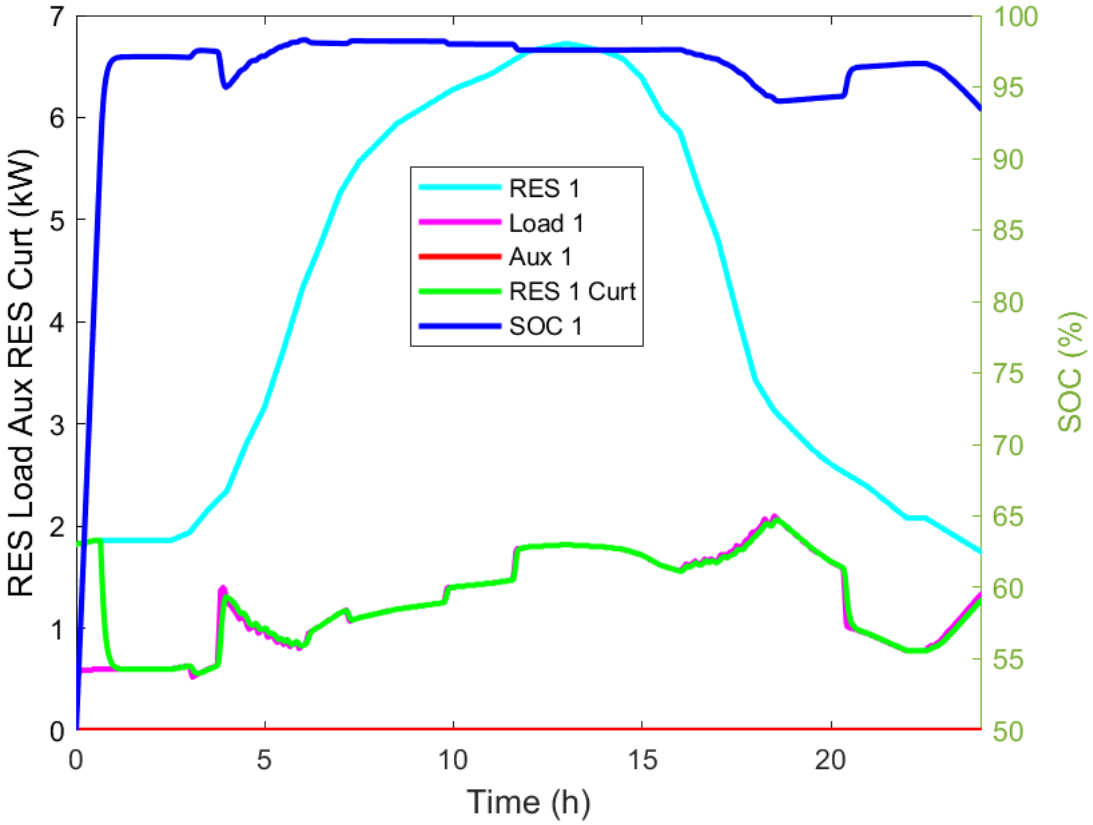
RES 1
Load 1
Aux 1
RES 1 Curt
SOC 1
RES Load Aux RES Curt (kW)
SOC (%)
Time (h)

(i)

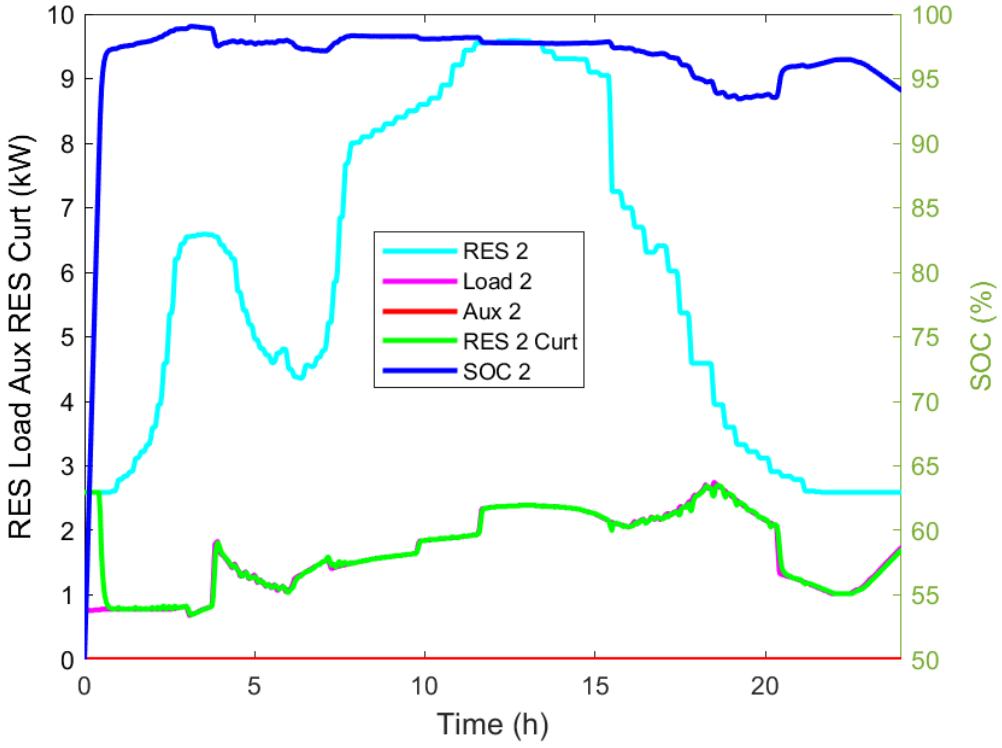
RES 2
Load 2
Aux 2
RES 2 Curt
SOC 2
RES Load Aux RES Curt (kW)
SOC (%)
Time (h)

(ii)

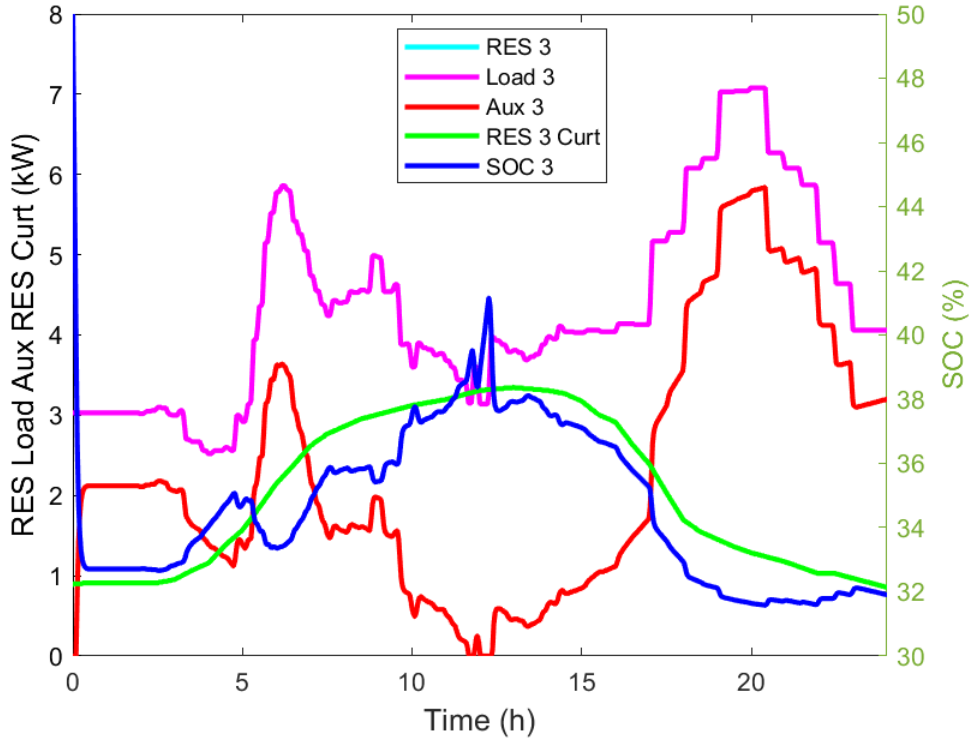

(iii)

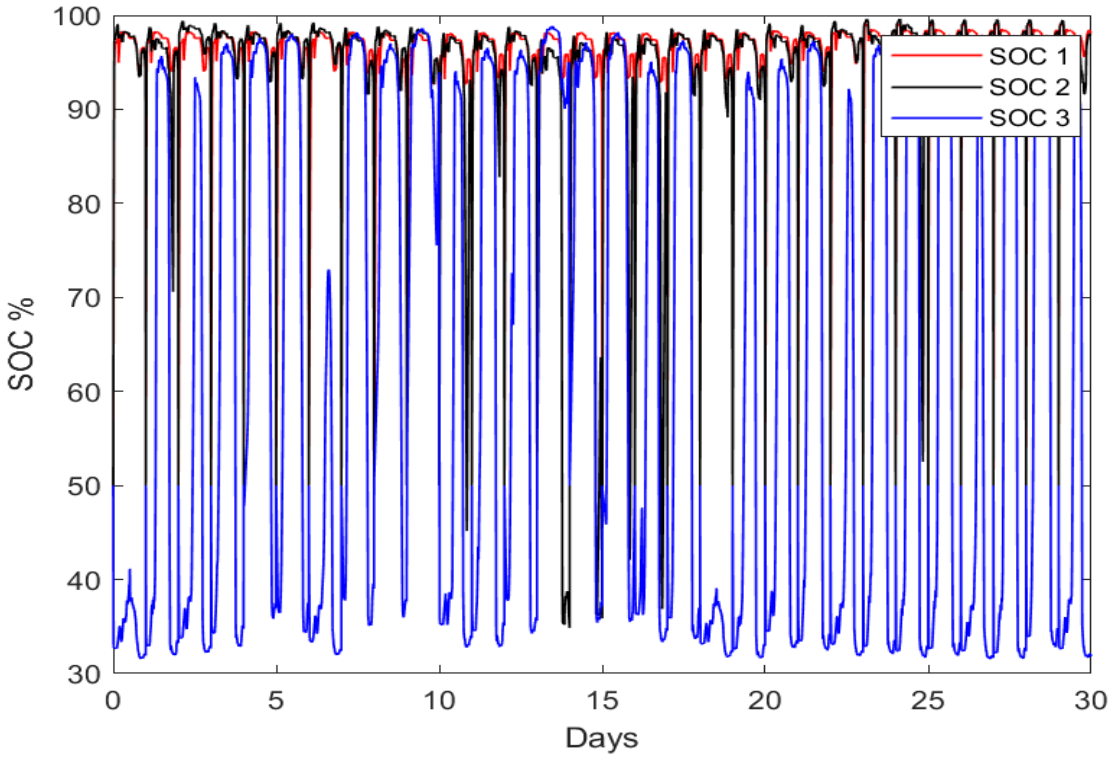

(iv)

Figure 4.8(i)-(iv): Output responses for multiple microgrids independently operated at a minimum SOC of 30% and Low SOC of 40%: (i) microgrid one, (ii) microgrid two, (iii) microgrid three, and (iv) 30-day SOC

Case 2: Multiple Interconnected Microgrids

Figure 4.9 shows the output responses for multiple microgrids interconnected with a global droop controller at a minimum SOC of 30% and low SOC of 40%. Figure 4.9 (i) shows the output power of the PV-based RES and the curtailed RES, the auxiliary unit, the 30-day SOC, the load, and the power exported for microgrid one. After power export, it is anticipated that any excess RES power should be curtailed, and the available PV power should be used to supply the load. In the case of insufficient supply from the RES, power should be imported from other microgrids with surplus power. The auxiliary unit supplies the shortage if the power export/import is insufficient to meet the load demand. The available RES power in microgrid one exceeds the load demand throughout the simulation. The RES profile supplies the power for the load, some RES power is fairly exported via P_1, and the surplus power is curtailed. The battery SOC goes up to its full limit most of the time, and the auxiliary unit is on standby and does not supply any power. At about t = 19 h, the SOC goes below 95%, corresponding to the highest point of the load, and the SOC goes back up to 95% as the load reduces. Figure 4.9(ii) shows the available RES power in microgrid two is greater than the load, indicating power export from microgrid two to deficient microgrids via the P_2. The RES supplies power to the load, the surplus power is fairly exported via P_2, and the remaining excess is curtailed. The battery SOC goes up and stays within its full limit, keeping the auxiliary unit on standby and not supplying. At about t = 18 h, the SOC slightly reduces below 95%, and this slight reduction of SOC corresponds to the highest point of load demand, and the SOC goes back up to 95% as the load demand and the curtailed RES power reduce. Figure 4.9(iii) shows the available PV power is less than the load demand in microgrid three, which implies the need for power import via P_1. The PV-based RES power is fully utilised to supply the load, which is insufficient to meet the demand. The two other microgrids supply the remaining power shortage equitably, starting from t = 0 h. Due to the less available PV, the SOC stays within its lowest limits at intervals between t = (0 -10) h and (16 – 24)h, which causes the auxiliary unit to supply

power during those intervals to meet demand. The auxiliary unit supplies power as required and stays on standby within t = (11 – 16)h, as the SOC exceeds the low limit. The SOC exceeds its high limit due to the load demand being met by the available RES and power equitably imported from the first and 2nd microgrids. Figure 4.9(iv) shows the 30-day simulation results for the SOC operated under different loads and RES conditions. The results show that despite the intermittent nature of the RES and changes in load requirements, the SOC maintains its boundaries. The maximum charging and minimum discharging levels of the battery are preserved. Figure 4.9(v) shows the frequency curve at the global bus with the global droop controller. The curve shows that frequency is maintained within its operating limits at the global bus, irrespective of the intermittent nature of the RES power and variations in the load demands.

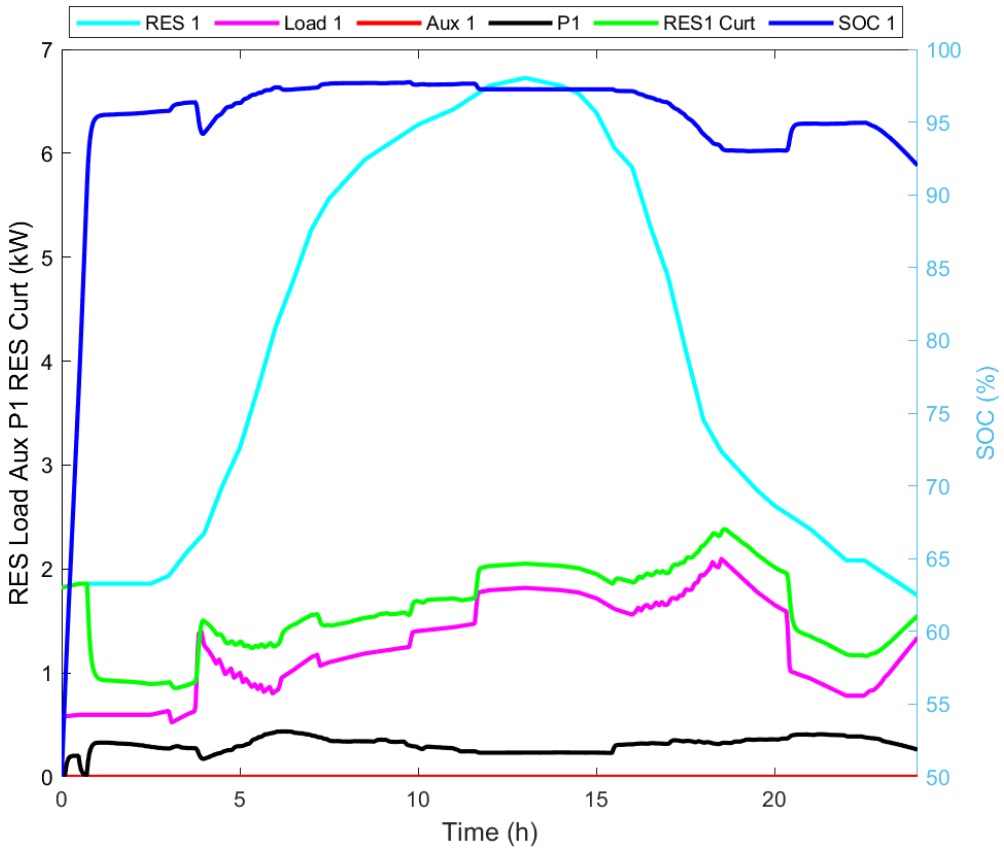

(i)

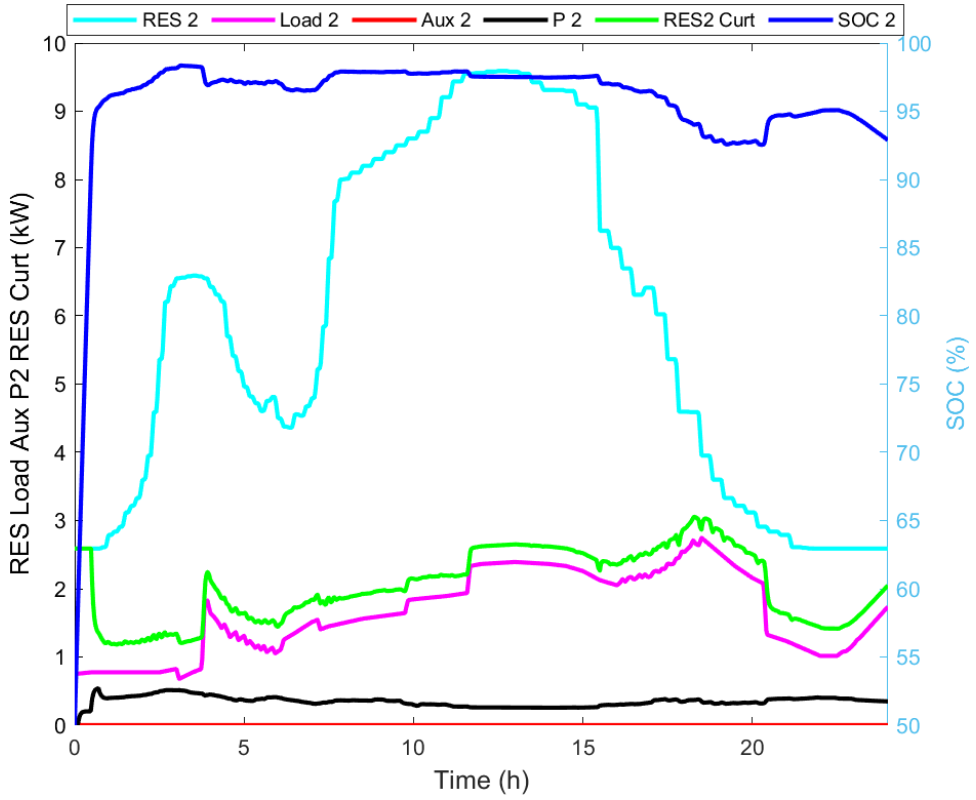
RES 2
Load 2
Aux 2
P 2
RES2 Curt
SOC 2
RES Load Aux P2 RES Curt (kW)
SOC (%)
Time (h)

(ii)

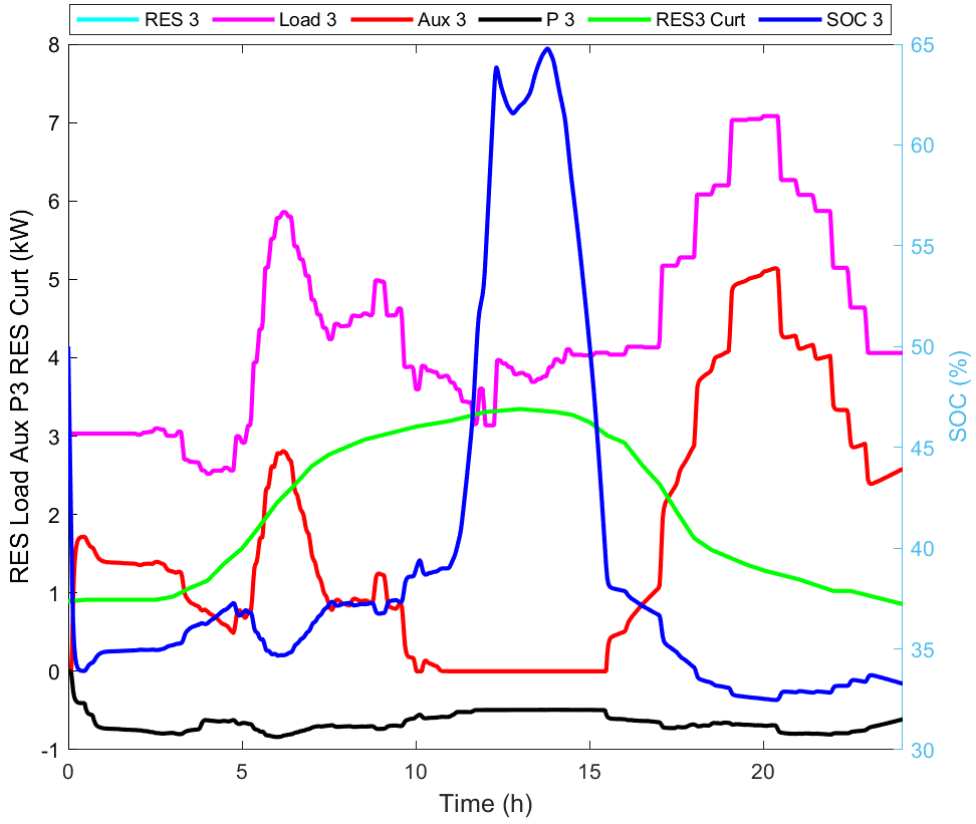
RES 3
Load 3
Aux 3
P 3
RES3 Curt
SOC 3
RES Load Aux P3 RES Curt (kW)
SOC (%)
Time (h)

(iii)

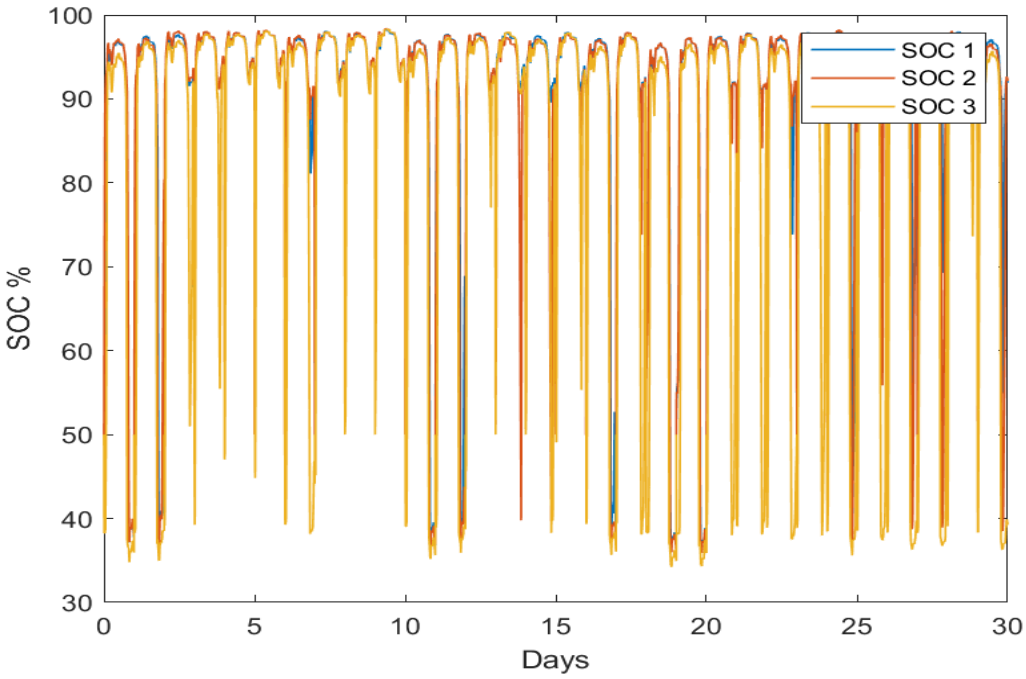

(iv)

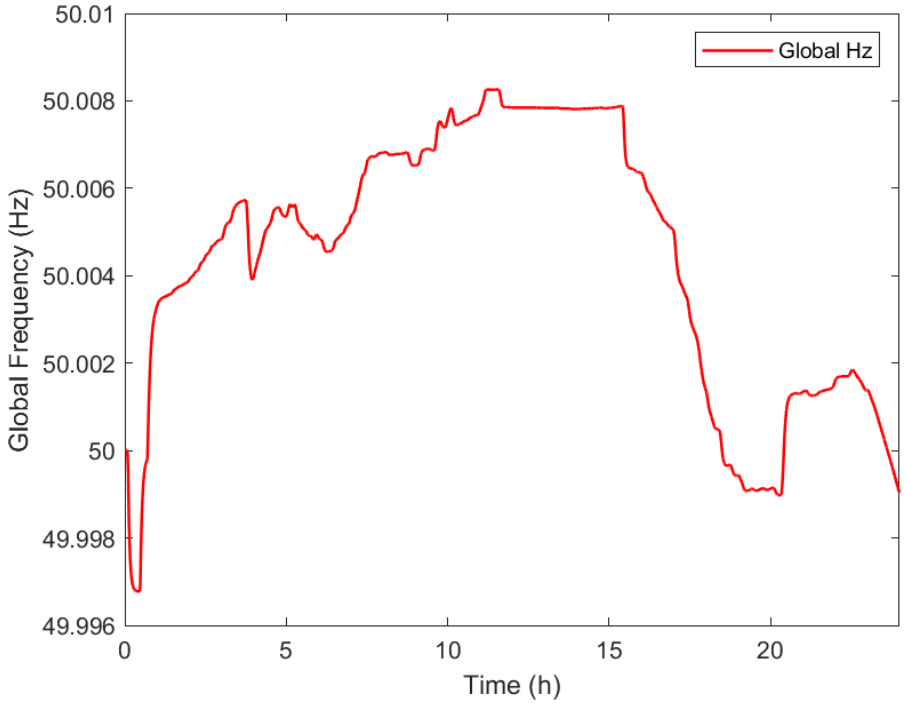

(v)

Figure 4.9(i)-(v): Output responses for multiple microgrids interconnected with global droop controller at minimum SOC of 30% and Low SOC of 40%: (i) Microgrid one, (ii) Microgrid two, (iii) Microgrid three, (iv) 30-day SOC, and (v) Global Frequency

Case 3: Multiple Interconnected Microgrids with Global Load

Figure 4.10 shows the output responses for multiple microgrids interconnected with a global droop controller and global load. Figure 4.10(i) shows the available PV-based RES and the curtailed RES power, the auxiliary unit, the SOC, the load profile, and the power exported for microgrid one. The available RES power is greater than the load, and the RES supplies power to meet the load and export power via P_1, and the surplus from the RES is curtailed. The auxiliary unit is on standby and does not supply power as the battery SOC significantly goes up to its full limit. At about t = 19 h, the SOC slightly goes down to about 85% while the system exhausts its available RES power due to increased load demand. At about t = 21 h, the battery SOC instantly goes back up to its full limit due to a sharp reduction in load. Figure 4.10(ii) shows the available RES power is greater than the load demand; therefore, power is exported via P_2, and the surplus is curtailed. The auxiliary unit is on standby and does not supply power while the battery SOC reaches its full limit. At about t = 18 h, the battery SOC gradually declined to about 85%, indicating a maximum utilisation from the available RES at the highest point of the load demand. Figure 4.10(iii) shows the available PV power is less than the load demand, indicating the need for power import into the microgrid via P_3. Due to an insufficient supply of RES power, the SOC goes down to its low limit, and the auxiliary unit starts to supply power at t = 0 h, while the available PV-based RES power is fully utilised to supply the load, and no RES is curtailed (hence RES 3 = RES 3 Curt). At t = 12 h, the SOC momentarily go up and down due to the point of intersection of the RES and load demand curve. After that, the SOC goes down to its low limit, and the auxiliary unit supplies more power. Figure 4.10(iv) shows that the global load demand at the global bus is equitably fulfilled at every instant such that the combined effect of the supply of the global load follows the demand. Figure 4.10(v) shows the 30-day simulation results for the SOC operated with the global droop controller and global load under different microgrid loads and RES profiles. The result illustrates that the SOC remains within its limits regardless of the variation in the supply of RES and

changing local and global load demands. However, the maximum charging and minimum discharging levels of the battery are preserved throughout the simulations. Figure 4.10(vi) shows the global frequency curve of the global bus operated with the global droop controller and global load. The curve illustrates that the frequency of the global bus is maintained within its operational limits, irrespective of the variations in RES power and local and global load demands.

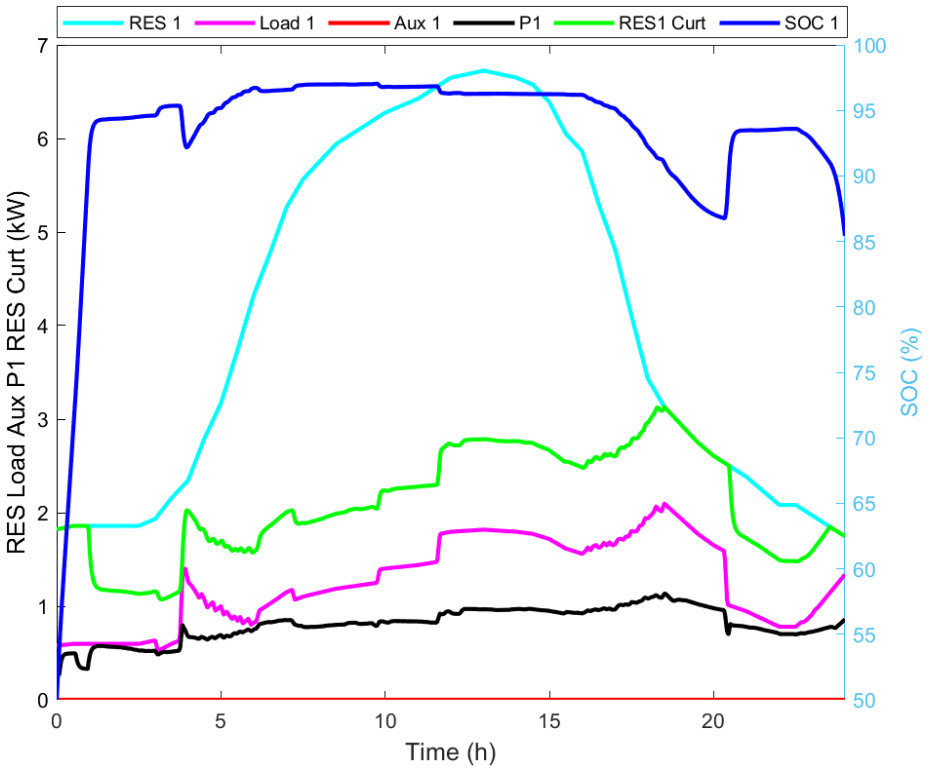

(i)

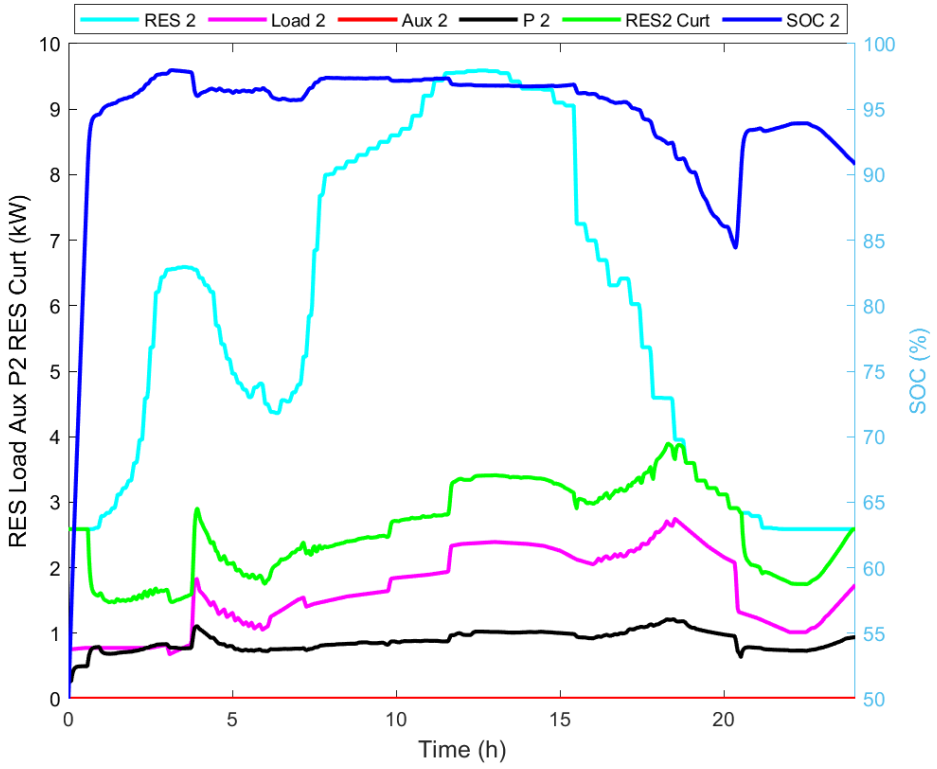

(ii)

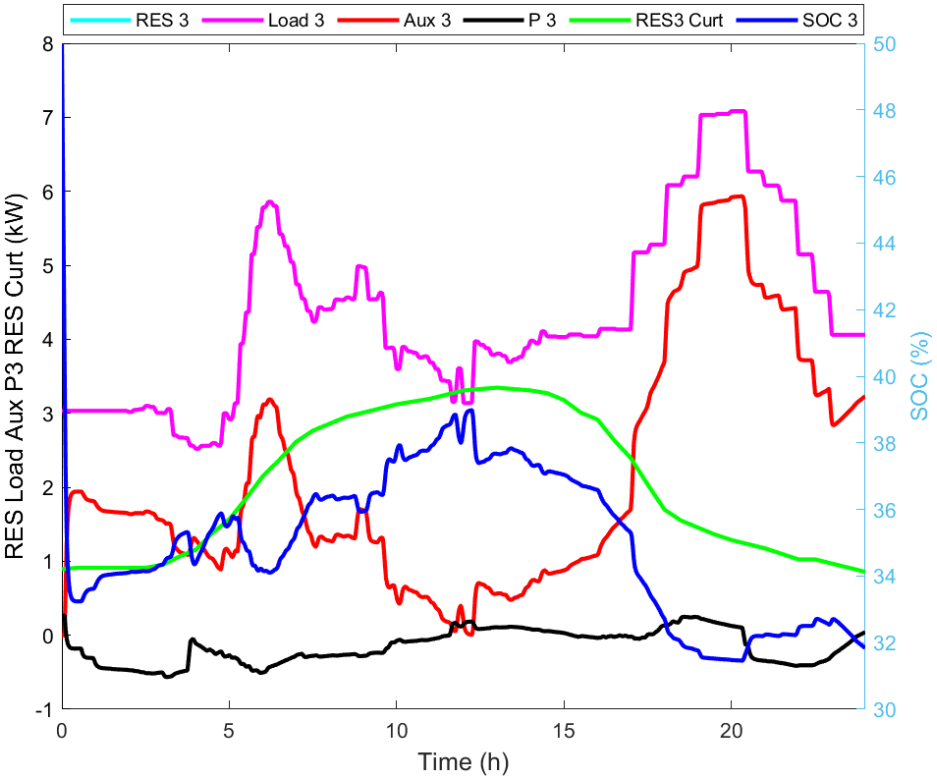

(iii)

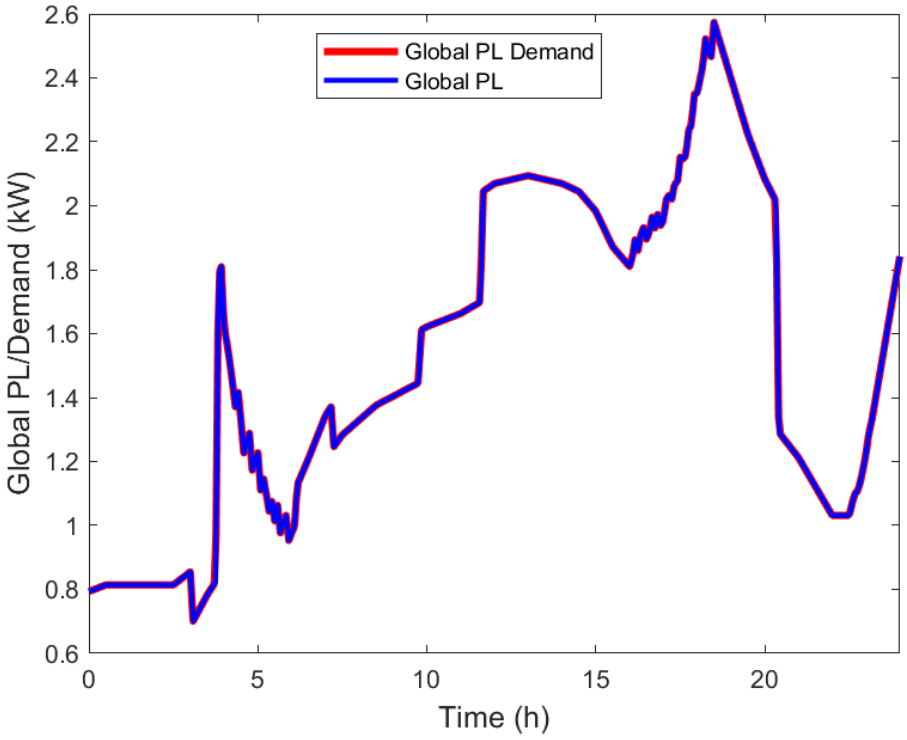

(iv)

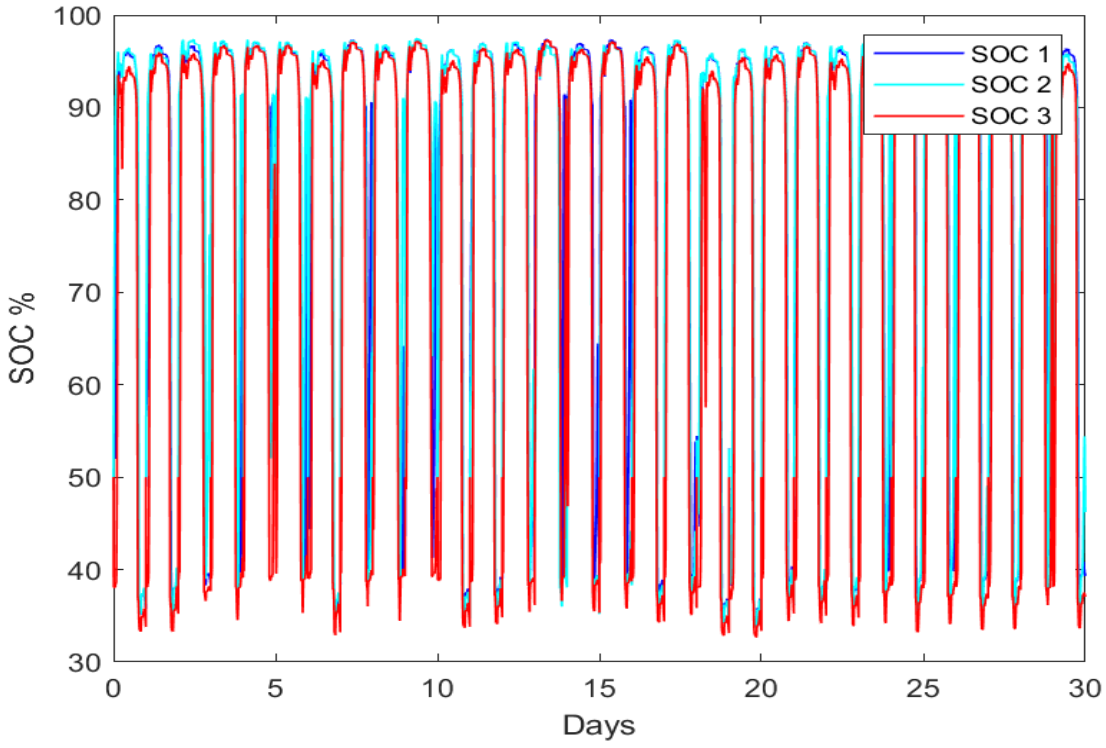

(v)

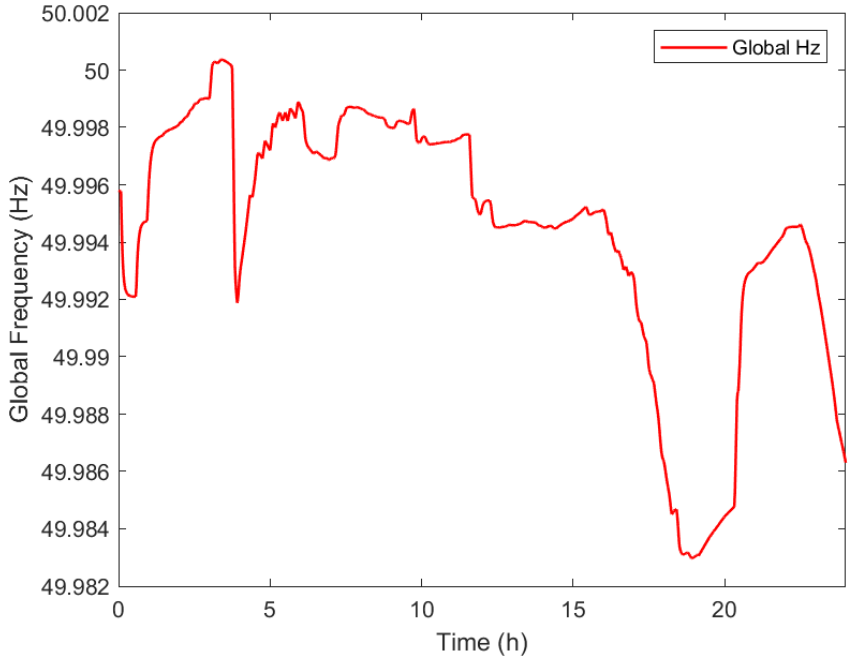

(vi)

Figure 4.10(i)-(vi): Output responses for multiple microgrids interconnected with global droop controller and global load at minimum SOC of 30% and Low SOC of 40%: (i) Microgrid one, (ii) Microgrid two, (iii) Microgrid three, (iv) global load, (v) 30-da day SOC, (vi) Global frequency

4.4 Performance Evaluation

It is important to reiterate that the main focus of this paper on energy management of interconnected AC microgrids using back-to-back converters is to maximise RES energy utilisation and minimise auxiliary energy usage. Therefore, this section compares simulation results for 30 days based on three operating scenarios:

i) independent operation of the microgrids,

ii) interconnected operation of multiple microgrids with the proposed control, and

iii) interconnected operation of multiple microgrids with the proposed control and global load. The performance of the three operating scenarios is assessed using a series of simulation data, and the results are shown in the subsequent sessions.

Figure 4.11 compares the RES energy curtailment simulation results evaluated over 30 days based on the three operating scenarios. The results show that in all 30 days, the most available RES energy is curtailed each day when the microgrids are independently operated compared with when multiple microgrids are interconnected with the proposed global droop controller with or without the global load in place.

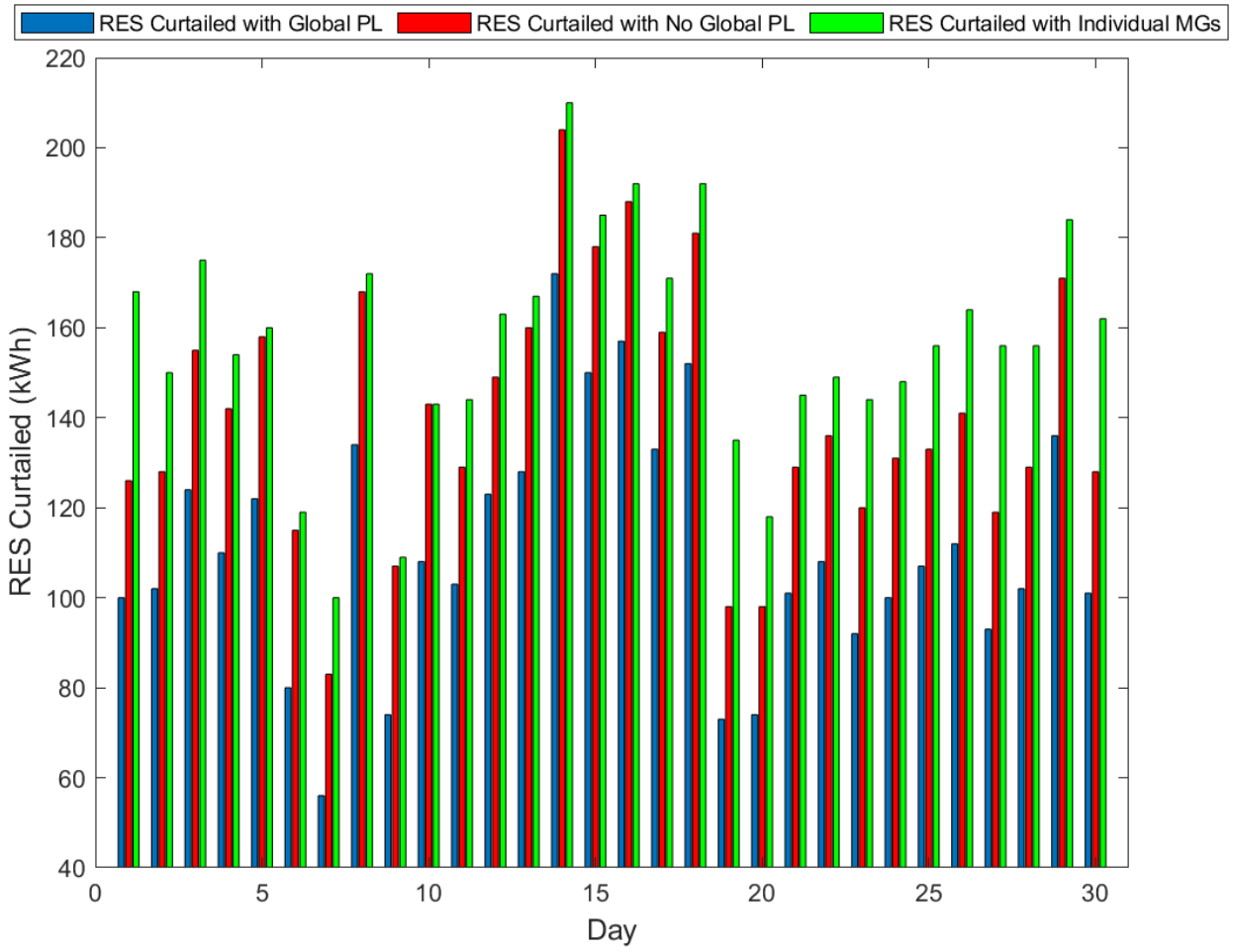

Figure 4.11: Comparing RES Energy curtailed for individually operated microgrids and with the proposed technique

Figure 4.12 compares the auxiliary energy utilisation for 30 days of simulation results and is evaluated based on the three operating scenarios. On day 1, about 55kWh of auxiliary energy is used when the microgrids are operated individually compared to about 20kWh and 10kWh energy utilised when the microgrids are interconnected with and without global load. The results show that the highest amount of auxiliary energy is supplemented daily when the microgrids are independently operated compared

to when multiple microgrids are interconnected with the proposed global droop controller with or without the global load. The smallest amount of auxiliary energy utilisation occurs when multiple microgrids are interconnected with the proposed global droop controller. However, there is a gradual increase in auxiliary energy utilisation when the global load is connected to the global bus.

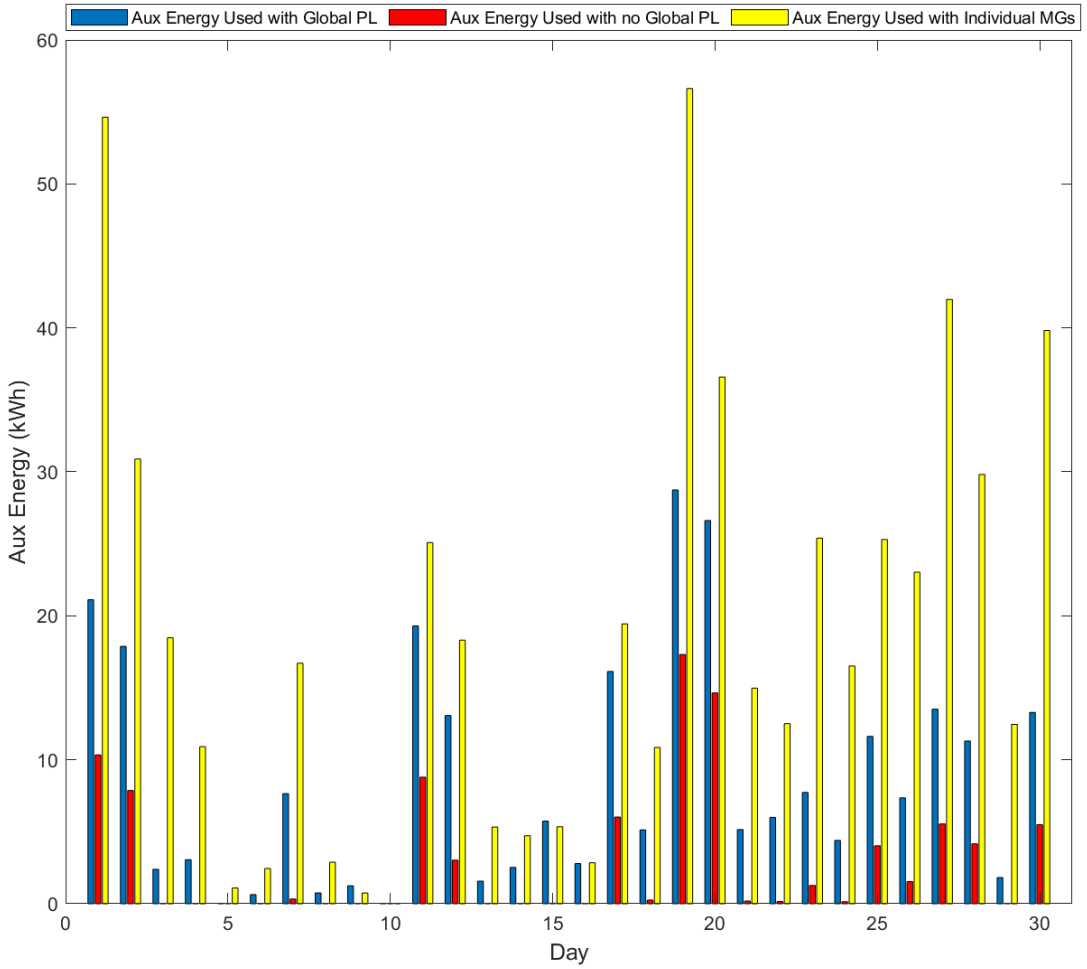

Figure 4.12: Comparing auxiliary energy utilised for individually operated microgrids with the proposed technique.

Figure 4.13(a) compares the total RES energy curtailed from overall simulation results evaluated based on the three operating scenarios. The results show that the most available RES energy of about 4.691 MWh is curtailed when the microgrids are independently operated compared to about 4.209 MWh of RES energy curtailed when multiple microgrids are interconnected with no global load. However, the least RES energy of about 3.327 MWh is curtailed when the global load is connected to the proposed control strategy. This implies that more RES energy is utilised with the proposed technique as the

global load is connected to the global bus. Figure 4.13(b) compares the total energy utilised from the auxiliary unit evaluated based on the three operating scenarios. The results show that the highest energy of about 0.566 MWh is utilised from the auxiliary unit when the microgrids are independently operated compared to the smallest of about 0.091 MWh obtained when multiple microgrids are interconnected with the proposed global droop controller. More energy of about 0.259 MWh is utilised from the auxiliary unit when multiple microgrids are interconnected with the proposed global droop controller with the global load. Hence, there is a gradual increase in energy utilisation from the auxiliary unit when the global load is connected to the global bus.

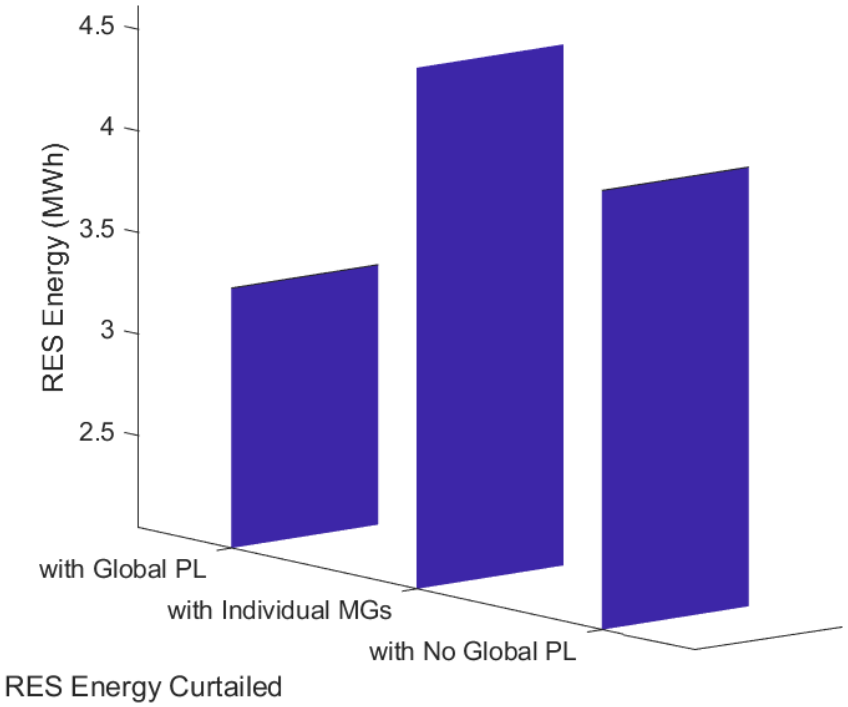

(a)

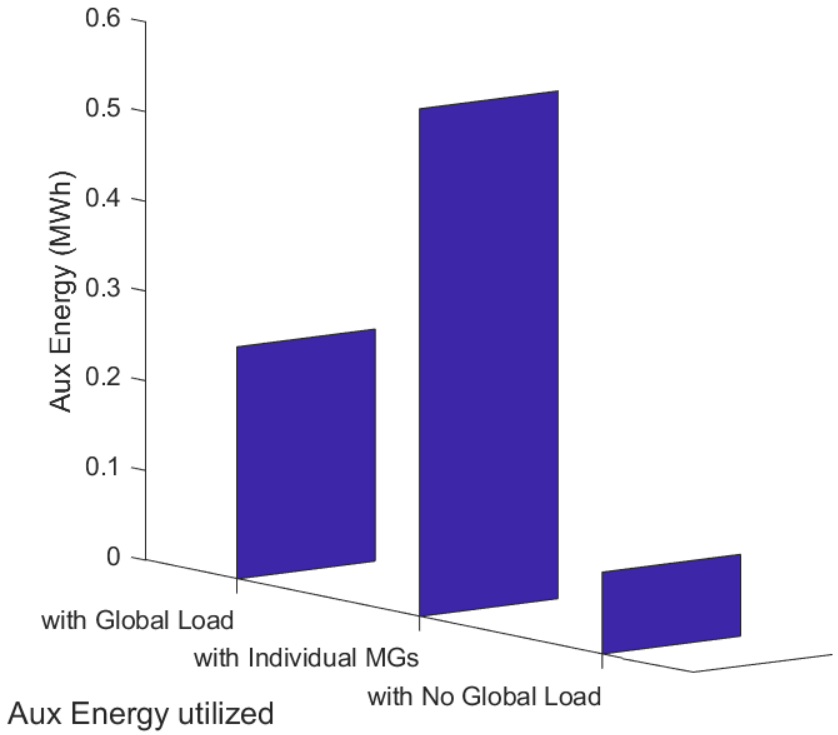

(b)

Figure 4.13: Comparing total energy curtailed and Auxiliary Energy utilised for individually operated microgrids and with the proposed technique

4.5 Summary

A new decentralised control scheme for the interconnected microgrids has been proposed. RES power curtailment and auxiliary power supplement mechanisms have been designed based on the bus frequency signalling technique to achieve balance and continuity of supply. In case of power shortage in one microgrid, priority will first be given to power import from other microgrids. A power supplement is used if this is not enough to control the battery SOC. A simplified model for multiple interconnected standalone microgrids has been formulated and tested in Matlab/Simulink. The step-varying and long-duration Matlab/Simulink simulations have been conducted for different minimum and low cases of the SOC. The proposed controller combines the global droop controller and the frequency bus-signalling techniques to manage the power flow between interconnected microgrids. The controller is implemented without any communication link between the microgrids based on the local and global droop controllers and varying the AC bus frequency within allowable standards. The

SOC and frequency at the global bus are maintained within the operational limits. The auxiliary unit is left to stay on standby and only supplies power when needed depending on the deviation in frequency and to avoid frequency degradation below allowable limits. However, The results presented from both the step-varying and long-duration simulations demonstrate the effectiveness and efficiency of the proposed interconnected microgrid structure and global droop controller, which can maintain the system requirements within the defined limitations. Both results show that more RES power is utilised when microgrids are interconnected with the proposed global droop controller than when they operate individually. Also, greater load demands are met with the proposed controller and also when the global loads are connected to the global bus. Hence, the proposed structure and controller have provided the right power flow management of interconnected microgrids, which comply with the design requirements.

CHAPTER 5: CENTRALISED CONTROL AND OPTIMISATION OF MULTIPLE INTERCONNECTED STANDALONE AC MICROGRIDS

5.1 Introduction

This chapter investigates the centralised control and energy management of multiple interconnected standalone AC microgrids. The proposed control and power flow management of interconnected microgrids, as presented in Chapter 4, carries out a decentralised control of interconnected microgrids and uses equations to relate from one microgrid to another to determine the power for different power demands. Also, the system is balanced as part of its model, representing the steady state power balance. Still, the system is yet to be investigated for its optimal performance in dealing with multiple interconnected microgrids as the existing system automatically exchanges power during surplus and shortage of power. Therefore, Chapter 5 carries out a centralised control and optimisation on the proposed model, and the results obtained are compared with those obtained from an unoptimised system. The main objective of this chapter is to minimise the total cost of energy from the auxiliary unit produced from gas. The performance results obtained are compared with the unoptimised results to determine the percentage optimal performance of the system. Furthermore, the optimised results are used to determine the total cost of auxiliary power minimised by the system.

5.2 System Description

The structure and control model of the standalone interconnected microgrids and the operating conditions to be optimised were described in detail in Chapter 4. Figure 5.1 presents the centralised control and energy management system (EMS) schematics for multiple interconnected standalone microgrids. The figure comprises three standalone microgrids interconnected to the common AC bus via their corresponding global connecting converters. The red dotted line shows a low-link communication network between each microgrid with the corresponding global converter and the EMS. Individual microgrids consist of the following main components: PV-based RES units, BESS units, auxiliary units like micro-gas turbines, and local loads. Each of the three microgrids is connected

with the associated global converter, a switch and a traditional power transformer to a common medium voltage AC (MVAC) bus (or global bus) and global load.

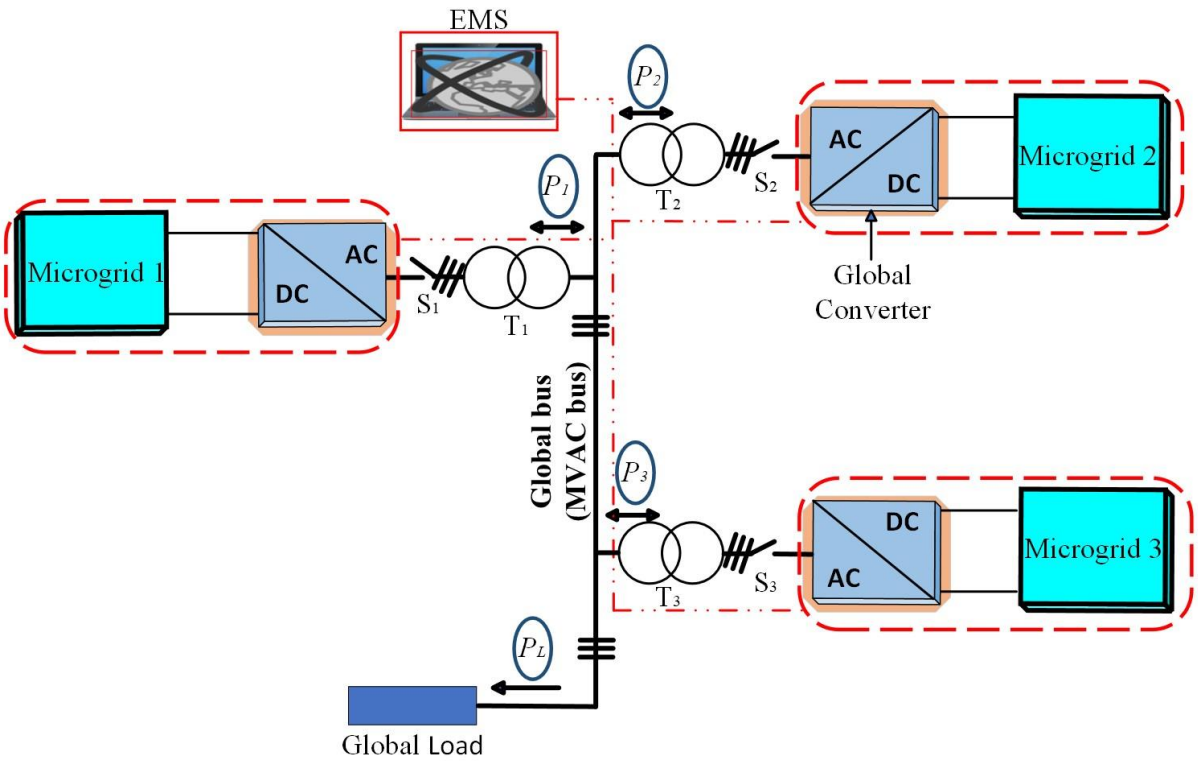

Figure 5.1: Schematics of EMS for Multiple Interconnected Standalone Microgrids

Considering the practicality of the overall existing model, each microgrid consists of PV-based RES and load profiles, daily and monthly. Each microgrid can operate individually to meet the local load demand regardless of the power balance in neighbouring microgrids. When the microgrids are not interconnected, if one microgrid has a shortage of power and another microgrid has a surplus of power, the microgrid with a shortage will be supplemented by power from the auxiliary unit (gas), and the microgrid with a surplus needs to be curtailed because the surplus power from PV-based RES cannot go anywhere else.

When the microgrids are interconnected, the balance between the power exported from the three microgrids and that consumed by the global load is continuously maintained to achieve optimal energy

balance. Microgrid units will put frequency up during a surplus of power or down during a power shortage to communicate with other microgrid units and tell other units about the battery's SOC. If there is a power shortage, the microgrid will start demanding power, and power will be imported from other microgrids. Suppose the microgrid is not getting the amount of power demanded. In that case, power will begin to be supplemented from the auxiliary unit (powered by gas) to maintain continuity of supply and reliable operation. The gas from the auxiliary unit has a unit price. The unit cost of gas is the per kWh unit of energy produced from the auxiliary unit (micro gas turbine) multiplied by the unit price. Hence, there is no direct communication, and power flows from one microgrid to another. However, the system prioritises exporting available power from the PV-based RES over curtailment. Therefore, the system exports power, and if there is a power surplus, it starts to curtail the PV power. Similarly, the system prioritises importing power from other neighbouring microgrid networks over supplementing from the auxiliary power supply. Centralised control and energy management of interconnected microgrids offer improved coordination and optimisation capabilities, enabling more efficient and reliable energy distribution across the network. It also facilitates the integration of renewable energy sources and enhances the overall sustainability of the energy system. However, it requires a sophisticated control infrastructure and careful planning to address potential challenges and vulnerabilities [147], [148]. However, most optimal control and energy management studies in [110], [132], [138], [144], [148]–[177] on interconnected microgrids are based on tie-line power flow control strategies in utility grid-connected or standalone mode or both modes considering the overall cost, emission cost from generator, storage, and operating cost minimisation.

This chapter carries out a centralised control and optimisation on the proposed structure as described in Chapter 4 to improve the efficiency and performance of the system in achieving the optimal result in minimising the total energy cost from gas used by the auxiliary supply. The system also ensures the right amount of power is exchanged between microgrids and that the global load demand is met at all times. The optimisation algorithm is expected to utilise optimal controller operation and balance power

among the interconnected microgrid network. The results from the optimisation algorithm are compared with those obtained in Chapter 4, where no optimisation algorithm was used.

5.3 Energy Management Formulation

The structure of three standalone interconnected microgrids is presented in Figure 5.1. The interconnected microgrid optimisation problem structure is modelled as a centralised economic dispatch (ED) model of the interconnected microgrids to determine the optimal dispatch solution. Centralised ED and energy management involves consolidating the control and optimisation of interconnected microgrids into a single central system with information on every microgrid to maximise the global benefit of the network. By globally controlling and coordinating the power exchange with the interconnected microgrid network, the gas utilisation by the auxiliary supply in each microgrid can be minimised, thereby maximising the overall use of RES in the interconnected network. The interconnected microgrids utilise RES power as much as possible to meet the demand of the global load automatically and equitably.

5.3.1 Objective Function

The centralised optimal economic dispatch of the interconnected microgrid is considered a non-linear problem and aims to minimise the total energy cost from gas; hence, the objective function considered is the total energy cost from gas utilised by the interconnected microgrids. The exchange of power flow between the global AC bus and the microgrids and vice versa makes the centralised ED problem a robust coupling operation. However, in this problem, the optimisation algorithm is expected to minimise the total cost of gas from the auxiliary supply. Hence, the objective function is formulated as follows:

$$Min: OF = \sum_{s} C_{gas,s} \ , \tag{5.1}$$

$$C_{gas,s} = \sum_{t=1}^{T} \lambda_{(t)} P_{gas,i}(t), \qquad (5.2)$$

where OF is the objective function, which is the summation of the cost of gas function C_{gas}. The C_{gas} is the summation of the total gas price $\lambda_{(t)}$ per kWh (£/kWh) multiplied by the amount of gas the auxiliary unit utilises. The function C_{gas} is optimised for each sample of iteration by the algorithm. Due to the complex nature of the existing Simulink model and the heavy computation time required for each iteration, a derivative-free and unconstraint optimisation strategy known as the Fminsearch optimisation toolbox in Matlab is employed.

5.4 Proposed Optimisation Algorithm

The proposed model can be solved using the Fminsearch optimisation algorithm, a non-derivative heuristic optimisation method, using the Nelder-Mead simplex algorithm as described in [178]. The algorithm uses a simplex of $n+1$ points for n-dimensional vectors x. Figure 5.2 illustrates how the algorithm first makes a simplex around the initial point guess at $x = 0$ or x_0 by adding 5% of each component $x_0(i)$ to x_0.

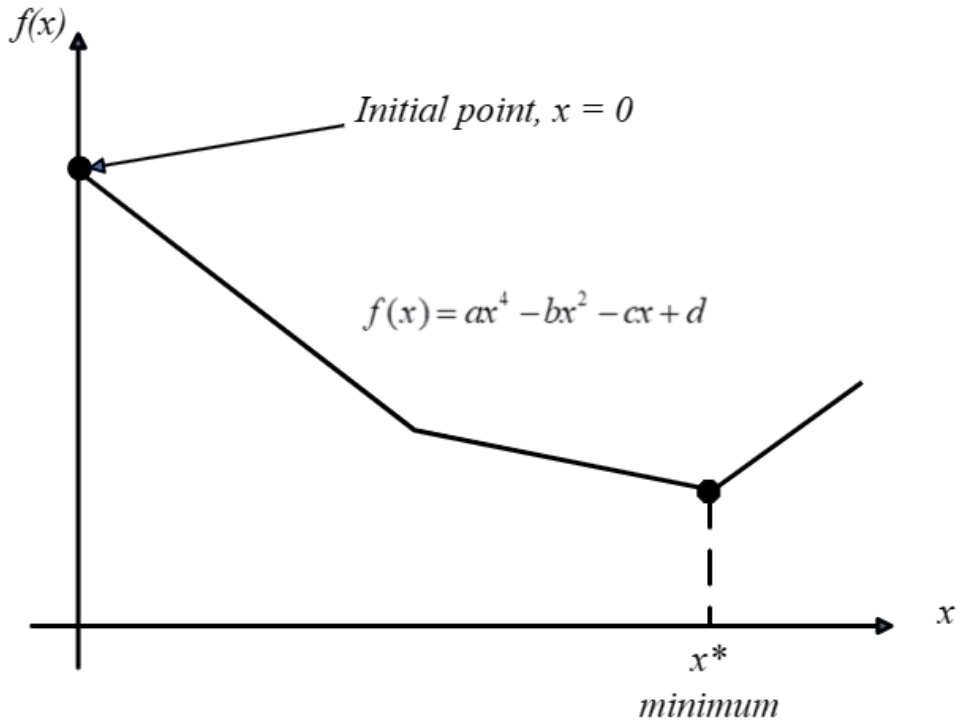

Figure 5.2: Illustrates the Plot of Objective Function Against Design Variables and Minimum

It is a design space with two dimensions if single variable optimisation is considered, and the objective function $f(x)$ is plotted against the design variables (x). Still, it can have any number of dimensions or sizes. However, the x^* is the notation for the minimum. Hence, Fminsearch minimises the objective function by starting from an initial point x_0 in the search space [178], [179]. This initial point guess does not have to be perfect because the Fminsearch algorithm searches the design space to find the minimum. It is important to note that Fminsearch is for unconstrained problems and does not require any derivative information from the system. It is referred to as unconstrained nonlinear optimisation because it finds the minimum of a scalar function of several variables, starting at an initial estimate.

5.5 Realisation of the Proposed Fminsearch Optimisation Algorithm

The proposed centralised control and optimal energy management of multiple interconnected standalone microgrids simulation was carried out in three cases. The first case simulation was carried out as a one-variable optimisation as described in the EMS flow model shown in Figure 5.3. This is an

unconstrained optimisation performed using a single gain value and the total auxiliary power from the three interconnected microgrids. The optimal operating cost is obtained and recorded at the minimal gas cost, representing the lowest objective function value. The second case is three-variable optimisation as illustrated in the EMS flow model in Figure 5.4, with simulation carried out in two phases viz with global droop controller equation as it is and with a modified global droop controller equation (by changing the droop equation from proportional to proportional-integral). Similarly, this is an unconstrained optimisation performed using three variables and the total auxiliary power from the three interconnected microgrids. The optimal operating cost is also obtained and recorded at the overall lowest gas cost, representing the lowest objective function value.

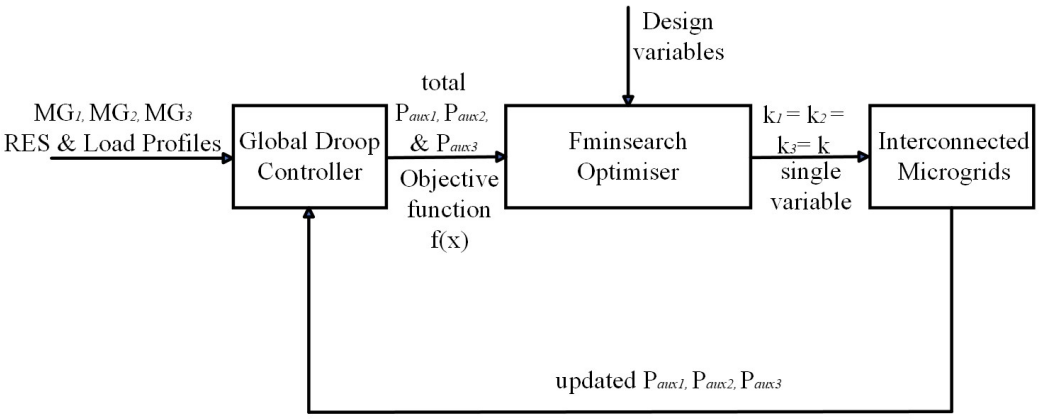

Figure 5.3: EMS flow model for One-Variable Optimisation

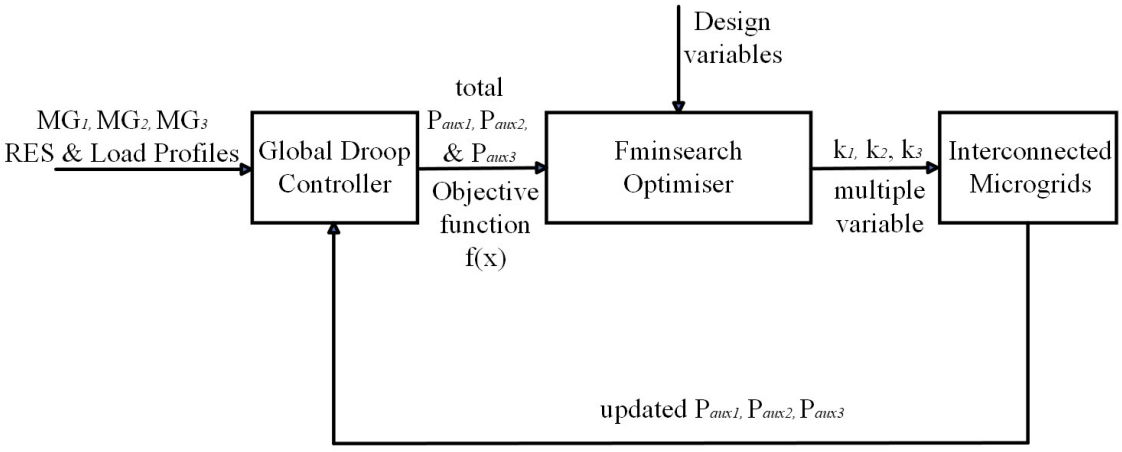

Figure 5.4: EMS flow model for Three Variable Optimisation

Hence, the algorithm has been run as follows:

i) Single-variable optimisation

(a) $k_1 = k_2 = k_3 = k$

ii) Three-variable optimisation

(a) $k_1 \neq k_2 \neq k_3$ (with global droop controller equation as it is)

(b) $k_1 \neq k_2 \neq k_3$, at $P^*_{\text{exp},i} = P_{\text{exp},i}$ (with a modified global droop controller equation)

Recall the droop equation (4.12) of Chapter 4; ii(b) is achieved by changing the droop equation from proportional to proportional-integral.

where k is the proportional gain that relates frequency deviation to power setpoints, as illustrated in Figure 4.4 of Chapter 4, $P^*_{\text{exp},i}$ is the power setpoint and $P_{\text{exp},i}$ is the power export.

The algorithm was run for different initial points at each optimisation operating case. The results show that the system performance improved, and the auxiliary unit's overall cost of gas utilisation was minimised in single and multiple objective cases compared to the results obtained in Chapter 4. It has been observed that no further cost minimisation of the objective function was possible after evaluating each of the last initial points. The initial points used for minimising the overall cost of gas utilised by the auxiliary unit are presented in Table 5.1. The first initial estimate is chosen as established in Chapter 4, while the rest are selected from the lowest function value of each iteration.

Table 5.1. Fminsearch Initial Points

Type of Optimisation	**Condition of Selecting Initial Points**	**Initial Points**
Single-variable	(i) $k_1 = k_2 = k_3 = k$	1000.0 1639350.0 1749959.5 1600000.0

		1603615.6 1603615.6 1603615.6
Multi-variable	(i) $k_1 \neq k_2 \neq k_3$	1000.0 1000.0 1000.0 1043533.3 476533.3 1879361.1 1142089.2 259445.9 2474492.1
	(ii) $k_1 \neq k_2 \neq k_3$, at $P^*_{\text{exp},i} = P_{\text{exp},i}$	1000.0 1000.0 1000.0 -36844.4 -41783.3 79772.2 -36844 -41783 79772

The first set of initial points is the case of single-variable optimisation, where a single gain k is selected at each iteration to minimise the objective cost function. The 2nd set of initial points is the multi-variable optimisation, where three sets of gains k_1, k_2, k_3 of different initial points are selected for the three microgrids at each iteration to minimise the objective cost function. Similarly, the 3rd set of initial points is by repeating the three-variable optimisation iterations with three different sets of gain k_1, k_2, k_3, with a modified global droop equation (by changing the droop equation from proportional to proportional-integral) such that the power export reference is the same as the power exported for each microgrid $(P^*_{\text{exp},i} = P_{\text{exp},i})$ and each iteration minimises the objective cost function.

The progression of the cost-based objective function values for the algorithm's three cases of optimisation runs for the different initial points are presented in Figure 5.5, Figure 5.6 and Figure 5.7, respectively. In contrast, the optimal cost comparison for the three cases against the benchmark as obtained from the proposed model in Chapter 4 is shown in Table 5.2.

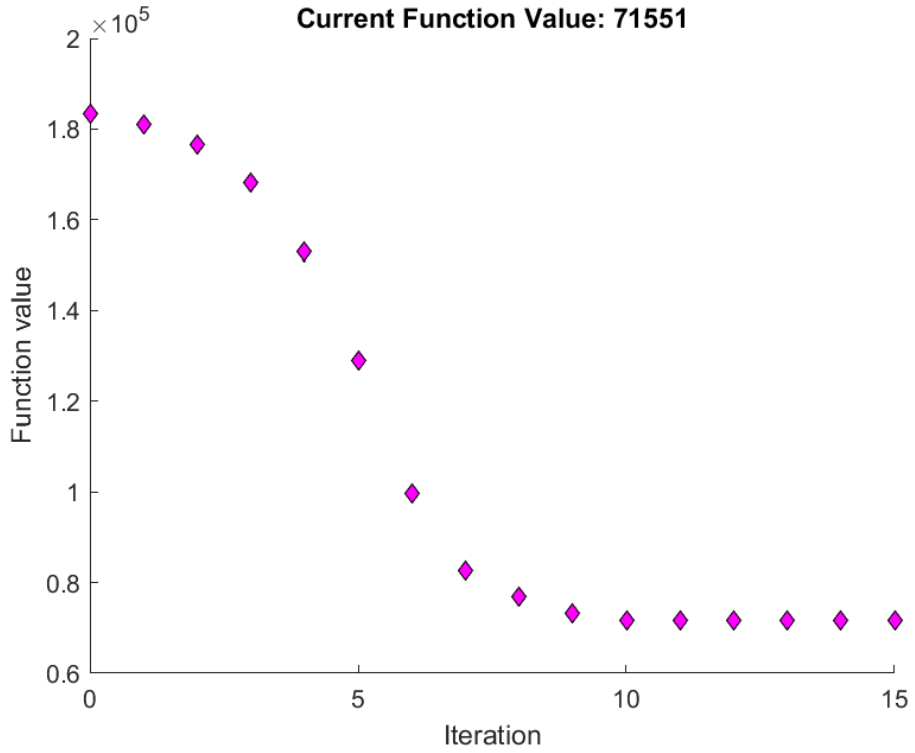

(a)

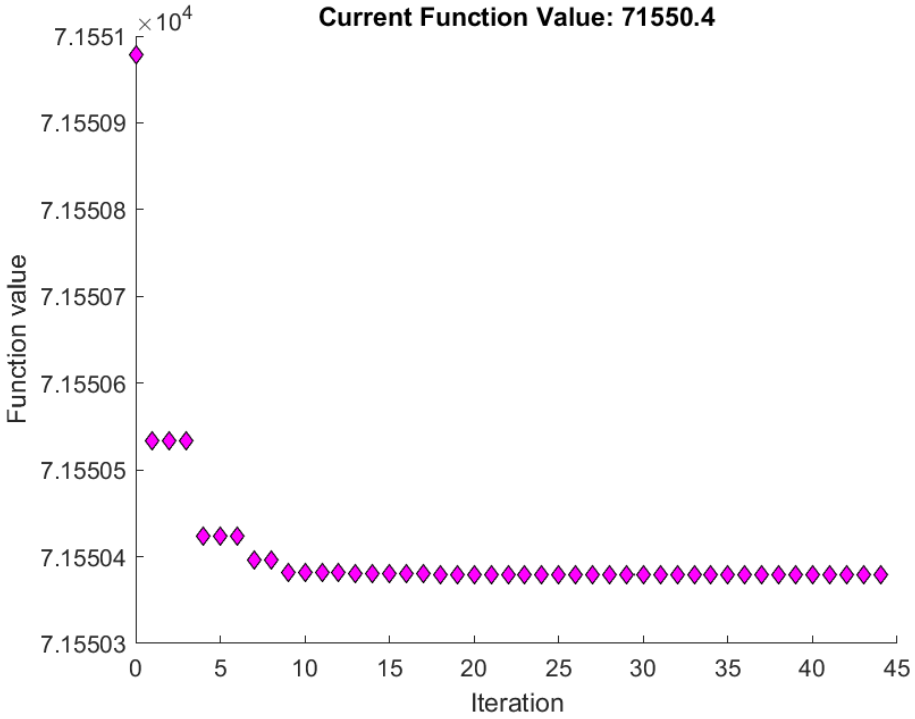

(b)

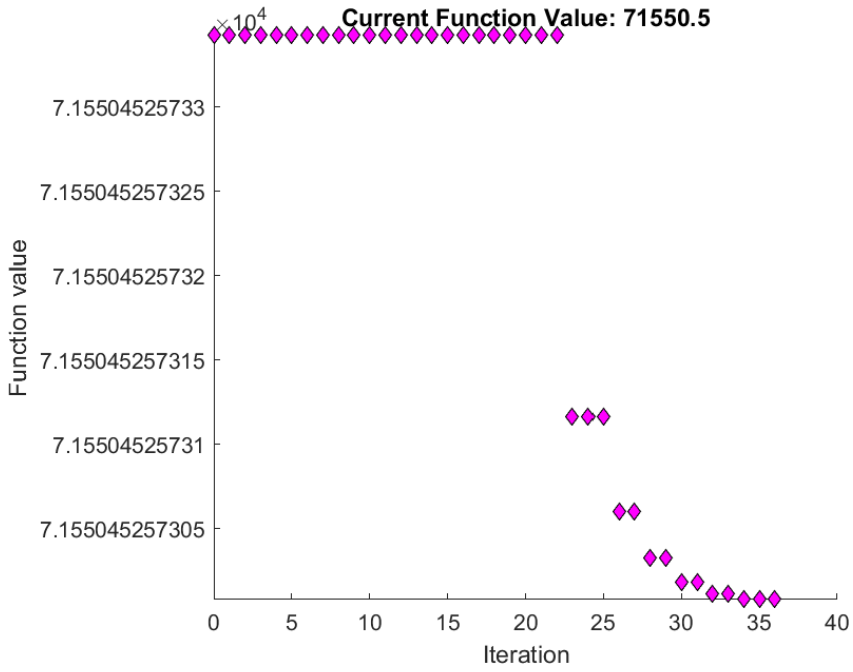

(c)

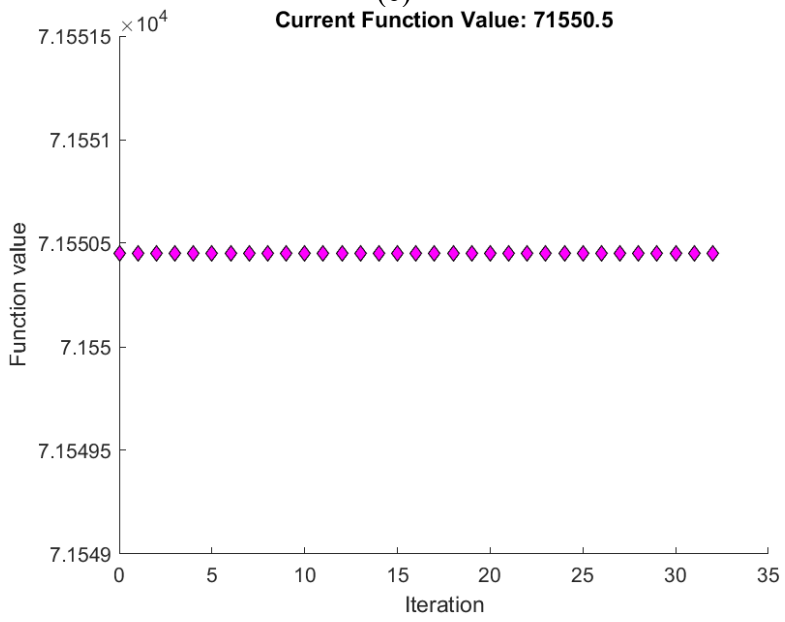

(d)

Figure 5.5(a-d): Fminsearch Objective Function Progression for Single-Variable Optimisation

Figures 5.5 (a-d) shows that the cost-based objective function values for single-variable optimisation starts to minimise from the initial estimate as presented in Figure 5.5(a). It continues to minimise in Figure 5.5(b) and Figure 5.5(c) and in Figure 5.5(d) the cost-based objective function maintained a constant value over 30 iterations.

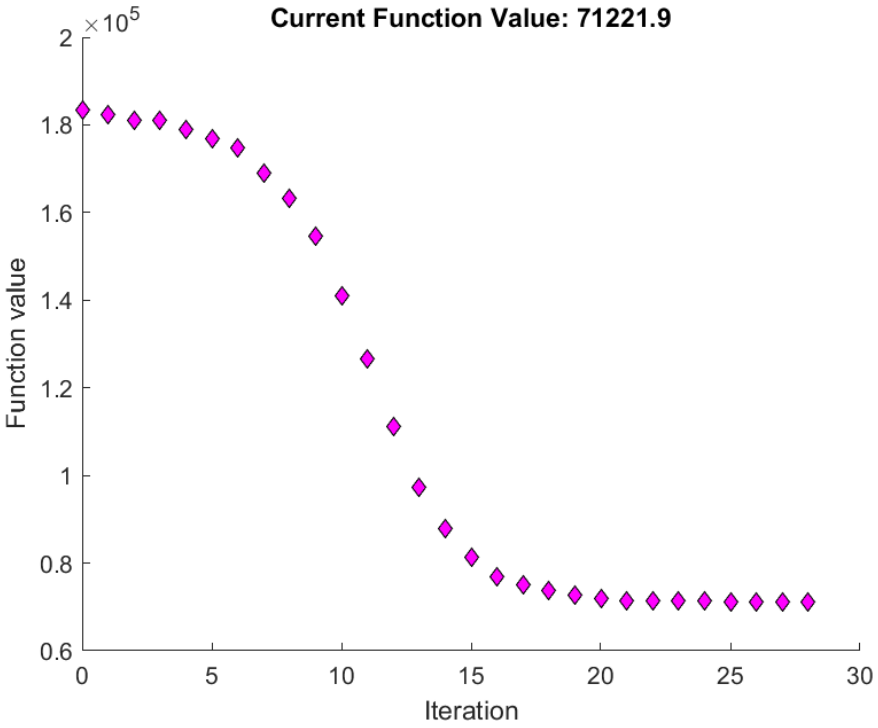

(a)

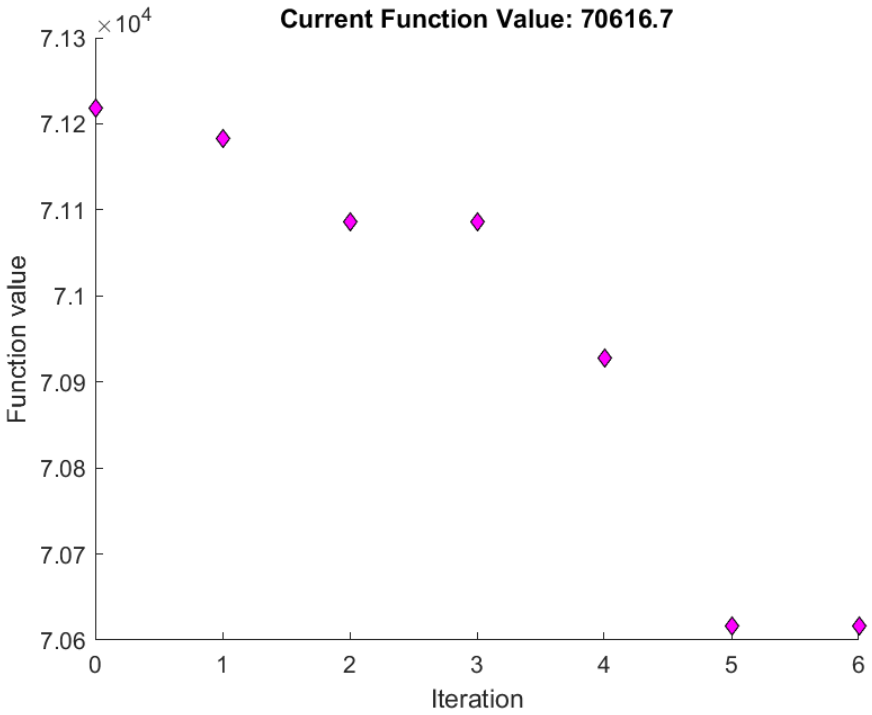

(b)

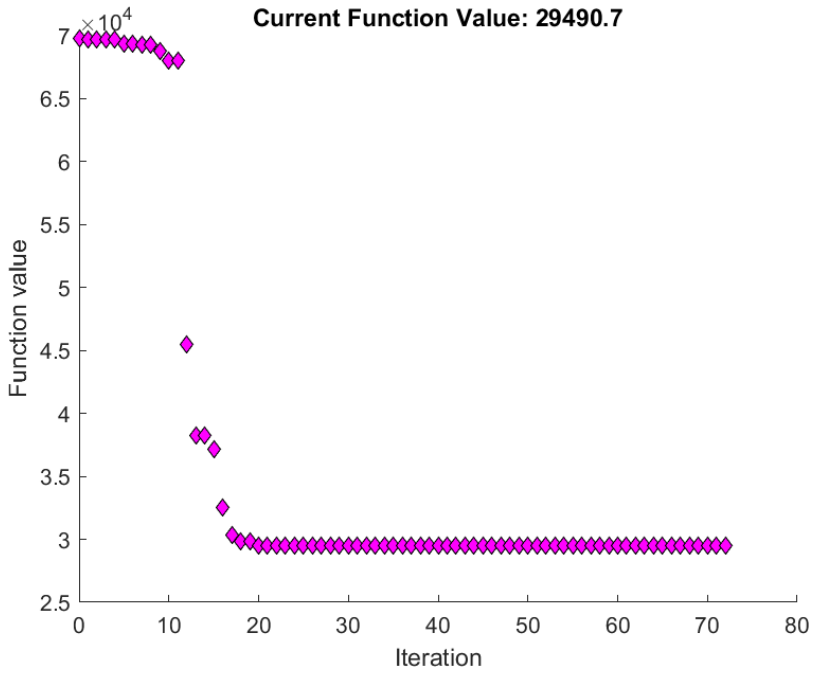

(c)

Figure 5.6(a-c): Fminsearch Objective Function Progression for Three-Variable Optimisation

Figures 5.6 (a-c) show that the cost-based objective function values for three-variable optimisation start minimising from the initial estimate, as presented in Figure 5.6(a). It continues to minimise in Figure 5.6(b), and in Figure 5.5(c), the cost-based objective function further minimised for about 15 iterations before maintaining a constant lowest value for over 50 iterations.

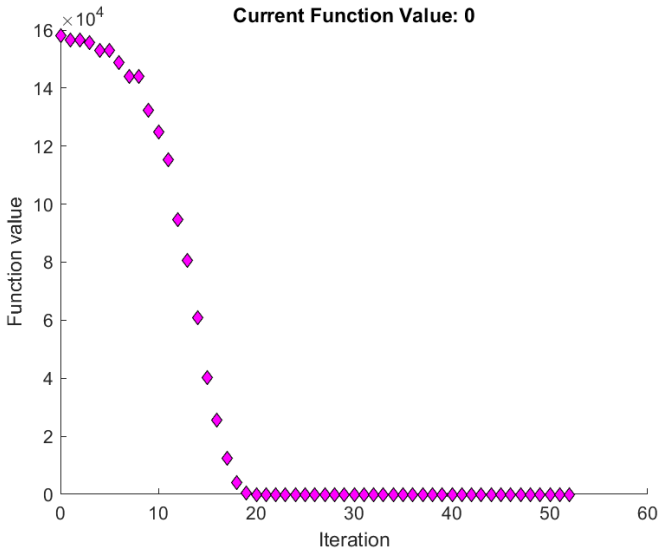

(a)

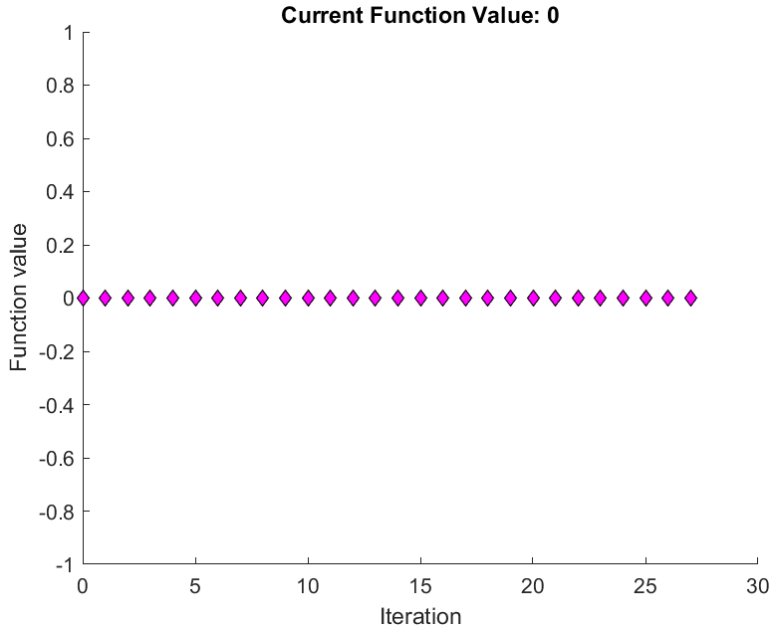

(b)

Figure 5.7(a-b): Fminsearch Objective Function Progression for Three-Variable Optimisation with Modified Global Droop Equation

Figures 5.7 (a-b) shows the cost-based objective function values for three-variable optmisation with a modified global droop equation starts to minimise from the initial estimate as presented in Figure 5.7(a) and got minimised to zero after about 19 iterations, The iteration continued and maintained a zero function value as shown in Figure 5.7(b) for over 26 iterations.

Table 5.2. Optimal Cost Comparison for the Three Cases Against the Benchmark

Type of Optimisation	**Condition of Optimisation**	**Unoptimised cost (£) (Benchmark)**	**Optimal cost (£) (Optimisation)**
Single-variable	(i) $k_1 = k_2 = k_3 = k$	183423.2	71550.5
Multi-variable	(ii) $k_1 \neq k_2 \neq k_3$	183423.2	30210.7
Multi-variable	(iii) $k_1 \neq k_2 \neq k_3$, at $P^*_{\text{exp},i} = P_{\text{exp},i}$	158203.1	0.0

5.6 Performance of the Algorithm on the Centralised Control System

The performance of the proposed Fminsearch algorithm on the centralised control for interconnected microgrids is analysed from the perspective of comparison with overall cost minimisation based on initial sensitivity, convergence and scalability. Table 5.3 summarises the performance evaluation category.

(i) Comparison based on initial sensitivity

The influence of the initial gain values is evaluated on the objective cost function, and different evolution sets of gain values are sampled during simulation, and their corresponding optimal objective costs represent good stability to their respective initial sensitivity. However, Figure 5.8 shows the initial sensitivity plot for single-variable optimisation, which shows that the objective cost appears stable at the 2nd sample of different initial sensitivity values irrespective of the fluctuations in the samples of initial gain values between the 2nd and 4th initial values.

(ii) Comparison based on convergence

The evaluation of convergence based on the three case optimisation simulation shows that the optimisation process converged at different numbers of iterations. Figure 5.9 shows the convergence curve of the objective cost after 418 iterations for the single-variable optimisation. The curve represents and maintains a consistent objective cost over 418 iterations. Whereas the cases (i) and (ii) for three-variable optimisation converged at about 106 and 72 iterations, respectively, both results made the system unstable.

(iii) Comparison based on scalability

Scalability, in this case, is the ability of the centralised control system of interconnected microgrids to continue functioning effectively, irrespective of its size, to meet the user demand. The performance of the centralised control method proposed in this chapter is used to solve the DED problem. The calculation result is compared with the benchmark based on the single-variable and multiple-variable centralised optimisation methods. Based on the performance of the results obtained after convergence,

the optimal solution is obtained in the case of single-variable optimisation in terms of maintaining the standard of comparison with the proposed model in Chapter 4. The two conditions for multi-variable optimisation show sub-optimal performance and instability evidenced due to high gain values; hence, they are not considered further in detailed simulation studies.

Table 5.3. Summary of the Performance Category

Type of Optimisation	Condition of Optimisation	Initial Sensitivity	Convergence	Scalability
Single-variable	(i) $k_1 = k_2 = k_3 = k$	✓	✓	✓
Multi-variable	(ii) $k_1 \neq k_2 \neq k_3$	✓	✓	-----
Multi-variable	(iii) $k_1 \neq k_2 \neq k_3$, at $P^*_{\exp,i} = P_{\exp,i}$	✓	✓	-----

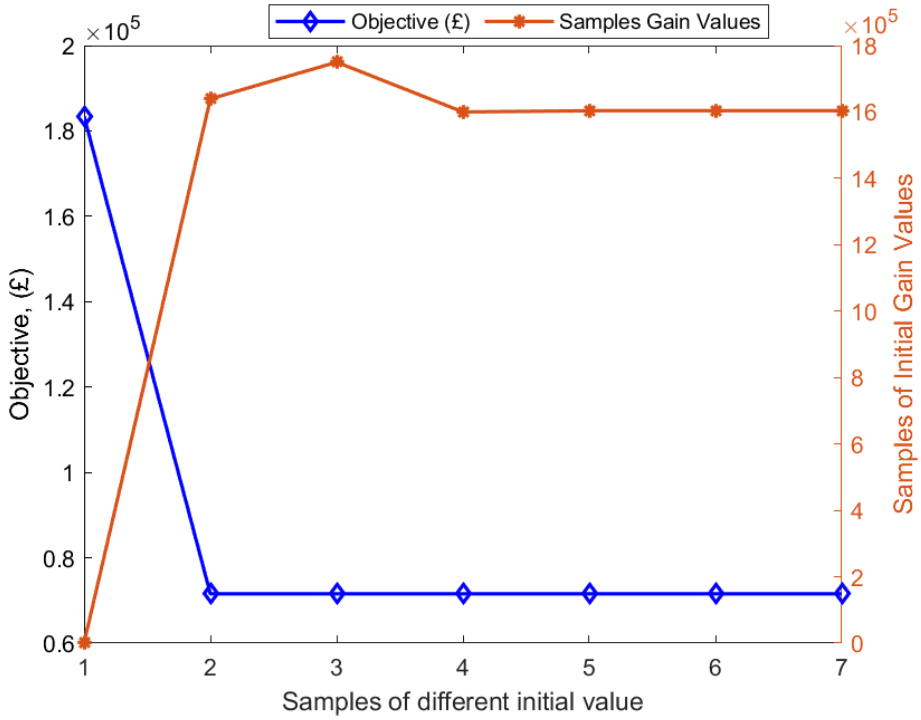

Figure 5.8: Plot of Initial Sensitivity to the Objective Cost for Single Variable Optimisation

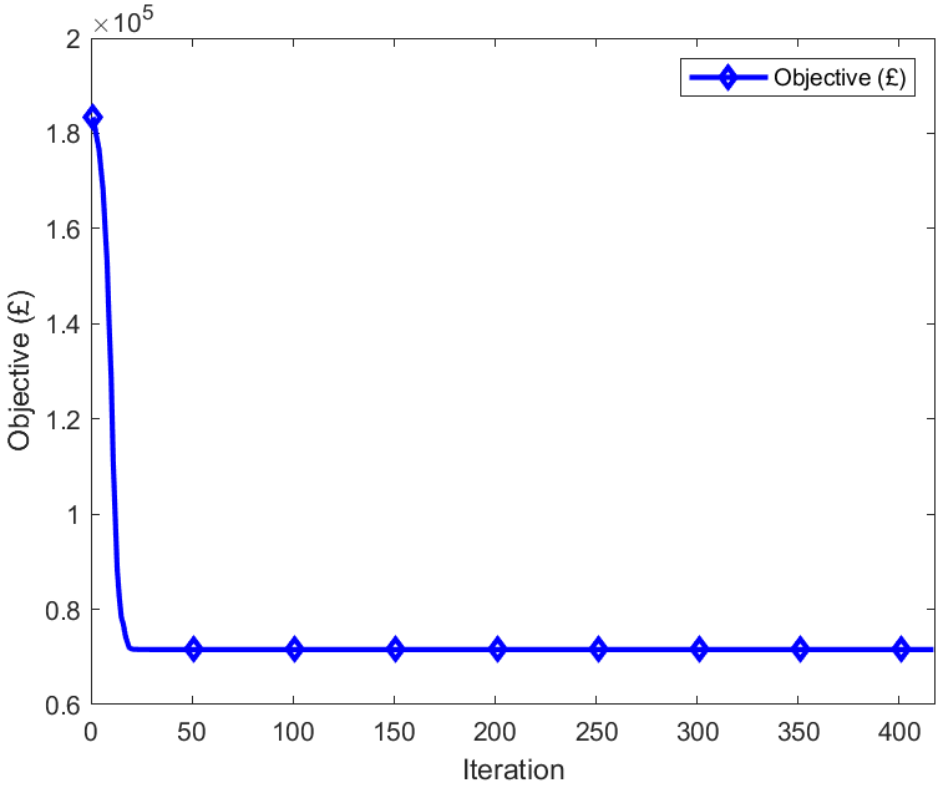

Figure 5.9: Convergence Curve of Single-Variable

5.7 Simulation Results and Discussion

This section shows the results of the proposed global control of multiple interconnected standalone microgrids tested on the Fminsearch optimisation algorithm based on the single-variable optimisation algorithm. Figure 5.1 shows the centralised control and energy management structure of three standalone microgrids interconnected to a common AC bus with a global load via a static switch, back-to-back converter and traditional power transformers. However, all the system parameters used during simulations are mentioned earlier in Chapter 4, and the method description is in Chapter 5.

This research aims to solve the optimal power dispatch of the centralised control and energy management of multiple interconnected standalone microgrids. Each microgrid consists of a PV-based RES unit, BESS unit, auxiliary unit and load. Daily data profiles measured over a 24-hour time span represent the available RES units and load demands. And as an economic dispatch problem, this research solves the centralised control and energy management of multiple interconnected microgrid economic dispatch problems based on the measured data of 24-hour. The detailed model for three

interconnected microgrids built in Matlab/Simulink is presented in Chapter 4. The effect of each standalone microgrid auxiliary power generation cost on the interconnected microgrid is not utilised based on the centralised control topology. Instead, the total cost of the auxiliary is used as input to minimise the total cost of gas. Therefore, the cost per kilowatt of power generated by the total auxiliary units varies based on individual microgrid consumption. This research is modelled as a centralised unit with single-variable optimisation having multiple area economic dispatch problems as each microgrid operates autonomously.

The proposed multiple standalone interconnected microgrids with three different microgrids and the global load is optimised, and the connection diagram is shown in Figure 5.1. The optimised results are compared with the unoptimised benchmark obtained, as described in the detailed design, model, and control in Chapter 5, regarding how much gas from the auxiliary unit is saved.

Therefore, using the proposed Fminsearch optimisation algorithm toolbox in Matlab/Simulink to solve the DED problem of the interconnected standalone microgrids, the following corresponding case-by-case optimal dispatching results of the three different microgrids are shown in Figures 5.10 -5.12 based on independently operated microgrids, interconnected microgrids with the global droop control and interconnected microgrids with the global droop control and global load respectively. The optimal dispatching results of Figure 5.10 show no difference, and all dispatch SOC curves are within range, implying the microgrids are not optimised when they operate independently. When operated with an optimised gain selected based on minimising the cost of auxiliary power, this implies that at some point, independent microgrids can be seen to minimise gas at different sets of profiles. The optimal dispatching results of Figures 5.11 and 5.12 show a drastic reduction in power from the auxiliary unit, and more power from the PV-based RES is exported and used to meet the load demand.

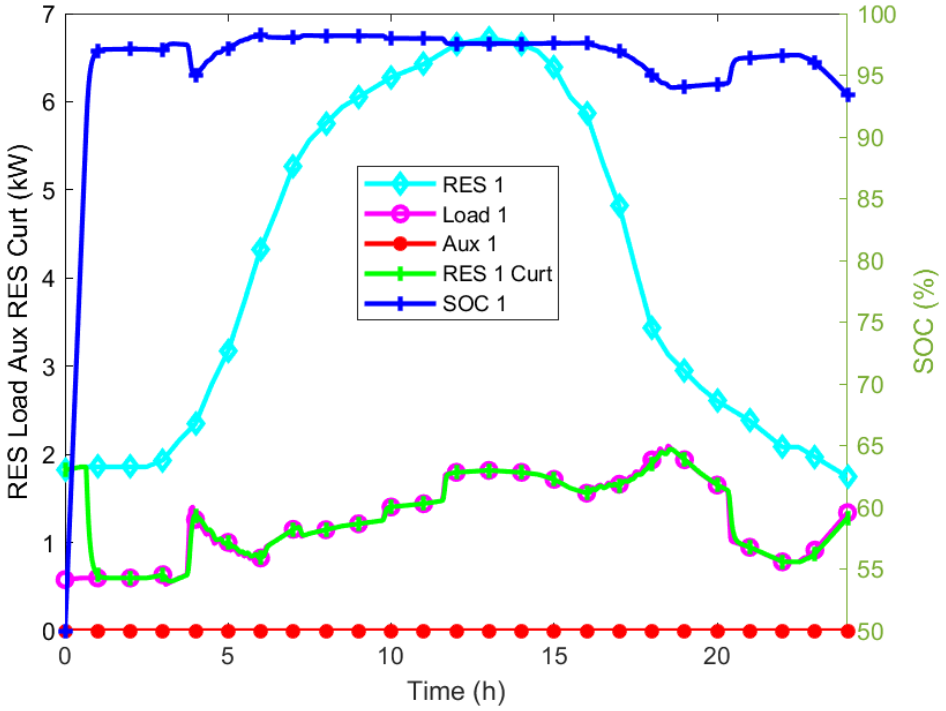
RES 1
Load 1
Aux 1
RES 1 Curt
SOC 1
RES Load Aux RES Curt (kW)
SOC (%)
Time (h)

(a)

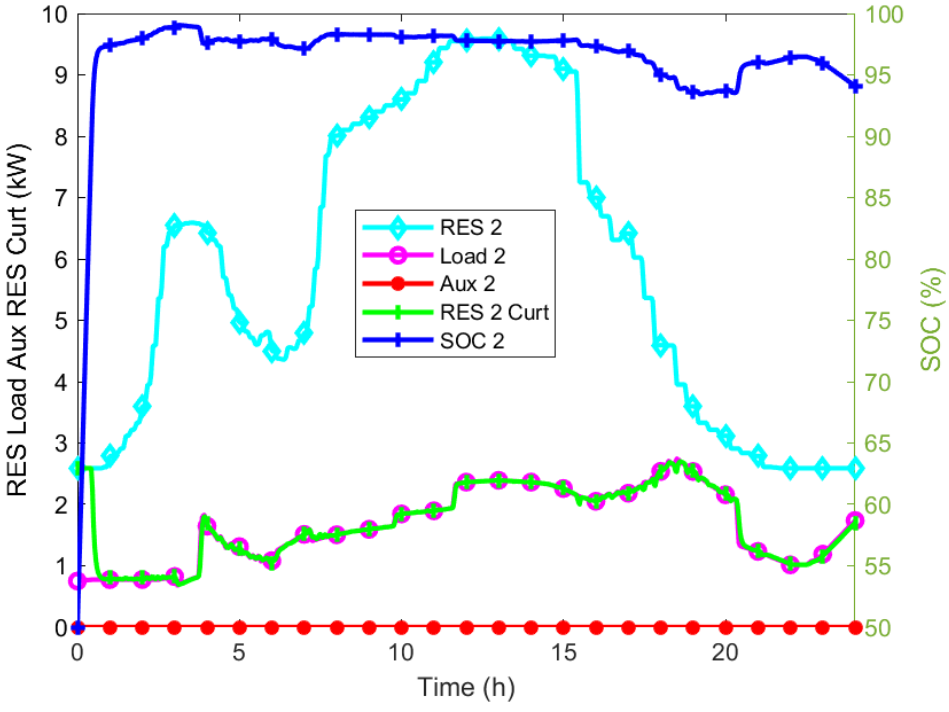
RES 2
Load 2
Aux 2
RES 2 Curt
SOC 2
RES Load Aux RES Curt (kW)
SOC (%)
Time (h)

(b)

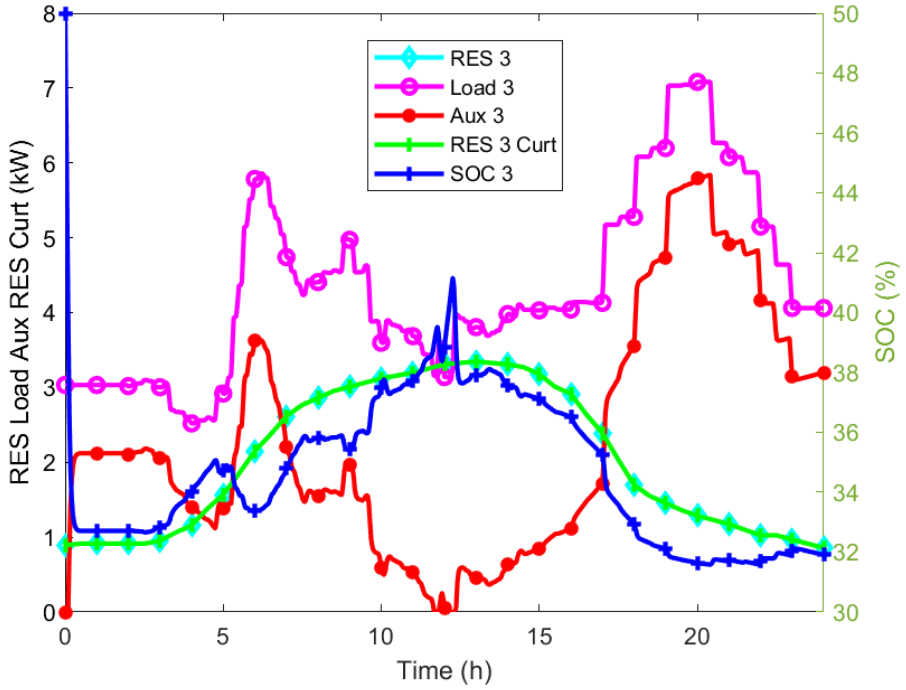

(c)

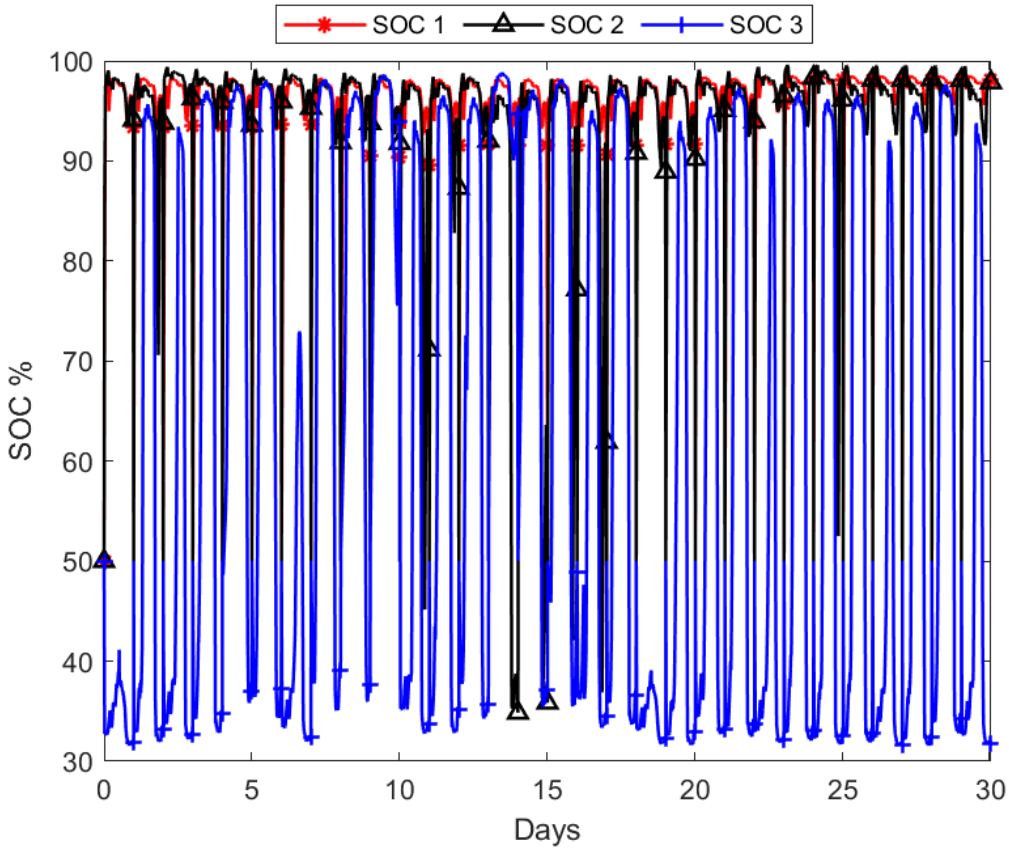

(d)

Figure 5.10(a)-(d): Optimal Dispatching Curves of Independently Operated Microgrids between (30 – 100)% SoC: (a) microgrid one, (b) microgrid two, (c) microgrid three, and (d) Dispatch Curves of 30-day SoC

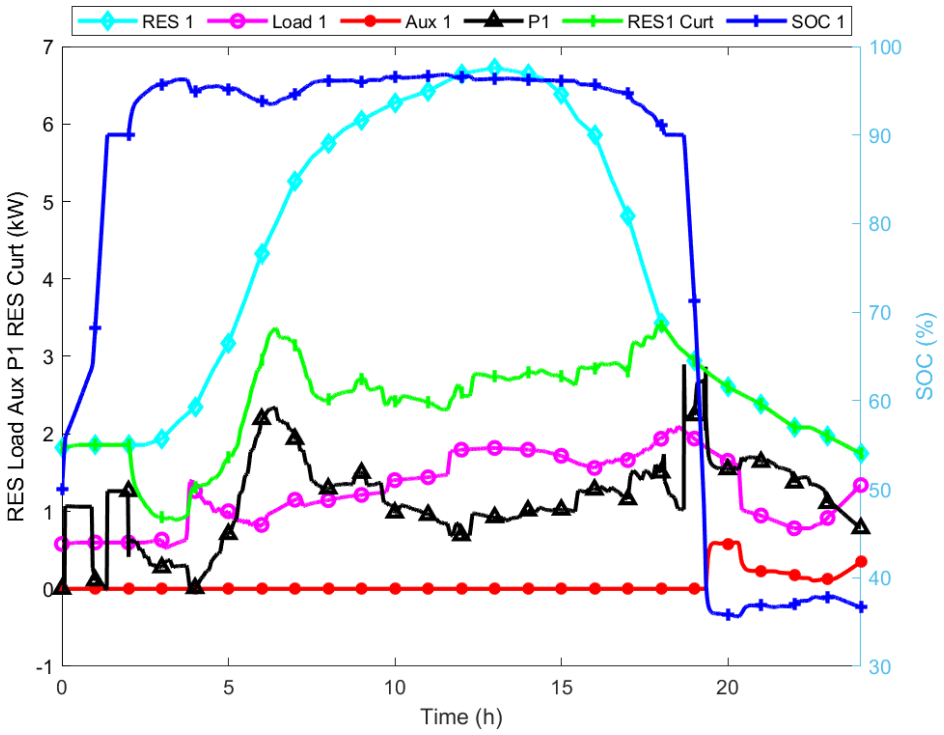

(a)

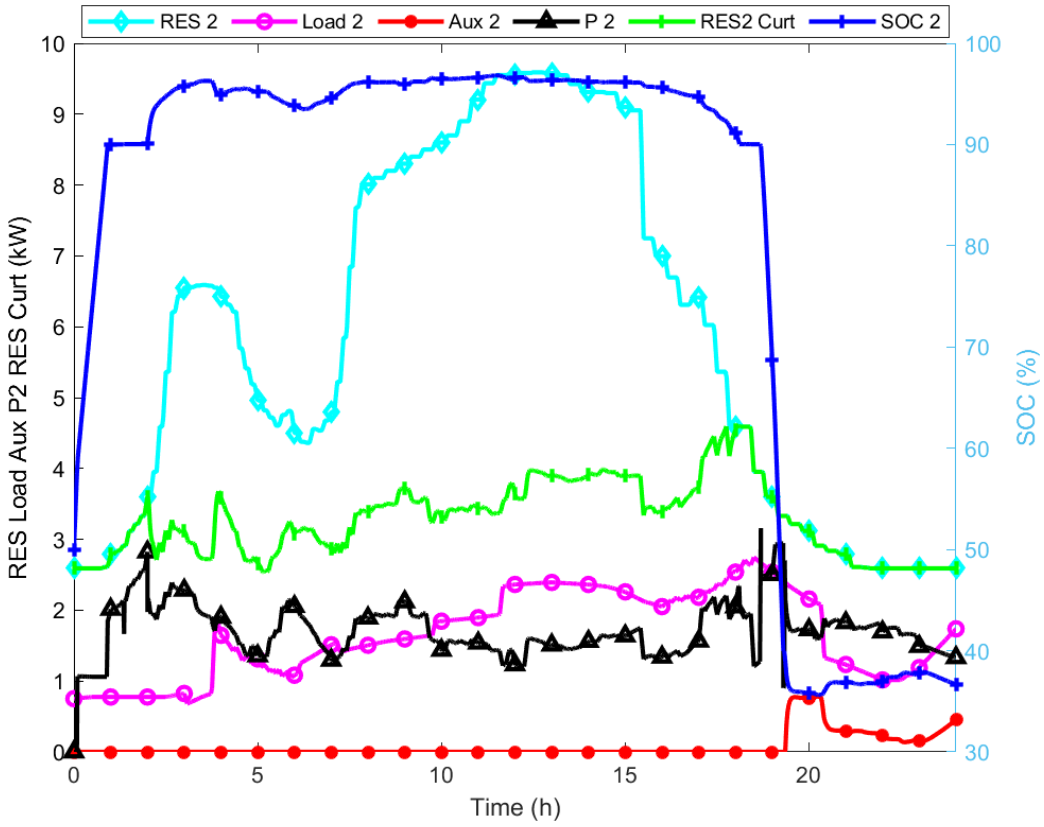

(b)

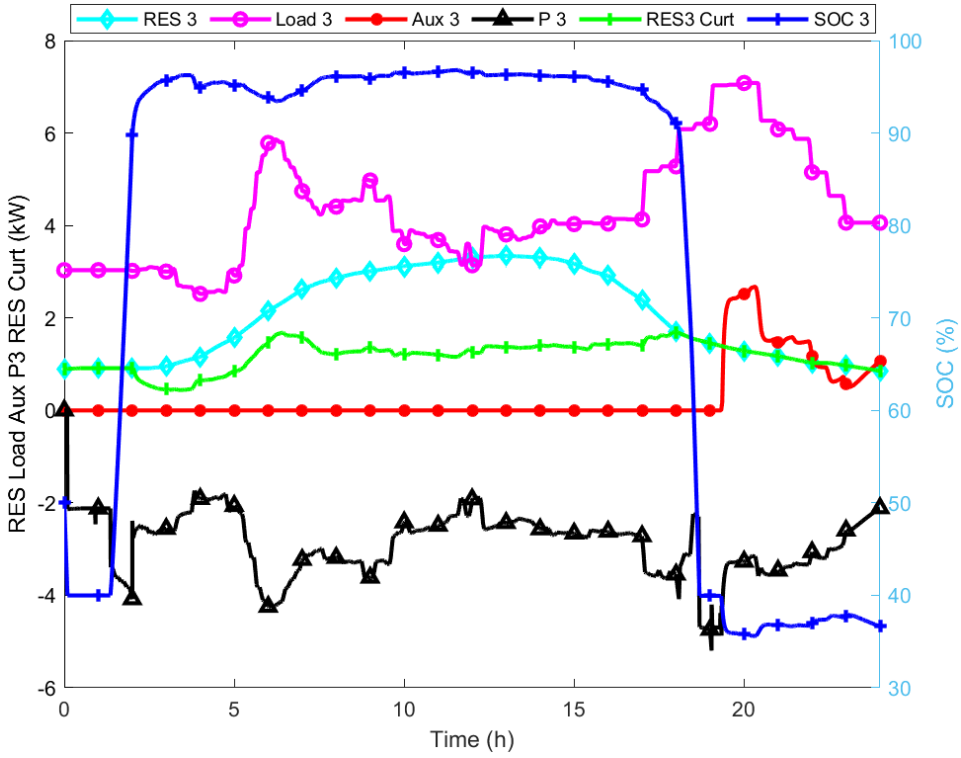

(c)

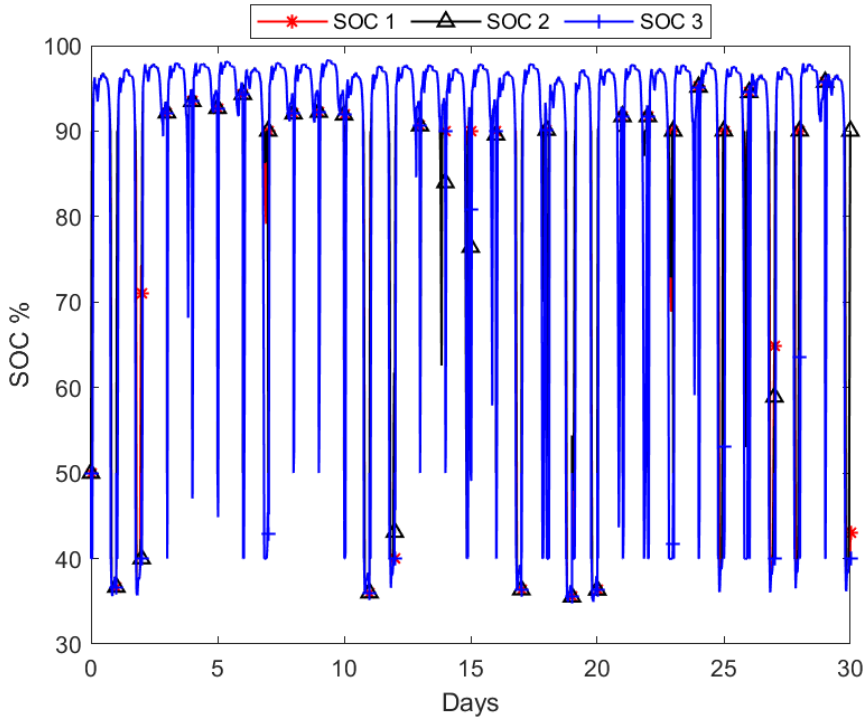

(d)

Figure 5.11(a)-(d): Optimal Dispatching Curves of Interconnected Microgrids with the Global Droop Control, Between (30 – 100)% SoC: (a) microgrid one, (b) microgrid two, (c) microgrid three, and (d) Dispatch Curves of 30-day SoC

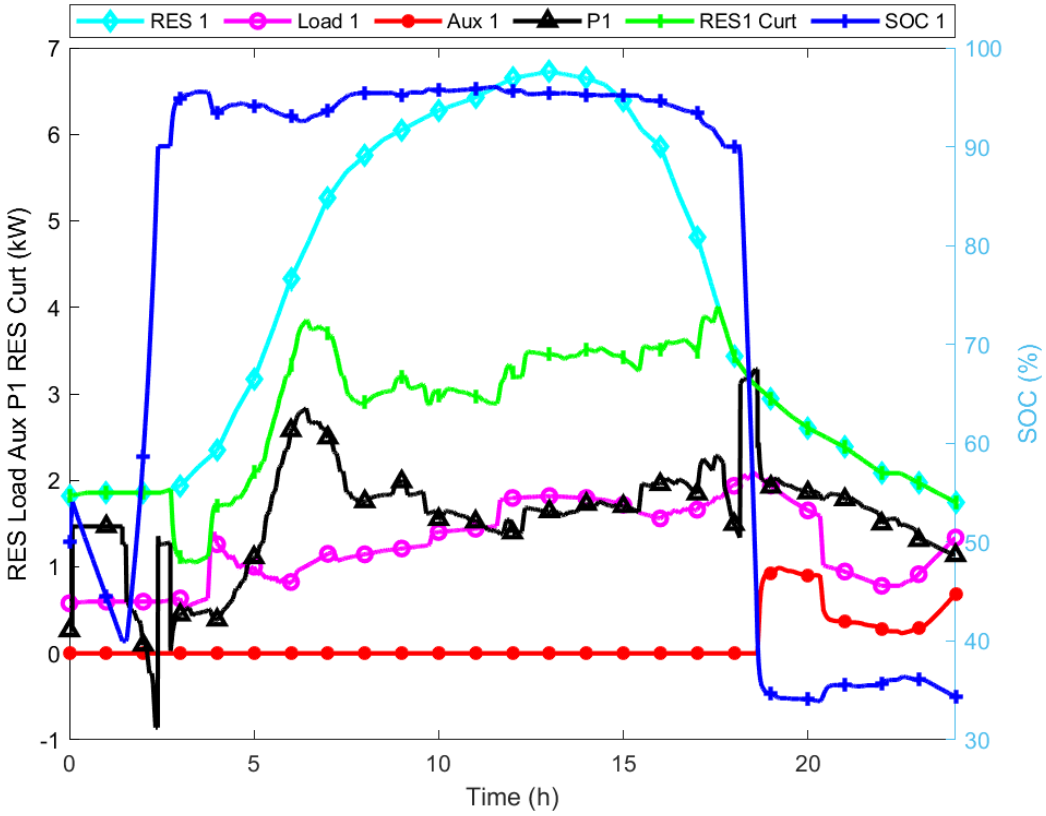

(a)

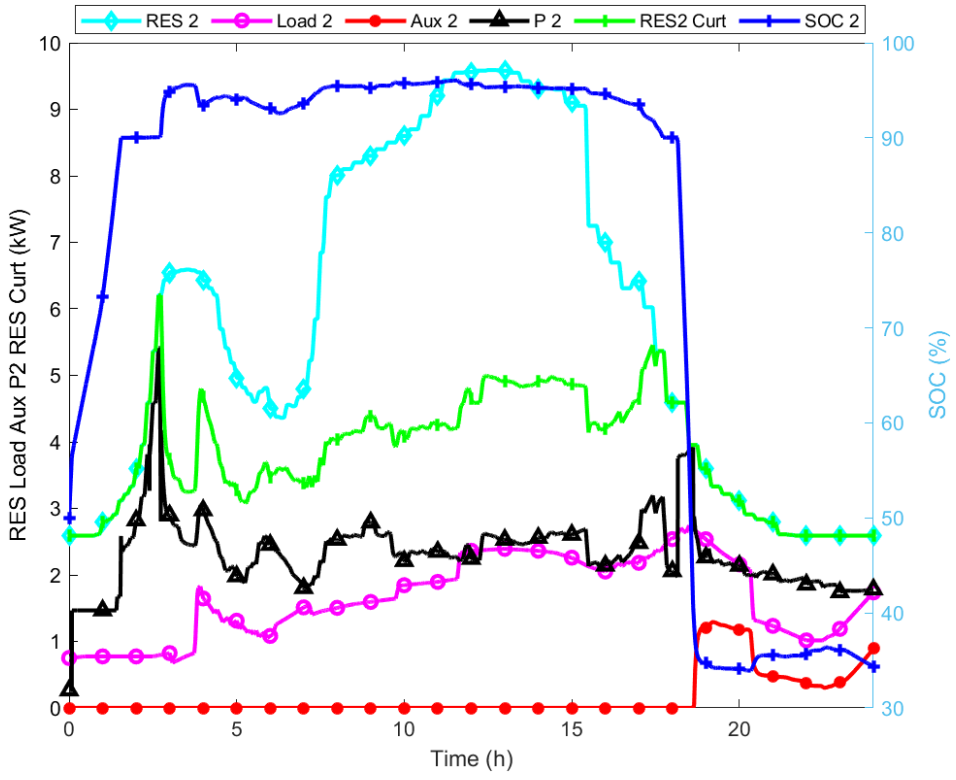

(b)

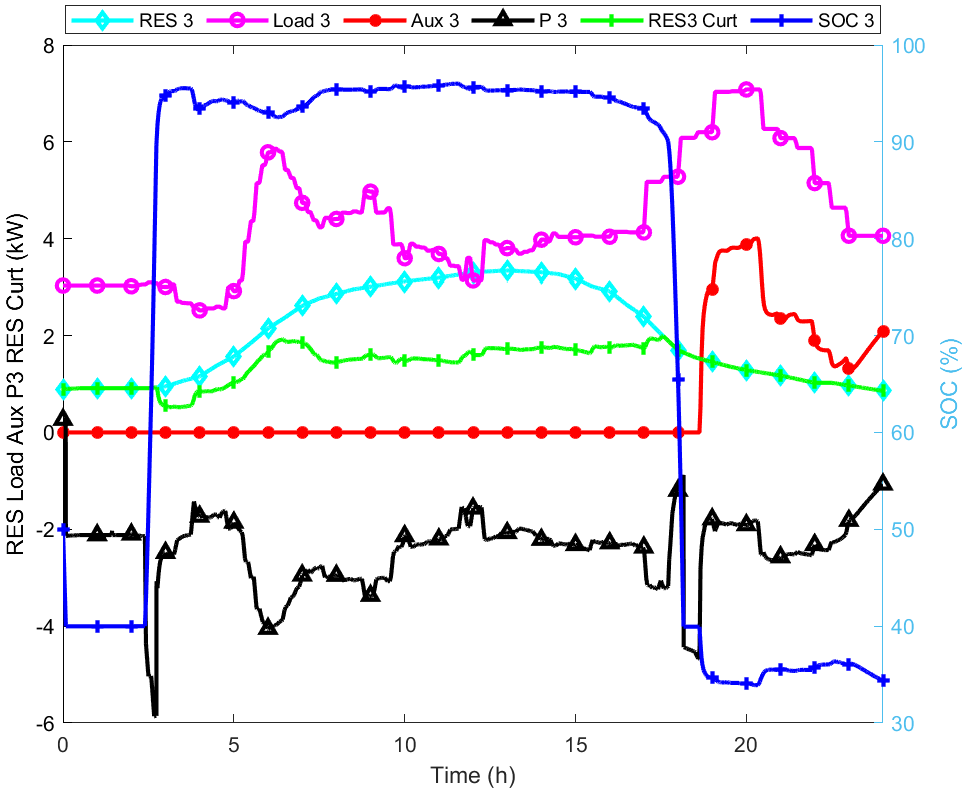

(c)

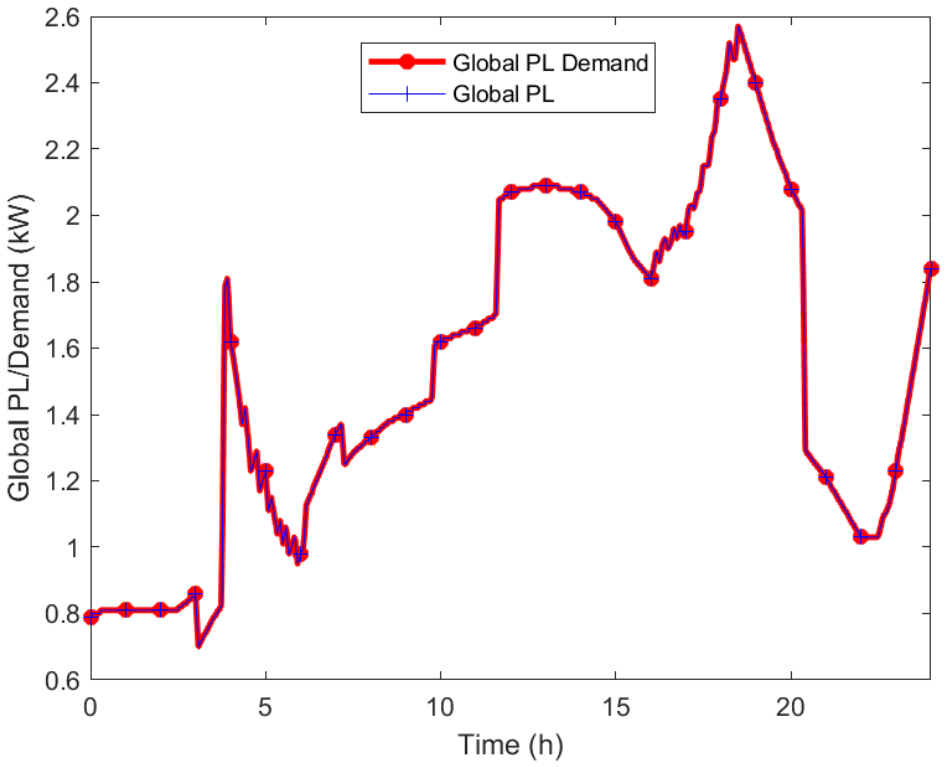

(d)

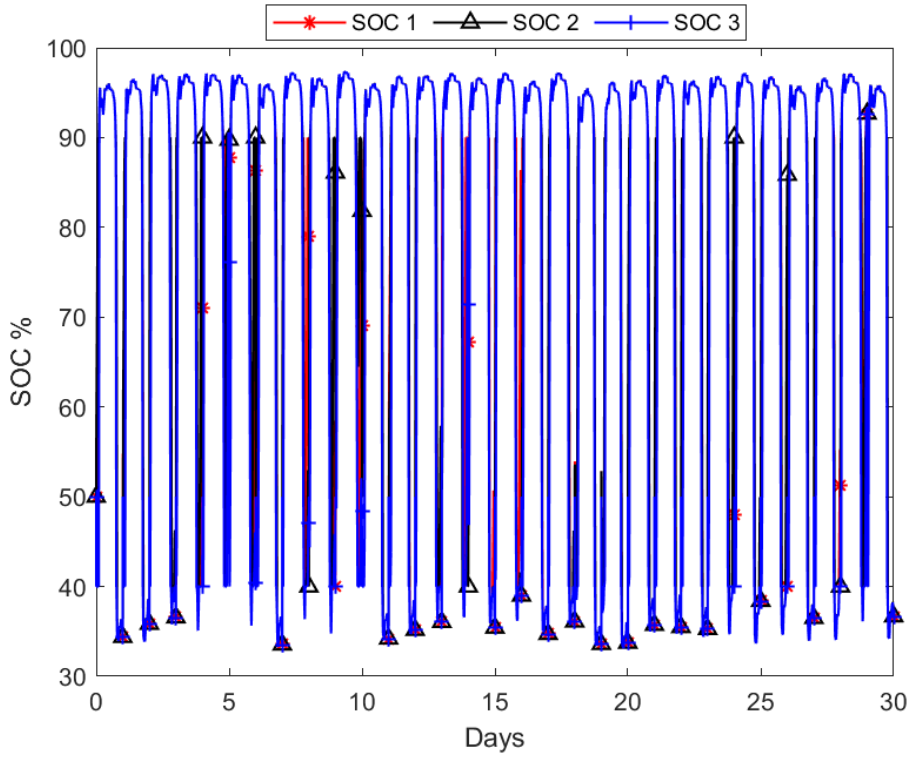

(e)

Figure 5.12(a)-(e): Optimal Dispatching Curves of Interconnected Microgrids with the Global Droop Control and Global Load, Between (30 – 100)% SoC: (a) microgrid one, (b) microgrid two, (c) microgrid three, and (d) Global Load Dispatch Curve (e) Dispatch Curves of 30-day SoC

Figures 5.13 and 5.14 show the optimal RES energy curtailed and optimal auxiliary energy utilised for over 30 days when the microgrids are independently operated, interconnected microgrids and interconnected microgrids with the global load, respectively. Figure 5.13 shows that more RES energy is utilised to meet load demand. Figure 5.14 shows massive reductions in the use of gas for 30 days, which increased when the interconnected microgrids were connected to the global load. However, the lowest use of gas from the auxiliary unit is recorded when the interconnected microgrids are operated with a global droop controller. The highest use of gas is recorded when the microgrids are operated independently, representing the unoptimised case.

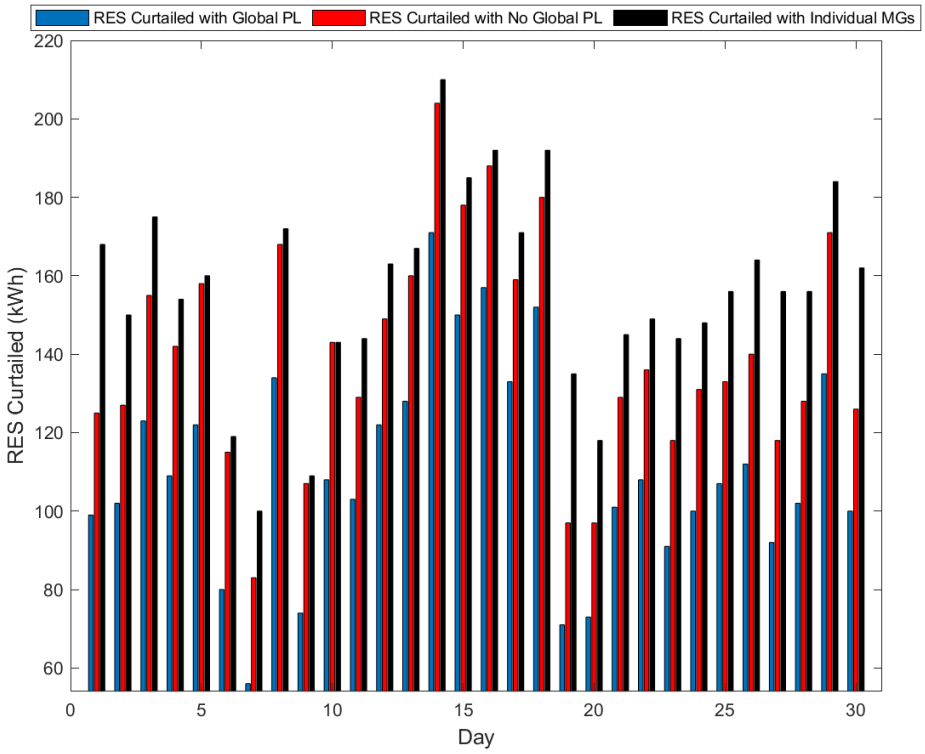

Figure 5.13: Optimal RES Energy Curtailed with Individually Operated Microgrids, with the Global droop controller and the Global Droop Controller and load.

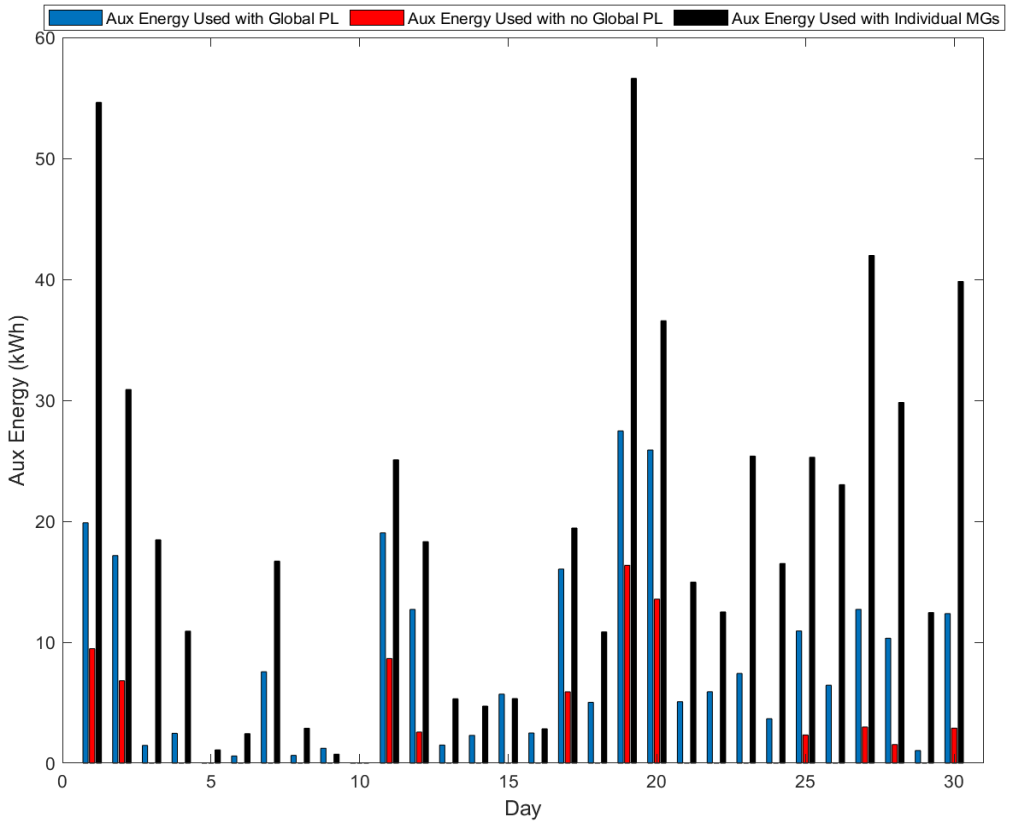

Figure 5.14: Optimal Auxiliary Energy Utilised with Individually Operated Microgrids, with the Global droop controller and the Global Droop Controller and load.

Figures 5.15 and 5.16 show the optimal total RES energy curtailed and optimal total auxiliary energy utilised when the microgrids are independently operated, interconnected microgrids with the global droop control and interconnected microgrids with the global droop control and global load, respectively. Figure 5.15 shows that, overall, more RES energy is utilised to meet the energy demand of the interconnected microgrids. In contrast, Figure 5.16 shows that overall, there is an optimal total reduction in the use of gas to meet the load demand. The case where the microgrids are interconnected with the global droop controller shows the highest reduction in gas, followed by when the interconnected microgrids are connected with the global load, while the individual microgrids operation case shows the optimal highest use of gas. Table 5.4 shows the details of the total optimal auxiliary energy comparison with the percentage reduction between the unoptimised and optimised cases. A detailed performance evaluation of the simulation results shows that the optimisation strategy is optimal, and the result shows that the total optimal auxiliary energy is reduced by about 9%. Hence, the optimised case outperformed the unoptimised case.

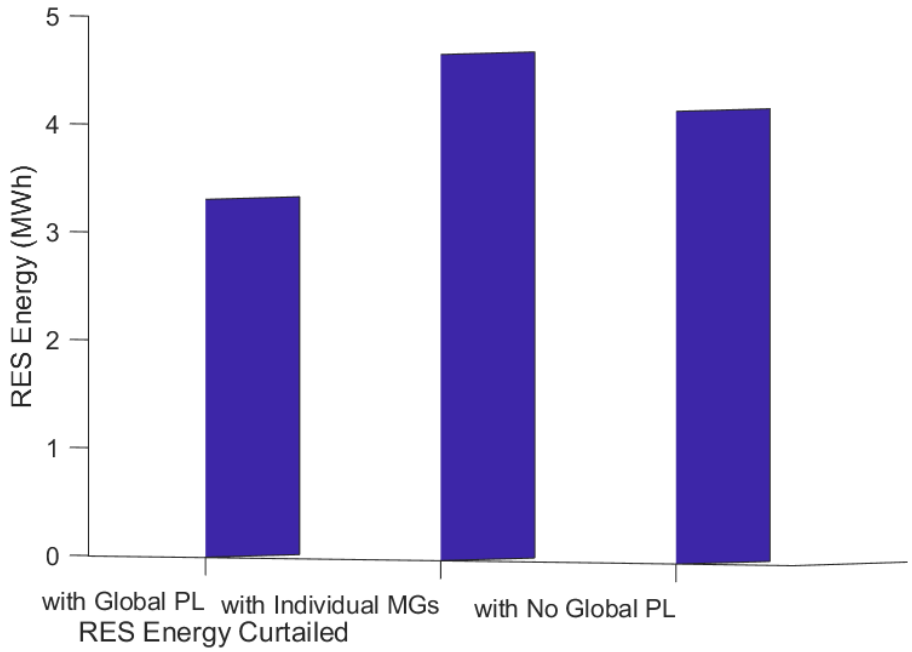

Figure 5.15: Optimal Total RES Energy Curtailed with Individually Operated Microgrids, with the Global droop controller and the Global Droop Controller and load.

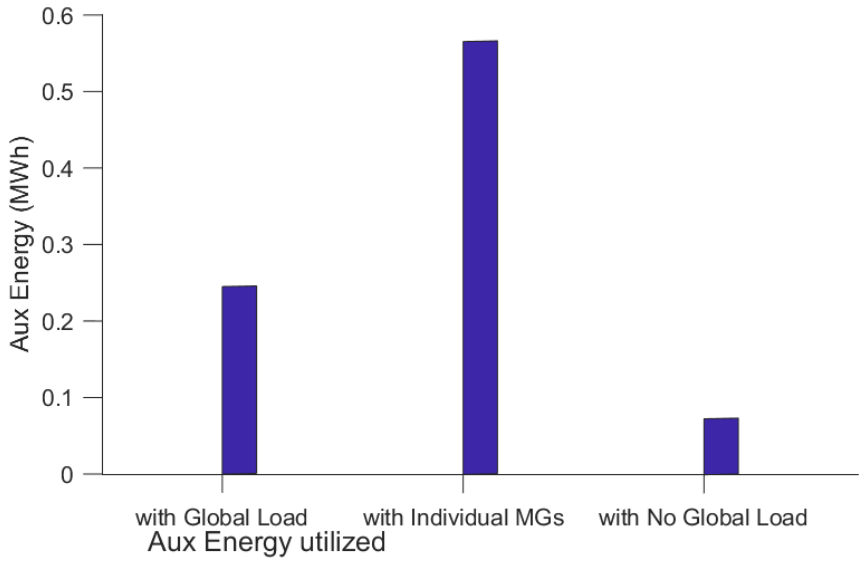

Figure 5.16: Optimal Total Auxiliary Energy Utilised with Individually Operated Microgrids, with the Global droop controller and the Global Droop Controller and load.

Table 5.4. Optimal Auxiliary Energy Comparison with % Reduction Between the Two Cases

Auxiliary Power Use Cases	**Unoptimised Case (Benchmark £/kWh)**	**Optimised Case (£/kWh)**	**%Reduction Between the Two Cases**
Aux. Energy used with Global Load	258.606	245.223	5.2%
Aux. Energy used with no Global Load	91.155	73.146	19.8%
Aux. Energy used with Individual MGs	565.773	565.773	0%
Total auxiliary energy minimised	349.761	318.369	8.98%

5.8 Summary

The chapter presented a centralised control and energy management of multiple interconnected standalone microgrids to minimise the overall cost of auxiliary energy while maximising the use of RES power. Based on the original concept of interconnected microgrids as in Chapter 4, created in this dispatching model, the interconnected network of microgrids is viewed as a single entity with diverse networks capable of operating independently to meet the local load demand and globally to meet the global load demand. Based on this, centralised control and energy management are carried out in a dispatching model using the Fminsearch optimisation toolbox Matlab. The daily total cost of energy

from the auxiliary unit was used to determine whether this optimisation technique was optimal. The optimisation algorithm was carried out based on three case scenarios: single-variable optimisation and multiple-variable optimisation, which considered two cases with the global droop equation left as it is in equation 4.12 in Chapter 4 and with a modified global droop equation (by changing the droop equation from proportional to proportional-integral. The results showed that the single-variable optimisation minimises the overall energy cost from the auxiliary unit and maintains the SOC within the predetermined limit. Whereas the results from the two cases of three-variable optimisation show some consistency in the objective cost minimisation, the system's performance was unstable over the iteration time. It did not tick the boxes in scalability summarised in the performance category of Table 5.3 compared with the single-variable results. Furthermore, the single-variable simulation studies show that the optimised centralised control network outperformed the benchmark in minimising the total cost of auxiliary energy use compared to the unoptimised case, as proposed in Chapter 4. This approach shows that based on a single-variable optimisation approach, it is possible to regulate the total energy utilisation from the auxiliary unit, thereby utilising more energy from the PV-based RES to meet the load demand.

CHAPTER 6: CONCLUSION AND RECOMMENDATION FOR FUTURE WORK

This final chapter of the thesis summarises the findings of the study and makes recommendations for future research work.

6.1 Conclusion

The thesis proposed a novel structure for the design, model, control and energy management of interconnected standalone AC Microgrids using back-to-back converters. The control and energy management of interconnected microgrids have been designed and modelled for standalone interconnected AC microgrids. The system considered in the study consists of three microgrids, and each is connected to a common medium voltage AC bus known as MVAC or global bus and global load via a back-to-back converter and a traditional power transformer. Each microgrid has a PV-based RES, BESS, auxiliary unit, and load. The high-level global droop controller exchanges power between the interconnected microgrids. Hence, the following summarily describes the conclusions of the thesis:

- The key research studies published in the literature concerning the structural design, control and optimal energy management of interconnected microgrids of both the grid-interconnected and standalone-interconnected microgrids have been evaluated. This thesis reviewed different structures and mediums for interconnection and control topologies of interconnecting microgrids in grid-connected and standalone modes. A thorough literature review provides more explicit knowledge to aid the advancement of structural design, control and energy management of interconnected microgrids. Contemporary literature revealed that the structural design, interconnecting medium, control and energy management of interconnected microgrids are not fully resolved yet, and further research into finding better, easier ways for large-scale penetration of RES continues to rise, as concluded in Chapter 2. The effect of changing load conditions at the local microgrid and global interconnected microgrid level and deviations in frequency on the operation of the battery's SOC has been studied.

- The various potential control approaches for back-to-back power electronic converters/two-stage converters have been analysed. The analysis defined different operations for different power converter units and how the identified converter units should operate. It further proposed a global droop control operation for connecting the global converter units to the MVAC bus and the other control operation for the local converter, the microgrid grid-forming converters for the BESS, grid-following converters of the PV-based RES and two-stage converter for the auxiliary unit that floats and only provides power automatically when needed at low deviation in frequency.
- A new structure and control mechanism of standalone interconnected microgrids using the back-to-back converter is proposed to maximise RES power utilisation and provide better load support. A detailed Matlab/Simulink interconnected standalone AC microgrid model has been developed to demonstrate the power exchange from a microgrid with a surplus of power to a microgrid with a power shortage. The interconnected AC microgrids consist of three microgrids. Each microgrid is connected to a common AC bus and global load via a back-to-back converter, a traditional power transformer and a static switch. Each microgrid comprises PV-based RES, BESS, auxiliary unit and load. The detailed model was based on ideal voltages and averaged models with all the required control loops. Each back-to-back converter is identified as either the local converter, the microgrid side converter, or the global converter, the global bus side converter. Both converter units are controlled differently using a modified droop controller to exchange power when required. The global converter is controlled to demand power from the global bus or send power to the global bus based on the frequency deviation from the local microgrid bus. The concept of one microgrid putting down its bus frequency below nominal value to reflect a shortage of power and the other microgrid putting up its frequency above nominal value to reflect a surplus in power among interconnected microgrids allows the exchange of power to automatically occur whenever there is a

shortage/surplus has been demonstrated. The amount of deviation in frequency below nominal determines the amount of power to be demanded from the microgrid with a shortage, while the amount of deviation in frequency above nominal determines the amount of power to be exported from the microgrid with a surplus and vice versa. The detailed model was tested using two cases using the proportional controller when the interconnected microgrid operates with power-sharing capability and reserves capacity to complement each and using the proportional-integral control when the interconnected microgrid operates with no power-sharing capability. The proportional control case achieved the desired result and allowed power to be exchanged among interconnected microgrids, thereby providing better support for the load. It is important to reiterate that the proposed structure and control using back-to-back converters only deals with real power management. This thesis does not address the reactive power component. Furthermore, the thesis does not consider the economics of the power units.

- A high-level controller was proposed and has been designed to manage power flow between multiple interconnected standalone AC microgrids using back-to-back converters. A Matlab/Simulink model of interconnected standalone AC microgrid was developed to assess the performance of the proposed high-level global droop controller. This controller uses a frequency bus-signalling technique as input and the proposed global droop controller to exchange the right amount of power between interconnected microgrids. The controller was implemented without any communication link between the microgrids. At the microgrid level, the auxiliary unit floats and only supplies power when needed, largely dependent on the deviation in frequency and to avoid frequency degradation below allowable limits. On the other hand, the PV-based RES power curtailment mechanism is utilised to curtail the surplus RES when required to prevent overcharging the battery. However, the deviation in frequency below or above the defined limit determines the amount supplemented by the auxiliary unit or curtailed as surplus from the PV-based RES. The BESS maintained the bus voltage and

frequency in the standalone AC microgrid. The BESS balances the difference between the PV-based RES power and that consumed by the load. This model considers the global droop control level and model of the BESS to speed up the simulation time to adequately assess the controller's performance, especially over long periods of time. Chapter 4 presented the results of short- and long-term simulations utilising this model, in which the system was evaluated using various RES and load profiles. The results obtained from both simulation cases validate the performance of the proposed controller. The results of both simulation cases indicate that the proposed global droop controller exchanges the right amount of power when needed. The controller prioritises PV power export over curtailment and imports over auxiliary power supplement. Furthermore, the controller under normal operation with the global droop was compared with the independent operation of microgrids and multiple microgrids interconnected with the global droop control and global load, and the results show that the global droop controller satisfies the control priorities and design requirements.

- A centralised control and energy management system for interconnected standalone AC microgrids has been designed and implemented in Chapter 5. A centralised control and optimisation approach has been applied to the proposed system in Chapter 4 to investigate the optimal cost of the total auxiliary power utilised every 24 hours in the whole network. Due to the complex nature of the interconnected microgrid network, a simple and unconstrained optimisation strategy is known as Fminsearch. Fminsearch finds the minimum of an unconstrained multivariable function using the derivative-free method. The proposed Fminsearch algorithm was executed considering three cases: single-variable and two cases of three-variable optimisation, namely when the global droop equation is left and when the global droop equation is modified. Simulation results on the three cases showed instability in the two cases of three-variable optimisation. The result from the single-variable optimisation case shows that the system is stable, and the optimised case outperformed the benchmark case in

terms of minimising the total cost of auxiliary power use compared to the unoptimised case, as proposed in Chapter 4. Detailed performance evaluation from the simulation results shows that the optimisation strategy is optimal, and the result shows that the total auxiliary energy is reduced to about 9% compared with the benchmark.

6.2 Future Works

In addition to the outcomes of this thesis, the following exciting areas can be looked into further as a future extension of the work:

- The reactive power can be included as an integral part of the power management for standalone interconnected microgrids. This can be done by formulating another global reactive droop control equation from the reactive power component of the droop control based on the number of interconnecting microgrids. It derives the global reactive droop and the related steady-state equations to enhance global reactive power requirements.
- Consider designing a structure of multiple standalone DC microgrids to the common DC bus (having a global DC bus) instead of the common AC bus. This structure can be used to transmit DC technology over a long distance, and a similar method of power management used for the common AC bus can be adopted for interconnected standalone microgrids connected to the common DC bus.
- An investigation into a detailed small-signal stability modelling and analysis can be done on the existing detailed structure of interconnected standalone AC microgrids. This study can consider the closed-loop control system of a microgrid, express them in the state-space domain, and use the stability of individual microgrids and interconnected microgrids. The expected results can be helpful as a stability criterion for interconnected microgrids.
- A study in the economics of implementation can be carried out to estimate the practical implementation and running cost of the different power units to inform or give any prospective

user an estimated cost of implementation and running. This study can help better understand the actual design capacities/size and overall cost of operating every power unit.

- Use another optimisation method, such as particle swarm optimisation (PSO), genetic algorithm (GA), random generation of solutions, etc, to optimise the system further and compare the results obtained to determine the best solution. This could help to improve the decision-making process in terms of implementation for the future.
- Build a laboratory simple scale of interconnected standalone AC microgrids that consist of three microgrids connected to a common AC bus via back-to-back converters and implement the global droop control scheme experimentally and observe to see power exchanged from one microgrid with surplus to another microgrid with a shortage of power. Also, compare results with proportional and proportional-integral control. Similarly, verify experimentally the power flow management of interconnected standalone AC microgrids using back-to-back converters, verify the proposed global droop control experimentally, and compare the results using the optimised gain value and unoptimised system.

References

[1] United Nations, “The Climate Crisis-A Race We Can Win,” https://www.un.org/en/un75/climate-crisis-race-we-can-win. Accessed: Jul. 01, 2023. [Online]. Available: https://www.un.org/en/un75/climate-crisis-race-we-can-win

[2] IRENA, “Reaching Zero with Renewables: Eliminating CO2 emissions from industry and transport in line with the 1.5^{0}C climate goal,” 2020.

[3] F. Birol, “World Energy Outlook 2021,” *International Energy Agency*, 2021.

[4] U. Nations, *The 2030 Agenda and the Sustainable Development Goals: An opportunity for Latin America and the Caribbean*. Santiago: United Nations publication, 2018.

[5] IEA, “Renewables 2022,” Paris, 2022. Accessed: Jul. 02, 2023. [Online]. Available: https://www.iea.org/reports/renewables-2022

[6] J. Hossain *et al.*, “Design of Robust Distributed Control for Interconnected Microgrids,” *IEEE Trans Smart Grid*, vol. 7, no. 6, pp. 2724–2735, 2016.

[7] W. Issa, “Improved Control Strategies for Droop - Controlled Inverter - Based Microgrid,” p. 202, 2015.

[8] S. S. Mavuri, J. Nakka, and A. Kotla, “Interconnected Microgrids: A Review and Future perspectives,” in *2022 IEEE 2nd International Conference on Sustainable Energy and Future Electric Transportation, SeFeT 2022*, Institute of Electrical and Electronics Engineers Inc., 2022. doi: 10.1109/SeFeT55524.2022.9908988.

[9] K. Prabakar *et al.*, “Remote Hardware-in-the-Loop Approach for Microgrid Controller Evaluation,” in *Clemson University Power Systems Conference (PSC)*, 2020. doi: 10.1109/PSC50246.2020.9131282.

[10] M. H. Spiegel, E. M. S. P. Veith, and T. I. Strasser, “The spectrum of proactive, resilient multi-microgrid scheduling: A systematic literature review,” *Energies*, vol. 13, no. 17. MDPI AG, Sep. 01, 2020. doi: 10.3390/en13174543.

[11] R. S. M. AI Badwawi, “Supervisory Control and Power Management of an AC Microgrid,” PhD Thesis, University of Exeter , Penryn, 2017.

[12] S. Chowdhury, S. P. Chowdhury, and P. Crossley, *Microgrids and Active Distribution Networks*, vol. IET Ren Ener Ser. 6. 2009.

[13] M. Naderi, Y. Khayat, Q. Shafiee, T. Dragicevic, H. Bevrani, and F. Blaabjerg, “Interconnected Autonomous ac Microgrids via Back-to-Back Converters — Part II : Stability Analysis,” *IEEE Trans Power Electron*, vol. 35, no. 11, pp. 11801–11812, 2020.

[14] L. Che, X. Zhang, M. Shahidehpour, A. Alabdulwahab, and A. Abusorrah, “Optimal Interconnection Planning of Community Microgrids with Renewable Energy Sources,” *IEEE Trans Smart Grid*, vol. 8, no. 3, pp. 1054–1063, May 2017, doi: 10.1109/TSG.2015.2456834.

[15] I. U. Nutkani, P. C. Loh, P. Wang, T. K. Jet, and F. Blaabjerg, “Intertied ac-ac microgrids with autonomous power import and export,” *International Journal of Electrical Power and Energy Systems*, vol. 65, pp. 385–393, 2015, doi: 10.1016/j.ijepes.2014.10.040.

[16] R. Al Badwawi, W. R. Issa, T. K. Mallick, and M. Abusara, "Supervisory Control for Power Management of an Islanded AC Microgrid Using a Frequency Signalling-Based Fuzzy Logic Controller," *IEEE Trans Sustain Energy*, vol. 10, no. 1, pp. 94–104, 2019.

[17] I. U. Nutkani, P. C. Loh, and F. Blaabjerg, "Power flow control of intertied ac microgrids," *IEEE Trans Power Electron*, vol. 6, no. 7, pp. 1329–1338, 2013, doi: 10.1049/iet-pel.2012.0640.

[18] B. Zhao *et al.*, "Energy Management of Multiple Microgrids Based on a System of Systems Architecture," *IEEE TRANSACTIONS ON POWER SYSTEMS*, vol. 33, no. 6, 2018, doi: 10.1109/TPWRS.2018.2840055.

[19] M. Grami, M. Rekik, and L. Krichen, "A Power management Strategy for Interconnected Microgrids," *Proceedings - STA 2020: 2020 20th International Conference on Sciences and Techniques of Automatic Control and Computer Engineering*, pp. 213–218, Dec. 2020, doi: 10.1109/STA50679.2020.9329333.

[20] M. Elshenawy, A. Fahmy, A. Elsamahy, S. A. Kandil, and H. M. E. Zoghby, "Optimal Power Management of Interconnected Microgrids Using Virtual Inertia Control Technique," *Energies (Basel)*, vol. 15, no. 19, p. 7026, 2022, [Online]. Available: https://doi.org/10.3390/en15197026

[21] J. L. Afonso *et al.*, "A review on power electronics technologies for power quality improvement," *Energies (Basel)*, vol. 14, no. 24, 2021, doi: 10.3390/en14248585.

[22] B. M. Eid, N. A. Rahim, J. Selvaraj, and A. H. El Khateb, "Control methods and objectives for electronically coupled distributed energy resources in microgrids: A review," *IEEE Systems Journal*, vol. 10, no. 2. pp. 446–458, 2016. doi: 10.1109/JSYST.2013.2296075.

[23] L. Huang, C. Wu, F. Blaabjerg, and D. Zhou, "Grid Impedance Impact on the Maximum Power Transfer Capability of Grid-Connected Inverter; Grid Impedance Impact on the Maximum Power Transfer Capability of Grid-Connected Inverter," *2021 IEEE 12th Energy Conversion Congress & Exposition - Asia (ECCE-Asia)*, 2021, doi: 10.1109/ECCE-Asia49820.2021.9479080.

[24] L. Huang, C. Wu, D. Zhou, and F. Blaabjerg, "Impact of Grid Strength and Impedance Characteristics on the Maximum Power Transfer Capability of Grid-Connected Inverters," *MDPI Appl. Sci*, 2021, doi: https://doi.org/ 10.3390/app11094288.

[25] D. Rogers, A. M. Herscowitz, and K. Auth, "Power Africa: A U.S Governament-led Partnership," 2019. [Online]. Available: www.usaid.gov/powerafrica/nigeria

[26] E. Udoha, S. Das, and M. Abusara, "Power Flow Management of Interconnected AC Microgrids Using Back-to-Back Converters," *Electronics (Basel)*, vol. 12, no. 18, p. 3765, Sep. 2023, doi: 10.3390/electronics12183765.

[27] P. Wu, W. Huang, N. Tai, and S. Liang, "A novel design of architecture and control for multiple microgrids with hybrid AC/DC connection," *Appl Energy*, vol. 210, pp. 1002–1016, Jan. 2018, doi: 10.1016/j.apenergy.2017.07.023.

[28] E. Bullich-Massagué, F. Díaz-González, M. Aragüés-Peñalba, F. Girbau-Llistuella, P. Olivella-Rosell, and A. Sumper, "Microgrid clustering architectures," *Appl Energy*, vol. 212, pp. 340–361, Feb. 2018, doi: 10.1016/j.apenergy.2017.12.048.

[29] T. by Qobad Shaee, "Multi-Functional Distributed Secondary Control for Autonomous Microgrids," Aalborg University, Aalborg, 2014.

[30] H. M. Kim, T. Kinoshita, and M. C. Shin, “A multiagent system for autonomous operation of islanded microgrids based on a power market environment,” *Energies (Basel)*, vol. 3, no. 12, pp. 1972–1990, Dec. 2010, doi: 10.3390/en3121972.

[31] F. Katiraei and M. R. Iravani, “Power management strategies for a microgrid with multiple distributed generation units,” *IEEE Transactions on Power Systems*, vol. 21, no. 4, pp. 1821–1831, Nov. 2006, doi: 10.1109/TPWRS.2006.879260.

[32] R. Zamora and A. K. Srivastava, “Multi-Layer Architecture for Voltage and Frequency Control in Networked Microgrids,” *IEEE Trans Smart Grid*, vol. 9, no. 3, pp. 2076–2085, May 2018, doi: 10.1109/TSG.2016.2606460.

[33] M. A. Hossain, “Energy Management of Community Microgrids using Particle Swarm Optimisation,” Thesis, The University of New South Wales, Canberra, 2020. [Online]. Available: https://www.researchgate.net/publication/360061396

[34] T. Dragicevic, J. M. Guerrero, J. C. Vasquez, and D. Skrlec, “Supervisory control of an adaptive-droop regulated DC microgrid with battery management capability,” *IEEE Trans Power Electron*, vol. 29, no. 2, pp. 695–706, 2014, doi: 10.1109/TPEL.2013.2257857.

[35] M. A. Hossain, H. R. Pota, M. J. Hossain, and F. Blaabjerg, “Evolution of microgrids with converter-interfaced generations: Challenges and opportunities,” *International Journal of Electrical Power and Energy Systems*, vol. 109. Elsevier Ltd, pp. 160–186, Jul. 01, 2019. doi: 10.1016/j.ijepes.2019.01.038.

[36] M. Zolfaghari, G. B. Gharehpetian, M. Shafie-khah, and J. P. S. Catalão, “Comprehensive review on the strategies for controlling the interconnection of AC and DC microgrids,” *International Journal of Electrical Power and Energy Systems*, vol. 136. Elsevier Ltd, Mar. 01, 2022. doi: 10.1016/j.ijepes.2021.107742.

[37] F. Nejabatkhah and Y. W. Li, “Overview of Power Management Strategies of Hybrid AC/DC Microgrid,” *IEEE Transactions on Power Electronics*, vol. 30, no. 12. Institute of Electrical and Electronics Engineers Inc., pp. 7072–7089, Dec. 01, 2015. doi: 10.1109/TPEL.2014.2384999.

[38] H. Xiao, A. Luo, Z. Shuai, G. Jin, and Y. Huang, “An improved control method for multiple bidirectional power converters in hybrid AC/DC microgrid,” *IEEE Trans Smart Grid*, vol. 7, no. 1, pp. 340–347, Jan. 2016, doi: 10.1109/TSG.2015.2469758.

[39] L. Che, M. Shahidehpour, A. Alabdulwahab, and Y. Al-Turki, “Hierarchical coordination of a community microgrid with AC and DC microgrids,” *IEEE Trans Smart Grid*, vol. 6, no. 6, pp. 3042–3051, Nov. 2015, doi: 10.1109/TSG.2015.2398853.

[40] J. G. Ciezki and R. W. Ashton, “Selection and Stability Issues Associated with a Navy Shipboard DC Zonal Electric Distribution System,” 2000.

[41] A. T. Elsayed, A. A. Mohamed, and O. A. Mohammed, “DC microgrids and distribution systems: An overview,” *Electric Power Systems Research*, vol. 119. Elsevier Ltd, pp. 407–417, 2015. doi: 10.1016/j.epsr.2014.10.017.

[42] D. Salomonsson and A. Sannino, “Low-voltage DC distribution system for commercial power systems with sensitive electronic loads,” *IEEE Transactions on Power Delivery*, vol. 22, no. 3, pp. 1620–1627, 2007, doi: 10.1109/TPWRD.2006.883024.

[43] Y. W. Li and C. N. Kao, “An accurate power control strategy for power-electronics-interfaced distributed generation units operating in a low-voltage multibus microgrid,” *IEEE Trans Power Electron*, vol. 24, no. 12, pp. 2977–2988, 2009, doi: 10.1109/TPEL.2009.2022828.

[44] J. J. Justo, F. Mwasilu, J. Lee, and J. W. Jung, “AC-microgrids versus DC-microgrids with distributed energy resources: A review,” *Renewable and Sustainable Energy Reviews*, vol. 24. pp. 387–405, 2013. doi: 10.1016/j.rser.2013.03.067.

[45] K. S. Rajesh, S. S. Dash, R. Rajagopal, and R. Sridhar, “A review on control of ac microgrid,” *Renewable and Sustainable Energy Reviews*, vol. 71. Elsevier Ltd, pp. 814–819, 2017. doi: 10.1016/j.rser.2016.12.106.

[46] J. Rocabert, A. Luna, F. Blaabjerg, and P. Rodríguez, “Control of power converters in AC microgrids,” *IEEE Trans Power Electron*, vol. 27, no. 11, pp. 4734–4749, 2012, doi: 10.1109/TPEL.2012.2199334.

[47] Hemanshu R. Pota, M. J. Hossain, M. A. Mahmud, and Rajit Gadh, “Control for Microgrids with Inverter Connected Renewable Energy Resources,” in *IEEE PES General Meeting | Conference & Exposition*, 2014.

[48] M. Dabbaghjamanesh, S. Mehraeen, A. Kavousi-Fard, and F. Ferdowsi, “A New Efficient Stochastic Energy Management Technique for Interconnected AC Microgrids,” *IEEE Power and Energy Society General Meeting*, vol. 2018-Augus. 2018. doi: 10.1109/PESGM.2018.8586362.

[49] J. G. De Matos, F. S. F. E Silva, and L. A. S. Ribeiro, “Power control in AC isolated microgrids with renewable energy sources and energy storage systems,” *IEEE Transactions on Industrial Electronics*, vol. 62, no. 6, pp. 3490–3498, Jun. 2015, doi: 10.1109/TIE.2014.2367463.

[50] L. ’Fusheng, L. ’Ruisheng, and Z. ’Fengquan, “Microgrid Technology and Engineering Application,” in *Elsevier*, Elsevier, 2016. doi: 10.1016/B978-0-12-803598-6.00015-2.

[51] M. B. Sigalo, A. C. Pillai, S. Das, and M. Abusara, “An energy management system for the control of battery storage in a grid-connected microgrid using mixed integer linear programming,” *Energies (Basel)*, vol. 14, no. 19, Oct. 2021, doi: 10.3390/en14196212.

[52] P. P. Vergara *et al.*, “A Generalized Model for the Optimal Operation of Microgrids in Grid-Connected and Islanded Droop-Based Mode,” *IEEE Trans Smart Grid*, vol. 10, no. 5, pp. 5032–5045, Sep. 2018, doi: 10.1109/TSG.2018.2873411.

[53] T. John, “Operation and Control of Multi-area Multi-microgrid Systems,” 2017.

[54] H. Karimi, H. Nikkhajoei, and R. Iravani, “Control of an electronically-coupled distributed resource unit subsequent to an islanding event,” *IEEE Transactions on Power Delivery*, vol. 23, no. 1, pp. 493–501, Jan. 2008, doi: 10.1109/TPWRD.2007.911189.

[55] F. Katiraei, M. R. Iravani, and P. W. Lehn, “Micro-grid autonomous operation during and subsequent to islanding process,” *IEEE Transactions on Power Delivery*, vol. 20, no. 1, pp. 248–257, Jan. 2005, doi: 10.1109/TPWRD.2004.835051.

[56] Y. Li, D. M. Vilathgamuwa, and P. C. Loh, “Design, analysis, and real-time testing of a controller for multibus microgrid system,” *IEEE Trans Power Electron*, vol. 19, no. 5, pp. 1195–1204, Sep. 2004, doi: 10.1109/TPEL.2004.833456.

[57] Prasenjit Basak, A. K. Saha, S. Chowdhury, and S. P. Chowdhury, "Microgrid: Control techniques and modeling," in *Proceedings of the IEEE 44th International Universities Power Engineering Conference (UPEC)*, 2009.

[58] H. Fathima, N. Prabaharan, K. Palanisamy, A. Kalam, S. Mekhilef, and J.J. Justo, *Hybrid-Renewable Energy Systems in Microgrids : Integration, Developments and Control*. Wood head Publishing Series in Energy, 2018.

[59] M. Jamil, B. Hussain, M. Abu-Sara, R. J. Boltryk, and S. M. Sharkh, "Microgrid Power Electronic Converters: State of the Art and Future Challenges," in *44th International Universities Power Engineering Conference (UPEC)*, Glasgow: 44th International Universities Power Engineering Conference (UPEC), Sep. 2009.

[60] J. M. Guerrero, M. Castilla, and J. Miret, "A Wireless Controller to Enhance Dynamic Performance of Parallel Inverters in Distributed Generation Systems," vol. 19, no. 5, pp. 1205–1213, 2004.

[61] H. Hasabelrasul, Z. Cai, L. Sun, X. Suo, and I. Matraji, "Two-Stage Converter Standalone PV-Battery System Based on VSG Control," *IEEE Access*, vol. 10, pp. 39825–39832, 2022, doi: 10.1109/ACCESS.2022.3165664.

[62] N. H. Selman and J. R. Mahmood, "Design and Simulation of two Stages Single Phase PV Inverter operating in Standalone Mode without Batteries," *International Journal of Engineering Trends and Technology*, vol. 37, no. 2, 2016, [Online]. Available: http://www.ijettjournal.org

[63] Y. Zeng, "Droop Control of Parallel-Operated Inverters," The University of Sheffield, Sheffield, 2015.

[64] M. N. Marwali and A. Keyhani, "Control of distributed generation systems - Part I: Voltages and currents control," *IEEE Trans Power Electron*, vol. 19, no. 6, pp. 1541–1550, Nov. 2004, doi: 10.1109/TPEL.2004.836685.

[65] I. M. de A. Estefanía Planas, Asier Gil-de-Muro, Jon Andreu, Iñigo Kortabarria, "General aspects, hierarchical controls and droop methods in microgrids: A review," *Renewable and Sustainable Energy Reviews*, vol. 17, pp. 147–159, 2013, doi: https://doi.org/10.1016/j.rser.2012.09.032.

[66] K. H. Ahmed, A. M. Massoud, G. P. Adam, and A. F. Zobaa, "A State of the Art Review of Control Techniques for Power Electronics Converter Based Distributed Generation Systems in Different Modes of Operation," *International Conference on Renewable Energy Research and Applications*, no. October, pp. 20–23, 2013.

[67] J. M. Guerrero, L. Hang, and J. Uceda, "Control of distributed uninterruptible power supply systems," *IEEE Transactions on Industrial Electronics*, vol. 55, no. 8, pp. 2845–2859, 2008, doi: 10.1109/TIE.2008.924173.

[68] B. Zhao, X. Zhang, and J. Chen, "Integrated microgrid laboratory system," *IEEE Transactions on Power Systems*, vol. 27, no. 4, pp. 2175–2185, 2012, doi: 10.1109/TPWRS.2012.2192140.

[69] X. Yu, A. M. Khambadkone, H. Wang, and S. T. S. Terence, "Control of parallel-connected power converters for low-voltage microgrid - Part I: A hybrid control architecture," *IEEE Trans Power Electron*, vol. 25, no. 12, pp. 2962–2970, 2010, doi: 10.1109/TPEL.2010.2087393.

[70] Paolo Piagi and Robert H. Lasseter, "Autonomous_control_of_microgrids," in *IEEE Power Engineering Society General Meeting*, 2006.

[71] J. M. Guerrero, J. C. Vasquez, J. Matas, L. G. De Vicuña, and M. Castilla, "Hierarchical control of droop-controlled AC and DC microgrids - A general approach toward standardization," *IEEE Transactions on Industrial Electronics*, vol. 58, no. 1, pp. 158–172, Jan. 2011, doi: 10.1109/TIE.2010.2066534.

[72] X. Hou, Y. A. O. Sun, J. Lu, and J. M. Guerrero, "Distributed Hierarchical Control of AC Microgrid Operating in Grid-Connected , Islanded and Their Transition Modes," *IEEE Access*, vol. 6, pp. 77388–77401, 2018, doi: 10.1109/ACCESS.2018.2882678.

[73] D. Cardoso, S. Junior, J. S. Dohler, P. M. De Almeida, and J. G. De Oliveira, "Droop Control for Power Sharing and Voltage and Frequency Regulation in Parallel Distributed Generations on AC Microgrid," no. Table I, pp. 5–10, 2018.

[74] M. D. Cook, E. H. Trinklein, G. G. Parker, R. D. Robinett, and W. W. Weaver, "Optimal and decentralized control strategies for inverter-based AC microgrids," *Energies (Basel)*, vol. 12, no. 18, Sep. 2019, doi: 10.3390/en12183529.

[75] J. M. Guerrero, C. Raj D, and D. N. Gaonkar, "Power sharing control strategy of parallel inverters in AC microgrid using improved reverse droop control," *International Journal of Power Electronics*, vol. 11, no. 1, p. 116, 2020, doi: 10.1504/ijpelec.2020.10025623.

[76] K. T. Tan, X. Y. Peng, P. L. So, Y. C. Chu, and M. Z. Q. Chen, "Centralized control for parallel operation of distributed generation inverters in microgrids," *IEEE Trans Smart Grid*, vol. 3, no. 4, pp. 1977–1987, 2012, doi: 10.1109/TSG.2012.2205952.

[77] P.Monica and M.Kowsalya, "Control strategies of parallel operated inverters in renewable energy application: A review," *Renewable and Sustainable Energy Reviews*, vol. 65, pp. 885–901, 2016.

[78] M. B. Delghavi and A. Yazdani, "An adaptive feedforward compensation for stability enhancement in droop-controlled inverter-based microgrids," *IEEE Transactions on Power Delivery*, vol. 26, no. 3, pp. 1764–1773, Jul. 2011, doi: 10.1109/TPWRD.2011.2119497.

[79] M. A. Roslan, S. A. Azmi, and K. H. Ahmed, "AC Power Flow Analysis for Inverters in Microgrid Application," in *Journal of Physics: Conference Series*, Institute of Physics, 2022. doi: 10.1088/1742-6596/2312/1/012053.

[80] E. Rokrok and M. E. H. Golshan, "Adaptive voltage droop scheme for voltage source converters in an islanded multibus microgrid," *IET Generation, Transmission and Distribution*, vol. 4, no. 5, pp. 562–578, May 2010, doi: 10.1049/iet-gtd.2009.0146.

[81] J. M. Guerrero, J. C. Vásquez, J. Matas, M. Castilla, and L. García de Vicuna, "Control strategy for flexible microgrid based on parallel line-interactive UPS systems," in *IEEE Transactions on Industrial Electronics*, 2009, pp. 726–736. doi: 10.1109/TIE.2008.2009274.

[82] N. Prabaharan, A. R. A. Jerin, E. Najafi, and K. Palanisamy, "An overview of control techniques and technical challenge for inverters in micro grid," in *Hybrid-renewable energy systems in microgrids: Integration, developments and control*, Elsevier, 2018, pp. 97–107. doi: 10.1016/B978-0-08-102493-5.00006-6.

[83] A. Elmouatamid, R. Ouladsine, M. Bakhouya, N. El Kamoun, M. Khaidar, and K. Zine-Dine, "Review of control and energy management approaches in micro-grid systems," *Energies*, vol. 14, no. 1. MDPI AG, Jan. 01, 2021. doi: 10.3390/en14010168.

[84] H. Zou, S. Mao, Y. Wang, F. Zhang, X. Chen, and L. Cheng, "A Survey of Energy Management in Interconnected Multi-Microgrids," *IEEE Access*, vol. 7. Institute of Electrical and Electronics Engineers Inc., pp. 72158–72169, 2019. doi: 10.1109/ACCESS.2019.2920008.

[85] G. Ma, J. Li, and X. P. Zhang, "A Review on Optimal Energy Management of Multimicrogrid System Considering Uncertainties," *IEEE Access*, vol. 10. Institute of Electrical and Electronics Engineers Inc., pp. 77081–77098, 2022. doi: 10.1109/ACCESS.2022.3192638.

[86] M. Naderi, Y. Khayat, Q. Shafiee, and T. Dragicevic, "An Emergency Active and Reactive Power Exchange Solution for Interconnected Microgrids," *IEEE J Emerg Sel Top Power Electron*, vol. 9, no. 5, pp. 5206–5218, 2021, doi: 10.1109/JESTPE.2019.2954113.

[87] N. Nikmehr and S. Najafi Ravadanegh, "Optimal Power Dispatch of Multi-Microgrids at Future Smart Distribution Grids," *IEEE Trans Smart Grid*, vol. 6, no. 4, pp. 1648–1657, Jul. 2015, doi: 10.1109/TSG.2015.2396992.

[88] Y. Liu, Y. Li, H. Xin, H. B. Gooi, and J. Pan, "Distributed Optimal Tie-Line Power Flow Control for Multiple Interconnected AC Microgrids," *IEEE Transactions on Power Systems*, vol. 34, no. 3, pp. 1869–1880, 2019.

[89] D. H. Tungadio and Y. Sun, "Optimal control of active power sharing capacity of microgrids interconnected," *Proceedings - 18th IEEE/ACIS International Conference on Computer and Information Science, ICIS 2019*, pp. 67–71, Jun. 2019, doi: 10.1109/ICIS46139.2019.8940237.

[90] D. H. Tungadio, "Optimal Control of Active Power Sharing Capacity of Microgrids Interconnected," pp. 67–71, 2019.

[91] L. P. M. I. Sampath, A. Krishnan, K. Chaudhar, H. B. Gooi, and A. Ukil, "A control architecture for optimal power sharing among interconnected microgrids." IEEE Power & Energy Society General Meeting, 2017. doi: 10.1109/PESGM.2017.8274333.

[92] M. Pham *et al.*, "Power management in multi-microgrid system based on energy routers," in *IEEE International Conference on Industrial Technology (ICIT)*, 2020. doi: 10.1109/ICIT45562.2020.9067200.

[93] I. U. Nutkani, P. C. Loh, and F. Blaabjerg, "Power flow control of interlinked hybrid microgrids," *15th International Power Electronics and Motion Control Conference and Exposition, EPE-PEMC 2012 ECCE Europe*, no. 2, pp. 2–7, 2012, doi: 10.1109/EPEPEMC.2012.6397327.

[94] M. Naderi, Y. Khayat, Q. Shafiee, T. Dragicevic, H. Bevrani, and F. Blaabjerg, "Interconnected Autonomous AC Microgrids via Back-to-Back Converters - Part I: Small-Signal Modeling," *IEEE Trans Power Electron*, vol. 35, no. 5, pp. 4728–4740, May 2020, doi: 10.1109/TPEL.2019.2943996.

[95] T. Nguyen, S. Member, H. Yoo, and S. Member, "A Droop Frequency Control for Maintaining Different Frequency Qualities in a Stand-Alone Multimicrogrid System," *IEEE Trans Sustain Energy*, vol. 9, no. 2, pp. 599–609, 2018, doi: 10.1109/TSTE.2017.2749438.

[96] B. Zhou *et al.*, "Multi-microgrid Energy Management Systems: Architecture, Communication, and Scheduling Strategies," *Journal of Modern Power Systems and Clean Energy*, vol. 9, no. 3, pp. 463–476, 2021, doi: 10.35833/MPCE.2019.000237.

[97] M. Naderi, Y. Khayat, Q. Shafiee, T. Dragicevic, H. Bevrani, and F. Blaabjerg, "Interconnected Autonomous AC Microgrids via Back-to-Back Converters — Part I : Small-Signal Modeling," *IEEE Trans Power Electron*, vol. 35, no. 5, pp. 4728–4740, 2020.

[98] X. Shen, D. Tan, Z. Shuai, and A. Luo, "Control techniques for bidirectional interlinking converters in hybrid microgrids," *IEEE Power Electronics Magazine*, vol. 6, no. 3, pp. 39–47, Sep. 2019, doi: 10.1109/MPEL.2019.2925298.

[99] P. Wu, W. Huang, N. Tai, J. Xie, and B. Lv, "An Advanced Architecture of Multiple Microgrids Interfacing with UCC," in *IEEE Power & Energy Society General Meeting*, 2017.

[100] A. M. Pasha *et al.*, "Enhanced transient response and seamless interconnection of multi-microgrids based on an adaptive control scheme," *IET Renewable Power Generation*, vol. 15, no. 11, pp. 2452–2467, Aug. 2021, doi: 10.1049/rpg2.12176.

[101] G. Turner, J. P. Kelley, C. L. Storm, D. A. Wetz, and W. J. Lee, "Design and active control of a microgrid testbed," *IEEE Trans Smart Grid*, vol. 6, no. 1, pp. 73–81, Jan. 2015, doi: 10.1109/TSG.2014.2340376.

[102] F. Katiraei, R. Iravani, N. Hatziargyriou, and A. Dimeas, "Microgrids management," *IEEE Power and Energy Magazine*, vol. 6, no. 3, pp. 54–65, May 2008, doi: 10.1109/MPE.2008.918702.

[103] A. Kargarian and M. Rahmani, "Multi-microgrid energy systems operation incorporating distribution-interline power flow controller," *Electric Power Systems Research*, vol. 129, pp. 208–216, Dec. 2015, doi: 10.1016/j.epsr.2015.08.015.

[104] D. Saha, N. Bazmohammadi, J. C. Vasquez, and J. M. Guerrero, "Multiple Microgrids: A Review of Architectures and Operation and Control Strategies," *Energies*, vol. 16, no. 2. MDPI, Jan. 01, 2023. doi: 10.3390/en16020600.

[105] N. O. Song, J. H. Lee, H. M. Kim, Y. H. Im, and J. Y. Lee, "Optimal energy management of multi-microgrids with sequentially coordinated operations," *Energies (Basel)*, vol. 8, no. 8, pp. 8371–8390, Aug. 2015, doi: 10.3390/en8088371.

[106] N. Nikmehr and S. Najafi Ravadanegh, "Reliability evaluation of multi-microgrids considering optimal operation of small scale energy zones under load-generation uncertainties," *International Journal of Electrical Power and Energy Systems*, vol. 78, pp. 80–87, Jun. 2016, doi: 10.1016/j.ijepes.2015.11.094.

[107] Hossein Farzin, Mahmud Fotuhi-Firuzabad, and Moein Moeini-Aghtaie, "Role of Outage Management Strategy in Reliability Performance of Multi-Microgrid Distribution Systems," *IEEE Transactions on Power Systems* , vol. 33, no. 3, pp. 2359–2369, 2018, [Online]. Available: http://www.ieee.org/publications

[108] C. S. Karavas, G. Kyriakarakos, K. G. Arvanitis, and G. Papadakis, "A multi-agent decentralized energy management system based on distributed intelligence for the design and control of autonomous polygeneration microgrids," *Energy Convers Manag*, vol. 103, pp. 166–179, Jul. 2015, doi: 10.1016/j.enconman.2015.06.021.

[109] Z. Wang, B. Chen, J. Wang, M. M. Begovic, and C. Chen, "Coordinated energy management of networked microgrids in distribution systems," *IEEE Trans Smart Grid*, vol. 6, no. 1, pp. 45–53, Jan. 2015, doi: 10.1109/TSG.2014.2329846.

[110] Z. Wang, B. Chen, J. Wang, and J. Kim, "Decentralized Energy Management System for Networked Microgrids in Grid-Connected and Islanded Modes," *IEEE Trans Smart Grid*, vol. 7, no. 2, pp. 1097–1105, Mar. 2016, doi: 10.1109/TSG.2015.2427371.

[111] C. Ceja Espinosa, "Energy Management Systems for Multi-Microgrid Networks Under Uncertainties," 2023.

[112] P. Kou, D. Liang, and L. Gao, "Distributed EMPC of multiple microgrids for coordinated stochastic energy management," *Appl Energy*, vol. 185, pp. 939–952, Jan. 2017, doi: 10.1016/j.apenergy.2016.09.092.

[113] M. J. Hossain, M. A. Mahmud, H. R. Pota, N. Mithulananthan, and R. C. Bansal, "Distributed control scheme to regulate power flow and minimize interactions in multiple microgrids," in *IEEE PES General Meeting | Conference & Exposition*, 2014.

[114] C. Bersani, H. Dagdougui, A. Ouammi, and R. Sacile, "Distributed Robust Control of the Power Flows in a Team of Cooperating Microgrids," *IEEE Transactions on Control Systems Technology*, vol. 25, no. 4, pp. 1473–1479, Jul. 2017, doi: 10.1109/TCST.2016.2611568.

[115] G. Liu, M. F. Ferrari, T. B. Ollis, A. Sundararajan, M. Olama, and Y. Chen, "Distributed Energy Management for Networked Microgrids with Hardware-in-the-Loop Validation," *Energies (Basel)*, vol. 16, no. 7, Apr. 2023, doi: 10.3390/en16073014.

[116] L. Gao and L. Ma, "Coordinated Energy Management Of Networked Microgrids In The Distribution Market," in *5th IEEE Conference on Energy Internet and Energy System Integration: Energy Internet for Carbon Neutrality, EI2 2021*, Institute of Electrical and Electronics Engineers Inc., 2021, pp. 3615–3620. doi: 10.1109/EI252483.2021.9713448.

[117] P. Sanjeev, N. P. Padhy, and P. Agarwal, "Autonomous Power Control and Management Between Standalone DC Microgrids," vol. 3203, no. c, pp. 1–10, 2017, doi: 10.1109/TII.2017.2773507.

[118] T. Dragicevic, D. Wu, Q. Shafiee, and L. Meng, "Distributed and Decentralized Control Architectures for Converter-Interfaced Microgrids," vol. 3, no. 2, 2017.

[119] P. Monica, M. Kowsalya, and P. C. Tejaswi, "Load sharing control of parallel operated single phase inverters," in *Energy Procedia*, Elsevier Ltd, 2017, pp. 600–606. doi: 10.1016/j.egypro.2017.05.156.

[120] M. Kumar, "Control Techniques for Interconnections of Cluster of Neighboring Islanded Hybrid Smart Microgrids," *Electric Power Components and Systems*, vol. 51, no. 3, pp. 225–239, 2023, doi: 10.1080/15325008.2022.2139872.

[121] N. L. Díaz, F. Guinjoan, G. Velasco-Quesada, A. C. Luna, and J. M. Guerrero, "Fuzzy-based cooperative interaction between stand-alone microgrids interconnected through VSC-based multiterminal converter," *International Journal of Electrical Power & Energy Systems*, vol. 152, p. 109226, Oct. 2023, doi: 10.1016/J.IJEPES.2023.109226.

[122] V. K. Singh, B. V. Suryakiran, A. Verma, and T. S. Bhatti, "Modelling of a renewable energy-based AC interconnected rural microgrid system for the provision of uninterrupted power supply," *IET Energy Systems Integration*, vol. 3, no. 2, pp. 172–183, Jun. 2021, doi: 10.1049/esi2.12015.

[123] H. J. Yoo, T. T. Nguyen, and H. M. Kim, "Multi-frequency control in a stand-alone multi-microgrid system using a back-to-back converter," *Energies (Basel)*, vol. 10, no. 6, Jun. 2017, doi: 10.3390/en10060822.

[124] D. Gamage, X. Zhang, A. Ukil, and A. Swain, "Energy Management of Islanded Interconnected Dual Community Microgrids," in *IECON 2020 The 46th Annual Conference of the IEEE Industrial Electronics Society*, 2020, pp. 1803–1807. doi: 10.1109/IECON43393.2020.9254619.

[125] Sandeep Bala and Giri Venkataramanan, "Autonomous power electronic interfaces between microgrids," in *IEEE Energy Conversion Congress and Exposition*, IEEE, 2009.

[126] C. Y. Tang, C. J. Tsai, Y. M. Chen, and Y. R. Chang, "Dynamic optimal AC line current regulation method for three-phase active power conditioners," *IEEE J Emerg Sel Top Power Electron*, vol. 5, no. 2, pp. 901–911, Jun. 2017, doi: 10.1109/JESTPE.2017.2647843.

[127] C. Y. Tang, Y. F. Chen, Y. M. Chen, and Y. R. Chang, "DC-Link Voltage Control Strategy for Three-Phase Back-to-Back Active Power Conditioners," *IEEE Transactions on Industrial Electronics*, vol. 62, no. 10, pp. 6306–6316, Oct. 2015, doi: 10.1109/TIE.2015.2420671.

[128] M. Khederzadeh, H. Maleki, and V. Asgharian, "Frequency control improvement of two adjacent microgrids in autonomous mode using back to back Voltage-Sourced Converters," *International Journal of Electrical Power and Energy Systems*, vol. 74, pp. 126–133, Aug. 2016, doi: 10.1016/j.ijepes.2015.07.002.

[129] S. A. Mehraban and R. Eslami, "Multi-microgrids energy management in power transmission mode considering different uncertainties," *Electric Power Systems Research*, vol. 216, Mar. 2023, doi: 10.1016/j.epsr.2022.109071.

[130] Y. Jia, P. Wen, Y. Yan, and L. Huo, "Joint Operation and Transaction Mode of Rural Multi Microgrid and Distribution Network," *IEEE Access*, vol. 9, pp. 14409–14421, 2021, doi: 10.1109/ACCESS.2021.3050793.

[131] Z. Wang, Z. Dou, J. Dong, S. Si, C. Wang, and L. Liu, "Optimal Dispatching of Regional Interconnection Multi-Microgrids Based on Multi-Strategy Improved Whale Optimization Algorithm," *IEEJ Transactions on Electrical and Electronic Engineering*, vol. 17, no. 6, pp. 766–779, Jun. 2022, doi: 10.1002/tee.23566.

[132] S. Fan, G. Xu, Q. Ai, and Y. Gao, "Community Market Based Energy Trading Among Interconnected Microgrids With Adjustable Power," *IEEE Trans Ind Appl*, vol. 59, no. 1, pp. 148–159, Jan. 2023, doi: 10.1109/TIA.2022.3212992.

[133] C. I. Chen, W. J. Chen, and C. H. Chen, "Power Dispatching Control Strategy of Interconnected Microgrid," in *Proceedings - 2022 IET International Conference on Engineering Technologies and Applications, IET-ICETA 2022*, Institute of Electrical and Electronics Engineers Inc., 2022. doi: 10.1109/IET-ICETA56553.2022.9971593.

[134] N. Liu and J. Wang, "Energy sharing for interconnected microgrids with a battery storage system and renewable energy sources based on the alternating direction method of multipliers," *Applied Sciences (Switzerland)*, vol. 8, no. 4, Apr. 2018, doi: 10.3390/app8040590.

[135] C. Wei, Z. Shen, D. Xiao, L. Wang, X. Bai, and H. Chen, "An optimal scheduling strategy for peer-to-peer trading in interconnected microgrids based on RO and Nash bargaining," *Appl Energy*, vol. 295, p. 117024, Aug. 2021, doi: 10.1016/J.APENERGY.2021.117024.

[136] X. Zhong, W. Zhong, Y. Liu, C. Yang, and S. Xie, "Optimal energy management for multi-energy multi-microgrid networks considering carbon emission limitations," *Energy*, vol. 246, p. 123428, May 2022, doi: 10.1016/J.ENERGY.2022.123428.

[137] K. Naz, F. Zainab, S. B. A. Mehmood, Khawaja Khalid Bukhari, H. A. Khalid, and C. Kim, "An Optimized Framework for Energy Management of Multi-Microgrid Systems," *Energies (Basel)*, pp. 1–15, 2021.

[138] D. I. Hidalgo-Rodríguez and J. Myrzik, "Optimal Operation of Interconnected Home-Microgrids with Flexible Thermal Loads: A Comparison of Decentralized, Centralized, and Hierarchical-Distributed Model Predictive Control," 2018. doi: 10.23919/PSCC.2018.8442807.

[139] M. Grami, M. Rekik, and L. Krichen, "Power Dispatch Strategy for Interconnected Microgrids Based Hybrid Renewable Energy System," *International Journal of Renewable Energy Research*, vol. 8, no. 2, 2018.

[140] M. Kermani, P. Chen, L. Goransson, and M. Bongiorno, "Optimal Energy Control, Hosting BESS and EVs through Multiport Converter in Interconnected MGs," in *2022 IEEE International Conference on Environment and Electrical Engineering and 2022 IEEE Industrial and Commercial Power Systems Europe, EEEIC / I and CPS Europe 2022*, Institute of Electrical and Electronics Engineers Inc., 2022. doi: 10.1109/EEEIC/ICPSEurope54979.2022.9854791.

[141] Morteza Dabbaghjamanesh, Shahab Mehraeen, Abdollah Kavousi-Fard, and Farzad Ferdowsi, "A New Efficient Stochastic Energy Management Technique for Interconnected AC Microgrids," *IEEE Power & Energy Society General Meeting (PESGM)*, 2018.

[142] S. K. Akula and H. Salehfar, "Energy Management System for Interconnected Microgrids using Alternating Direction Method of Multipliers (ADMM)," *2018 North American Power Symposium, NAPS 2018*. 2019. doi: 10.1109/NAPS.2018.8600647.

[143] B. Zhao *et al.*, "Energy Management of Multiple Microgrids Based on a System of Systems Architecture," *IEEE Transactions on Power Systems*, vol. 33, no. 6, pp. 6410–6421, 2018.

[144] M. Xie, X. Ji, X. Hu, P. Cheng, Y. Du, and M. Liu, "Autonomous optimized economic dispatch of active distribution system with multi-microgrids," *Energy*, vol. 153, pp. 479–489, Jun. 2018, doi: 10.1016/j.energy.2018.04.021.

[145] W. R. Issa, M. A. Abusara, S. M. Sharkh, and A. In, "Control of Transient Power During Unintentional Islanding of Microgrids," vol. 30, no. 8, pp. 4573–4584, 2015.

[146] R. Al Badwawi, W. Issa, T. Mallick, and M. Abusara, "Power management of AC islanded microgrids using fuzzy logic," in *IET Conference Publications*, Institution of Engineering and Technology, 2016. doi: 10.1049/cp.2016.0348.

[147] W. Liu, J. Zhan, and C. Y. Chung, "A novel transactive energy control mechanism for collaborative networked microgrids," *IEEE Transactions on Power Systems*, vol. 34, no. 3, pp. 2048–2060, May 2019, doi: 10.1109/TPWRS.2018.2881251.

[148] Tianguang Lu, Zhaoyu Wang, Qian Ai, and Wei-Jen Lee, "Interactive model for energy management of clustered microgrids," in *IEEE Industry Applications Society Annual Meeting*, 2016.

[149] S. A. Arefifar, M. Ordonez, and Y. A. R. I. Mohamed, "Energy Management in Multi-Microgrid Systems - Development and Assessment," *IEEE Transactions on Power Systems*, vol. 32, no. 2, pp. 910–922, Mar. 2017, doi: 10.1109/TPWRS.2016.2568858.

[150] F. Li, J. Qin, Y. Wan, and T. Yang, "Decentralized Cooperative Optimal Power Flow of Multiple Interconnected Microgrids via Negotiation," *IEEE Trans Smart Grid*, vol. 11, no. 5, pp. 3827–3836, Sep. 2020, doi: 10.1109/TSG.2020.2989929.

[151] W. Liu, J. Zhan, and C. Y. Chung, "A novel transactive energy control mechanism for collaborative networked microgrids," *IEEE Transactions on Power Systems*, vol. 34, no. 3, pp. 2048–2060, May 2019, doi: 10.1109/TPWRS.2018.2881251.

[152] Z. Liu *et al.*, "Optimal planning and operation of dispatchable active power resources for islanded multi-microgrids under decentralised collaborative dispatch framework," *IET Generation, Transmission and Distribution*, vol. 14, no. 3, pp. 408–422, Feb. 2020, doi: 10.1049/iet-gtd.2019.0796.

[153] F. Mthethwa, C. Gomes, and D. Dorrell, "Development of optimal algorithm to interconnect multiple microgrids in an agricultural-based remote community," in *IEEE AFRICON Conference*, Institute of Electrical and Electronics Engineers Inc., Sep. 2021. doi: 10.1109/AFRICON51333.2021.9571000.

[154] K. P. Schneider, C. Miller, S. Laval, W. Du, and D. Ton, "Networked Microgrid Operations: Supporting a Resilient Electric Power Infrastructure," *IEEE Electrification Magazine*, vol. 8, no. 4, pp. 70–79, Dec. 2020, doi: 10.1109/MELE.2020.3026442.

[155] Stella Kampezidou, Orestis Vasios, and Sakis Meliopoulos, "Multi-Microgrid Architecture: Optimal Operation and Control," in *North American Power Symposium (NAPS)*, 2018.

[156] A. Ouammi, H. Dagdougui, and R. Sacile, "Optimal control of power flows and energy local storages in a network of microgrids modeled as a system of systems," *IEEE Transactions on Control Systems Technology*, vol. 23, no. 1, pp. 128–138, Jan. 2015, doi: 10.1109/TCST.2014.2314474.

[157] B. Zhao *et al.*, "Energy Management of Multiple Microgrids Based on a System of Systems Architecture," *IEEE Transactions on Power Systems*, vol. 33, no. 6, pp. 6410–6421, 2018.

[158] P. Sheikhahmadi, S. Bahramara, A. Mazza, G. Chicco, M. Shafie-Khah, and J. P. S. Catalao, "Multi-Microgrids Operation With Interruptible Loads in Local Energy and Reserve Markets," *IEEE Syst J*, vol. 17, no. 1, pp. 1292–1303, Mar. 2023, doi: 10.1109/JSYST.2022.3177637.

[159] W. Zhang and Y. Xu, "Distributed Optimal Control for Multiple Microgrids in a Distribution Network," *IEEE Trans Smart Grid*, vol. 10, no. 4, pp. 3765–3779, Jul. 2019, doi: 10.1109/TSG.2018.2834921.

[160] A. Hussain, V. H. Bui, and H. M. Kim, "A Resilient and Privacy-Preserving Energy Management Strategy for Networked Microgrids," *IEEE Trans Smart Grid*, vol. 9, no. 3, pp. 2127–2139, May 2018, doi: 10.1109/TSG.2016.2607422.

[161] N. Nikmehr, S. Najafi-Ravadanegh, and A. Khodaei, "Probabilistic optimal scheduling of networked microgrids considering time-based demand response programs under uncertainty," *Appl Energy*, vol. 198, pp. 267–279, 2017, doi: 10.1016/j.apenergy.2017.04.071.

[162] S. Haghifam, M. Dadashi, K. Zare, and H. Seyedi, "Optimal operation of smart distribution networks in the presence of demand response aggregators and microgrid owners: A multi follower Bi-Level approach," *Sustain Cities Soc*, vol. 55, Apr. 2020, doi: 10.1016/j.scs.2020.102033.

[163] M. Mohiti, H. Monsef, A. Anvari-moghaddam, J. Guerrero, and H. Lesani, "A decentralized robust model for optimal operation of distribution companies with private microgrids," *International Journal of*

Electrical Power and Energy Systems, vol. 106, pp. 105–123, Mar. 2019, doi: 10.1016/j.ijepes.2018.09.031.

[164] A. Hussain, V. H. Bui, and H. M. Kim, "Robust optimization-based scheduling of multi-microgrids considering uncertainties," *Energies (Basel)*, vol. 9, no. 4, Apr. 2016, doi: 10.3390/en9040278.

[165] Y. Du, J. Wu, S. Li, C. Long, and S. Onori, "Coordinated Energy Dispatch of Autonomous Microgrids With Distributed MPC Optimization," *IEEE Trans Industr Inform*, vol. 15, no. 9, pp. 5289–5298, Feb. 2019, doi: 10.1109/tii.2019.2899885.

[166] X. Wu *et al.*, "A Two-Layer Distributed Cooperative Control Method for Islanded Networked Microgrid Systems," *IEEE Trans Smart Grid*, vol. 11, no. 2, pp. 942–957, Mar. 2020, doi: 10.1109/TSG.2019.2928330.

[167] X. Kong, D. Liu, C. Wang, F. Sun, and S. Li, "Optimal operation strategy for interconnected microgrids in market environment considering uncertainty," *Appl Energy*, vol. 275, Oct. 2020, doi: 10.1016/j.apenergy.2020.115336.

[168] A. Jafari, H. Ganjeh Ganjehlou, T. Khalili, and A. Bidram, "A fair electricity market strategy for energy management and reliability enhancement of islanded multi-microgrids," *Appl Energy*, vol. 270, Jul. 2020, doi: 10.1016/j.apenergy.2020.115170.

[169] A. El Zerk, M. Ouassaid, and Y. Zidani, "Decentralised strategy for energy management of collaborative microgrids using multi-agent system," *IET Smart Grid*, vol. 5, no. 6, pp. 440–462, Dec. 2022, doi: 10.1049/stg2.12077.

[170] B. Mukhopadhyay and D. Das, "Comprehensive multi-benefit planning of sustainable interconnected microgrids," *Sustainable Energy, Grids and Networks*, vol. 36, Dec. 2023, doi: 10.1016/j.segan.2023.101226.

[171] X. Chen, J. Zhai, Y. Jiang, C. Ni, S. Wang, and P. Nimmegeers, "Decentralized coordination between active distribution network and multi-microgrids through a fast decentralized adjustable robust operation framework," *Sustainable Energy, Grids and Networks*, vol. 34, Jun. 2023, doi: 10.1016/j.segan.2023.101068.

[172] Y. Li *et al.*, "Optimal operation of multimicrogrids via cooperative energy and reserve scheduling," *IEEE Trans Industr Inform*, vol. 14, no. 8, pp. 3459–3468, Aug. 2018, doi: 10.1109/TII.2018.2792441.

[173] Y. Du and F. Li, "Intelligent Multi-Microgrid Energy Management Based on Deep Neural Network and Model-Free Reinforcement Learning," *IEEE Trans Smart Grid*, vol. 11, no. 2, pp. 1066–1076, Mar. 2020, doi: 10.1109/TSG.2019.2930299.

[174] C. Ceja-Espinosa, M. Pirnia, and C. A. Cañizares, "A Privacy-Preserving Energy Management System for Cooperative Multi-Microgrid Networks," in *11th Bulk Power Systems Dynamics and Control Symposium*, 2022.

[175] Z. Wang, Z. Dou, J. Dong, S. Si, C. Wang, and L. Liu, "Optimal Dispatching of Regional Interconnection Multi-Microgrids Based on Multi-Strategy Improved Whale Optimization Algorithm," *IEEJ Transactions on Electrical and Electronic Engineering*, vol. 17, no. 6, pp. 766–779, Jun. 2022, doi: 10.1002/tee.23566.

[176] K. Thirugnanam, M. S. El Moursi, V. Khadkikar, H. H. Zeineldin, and M. Al Hosani, "Energy Management of Grid Interconnected Multi-Microgrids Based on P2P Energy Exchange: A Data Driven Approach," *IEEE*

Transactions on Power Systems, vol. 36, no. 2, pp. 1546–1562, Mar. 2021, doi: 10.1109/TPWRS.2020.3025113.

[177] A. Ouammi, H. Dagdougui, L. Dessaint, and R. Sacile, "Coordinated Model Predictive-Based Power Flows Control in a Cooperative Network of Smart Microgrids," *IEEE Trans Smart Grid*, vol. 6, no. 5, pp. 2233–2244, Sep. 2015, doi: 10.1109/TSG.2015.2396294.

[178] J. C. Lagarias, J. A. Reeds, M. H. Wright, and P. E. Wright, "Convergence properties of the Nelder-Mead simplex method in low dimensions," *SIAM Journal on Optimization*, vol. 9, no. 1, pp. 112–147, 1998, doi: 10.1137/S1052623496303470.

[179] I. Vasiliev, L. Luca, R. Vilanova, and S. Caraman, "Optimal Control of a Sewer Network," in *2022 26th International Conference on System Theory, Control and Computing, ICSTCC 2022 - Proceedings*, Institute of Electrical and Electronics Engineers Inc., 2022, pp. 80–85. doi: 10.1109/ICSTCC55426.2022.9931810.